Research Center

Bethesda, MD 20084–5000

DTRC–SME–91/12 April 1991

Ship Materials Engineering Department

Research and Development Report

Vibration Damping Response of Composite Materials

by

Roger M. Crane

DTRC–SME–91/12 Vibration Damping Response of Composite Materials

MAJOR DTRC TECHNICAL COMPONENTS

CODE 011 DIRECTOR OF TECHNOLOGY, PLANS AND ASSESSMENT

12 SHIP SYSTEMS INTEGRATION DEPARTMENT

14 SHIP ELECTROMAGNETIC SIGNATURES DEPARTMENT

15 SHIP HYDROMECHANICS DEPARTMENT

16 AVIATION DEPARTMENT

17 SHIP STRUCTURES AND PROTECTION DEPARTMENT

18 COMPUTATION, MATHEMATICS & LOGISTICS DEPARTMENT

19 SHIP ACOUSTICS DEPARTMENT

27 PROPULSION AND AUXILIARY SYSTEMS DEPARTMENT

28 SHIP MATERIALS ENGINEERING DEPARTMENT

DTRC ISSUES THREE TYPES OF REPORTS:

1. **DTRC reports, a formal series,** contain information of permanent technical value. They carry a consecutive numerical identification regardless of their classification or the originating department.

2. **Departmental reports, a semiformal series,** contain information of a preliminary, temporary, or proprietary nature or of limited interest or significance. They carry a departmental alphanumerical identification.

3. **Technical memoranda, an informal series,** contain technical documentation of limited use and interest. They are primarily working papers intended for internal use. They carry an identifying number which indicates their type and the numerical code of the originating department. Any distribution outside DTRC must be approved by the head of the originating department on a case-by-case basis.

NDW-DTNSRDC 5602/50 (Rev. 2-88)

David Taylor Research Center
Bethesda, MD 20084-5000

DTRC-SME-91/12 April 1991
Ship Materials Engineering Department
Research and Development Report

Vibration Damping Response of Composite Materials

by
Roger M. Crane

TABLE OF CONTENTS

LIST OF TABLES

LIST OF FIGURES

LIST OF ABBREVIATIONS

A-D	Analogue to digital
CFRP	Carbon fiber reinforced plastic
cm	Centimeter
dB	Decibels
DMA	Direct memory access
°F	Degrees Fahrenheit
FFT	Fast Fourier Transform
GPa	Giga Pascals
GFRP	Glass fiber reinforced plastic
Hz	hertz
in	Inch
J	Joule
kg	Kilogram
kHz	Kilohertz
°K	Degrees Kelvin
ksi	Thousand pounds per square inch
lbf	Pounds force
m	Meter
mm	Millimeter
MPa	Mega Pascals
N	Newton
psi	Pounds per square inch
sec	Seconds
sq	Square

ABSTRACT

This report involves the investigation of the mechanical vibration damping characteristics of glass/epoxy and graphite/epoxy composite materials. The objective was to develop an analytical model which incorporates the frequency dependence of the vibration damping loss factor and to experimentally characterize the loss factor for frequencies up to 1000 Hz.

Numerous analytical models have been proposed to determine the loss factor of composites, including micromechanical, macromechanical and structural models. Of these generic types, the macromechanical models incorporate important material characteristics which can affect the loss factor. The most widely accepted model utilizes the elastic viscoelastic correspondence principle. Although investigators acknowledge the viscoelastic characteristic of composites, they fail to incorporate the frequency dependence in their analysis. In this effort, the elastic viscoelastic correspondence principle is extended to incorporate the frequency dependence of the composite material.

The analytical model requires as input the inplane material loss factors as a function of frequency. An experimental apparatus was designed and fabricated to accomplish this. Cantilever beam specimens were utilized, which were excited using an impulse from an instrumented force hammer. The loss factor was calculated using the half power band width technique. The apparatus was calibrated using a well characterized low damping material. The effect of clamping pressure and of the clamp block to specimen interface material was also investigated.

While testing the composites, it became evident that the amplitude of vibration had a pronounced effect on the calculated loss factor. Calculated loss factor were significantly reduced if the tip displacement amplitudes vs. time were lower than 0.001 in. for more than 25% of the data set. To alleviate this problem, a robust testing methodology was proposed and tested. This test method is then utilized to determine the composite inplane loss factors.

The analytical model was validated using two generic laminated configurations. The model predictions were within the scatter of the experimental data. Parametric studies were also performed using the model. Trends shown by other investigators as well as inconsistencies between them were accounted for by this model.

EXECUTIVE SUMMARY

This report presents information on a multiyear research investigation of the mechanical vibration damping of thermoset matrix composite materials. The objective of this effort was to develop an analytical model which could determine the mechanical vibration damping of an arbitrary composite laminate in a specified frequency range. A detailed discussion on the objective of this program is presented in Chapter 1 following the Introduction..

Chapter 2 presents a detailed chronological literature survey of the vibration damping research performed on composite materials. This survey is divided into two main sections; test procedures and experimental results, and analytical models for determination of the damping loss factor. The experimental technique that has gained wide acceptance for the determination of the damping loss factor of composites utilizes a cantilever beam. The beam is excited using an instrumented impact hammer and the beam response is measured with a noncontact eddy current probe. The mechanical vibration damping loss factor is then determined using the half power band width technique.

The damping loss factor for composite materials has been shown experimentally to be dependent on the fiber angle, specimen thickness, the resin system used, the frequency of test, the fiber volume fraction, fiber diameter, beam stiffness, state of damage in the

material, and, in some cases, on the stress amplitude. The type of fiber used also affects the damping loss factor due to the fiber's contribution to the damping or to the difference in the interface properties of the fiber and resin systems investigated. Increasing the fiber volume fraction, the fiber diameter, the specimen thickness, and the beam stiffness reduces the damping loss factor. In most cases, increasing the amount of damage in the material, the stress amplitude of test, or the frequency of test increases the damping loss factor.

The theoretical models presented in Chapter 2 can be categorized as micromechanical, macromechanical or structural. The models discussed are currently inadequate for design purposes. The micromechanical approaches for determining the loss factor of composite laminae do not incorporate the material characteristics that have been shown to affect the loss factor. In addition, they do not take into account the frequency dependence loss factor characteristic of the matrix. The macromechanical approaches also do not account for the frequency dependence, i.e the viscoelastic characteristic, of the composite material. In addition, there does not exist an adequate characterization of the material loss factor which could be utilized as input to these macromechanical models. The structural approaches do not account for either the frequency dependence of the loss factor or the anisotropic variation in loss factor.

Chapter 3 presents the analytical model developed in this research. The model is based on the elastic viscoelastic correspondence principle. In this research, the frequency dependence of the damping loss factor is included, thereby extending the model as it is currently used in the literature. The frequency dependent complex moduli of a lamina is utilized in classical lamination theory to determine the various complex reduced stiffnesses

of the composite laminate. The laminate loss factors at any frequency can then be determined as the ratio of the complex to real part of the specific component of the effective moduli. The importance of this model is that from limited lamina complex moduli, the damping loss factor at a specific frequency can be determined, in the analogous manner to the methodology used for determining the effective material properties of a composite.

Chapter 4 presents the experimental set-up, the computer hardware utilized and the software written to determine the damping loss factor of the composites. In order to ensure that the loss factor results obtained were of the material and not from any other sources of energy dissipation, such as friction at the clamped area of the specimen, aerodynamic damping, or inadequacies in the acquisition system, the set-up and procedure were calibrated using a well characterized, low damping material system, 2024 T-4 aluminum.

Chapter 5, a robust testing methodology is proposed for the determination of the material damping loss factor of composite materials. This is shown to be necessary for composites because of their high damping loss factor. During the experimental testing of the composite specimens, it was shown that it is necessary to determine the applicability of the displacement information prior to performing data reductions for loss factor determination. Incorporation of near zero displacement information, or displacements that are on the same order of magnitude as the noise of the system, has the effect of lowering the calculated value of the loss factor. This occurs because of the effective averaging of this loss factor with the losses that occur at the larger more resolvable displacements. Another reason for errors occurring when the near zero displacements are included in the determination of the damping loss factor is due to the reduction of the sensitivity of the

sensors measuring the beam tip displacements as the tip displacements are reduced.

The proposed robust testing methodology initially requires a well designed apparatus that has been calibrated using a well characterized test specimen, as has been described in Chapter 4. Following the beam excitation, the magnitude of the beam tip displacement vs. time must be visually or numerically interrogated to insure that the displacements remain greater than the noise and resolution of the sensor and data acquisition system. If not, the resultant experimentally determined loss factor may be lower than the actual material loss factor. If measured displacements less than 0.001 in. (0.025 mm) are incorporated in the FFT analysis, and constitute more than 25% of the displacement vs. time curve, the loss factor that is calculated will be lower than the actual material loss factor.

The damping loss factor results are shown to be dependent on the amplitude of beam tip displacements. It is proposed that the material loss factor can be obtained by determining the loss factor versus tip displacement by partitioning the beam vibration response into subsets. The loss factor within each of these subsets are then determined and plotted versus the maximum beam amplitude within the subset. The material loss factor is then obtained by performing a linear fit on this data and extrapolating to zero displacement. This zero displacement loss factor is then assumed to be the material loss factor. The extrapolation to zero displacement should reduce the extraneous losses, providing a more robust testing protocol. In addition, it is hypothesized that the loss factors that result are more representative of that which would be experienced by an actual structure since, in the majority of cases, displacements are small and/or the structures are restrained from experiencing large displacements.

In Chapter 6, the results of the experimental testing of the material loss factors for AS4/3501-6 and S-2 Glass/3501-6 composites are presented. The loss factor for the 90 degree S-2 glass/3501-6 and AS4/3501-6 unidirectional composites is a nonlinear function of frequency, showing an increase in loss factor with increasing frequency. The loss factor for the 0 degree S-2 glass/3501-6 and AS4/3501-6 unidirectional composite appears to be linear, showing an increase with increasing frequency. From experimentally determined 0° and 90° loss factor information, a methodology is given to determine the shear loss factor based on the loss factor results obtained in a $\pm$ 45° beam specimen. The results of experimental investigations in the literature which attempt to determine the effect of fiber orientation on loss factor are analytically investigated using the model described in Chapter 3 and the experimental data obtained in this chapter. The incorporation of the frequency dependence of the loss factor is shown to analytically explain the discrepancies in the literature on the loss factor as a function of fiber orientation. The results of the model show that for different frequencies, the fiber orientation at which the maximum damping loss factor occurs can be different. In addition, the differences that occur when considering angle-ply versus off-axis results is shown, using the analytical model, to be the result of the stress coupling effects on loss factor.

In Chapter 7, results are presented on the experimental validation of the analytical model. The validation is performed on quasi-isotropic S-2 Glass/3501-6 beams. Two configurations were used: $(90/0/-45/45)_{2s}$ and $(45/-45/90/0)_{2s}$. The analytical model based on the elastic viscoelastic correspondence principle appears to provide an excellent prediction of the damping loss factor of a general laminated composite configuration over a given frequency range. Trends occurring experimentally in the material are shown to occur using the analytical model. The analytical model has been shown to provide a loss factor

which is within 15% of the experimentally determined values in the frequency range of 50 to 500 Hz.

Chapter 8 discusses the conclusions from this research investigation. The analytical model, an extension of the elastic-viscoelastic correspondence principle incorporating the frequency dependence of the loss factor, is an accurate analytical tool that can be used to determine the loss factor of a general laminated composite plate. In addition, the proposed robust testing methodology is summarized.

Chapter 9 presents five areas of investigation which would add to the knowledge base and testing capability of the vibration damping of composites. The areas identified are: embedded fiber optic displacement sensor; effects of defects; effects of beam orientation on damping loss factor; damping optimization using hybrid composite design; generalized 3-D elastic viscoelastic model.

ADMINISTRATIVE INFORMATION

This project was financially supported by several Agencies. The DTRC Independent Exploratory Development Program, sponsored by the Space and Naval Warfare Systems Command Director of Navy Laboratories, SPAWAR 05 and administered by the Research Coordinator, DTRC 0113 under Work Unit 1-2802-454 supported the development and calibration of the test apparatus and some of the initial results of the composite testing. The development of the robust testing methodology was supported by Dr. A.K. Vasudevan, ONR Code 1216, under Work Unit 1-2802-150. The analytical model development and the composite test results were supported by Mr. James Kelly, the Program Area for Materials of the DARPA AST Program, under Work Unit 1-2802-300 and 1-2802-301.

INTRODUCTION

The vibration damping characteristics of various structural applications play a dominant role in the choice of configuration and materials. Metals, in general, possess a very low vibration damping loss factor. For the majority of structures that are manufactured using metal, however, damping is not considered to be a problem. For example, cantilevered structures such as aircraft wings have potential vibration problems. In these structures, aerodynamic and/or structural loading can set up vibrations within the structure. Since the materials used in many of these applications (aluminum or titanium) have very low material damping loss factors, an excitation at resonance could lead to

potential failure from fatigue overloading caused by the growing amplitude of vibration. In reality, this is not a problem, not because of the material, but because of the structural configuration typically employed. In the above example, the wing is manufactured using thousands of mechanical fasteners. When the wing is set into vibration, each of these fasteners becomes a site of energy dissipation by virtue of the friction occurring there. The structural configuration therefore possesses adequate energy dissipation to prevent structural degradation from in-service loading.

Energy dissipation around fastener sites is also possible in composites as well. In practice, however, one advantage of composites lies in the ability to reduce the number of parts and thereby the number of fasteners. Because of this reduction, the damping of the composite material becomes more important in the overall damping of the structure.

There has been only a limited number of investigators who have been concerned with the vibration damping response of composites. Typically, their investigations have dealt with either the development of experimental procedures and subsequent determination of the quantitative values of the damping loss factor, or with the development of analytical models capable of determining the composite material loss factor.

The majority of composite structures that are under consideration are manufactured using thermoplastic or thermoset polymer matrices. These matrix systems are viscoelastic. This means that as the material is loaded, the strain and stress are not in phase; rather the strain lags the stress(1). A composite material that is manufactured with these viscoelastic materials will also exhibit this viscoelastic characteristic. In general, the composite's

vibration damping response will be a combined response of the matrix and fibers that are used.

Typically, the damping loss factor of the polymer matrix materials normally used in composites is temperature dependent with certain characteristic features. Figure 1 is a generic representation of the loss factor of a polymer as a function of temperature at constant frequency. In general, there are three peaks present. These peaks are denoted as the alpha, beta and gamma transitions. It has been proposed that different mechanisms are responsible for the high energy dissipation associated with each of these transitions. The low temperature or high frequency transition, also called the alpha transition, has been associated in the literature with chain segment mobility (2). The largest peak in loss factor, the beta transition, is associated with the glass transition temperature. It has been proposed that losses occur here from long range motions of the amorphous polymer chains or rotations that can occur with the material passing from the glassy to rubbery or liquid state (1,3). The third peak that has been detected at temperatures above the glass transition, the gamma peak, is associated with net translatory motions of the amorphous chains and decrease in elastic modulus of the polymer (4).

For a generic polymer system, the frequency dependence of the loss factor has an inverse correspondence to the temperature dependence. As discussed above, a polymer may exhibit either an increase or decrease in loss factor with increasing frequency depending on the specific characteristics of that polymer. When incorporated into a composite system with continuous fibers, this frequency dependence of the loss factor should also be present.

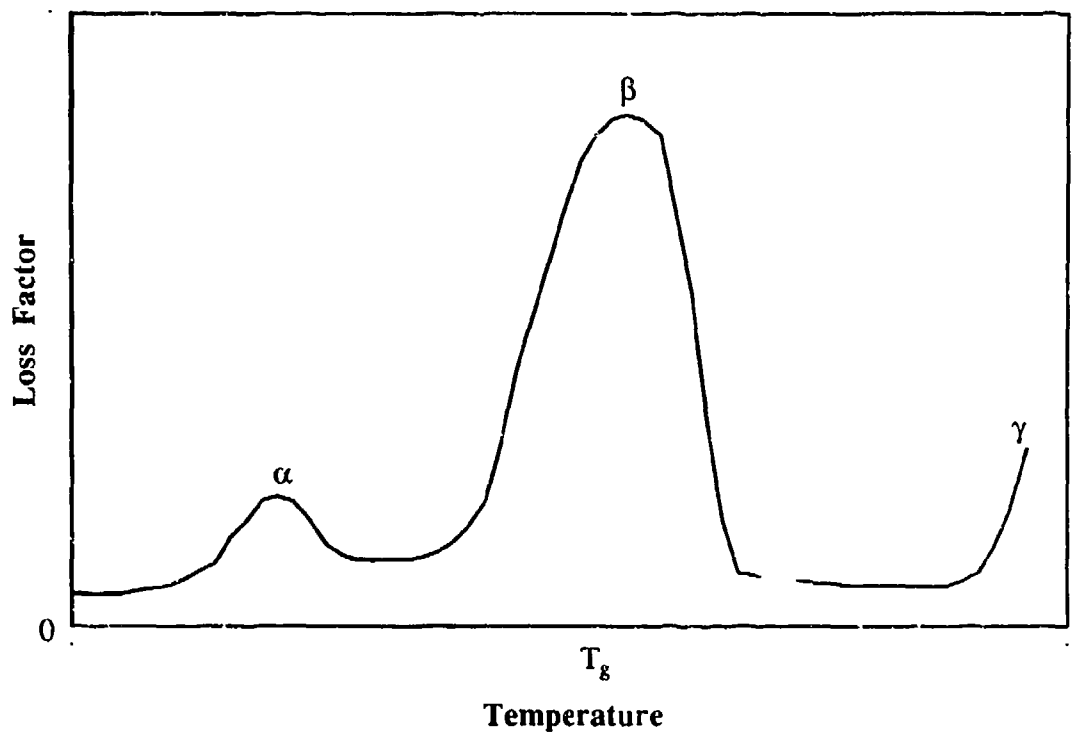

Figure 1: Schematic variation of loss factor with temperature for an amorphous polymer at constant frequency.

For a generic polymer system, the frequency dependence of the loss factor has an inverse correspondence to the temperature dependence. As discussed above, a polymer may exhibit either an increase or decrease in loss factor with increasing frequency depending on the specific characteristics of that polymer. When incorporated into a composite system with continuous fibers, this frequency dependence of the loss factor should also be present.

Previously, neither experimental nor analytical studies have taken this frequency dependence into account. Yet, the composite material loss factor needs to be determined as

a function of frequency to obtain an accurate characterization of the material. In addition, to determine the effects of various material characteristics on loss factor, it is necessary that comparisons be made at identical frequencies.

The purpose of this research is to develop a frequency dependent analytical model, based on material characteristics, that is capable of determining the material loss factors of a general laminated composite configuration. The material loss factor can then be used as input for structural analysis of composite components. To ensure that the material characteristics that have been shown to affect the loss factor are incorporated into the analytical model, a detailed literature survey was carried out. This survey will be presented in chronological order, detailing the experimental techniques used and the results obtained for the damping loss factor of composites, as well as proposed analytical models.

A macromechanical analytical model is presented that incorporates the relevant micromechanical effects of the material. An experimental apparatus is described as well. To ensure that environmental sources of energy dissipation are minimized, the apparatus is calibrated using a well characterized metallic material. A robust testing methodology is then proposed for use in the determination of the material loss factors. This testing methodology is then used to determine the material loss factors of AS4/3501-6 graphite/epoxy and S-2 Glass/3501-6 composites.

The loss factors of two generic S-2 glass/epoxy configurations are then determined using the analytical model. The results of this model are compared with the experimentally determined loss factors to assess the validity of the proposed model. In addition,

parametric studies are performed using the proposed model to determine the effect of fiber orientation and stress couplings on the loss factor of S-2 glass/epoxy composites.

Finally, topics for future work are proposed in an attempt to provide improvements to the experimental technique, to experimentally examine the effects of specific material characteristics on loss factor, and to provide a more universal analytical model for incorporation into structural analysis routines.

Chapter 1

RESEARCH OBJECTIVE

Organic matrix composite materials are viscoelastic because of their material constituents. This means that they have rate and temperature dependent properties. One property that has yet to be taken advantage of is their inherent vibration damping.

There are two plausible reasons that composite design does not incorporate considerations for damping. One is the lack of an analytical model that can be easily incorporated by the designer using existing structural analysis codes. The second reason is that there is a lack of experimental information available which can be used to either determine the frequency dependent loss factor or to verify proposed analytical models.

The purpose of this research is two fold. The first goal is to develop an analytical model which can account for the frequency dependent damping loss factor characteristic of organic matrix composites. This model should be capable of determining the various directional dependent loss factors that the material will possess. These directional dependent loss factors occur because of the directional dependence of the material properties of composites. The analytical model will attempt to incorporate the material characteristics which can affect the damping loss factor and will be formulated to provide information that the structural analyst can utilize in the design of high damping structurally

efficient composite components.

In addition to the development of an analytical model, the experimental determination of the damping loss factor will be undertaken. This experimental investigation will be used to verify the analytical model and to provide insight into the material characteristics which affect the vibration damping. This experimental effort will consider first and foremost the appropriateness of the technique. In the testing of materials for damping properties, the damping of the material as well as the damping provided by the test environment must be determined. To obtain an accurate characterization of the material loss factor, the developed experimental technique considers methodologies to minimize all sources of possible energy dissipation. To ensure that the technique minimizes external sources of energy dissipation, the system will be calibrated using a material which has a low damping loss factor and has a loss factor which can be analytically determined over an appropriate frequency range.

With this developed, calibrated experimental technique, the damping loss factor of two composite systems will be determined over a frequency range of interest for structural applications, up to 1000 Hz. The materials which will be tested are AS4/3501-6 graphite epoxy and S-2 Glass/3501-6 glass epoxy. These two systems are being investigated because of their present consideration for numerous structural applications. Determination of the loss factor as a function of frequency will provide information with which to verify the analytical model as well as specific information which can be used for structural damping designs.

Chapter 2

BACKGROUND

In order to assess the state of technology on the mechanical vibration damping of composites, a chronological historical review of the research published to date on the damping loss factor of composites will be given. This survey will be limited to continuous fiber organic matrix composite materials. This background is divided into two main sections: experimental results of the vibration damping of monolithic composites and the analytical models that have been developed to predict the vibration damping of these composites. The information presented is for test specimen geometries only, so that material characteristics that affect loss factor can be identified. The experimental values of loss factor and the techniques used are reported so that the material and procedural characteristics that affect the damping loss factor, such as specimen geometry and mode of excitation, can be identified. In addition, the results of the research performed by the various authors are compared to highlight inconsistencies in their results. These inconsistencies are considered in the design and development of a robust testing methodology.

Another configuration that has been intentionally omitted from this discussion is the constrained layer configuration. Several reviews have been written on this area. Interested readers are referred to references 5-7.

Continuous fiber organic matrix composites have been utilized for numerous structural applications because of their structural performance, the weight savings achievable and the reduction in life cycle costs they may allow. Composite structures also have the added advantage of corrosion resistance and design flexibility. An additional property possessed by the composite materials is their inherent vibration damping characteristics resulting from the numerous loss mechanisms within the material.

In general, the damping loss factor for metals is a function of frequency. A typical maximum value of the damping loss factor for 2024-T4 aluminum is approximately 22×10^{-4} [Crandall (8)], mild steel has a maximum loss factor of approximately 17×10^{-4} [Friend and coworkers (9)], and brass has a maximum loss factor of approximately 8×10^{-4} [Macander and Crane (5)]. Composite materials, by comparison, have shown damping loss factors as high as 325×10^{-4} for a standard GY-70/934 unidirectional composite oriented in the 90 degree direction [Haines (10)]. In the 0 degree direction, the loss factor for a general graphite/epoxy composite is approximately 30×10^{-4} [Suarez and Gibson(11)]. These examples of composite loss factor show that composite materials offer the possibility of an order of magnitude increase in damping over conventional structural metallic systems.

The literature was searched using the following search data bases: DIALOG, NTIS data base; DIALOG, Aerospace data base; DIALOG, METADEX data base; DIALOG, ISMEC Mechanical engineering data base; DIALOG, SCI data base; and DTIC (Defense Technical Information Center). In addition to these data bases, independent searches through the Journal of Composite Materials, Composites, ASTM Conference Proceedings, SESA Conference Proceedings, AIAA Conference Proceedings, and other composite

related publications were carried out to identify articles on composite vibration damping. This latter independent search was to ensure that important publications not in the above mentioned data bases were not overlooked.

Review of Terminology

Dynamic mechanical vibration damping is defined as any process that transforms the energy of a mechanical vibration into some other form of energy which is irrecoverable. From an energy standpoint, then, the mechanical vibration damping is the ratio of the change in stored energy of the system, ΔW, to the maximum stored energy during a cycle, W. The change in stored energy per cycle is therefore the energy loss per cycle. This value has then been defined using other terminologies such as the specific damping capacity, ψ, the damping loss factor, η, the dynamic amplification factor, Q, and the logarithmic decrement, δ. The relation between these various values is given as follows;

$$\frac{\Delta W}{W} = \psi = 2\pi\eta = \frac{2\pi}{Q} = 2\delta \qquad (1)$$

In this disssertation, the damping values are reported in units of damping loss factor, η. From the relations given in equation 1, then, if all of the energy is dissipated in one cycle, the value of η will be 0.159. A material loss factor of 0.1 for a structural applications is in general very desirable.

Experimental Testing of Laminated Composites

There has been a proliferation of work on the mechanical vibration damping of laminated composite materials. The composite material that has been investigated most often for its vibration damping response is graphite/epoxy. This material has been utilized in fatigue critical applications. As such, if a graphite/epoxy structure is set into undamped resonant vibration, fatigue degradation is possible, which can severely reduce the service life of the structure.

Because of this fatigue problem, it is not surprising that the earliest research on the problem of damping was conducted by the Air Force. Kurtze and Mechel (12) investigated the use of various materials that could be utilized as a core material for sandwich structures. Instead of considering single composite systems, various hybrid combinations of systems were investigated in order to possibly maximize the damping over a wide range of frequencies. The core material used included glass fiber and asbestos embedded in various fluorine-containing polymers and viscoelastic materials. In this work, they investigated, among other things, the effect of fabricating a structure with a stratified arrangement of different materials. Each material had a different frequency and temperature at which the maximum damping loss factor occurred. They assumed that it might be possible in this type of arrangement to achieve a structure having the additive qualities of the various subsystems, and that this would result in a structure with high damping characteristics over a large temperature and frequency range. Their testing, however, showed that, in the stratified arrangement, achieving these additive qualities of the various subsystem materials was not possible. The reason is that when a material having a high shear loss factor at a

correspondingly higher temperature is covered by a material which has a lower shear loss factor and shear modulus, the first material cannot experience a full shear deformation. The reason is that the majority of the shear motion occurs in the softer layer. If the shear properties of the various materials are nearly equal at the various temperatures, and these materials have maximum loss factors at various frequencies, then it may be possible for an additive type vibration damping effect to result. In most cases, however, the shear moduli of these different materials are very different, thereby nullifying the additive effect.

Kurtze and Mechel (12) then investigated the properties that would result if the materials with various loss factors at various frequencies and temperatures were arranged in a parallel strip arrangement. Using the same material as in the first study, they achieved a partial additive effect in the damping characteristics of the parallel strip sandwich structure. However, no quantitative data are presented concerning the results of the parallel arrangement of the materials.

Schultz and Tsai (13) investigated the damping ratios of unidirectional glass fiber reinforced composite beams. These beams were tested in free and forced vibration in a cantilever beam configuration. The E-glass beams were 0.005 in.(0.127 mm) thick and had widths of 0.75 or 1.0 in.(19.0 or 25.4 mm). These beams had a total length of 13.5 in. (343 mm). The specimens were tested by securing them midway along their length via two hardened steel cylinders which were in turn attached to the moving element of an electromagnetic vibration exciter. These beams were excited via a sine wave mode into their various natural frequencies. The excitation amplitude of oscillation was monitored by an accelerometer while the response was monitored by a foil strain gage mounted on the top

of the specimen near the clamped end. The excitation and response signals were observed on an oscilloscope. The resonant frequencies were determined by observing the peaking of the response on the oscilloscope trace while varying the input excitation frequency, keeping a constant excitation amplitude. For the low frequencies of vibration, the free vibration decay measurements were used to determine the damping loss factor. In this method, the beam is excited into its resonant vibration, the power to the exciter is cut, and the response amplitude decay is measured on an oscilloscope trace. The decay response is measured over 10 and 50 cycles. The loss factor is then determined using the following equation

$$\eta = \frac{\ln\left[\frac{a_n}{a_0}\right]}{n} \tag{2}$$

where a_0 is the amplitude of the forced resonant vibration when the excitation is removed, a_n is the amplitude of the vibration at the n^{th} cycle after the power is cut to the exciter and n is the cycle at which the amplitude a_n is measured. The damping loss factor for higher mode excitation was determined using the half power band width method [Newland (14)]. In this method, the width of response at -3dB of the peak of the resonant frequency, f_n, is determined. The ratio of this value to the resonant frequency, f_n, is the damping loss factor for the material at a particular frequency. The loss factor is therefore given by

$$\eta = \frac{\Delta f_n}{f_n} \tag{3}$$

The frequency and the band width necessary for determining the damping loss factor were determined by direct measurements on the oscilloscope trace.

These methods had the disadvantage that they required a visual interpretation of either the decay of the amplitude of oscillation, since this decay was read directly from the oscilloscope trace, or the band width at -3dB of the resonance peak. Also, the actual determination of the decay was a time-consuming process. In addition, direct comparisons with other samples were difficult since the only hard copy of the data was from the photographs of the oscilloscope traces.

Four angle-ply orientations were tested. These included 0, 22.5, 45, and 90 degree specimens. Results showed that the materials could be ranked in decreasing order of damping as follows: 45 > 90 > 22.5 > 0. In all cases, the damping tended to increase with increasing frequency.

In this investigation, the effect of environmental sources of energy dissipation appears to have been neglected, such as aerodynamic damping and the effect of the clamping on the specimen. Because of this, the magnitudes of the loss factor are in question.

Adams and coworkers (15) investigated the damping of unidirectional carbon and glass polyester reinforced composites. The purpose of the work was to determine if the damping capacity of the composite could be predicted from knowledge of the fiber content, the matrix, and the macroscopic stress system, and the effect, if any, of the fiber-matrix interface. The damping values reported in the paper are in units of damping capacity, ψ. The relationship between the damping capacity and the damping loss factor, η , was previously given in equation 1.

The carbon fiber used in this investigation had a tensile modulus of 55 x 10^6 psi (379 GPa) and a tensile strength of 250 ksi (1.72 GPa). The glass fiber was an E-glass with typical tensile modulus and strength of 10.5 x10^6 psi (72.4 GPa) and 500 ksi (3.45 GPa). The specimens were tested in both torsion, to measure the specific damping capacity of the forced vibration, and in flexure, to measure the damping capacity in the free mode oscillation. The latter technique had the specimen supported at its node points by knife edges. This is the only investigation presented herein which tested the composite using knife edge supports. The experimental procedure that is currently used suspends the beam specimens from two of its node points by strings. The fiber volume fraction of the glass specimens investigated by Adams and coworkers (15) was varied from 0 to 70%. The fiber volume fraction of the graphite composite specimens was varied from 0 to 50%.

In the torsion testing, the authors reported that the damping loss factor of the carbon fiber composite was dependent on the stress amplitude. This dependence was attributed to the development of internal damage in the material which led to the increased damping as the stress amplitude was increased. In the glass system, however, the damping loss factor was independent of the stress amplitude. Both fiber systems showed a decrease in the damping loss factor by approximately a factor of two as the fiber volume fraction of the systems was increased (Figure 2). This decrease can be attributed to the fact that the resin makes a strong contribution to the damping capacity of the material, whereas the fibers' contribution is substantially less.

In the flexural testing, the damping loss factor showed a decrease as the fiber volume fraction was increased, similar to the decrease seen in the torsion testing (see Figure 3). It

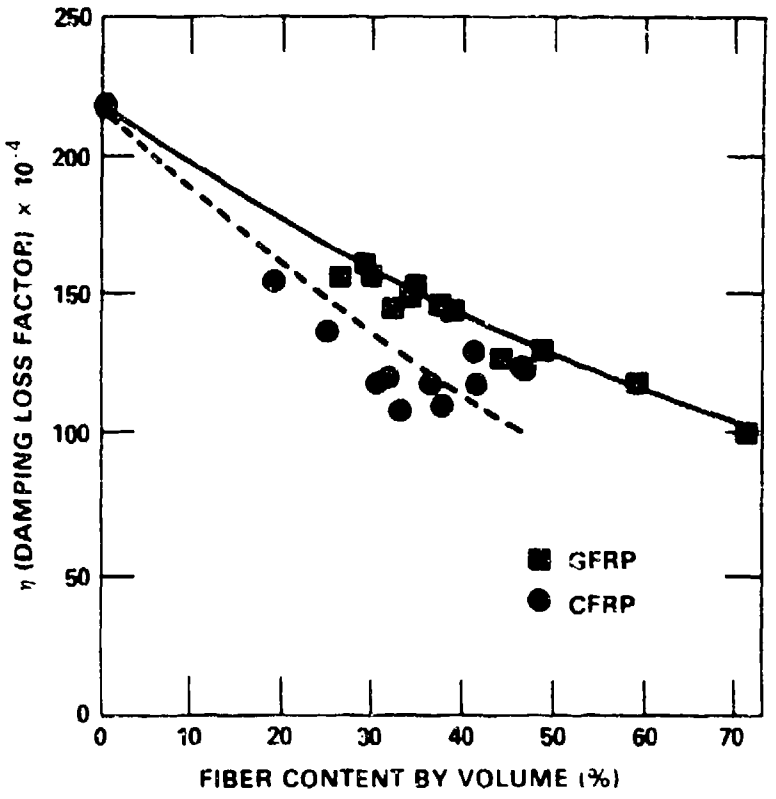

Figure 2 Comparison for the damping loss factor for graphite/epoxy (CFRP) and glass/epoxy (GFRP) unidirectional composite materials as a function of fiber volume fraction at constant maximum shear stress of 200 lbf/in^2 (1.4 MPa) tested in torsion (after Adams and coworkers (15)).

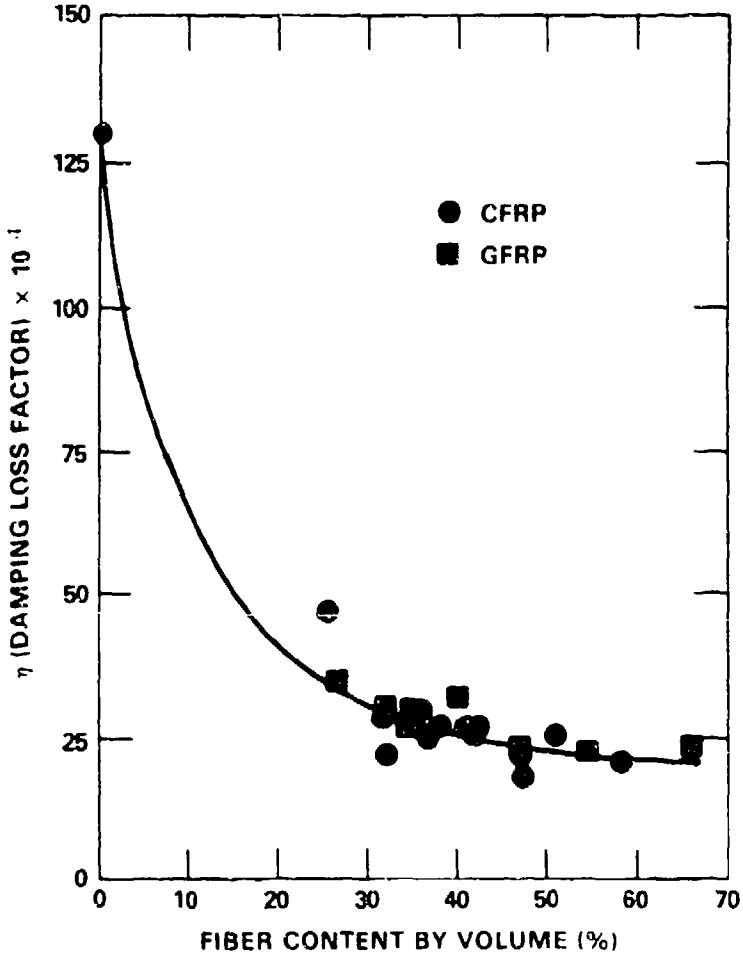

Figure 3 Variation of the damping loss factor for graphite/epoxy (CFRP) and glass/epoxy (GFRP) unidirectional composite materials as a function of fiber volume fraction tested in flexure (after Adams and coworkers (15)).

was shown that the stress amplitude had a mild effect on the damping loss factor, with the carbon fiber experiencing a slight increase similar to the increase seen in the torsion testing. In the glass fiber composite, a slight decrease occurred as the stress amplitude was increased, unlike the effect that was seen in the torsion testing. The damping loss factor of the two systems experienced nearly identical degradations as a function of the fiber volume fraction, reaching an asymptotic value of damping loss factor of 16×10^{-4} at a fiber volume fraction of approximately 60%. This result - that the damping loss factor of the glass/epoxy decreased as the amplitude of vibration increased - is contrary to what was expected, since aerodynamic damping should provide a contribution to the material damping; no explanation of its cause was given. In the torsion testing, the damping loss factor showed a linear decrease with increasing fiber content, whereas the damping loss factor for the flexural testing showed a rapid dropoff with increasing fiber content.

Adams and coworkers (15) identified the possible sources for the energy dissipation as the fibers, the resin, the fiber-resin interface, and cracks in the material. All of these variables, with the exception of the cracks, can be modified to fit the specific needs of an application. The factors having the largest contribution to the damping loss factor are the resin and the fiber-resin interface, both of which can be readily varied.

Another variable that was not considered in this investigation was the effect of frequency on loss factor. As the material is made stiffer, the resonant frequency is increased when identical specimen geometries are utilized. The frequency dependence of the matrix material loss factor is unknown, although it can be assumed that a frequency dependence exists. The effect of fiber volume fraction on loss factor given in this

investigation cannot be explicitly extracted.

Clary (16) investigated the effect of fiber angle and panel thickness on the damping of boron epoxy composite panels. In all cases, the panel configuration was that of an angle ply, $\pm\theta$. The fiber angles investigated were 0,10,30,45,60,and 90. Panel thicknesses were 0.033, 0.060, and 0.111 in. (0.84, 1.53 and 2.82 mm) corresponding to 6, 12 and 24 ply laminates. Typical fiber volume fraction was between 48 and 50%.

The specimens were tested by suspending them from two node points which were experimentally determined for each frequency of vibration used. The panels were set into resonant vibration via an electromechanical shaker with the peak amplitude determined by an accelerometer attached to the specimen. After steady state vibration was achieved, the power to the shaker was cut and the decay in the vibration amplitude determined. Polar plots of the form of magnitude and phase of the input acceleration normalized to the input force were obtained. The damping loss factor was obtained from these plots.

The results of the testing indicated that the damping loss factor was inversely proportional to the number of layers of the composite. As the number of layers increased, it was shown that the fiber angle at which the maximum damping loss factor occurred decreased from 60 degrees for the 6 ply laminates to 30 degrees for the 24 ply laminates. The damping loss factor of the composite panel showed only a moderate increase over that of aluminum. The maximum damping loss factor of the boron/epoxy specimens tested was 62×10^{-4}. This value is high compared with some of the other composite samples that will be discussed later.

It should be noted that as the thickness of the material is increased, the effective beam stiffness is also increased. This results in an increase in the resonant frequency of the beam. As such, the effect of thickness on the beam loss factor determined by Clary (16) is in actuality a combined thickness/frequency effect.

The investigation by Clary (16) complements the earlier experimental investigation on the effect of fiber orientation on the damping loss factor performed by Schultz and Tsai (13) who determined the damping loss factors at only one thickness. The results from these two experimental programs show the complexity involved when one must design a composite structure to maximize damping. In one case, one could first specify the fiber angle so as to maximize damping. This would then dictate the thickness of the composite necessary to meet the design loadings. However, from the results of Clary (16), it is seen that increasing the thickness of the composite has the effect of reducing the material damping loss factor, as a result of either the thickness itself or the variation in the resultant resonant frequency of the structure. This means that the damping provided by the specific fiber orientation may be partially negated by the added thickness. Another fiber angle which has a lower damping loss factor may require a structural thickness less than the first design, which may actually result in a structure with increased damping. Therefore, the design to maximize the damping of a structure will obviously be an iterative process on both fiber orientation and thickness.

In addition to the frequency effect, one other factor was not taken into consideration for the material tested. For the off-axis materials tested by Clary (16), a bending twisting coupling occurs when the specimen is placed in bending because the material is

unbalanced. The twisting that is occurring may alter the damping through additional energy dissipation. The magnitude of the twisting effect is reduced as the material thickness is increased. This would result in a decrease in the contribution to the specimen damping loss factor due to the reduction in twisting as the material is made thicker.

In another experimental study, Schultz and Tsai (17) investigated the effect of panel stiffness and frequency of test on the damping loss factor of glass fiber reinforced laminates. To determine the effect of stiffness on damping, they experimentally determined the storage and loss moduli of quasi-isotropic E-glass panels. Two panel configurations were used, $(0/60/-60)_S$ and $(0/90/45/-45)_S$. The experimental procedure utilized the free vibration decay of a sinusoidally excited double cantilever beam specimen that was excited to its natural frequencies up to the tenth mode. The damping loss factor was determined using the half power band width method, equation 3. The same test apparatus was used as one described previously [Schultz and Tsai (13)].

To verify that their results were a function of the material and not of the test procedure, Schultz and Tsai (17) performed additional tests on the specimens. First, the test apparatus was placed in a vacuum chamber evacuated to a pressure of 10^{-2} torr. Second, they varied the clamping pressure of the specimens in the test fixture. Neither of these two experimental setups changed values of the loss factor obtained in the routine procedure described previously.

The results of the testing indicated that the static modulus was between 0 and 20% lower than the dynamic modulus. There was also an increase in modulus with increasing

frequency. The relation between the resonant frequency and the modulus is given by the following equation:

$$F_n = \frac{(B_n L)^2}{2\pi [Ebh^3/ 12 \mu L^4]^{.5}} \quad (4)$$

where F_n is the n^{th} mode resonant frequency; B_n is the corresponding eigenvalue of the frequency equation governing the motion of a uniform cantilever beam; E is the effective storage modulus; μ is the mass per unit length; and b, h and L are the beam width, thickness and length, respectively.

As part of their experimental program, Schultz and Tsai(17) determined the dynamic properties of the material, i.e. E_1, E_2, G_{12}, and ν_{12} . Their results showed that the analytically determined static and dynamic moduli were predictable with the knowledge of the ply properties for the two configurations used in this study. The static and dynamic moduli of the material were then used to predict the complex moduli of various laminate configurations using standard transformation procedures. The damping loss factor was then analytically determined from the predicted complex moduli of the laminate using the following equation:

$$\eta_{11} = \frac{e_{11}}{E_{11}} \quad (5)$$

where e'_{11} is the imaginary part of the complex modulus and E'_{11} is the real part of the complex modulus of the particular laminate configuration in the primary loading direction. Predicted properties of the unidirectional laminate were in good agreement with properties

determined experimentally. The experimentally determined damping loss factor for the quasi-isotropic laminates was as much as 55% higher than that predicted analytically. Plotting their results of the damping loss factor versus the direction of the outer ply fibers to the flexural loading direction, Schultz and Tsai (17) obtained an asymmetric curve about 0 degrees. This asymmetry was present for both of the laminates tested. This result is expected, since the stiffness of the beams tested with the outer fibers oriented at different angles to the longitudinal axis of the beam have inner plies which have different orientations. For example, if the $(0/\pm 60)_s$ quasi-isotropic beam is rotated 30 degrees, the beam effectively becomes $(30/90/-30)_s$, whereas when the beam is rotated by -30 degrees it effectively becomes $(-30/30/90)_s$, an obviously stiffer configuration in flexure. In addition, the analytical predictions also showed this asymmetry.

Another factor not noted explicitly in the curves which presented the loss factor as a function of fiber orientation was this: the frequency at which the results were plotted was not the same for each fiber orientation tested. In the same paper, however, Schultz and Tsai (14) experimentally showed that there is a frequency dependence on the loss factor, as will be discussed below. The results that were actually reported did not indicate the fiber angle dependence of loss factor, but instead a combination of the effect of fiber angle and frequency on the loss factor.

In their investigation on the effect of frequency, Schultz and Tsai (17) again used the quasi-isotropic E-glass laminates. They varied the outer fiber orientation, thereby varying the flexural stiffness of the material. For both laminates, the loss factor was determined with outer ply angles of 0, 45 and 90. As the frequency was increased from the first

resonance, the damping decreased to a frequency of approximately 800 Hz. As the frequency was increased from this level, the damping loss factor increased with frequency up to the highest frequency of test, approximately 10000 Hz. The maximum damping loss factor was obtained from the $(0/60/-60)_s$ laminate tested in the 90 degree direction, having a value of approximately 151×10^{-4}. The minimum value of the damping loss factor was for the $(0/60/-60)_s$ panel tested with the outer fibers in the 0 degree direction, having a value of approximately 25×10^{-4}.

Friend and coworkers(9) described some of the general test methodologies and commented about the vibration damping characteristics of composites. They reported that five methods are used for testing these materials to determine the mechanical vibration damping characteristics of the material. Two of these are more prevalent than the others. The first method utilizes a forced vibration at the resonant frequency. The damping loss factor is calculated from the curve of amplitude versus frequency by dividing the bandwidth at the half power points for the resonance of the n^{th} mode, Δf_n, by the response frequency of the n^{th} mode, f_n, as given by equation 3. The second method involves striking the material and measuring the free decay in the amplitude of the vibration. The damping loss factor is then determined as the ratio of the successive amplitudes of vibration of the specimen as given previously by equation 2.

Friend and coworkers (9) indicated that the damping of the material is a function of many variables, including the thermal conductivity, modulus, void content, and fiber to resin bond effectiveness, among others. They summarized the vibration damping of various metallic and composite systems. This information is shown in Table 1. Here it can

be seen that the damping loss factor is a function of angle for the composite systems. The 90 degree orientation has the highest damping, the 0 degree orientation the lowest. These results are contrary to those presented by Schultz and Tsai (17), where the 45 degree off-axis specimen had the highest damping. This table also shows that the damping loss factors for composite systems have values typically an order of magnitude or greater than those of the metallic systems, indicating the inherent damping characteristics of the material.

Table 1: Comparison of Damping Loss Factors of Various Materials Systems (after Friend, Poesch, and Leslie(9))

Material	Orientation	Frequency (Hz)	Damping Loss Factor ($\times 10^{-4}$)	Modulus $\times 10^{-6}$psi (GPa)
2024 Al		3000	9.0	10 (69.0
6061 Al		4000	55.0	10 (69.0)
Mild Steel		4000	17.0	28 (193.1)
1020 Steel		6900	38.0	29 (200.0)
Scotch ply 1002 E glass/epoxy	0	4200	70.0	5.1 (35.2)
		9100	90.0	5.1 (35.2)
SP-272 Boron/Epoxy	0	4000	67.0	26.8 (184.8)
	0/90	4400	57.0	18.3 (126.3)
	90	4200	330.0	3.2 (21.2)
2002M Graphite/Epoxy	0	4000	157.0	27.4 (188.9)
	22.5	4000	164.0	4.7 (32.4)
	45	3800	186.0	1.8 (12.4)
	90	4000	319.0	1.0 (6.8)
	(0/22.5/45/90)	4000	201.0	10.0 (69.0)

Adams and Short (18) investigated the effect of fiber diameter on the vibration damping of glass/polyester composites. They fabricated beams using glass fibers having diameters of 10, 20, 30, and 50 μm. As the fiber diameter is decreased, the ratio of the surface area to volume increases. Thus, for a given fiber volume fraction of the laminate, the contribution to the damping from the interfacial bond between the resin and the fiber increases. This increase is not only the result of the increase in the bond area but is also attributed by Adams and Short (18) to the increase in the stress concentration in the matrix as the fiber diameter is decreased. This increased stress concentration results in an increase in the strain energy per unit volume of the matrix. As the fiber volume fraction was decreased from 70% to 35%, the sensitivity of the loss factor to the surface to volume ratio of the fibers was greater, which gives credence to the hypothesis that there is an additional effect on the loss factor besides the increase in the surface to volume ratio. Adams' and Short's (18) test results, shown in Figure 4, indicate that the damping loss factor of the beam increased as the fiber diameter was decreased. This shows that the fiber/matrix interface can be a major damping mechanism in composite materials, not only due to the bond itself but also to the stress concentrations that occur. In addition, the viscoelastic character of the interphase region around the fiber may be providing an additive effect on the damping for the smaller diameter fibers. Although the fiber diameter affected the damping loss factor, it should be mentioned that the fiber diameter did not affect the storage modulus of the material.

Adams and Bacon (19) studied the effect of fiber orientation and laminate geometry on the damping properties of graphite/epoxy composites as measured in flexural and torsion tests. For the flexural tests, the material was in the form of beams. These were clamped in the center with cylindrical steel clamps, which were subsequently attached to

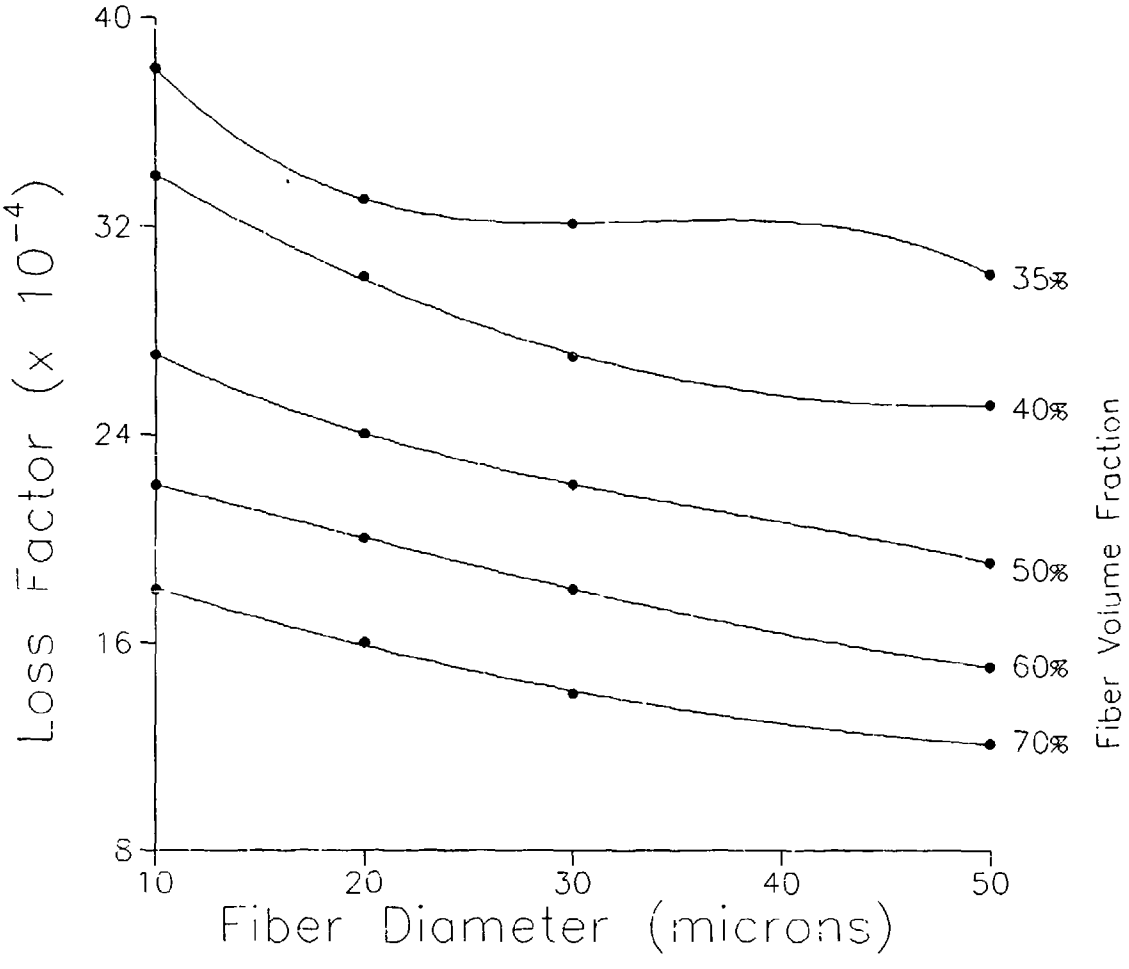

Figure 4 Effect of fiber diameter on the damping loss factor at varying fiber volume fractions for E-glass fi[illegible] (after Adams and Short (18)).

electromagnetic coils. These coils provided the necessary mechanical vibration. The system was set to the resonance of the beam and then stopped. The beam was then set into free vibration and the resulting decay in amplitude of oscillation measured. These authors' results of the testing of 0 degree graphite/epoxy revealed that, since there was only minimal damping, aerodynamic damping played a significant role in the measured values of the damping loss factors for the beam. Because of this, Adams and Bacon (19) tested their remaining beams in a vacuum. They also suggested that, since aerodynamic damping can significantly contribute to the apparent damping provided by the material, other investigators who did not consider this additional contribution may have spurious results. The specimens used in this investigation were approximately 0.5 x 0.1 x 9.0 in. (12.7 x 2.5 x 229 mm). Adams and Bacon (19) made theoretical predictions for the damping loss factor of the material, based on the strain energy of the material associated with the stresses in the specimen geometry directions. Their predictions of the material's strain energy dissipation are dependent on the compliance coefficients and the stresses induced in the material. Their theory indicates that the damping is a nonlinear function of stress, thereby having no closed form solution and requiring numerical evaluation.

In the flexural mode, Adams and Bacon (19) found a strong dependence of the damping loss factor on the laminate orientation. They found a peak in the damping loss factor at +35 degrees for the off-axis specimen tested in vacuum. This is a result of a large energy dissipation in shear. The damping-associated stresses in the fiber direction become negligible when fiber angles are greater than 10 degrees. In the case of angle-ply laminates, a maximum in the specific damping factor was found to be approximately 45 degrees. Graphs of the two results are shown in Figures 5 and 6. In all cases, the experimental values are greater than the theoretical values, although they follow the trends

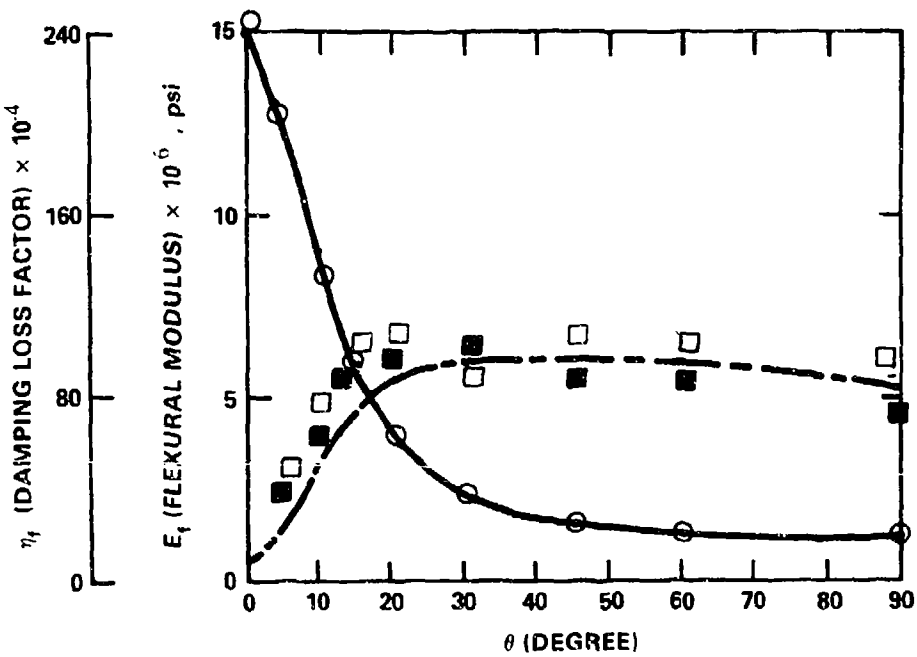

Figure 5 Variation of flexural modulus, E_f, and damping loss factor, η_f, of unidirectional high tensile strength graphite fibers embedded in DX210 epoxy resin with fiber volume fraction of 50%, as a function of angle that the fibers make with the longitudinal axis of the beam tested in flexure with a maximum bending moment of 2 lbf-in. (0.226 N-m); ○ E_f, □ η_f, 1.0 in. (25.4 mm) wide specimen, • E_f, ■ η_f 0.5 in (12.7 mm) wide specimen. Prediction for free flexure —— E_{ff}, — · — · — η_{ff} (after Adams and Bacon (19)).

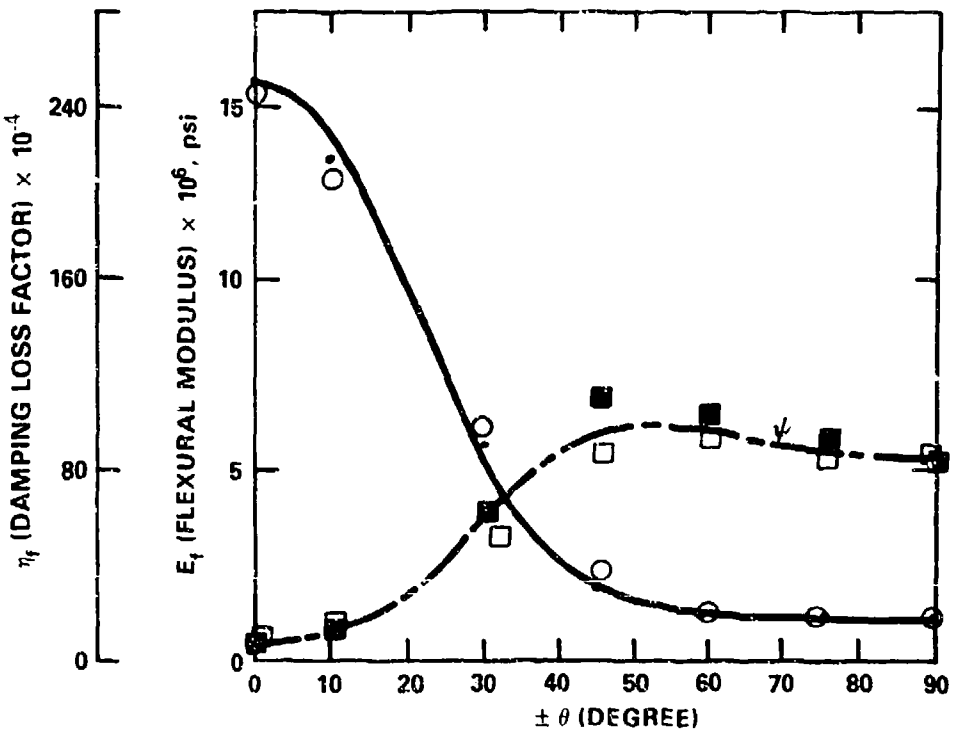

Figure 6 Variation of flexural modulus, E_f, and damping loss factor, η_f, of cross-ply, $\pm\theta$, high tensile strength graphite fibers embedded in DX210 epoxy resin with fiber volume fraction of 50%, as a function of angle that the fibers make with the longitudinal axis of the beam tested in flexure with a maximum bending moment of 1 lbf-in. (0.113 N-m); ○ E_f, ❑ η_f, 1.0 in. (25.4 mm) wide specimen, • E_f, ■ η_f 0.5 in (12.7 mm) wide specimen. Prediction for free flexure —— E_{ff}, —·— η_{ff} (after Adams and Bacon (19)).

quite closely.

When an off-axis material configuration is subjected to bending, the material also experiences a twist, since the material is unbalanced. The magnitude of the twist varies with fiber orientation, monitonically increasing from 0°, reaching a maximum at a fiber orientation of approximately 30°. For an angle-ply laminate, there is no bending-twisting coupling. The variation in the fiber orientation at which the loss factor reaches a maximum for the off-axis and angle-ply laminates would therefore be expected to be different.

Another point not indicated specifically in the figures, but evident in additional test results, is that the damping was amplitude dependent. Since the specimens were tested in a vacuum, aerodynamic damping, which has been previously shown to contribute significantly to the damping of a material, should not have arisen. However, this increase in damping with increasing amplitude of vibration could have arisen due to the increase in stress discontinuity at the clamped section of the beam or from the frictional losses at the clamped region. In both cases, the energy dissipation would have probably been in the form of localized heating of the specimen or from viscoelastic effects in the resin at these higher stress levels.

When cross-ply laminates were tested, it was found that the orientation of the outer plies had a pronounced effect on the damping of the laminate. As the beam stiffness was increased, the damping loss factor of the material decreased. The damping loss factor values that were obtained ranged from 13×10^{-4} for the beam with a stiffness of 14×10^{6} psi (96.5 GPa) to a minimal value of 10×10^{-4} for a beam with a stiffness of approximately

25×10^6 psi (172.4 GPa). Since the damping loss factor is so low for the cross-ply arrangement, it would not be a satisfactory material for structural damping in flexure. In addition to varying the beam stiffness in their tests, by using beams with identical dimensions Adams and Bacon(19) also changed the resonant frequency at which the loss factors were calculated.

In one of the specimens tested, Adams and Bacon (19) obtained a damping loss factor that was approximately six times higher than what they predicted theoretically. Upon examining the specimen, they found that it contained an interlaminar crack running approximately 1 in. (25.4 mm) along its length. This shows that the damping of the composite material is very dependent on the quality of the test specimen. Whereas the structure should be as free of defects as possible to maximize the mechanical properties, imperfections present in the material will enhance the damping.

For investigations on the material loss factor, then, it is therefore imperative that the quality of the material be determined; this will ensure that the losses determined are due to the material and not imperfections in the material. The energy dissipation which can occur in composites having internal defects results from dissipation of heat from the friction occurring at the imperfection sites. The heat generated at these material imperfections, such as cracks in the fibers and matrix and delaminations, can be readily detected at the surface of the composite. This characteristic has led to the development of a nondestructive evaluation technique called thermography(20,21,22) which assesses the material quality by monitoring thermal patterns on the surface of the specimen which has been either passively heated or actively heated by vibration. These defects are beneficial in that they enhance the

mechanical vibration damping, but are obviously deleterious in that they reduce the mechanical properties of the structure. Parker (23) reported that the heat generated will adversely affect the properties of the composites due to the possible degradation of the matrix when nonconductive fibers such as glass are used, but may not be a problem if conductive fibers such as graphite are used.

Adams and coworkers (24) experimentally determined the damping loss factor of various composite systems in angle-ply, off-axis and quasi-isotropic configurations. They attributed the vibration damping achieved in composites to the interfacial damping present by virtue of the laminated structure of the material. They reported that vibration damping limits the amplitude of the resonant vibration and, therefore, limits the radiated noise and onset of fatigue degradation. The materials used in their investigation were graphite and glass fibers embedded in an epoxy matrix. The specimens tested were beams which were clamped at their centers and vibrated using a coil/magnet pair at the material's resonant frequencies in a free-free flexural mode. The results obtained on the effect of vibration amplitude on the damping indicated that increasing the stress level from very low levels to 10% of the failure load did not affect the resultant damping. This is contrary to the results shown earlier by Adams and Bacon (19), who found that the damping loss factor increased with increasing cyclic bending moment. It should also be noted that Adams and coworkers (24) did not explicitly state that the tests were conducted in vacuum. If the specimens were tested in air, then the nondependence of loss factor on the amplitude of vibration would be contrary to the earlier work of Adams and Bacon (19).

Adams and coworkers (24) investigated the effect of specimen dimensions on the

damping loss factor of the graphite/epoxy specimens. The aspect ratio of the beams, l/h, was varied from 90 to 53. It was experimentally shown that as the aspect ratio was decreased in the range indicated above, the damping loss factor increased by approximately 25%. Adams and coworkers (24) attributed the increase in loss factor to the increase in the shear damping contribution to the damping of the beam in flexure. They theoretically indicate that the damping in longitudinal shear is of the order of 50 to 100 times larger than the tension or compression component. They also indicate that although the amount of energy stored in shear is small, the large damping that is attributable to the shear component can substantially contribute to the total predicted value of the damping loss factor in flexure. Another factor that changed as the aspect ratio was varied was the natural frequency of vibration. As the aspect ratio increased, the frequency should have decreased. The direct effect of aspect ratio on the damping loss factor was therefore not measured explicitly in the above tests.

For the angle ply specimens, Adams and coworkers (24) showed a maximum in the damping loss factor occurring at approximately 45 degrees with a value of approximately 146×10^{-4} and decreasing slightly as the angle is increased to 90 degrees to a value of approximately 108×10^{-4}. It was also mentioned that the off-axis specimen had a maximum in its damping loss factor at an angle of 35 degrees, which is probably the result of the stress couplings as was previously discussed. The final configuration tested was a $(0/-60/60)_s$ quasi-isotropic laminate. Testing revealed a nonsymmetric relation of damping capacity vs. angle as measured from the 0 degree direction, which is similar to the earlier findings of Schultz and Tsai (17). The minus angle side had a peak in the damping loss factor at 45 degrees with a value of approximately 108×10^{-4}, whereas the plus angle side had its peak in the damping loss factor at 90 degrees with a value of approximately 93×10^{4}

(see Figure 7). Also given in Figure 6 is the flexural modulus as a function of outer ply orientation. It can be seen that the flexural modulus, like the damping loss factor, is nonsymmetric about the 0 degree orientation.

Figure 7 shows that the loss factor varies inversely with the flexural stiffness. In general, as the stiffness of the material is increased, the loss factor is decreased. However, this direct observation is still obscured by the fact that the frequency of test for the various orientations must have been different since the natural frequencies of the material vary with stiffness also.

Paxson (25) investigated the damping capacity of boron fiber reinforced epoxy. He used the double cantilever beam configuration previously described. In addition, he had epoxy shoulders molded onto the upper and lower surfaces of the specimen at the center of the beam where it was to be clamped. This alleviated any stress concentrations that may have arisen if the specimen was clamped directly. The specimen was tested in a vacuum chamber. The experimental apparatus was also tested for additional energy losses by testing an aluminum beam and comparing the results with the well established thermoelastic model developed for determining the damping in metals developed by Zener (26). The specimen was excited in a sine wave mode with a frequency centered near the first resonant frequency of the beam via an electromagnetic shaker attached to the epoxy shoulders. The specimen was also dynamically balanced to ensure that each beam had equivalent vibration characteristics of the same maximum amplitude at the same frequency. Paxson (25) used an optical displacement follower to measure the tip deflections during the testing. The damping loss factor was determined using the half power band width method.

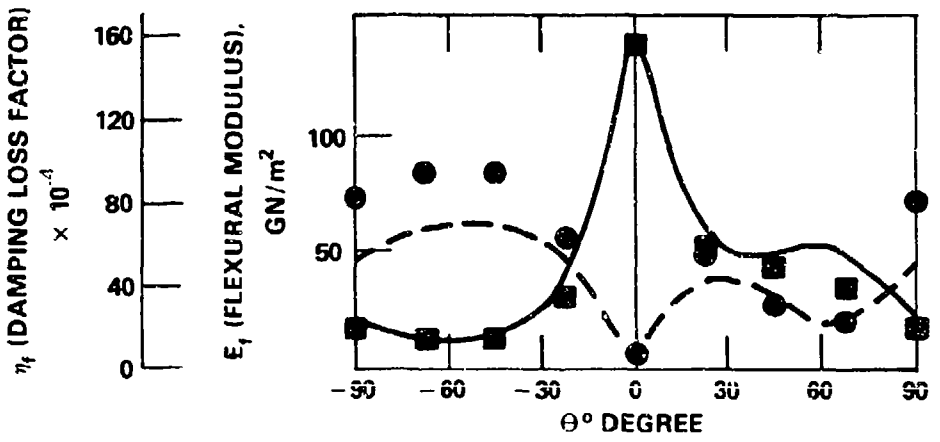

Figure 7 Variation of flexural modulus, E_f, and damping loss factor, η_f, of a $(0/-60/60)_{2s}$ laminate consisting of high modulus graphite fibers embedded in DX209 epoxy resin with fiber volume fraction of 50%, as a function of angle that the outer ply fibers make with the longitudinal axis of the beam tested in flexure, ■ E_f, • η_f 0.5 in (12.7 mm) wide specimen. Prediction for free flexure — E_{ff} — · — η_{ff} (after Adams and coworkers (24)).

Paxson's (25) results indicated that the $(45/-45)_{4s}$ specimen had the maximum damping factor; the 90 degree specimen had values slightly lower, and the 0 degree specimen had values approximately an order of magnitude lower than the former two. These results, given in Table 2, show the same angular dependence demonstrated by Adams and coworkers (24) for the graphite/epoxy composite beams.

Table 2: Effect of Fiber Orientation on the Damping Loss Factor of Boron Fiber Reinforced Epoxy Composites in the Forced Vibration Mode(after Paxson (25)).

Fiber Orientation (degrees)	Thickness mm (in)	Frequency (Hz)	Storage Modulus x 10^6psi (GPa)	Loss Modulus x 10^6psi (GPa)	Damping Loss Factor (x 10^{-4})
0	1.96(.077)	34.33	26.5 (182.7)	6.5 (44.8)	24.8
0	1.96(.077)	135.02	23.5 (162.0)	6.3 (43.4)	27.0
0	1.96(.077)	302.40	22.5 (155.1)	8.6 (59.3)	38.3
45/-45	2.11(.083)	32.25	4.0 (27.6)	7.8 (53.8)	197.0
45/-45	2.11(.083)	106.10	3.7 (25.5)	9.5 (65.5)	259.0
45/-45	2.11(.083)	153.25	3.7 (25.5)	10.5 (72.4)	283.0
90	1.93(.076)	29.25	3.9 (26.9)	5.5 (37.9)	144.0
90	1.93(.076)	53.20	4.0 (27.6)	6.3 (43.4)	159.0
90	1.93(.076)	136.25	2.9 (20.0)	8.3 (57.2)	290.0
90	1.93(.076)	262.00	2.8 (19.3)	8.1 (55.9)	290.0

Paxson (25) also tested the material in a free-free vibration mode. The specimen was suspended from a rigid support structure with no. 50-sized cotton thread and attached to the beam at its node points for the first mode of vibration for a free-free beam. The purpose of the threads was to decouple the specimen from the support structure, alleviating any transfer of energy from the beam specimen to the support apparatus. The beam was excited at one end and the displacement of the other end measured by a noncontact displacement follower. The damping loss factor was determined by the amplitude decay method using

equation 2.

In this mode of vibration, again the $(45/-45)_{4s}$ beam had the highest damping factor, the 90 degree material had values slightly lower, and the 0 degree material had values approximately an order of magnitude lower than the former two. The results are shown in Table 3. It should also be noted that the frequencies of testing for these specimens were not equivalent.

Table 3: Experimental Results on the Effect of Fiber Orientation on the Damping Loss Factor of Boron Fiber Reinforced Epoxy Composites in Free-Free Vibration (after Paxson (25)).

Fiber Orientation (degrees)	Thickness in. (mm)	Frequency (Hz)	Damping Loss Factor ($\times 10^{-4}$)
0	.077 (1.96)	34.2	11.7
0	.077 (1.96)	140.1	12.3
0	.077 (1.96)	300.0	13.5
45/-45	.083 (2.11)	32.1	219.0
45/-45	.083 (2.11)	106.4	217.0
45/-45	.083 (2.11)	155.0	199.0
45/-45	.083 (2.11)	313.0	239.0
90	.076 (1.93)	29.1	154.0
90	.076 (1.93)	52.6	165.0
90	.076 (1.93)	134.2	195.0
90	.076 (1.93)	262.8	210.0

Comparing the two experimental procedures used in his testing, Paxson (25) suggested that the damping loss factor determined using the forced vibration technique is generally higher than that determined from the free-free method. This difference is due

primarily to the different states of stress in each of the specimens. In the forced vibration technique, the maximum bending moment and maximum shear stress occur at the root of the specimen. In the free-free case, the maximum bending moment occurs where there is essentially no shear. In the forced vibration technique, then, energy is dissipated not only by cyclic tensile and compressive stresses, but also by cyclic shear stresses, which therefore results in a high loss factor.

Gibson and Plunkett (27) investigated the vibration damping characteristics of glass fiber reinforced composite materials. They investigated the effect of geometry, vibration frequency and amplitude on the damping of laminated beams. They subjected unidirectional and (0/90) crossply composite beams to flexural vibration. The specimens were tested using the double cantilever beam configuration, having epoxy shoulders molded to the center of the specimen, similar to that arrangement described by Paxson (25). This allowed the specimen to be clamped without introducing damage and reduced stress concentrations by shifting the clamping surface away from the region of high bending strain, thereby reducing the energy dissipation that may occur at the mounting surface. Each beam specimen was a 51 ply laminate with dimensions 35.9 x 1.0 x 0.5 in. (91.2 x 2.54 x 1.275 cm.). These beams were excited with an electromagnetic shaker attached to the epoxy shoulders. The bending strain of the material was monitored with a strain gage mounted on the specimen surface. The specimen acceleration was measured using an accelerometer mounted to the specimen support clamp. The acceleration Lissajous patterns were used to determine the damping loss factor of the composite. Gibson and Plunkett (27) point out that this type of analysis is valid only for small amplitude vibrations. For large amplitude vibrations, the shear force and the bending moment had to be determined from the characteristic function describing the mode shape [Bishop and

Johnson (28)] and the measured strain at a particular location on the beam. Because this method is much more complex, requiring visual interpretation of the acceleration Lissajous patterns, and has been abandoned for other techniques, it will not be elaborated upon further.

The beams were to be tested at large amplitudes. Since aerodynamic damping on the composite has been shown to be significant at high amplitude vibration, the test on the composite specimens was performed in a vacuum. For small amplitude vibration with the cross-ply specimen oriented in the transverse direction, damping was primarily from the 90 degree plies, with little contribution from the 0 degree plies. This is because the resin, which has the highest damping, is subjected to the highest strain in the 90 degree plies.

When thick beams in a cross-ply configuration are subjected to large amplitude vibration, the 90 degree plies near the surfaces of the beam will reach their failure stress, resulting in cracks in the material. At this load, however, the 0 degree plies have not yet failed and the beam can therefore still carry load. The mechanical degradation of the beam is thus minimal, since the 0 degree plies are the primary load carrying components. However, due to the material discontinuities as a result of the material damage, there is a strain concentration in the matrix. Although the failure strain of the flexural specimens was shown to be nearly the tensile failure strain when large amplitudes are used, the damping increased by 20% at failure, indicating the positive effect that damage and defects have on the damping in composites. Gibson and Plunkett (27) obtained experimental values for the damping loss factor of 20×10^{-4} for the initial test of the specific specimen to values as high as 100×10^{-4} for the third test of the same specimen. This result was also shown to occur in

the unidirectional 90 degree specimens as long as the failure strain of the material was not exceeded. This series of tests indicated that a damping loss factor variation is a more sensitive measure of damage than a stiffness variation.

Maymon and coworkers (29) presented experimental results on the effect of moisture and elevated temperature on the vibration damping characteristics of graphite/epoxy composites. The specimens were tested in a cantilever beam configuration both at room temperature dry and at 200° F (93°C) in a moisture saturated condition. The specimens were approximately 1 x 8 x 0.065 in.(25.4 x 203 x 1.65 mm) with a fiber volume fraction of 62% and both longitudinal and cross-ply fiber orientations. The specimens were subjected to various conditionings prior to vibration damping testing. First the specimens were dried for six days at 200° F (93°C), then tested in the flexural vibration mode at their natural frequencies. Next, the same specimens were placed in a 200° F (93°C) constant temperature bath for 45 days, after which they were weighed and the vibration damping properties determined by testing in an environmental chamber at a temperature of 200° F (93°C) and 70 to 80% relative humidity. After the specimens were tested, they were weighed to determine if moisture loss occurred during testing. The specimens were then redried at 200° F (93°C) for six days, and the dry condition vibration damping properties were again determined. The results from the conditioning indicated that the average weight gain for the hot/wet conditions was approximately 1.53% for all configurations tested. After testing in the hot/wet condition, the average weight loss experienced by the specimens was 0.078%. After redrying, the average weight loss of the specimens from their original weight was approximately 0.051%.

The vibration damping results are presented in Table 4. The testing of the specimens in such environmental conditions is relevant to the majority of composite structural applications, since composites are normally subjected to various humidity and temperature conditions. Maymon and coworkers (29) had assumed that the vibration damping experienced by the specimens would increase in the hot wet condition due to the plasticizing of the epoxy resin in this environment. However, the results showed that moisture increases the damping loss factor in specimens only where the matrix properties are less dominant. In the ($\pm$ 45) and the $(0/45/90/-45)_s$ specimens, where the matrix is strained to a higher level, the damping loss factor is actually decreased. These results show that the stress state in the material affects damping in the material. Moisture causes swelling in the matrix material. When a conditioned specimen is subjected to the same amplitude of vibration as an unconditioned specimen, the stress states in the material are different, which was shown to affect the vibration damping of the material. After redrying, these authors showed that the specimens' vibration damping loss factors were the same or in general greater than those obtained in the initial dry test condition. Examination of these specimens using both ultrasonic C-scan, and sectioning and subsequent examination with a scanning electron microscope revealed that microcracks had developed in the specimen. Such cracks enhance the damping characteristics of the test specimens (19). These results show the possibilities for using the damping loss factor to measure the damage state of a composite specimen.

Gibson and Plunkett (30) investigated the effect of amplitude and frequency on the vibration damping of composite materials subjected to flexural vibration. The specimens were subjected to a forced vibration so that a particular frequency and amplitude could be input and the direct effects on damping could be observed. To measure damping, the

Table 4: Experimentally Determined Damping Loss Factor as a Function of Temperature and Moisture Environmental Conditioning (after Maymon and coworkers (29)).

Material Orientation (degrees)	Average Effective Damping Modulus x 10^6 psi (GPa)			Average Damping Loss Factor (x 10^{-4})		
	Dry 77° F	Wet 200° F	Redried 77° F	Dry 77° F	Wet 200° F	Redried 77° F
0	17.0 (117.2)	17.1 (117.9)	16.4 (113.1)	92	120	140
45/-45	3.3 (22.8)	2.7 (18.6)	3.2 (22.1)	210	160	240
$(0/45/90/-45)_S$	10.0 (69.0)	9.9 (68.3)	9.8 (67.6)	130	75	120

resonant dwell technique was used. In this technique, the specimen is set into resonance with an electromagnetic shaker. The base acceleration and the strain on the surface measured by a foil resistance strain gage were used as inputs to an oscilloscope. The damping was then determined from the Lissajous patterns on the oscilloscope trace. To ensure that losses that were measured by the experimental procedure were from the specimen and not the result of the experimental setup, Gibson and Plunkett (30) first used 2024 T-351 aluminum as a calibration specimen and then compared their result to the theoretical prediction of the damping using the Zener thermoelastic theory (26). According to this theory, the loss factor for a beam vibrating in flexure is given by

$$\eta = \frac{\alpha^2 E T}{C} * \frac{\omega \tau}{(1 + \omega^2 \tau^2)} \qquad (6)$$

where α is the coefficient of thermal expansion, E the Young's modulus, T the absolute temperature, C the heat capacity, ω the angular frequency, and τ the relaxation time for heat

flow across a beam of rectangular cross section. The value of τ is determined as

$$\tau = \frac{h^2 C}{\pi^2 K} \tag{7}$$

where h is the beam thickness, and K is the thermal conductivity of the beam material.

The specimens were tested in the double cantilever beam configuration, clamped at its center to a vibration table. The vibration amplitude was controlled by varying the amplitude of vibration of the table. The resonant frequency of the specimens was varied by removing material from the ends of the specimens after results were obtained for the particular frequency. The difference in the damping loss factor between the experimental results and the theoretical predictions was less than 5% for aluminum, indicating that the experimental setup provided an accurate measure of the material loss factor. Results for the variation with amplitude for the aluminum calibration sample showed that, under a vacuum of 1 mm Hg, the loss factor did not vary with amplitude. However, at atmospheric pressure, as the amplitude of vibration increased, the loss factor also increased.

For the cross-ply E-glass reinforced epoxy composite samples (3-M Scotchply), Gibson and Plunkett (30) show that initial increases in the amplitude of vibration had little effect on the resultant material damping. As the amplitude of vibration increased to the point where permanent degradation occurred in the material, the damping loss factor showed a permanent increase. This result matches the work of Adams and Bacon (19) who showed that as damage in the material increases, damping also increases. When the amplitude of vibration was kept below the level at which permanent damage occurred,

damping increased as the frequency increased. The magnitude of the increase was approximately a factor of 2 from a value of 25×10^{-4} at a frequency of approximately 38 Hz to a value of 42×10^{-4} at a frequency of approximately 450 Hz. This result conflicts with the earlier results of Schultz and Tsai (17), who showed that initial increases in frequency caused a decrease in the damping loss factor of beams in the quasi-isotropic configuration. Since the experimental apparatus in the work of Gibson and Plunkett (30) was carefully evaluated to insure that measurements of the damping obtained would be of the material and not the apparatus, it is assumed that the results of Schultz and Tsai (17) may have been a function of the experimental apparatus and that the results of Gibson and Plunkett (30) are more accurate. If this is correct, this would indicate that if one is concerned with determining the damping experienced with a particular structure, then the measurement of the damping from the first mode of vibration should result in an expected lower bound. This assumption, however, needs further validation.

Pulgrano and Miner (31) conducted an experimental program to determine the loss factor of Kevlar, glass, and graphite composites with unidirectional and fabric configurations. In addition, the effect of resin was investigated by fabricating specimens using the above fibers with epoxy, polyester, and vinylester resin systems. These authors tested the samples in the double cantilever beam configuration. They determined the loss factor of the specimens using the logarithmic decay method.

The results from the investigation, given in Table 5, indicate that the Kevlar composite exhibited the highest loss factor of the three fiber systems tested. In addition, the loss factor for the Kevlar composite in both the unidirectional and fabric configurations

Table 5: Damping loss factor determination of graphite, Kevlar and glass composites in the double cantilever beam configuration using the log decrement technique with an initial maximum bending stress of 1000 psi. (after Pulgrano and Miner (30)).

Material	Configuration	Frequency (Hz.)	Loss Factor (x 10^{-4})
Kevlar 49/Epon 826 Epoxy	Unidirectional	87	130
		597	260
Kevlar 49/Epon 826 Epoxy	Fabric	50	140
	Fabric	340	160
S-Glass/Epon 826 Epoxy	Unidirectional	65	18
		438	28
E-Glass/Epon 826 Epoxy	Fabric	41	46
	Fabric	340	59
AS Graphite/Epon 826 Epoxy	Unidirectional	109	13
AS Graphite/Epon 826 Epoxy	Fabric	53	33
	Fabric	353	43
Kevlar 49 + AS Graphite Epon 826 Epoxy	Fabric	49	110
	Fabric	328	120
Kevlar 49/Polyester	Fabric	51	140
	Fabric	338	150
Kevlar 49/Polyester	Fabric ($\pm$45°)	46	190
	Fabric ($\pm$45°)	318	170
Kevlar 49/Vinylester	Fabric	60	140
	Fabric	375	240
Kevlar 49/Vinylester	Fabric ($\pm$45°)	52	160
	Fabric ($\pm$45°)	334	150

were approximately equivalent. This result is interesting from two aspects. First, the fabric composite has a much lower modulus than the unidirectional composite, approximately 50% lower for the same fiber volume fraction. The fabric composite samples fabricated were thicker than the unidirectional samples, as given by the number of plies of material used in both cases, although the measured thicknesses were not specifically given. Although the samples were subjected to the same initial outer fiber

stress, the authors did not report whether the initial amplitude of vibration was the same in both cases. Aerodynamic damping may therefore have been a larger contributing factor in one of the configurations. Second, in the fabric configuration, to achieve the same outer ply stress, the stress distribution in the fibers and resin will be different than in the unidirectional material. In addition, the amount of material available to dissipate the energy is greater in the fabric specimen than in the unidirectional specimen. In regard to the effect of resin on the loss factor for Kevlar fiber composites, the results of Pulgrano and Miner (31) would indicate that vinylester, polyester and epoxy have loss factor characteristics that differ little in the composite configuration.

Shimizu (32) conducted an experimental program to determine the effect of fiber volume fraction, quantity of flexibilizer, effect of foam matrix, and ply angles of angle-ply laminates on the damping of carbon fiber reinforced composites. He indicated that some contradictory statements have been made regarding the damping of carbon fiber composite materials. First, it has been reported that damping in these materials is due mainly to the resin and the fiber matrix interface with little contribution from the fibers. The contribution of the fiber resin interface to the damping in composites has been experimentally proven since the experimentally determined damping loss factor has been shown to be several times larger than the rule of mixtures prediction. This shows that the interface has a significant contribution to the damping of the composite. If, however, one considers the temperature and frequency dependence of the composite, one can see that the damping of the carbon fiber composite follows that which is expected of the matrix [Adams and Bacon (33) and Yoshida (34)]. This indicates that the resin properties, not the interface, are the dominant factor in determining the vibration damping as a function of frequency and temperature. Shimizu (32) reported that he could find no satisfying explanation as to why

there is no apparent temperature and frequency dependence on the fiber resin interface.

Shimizu (32) used high tensile strength carbon fiber made by Toray Corp. called " Torayca T-300." Measurements of the damping loss factor were obtained using a Bruel and Kjaer type complex modulus apparatus. The loss factor was determined using the half power bandwidth method that has been previously described. In this technique, using this equipment, the value of the damping loss factor depends on the amplitude of vibration, making this experimental procedure applicable for small amplitude vibrations only. The specimens were tested in flexure in a cantilever beam configuration.

Shimizu (32) showed that adding a flexibilizer to the matrix increases the damping loss factor of the system. With the addition of 25 parts of flexibilizer, the loss factor increased by as much as a factor of four for a (45/-45) laminate to as little as a factor of two for the 0 degree laminate. The damping loss factor for the resin itself also increased by approximately a factor of four when tested without the addition of fibers. The experimental values for the loss factor of the flexibilized resin is much higher than that predicted using the modified rule of mixtures approach by Hashin (35), the details of which are discussed later.

Shimizu (32) showed that by modifying the Hashin equation, the theoretical predictions could be made to provide an excellent fit to the experimental data. The necessary change was use of a different value of the resin's storage modulus in the Hashin equation (35)

$$\eta = \frac{\eta_m}{1 + \left[\frac{E_f V_f}{E_m (1 - V_f)}\right]} \qquad (8)$$

where η is the flexural loss factor, η_m is the loss factor of the matrix, E_f and E_m are the real parts of the complex modulus of the fiber and resin respectively and V_f is the fiber volume fraction. Shimizu (32) indicated that the storage modulus of the matrix in the composite is larger than that of the matrix alone due to the restriction provided by the fibers to the movement of the molecular chains of the resin. In this work Shimizu (32) showed the storage modulus of the matrix in the composite configuration to be 16 times that of the matrix itself.

Shimizu (32) tested the effect of foaming the matrix on the damping of the composite. Increasing the volume of the composite by as much as 50% had the effect of increasing the damping loss factor only by about a factor of two. This type of enhancement scheme to improve the damping of structural composites is therefore not a viable one. In addition, there is a variation in the resonant frequencies of these systems, which may also have affected the damping results.

For each of the angle ply configurations tested, the loss factor as a function of frequency had a minimum between 100 and 10000 Hz. The graph of loss factor vs. frequency for each angle ply orientation was concave up, with an initial decrease in loss factor to a minimum, followed by an increase as the frequency was increased. This result appears to support the earlier work of Schultz and Tsai (17) and to contradict the work of Gibson and Plunkett (30). What is probably occurring here is that the flexibilizer and

foams that are being used exhibit maximum damping at different frequencies as was previously discussed by Kurtze and Mechel (12). This may be the result of a variation in the fiber/matrix interface characteristics, as well as the frequency effect of the loss factor of these additives. This therefore shows that if various constituents are added to the composite, the effect of frequency on damping must be experimentally investigated to determine the frequency dependence on the loss factor of the particular system. The angle-ply laminates can be listed in order of decreasing loss factor in the following manner: $\pm 45 > \pm 60 > \pm 75 > 90 > \pm 30 > \pm 15 > \pm 0$. Also, the damping loss factor increases approximately eightfold from the 0 to the45. The result of the maximum in the loss factor occurring at the 45 degree orientation again matches the results of other previously mentioned investigators.

Plunkett (36) has investigated the effect of damage on the damping loss factor of cross-ply composites. The type of damage used in the investigation was microcracks in the transverse plies of the cross-ply composite. Many investigators have shown that the matrix material in a composite with this configuration will crack under a combination of residual and applied stresses, so that such cracks are a common defect that is easily created (37-40). In addition, Adams and Bacon (19) have shown that the presence of cracks in the composite material increases the damping loss factor of the material. Plunkett (36) used a 51-layer cross-ply Scotchply composite to investigate the effect of strain amplitude, and therefore the transverse crack density, on the damping loss factor of the composite material. The specimen was tested in the double cantilever beam configuration. As the amplitude of vibration was increased, an increase in the damping was observed corresponding to the development of permanent damage in the material. The crack density was easily correlated with the loss factor. Plunkett (36) also showed that after a particular level of damage

corresponding to the strain level of 2%, there was no increase in the loss factor for the system. This damage level corresponds to the minimum spacing of the cracks in the transverse plies of the cross-ply composite. The increase in the damping loss factor from the undamaged to the damaged specimen having the minimum crack spacing was approximately a factor of 3. Although he measured the increase in damping experimentally, Plunkett (36) indicated that there is no physical mechanism to explain why the magnitude of the dissipation is so large.

Macander and Crane (5) conducted an experimental program to obtain information on the vibration damping of advanced composite systems using monolithic composite beams. This testing differed from that described previously by the size of the beams tested. In this study, the beam thicknesses ranged from 1.25 to 1.94 in. (31.8 to 49.2 mm), approximately an order of magnitude greater than beams used in the other studies previously discussed. The beams were approximately 39.625 x 4.375 in. (100.6 x 11.1 cm) in length and width, respectively.

The experimental technique used in this investigation was also different from the other techniques previously mentioned. Here, the beams were excited with an impulse. The rate at which the excitation acceleration decays is a measure of the damping of the structure. The vibration of the structure can be approximated by a decaying sinusoid. The damping is then related to the time constant of vibration decay. When the specimen is set into vibration, the resulting mode has associated with it a particular reverberation time. The reverberation time is the time required for the vibration of the structure at a particular frequency to reach one thousandth of some initial value, i.e., 60 dB referred to some initial

value. The loss factor is then determined as being inversely proportional to this measured time at the particular frequency. Specifically, the decaying filtered electronic signal of the response of the structure at a particular modal frequency is compared with a signal whose reverberation time is known, thus determining the reverberation time of the specimen.

The experimental investigation of Macander and Crane (5) was designed to determine effect of fiber orientation, fiber type and material hybridization on the loss factor of thick [greater than 1.5 in. (38 mm)] composite beams. The four configurations tested were 1) a graphite/epoxy beam with fiber orientation $(0/45/-45)_{225T}$, 2) a Kevlar/epoxy beam with fiber orientation $(0/90)_{228T}$, 3) a graphite/glass/graphite epoxy beam with the graphite layers having fiber orientations of $(0/90)_{42T}$ and the glass/epoxy having fiber orientation $(0/90)_{108T}$, and 4) a hybridization of Kevlar/graphite/Kevlar epoxy with the Kevlar layers having fiber orientation of $(0)_{21T}$ and the graphite/epoxy having fiber orientations of $(0/45/-45)_{200T}$. In addition to the composite beams, a brass beam 1.5 in. (38.1 mm) thick was also tested to provide a reference for comparison with the composite results, since it was unknown if a size effect on the loss factor would be prevalent. The beams were constructed using the above combination of materials so that they would have the same bending stiffness as a 1.5 in. (38.1 mm) thick brass beam.

The results, given in Figure 8, indicate that all of the composite configurations tested have a loss factor that is at least an order of magnitude greater than the brass beam over the frequency range of 200 to 20000 Hz. The loss factor for the graphite beam is in the range of 20×10^{-4} to 100×10^{-4} and is comparable to the graphite/glass/graphite hybrid beam. These values are similar to those found in the literature. The graphite/Kevlar/ graphite

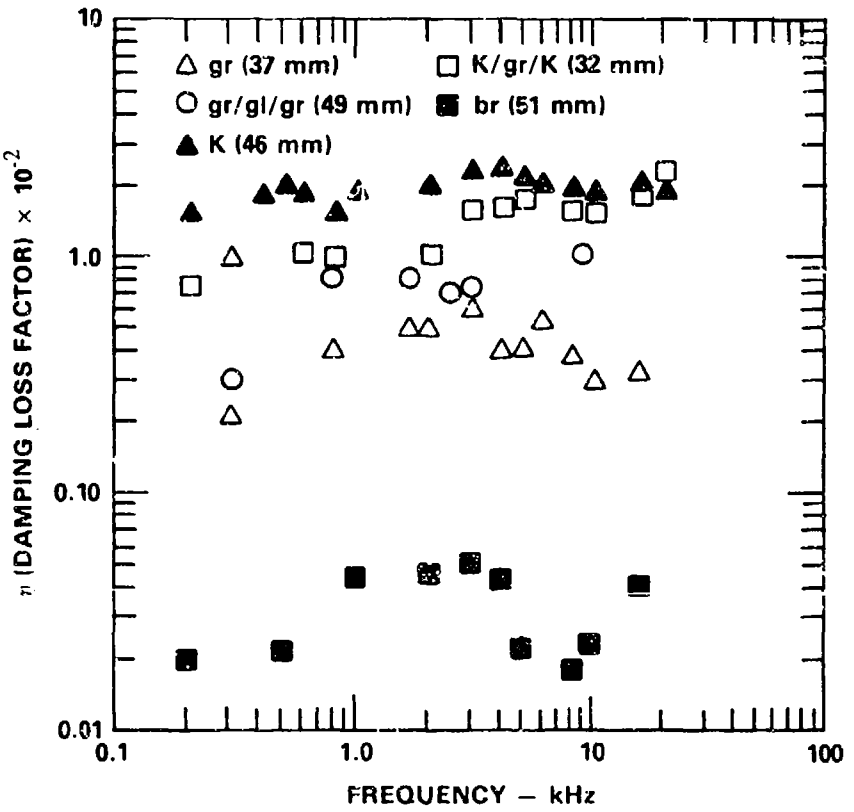

Figure 8 Comparison of damping loss factors for thick section composite and brass beams with nominal dimensions 39 x 4 in (99 x 10 cm), graphite/epoxy 1.46 in (37mm) thick (gr), graphite/glass/graphite/epoxy 1.93 in (49 mm) thick (gr/gl/gr), Kevlar/epoxy 1.26 (32 mm) thick (K), Kevlar/graphite/Kevlar/epoxy 1.26 in (32 mm) thick (K/gr/K), and brass 2.01 in (51 mm) thick (br) tested in flexure (after Macander and Crane (5)).

hybrid beam had a loss factor that was slightly greater than the previous two beams with a loss factor ranging from $70x10^{-4}$ to $230x10^{-4}$. The Kevlar beam had the highest loss factor with minimal variance over the frequency range tested; its loss factor ranged from $120x10^{-4}$ to $230x10^{-4}$. It should be noted that the brass beam results were approximately an order of magnitude lower than results reported for steel and aluminum beams.

The results of this testing showed no specific trends in regard to the effect of frequency on the loss factor, in contrast to the earlier results of Schultz and Tsai (13) which indicated that the loss factor increased with increasing frequency in a continuous manner. The results shown in Figure 8 show a general trend of increased loss factor with increasing frequency, but not in the same smooth continuous manner. One possible explanation for this is that various modes of vibration were investigated as opposed to utilizing the first resonant frequency only.

Gibson and coworkers (41) have developed a new technique for testing the vibration damping characteristics of composite systems. The improvements in this technique are a result of the improved electronic systems available for data acquisition. In addition, measurements of displacement can be improved by replacing the previously used strain gages with a noncontacting proximity transducer. The apparatus used by Gibson and coworkers (41) was the Kaman KD-2310-3U eddy current displacement measurement system. This apparatus was used to measure the resonant amplitude ratio for the determination of the loss factor. It was shown earlier that the damping of a beam can be determined by measuring the base and tip displacement amplitudes when the beam is subjected to vibrations at its fundamental frequency in a double cantilever beam

configuration. An analysis was presented where the damping loss factor is derived from the predicted tip displacement of the beam. This technique was used in previously described investigations. The problem with this experimental technique is that the monitoring probe cannot be placed at the tip of the beam due to physical constraints. An analytical solution was derived by Yau (42) where the displacement of the beam at any location can be predicted. The results of the analysis give the loss factor in flexure as

$$\eta = \frac{C_r \, \varphi_r \, X_0 \, \ddot{a}(0)}{\varphi_r(L) \, \omega_r^2 \, a(X_0)} \tag{9}$$

where C_r ,and ϕ_r are given by

$$C_r = \frac{4 (\cos \lambda_r L + \cosh \lambda_r L)}{\lambda_r L (\sin \lambda_r L * \cosh \lambda_r L - \cos \lambda_r L * \sinh \lambda_r L} \tag{10}$$

$$\varphi_r(x) = \cosh \lambda_r x - \cos \lambda_r x - \sigma_r(\sinh \lambda_r x - \sin \lambda_r x) \tag{11}$$

$$\lambda_r = \left(\frac{\rho A \omega_r^2}{EI} \right)^{\frac{1}{4}} \tag{12}$$

$$\sigma_r = \frac{\sin \lambda_r L * \cosh \lambda_r L + \cos \lambda_r L * \sinh \lambda_r L}{\sin \lambda_r L + \sinh \lambda_r L} \tag{13}$$

an

L	= specimen length
ω_r	= angular resonant frequency of the r^{th} mode
A	= cross sectional area of beam
I	= area moment of inertia of specimen cross section
ρ	= density of the beam
x	= distance along the beam from the base
X_0	= location of strain gages
$\ddot{a}(X_0)$	= base acceleration amplitude of beam

$a(X_o)$ = displacement amplitude at location of probe

All of the above values are measured in the experimental apparatus previously described.

To use the eddy current probe for the nonconductive composite specimens, aluminum foil targets had to be bonded to the ends of the specimen. These targets constitute only 0.08% of the total specimen weight and therefore add only minimally to specimen damping. The previously used accelerometers could substantially affect the measured damping by adding weight to the specimen at a specific location. The accelerometer would also affect the mode shape of the composite beam, thereby further complicating the measurement of the composite damping loss factor. An alternative technique, which does not add to the weight of the specimen, is use of an electro-optic follower. The cost of this equipment, however, is well in excess of the cost of the eddy current apparatus.

The specimens were clamped using square aluminum clamping blocks instead of epoxy blocks molded onto the specimen. These removable aluminum blocks were positioned using an alignment pin for centering the specimen. The amplitude of the input oscillation was determined using an ac-dc converter instead of the conventional oscilloscope. With an oscilloscope, the amplitudes are scaled from the acceleration Lissajous patterns. The ac-dc converter has the advantage of being automated, which reduces analysis time and errors in the measurement of the input amplitude caused by errors in measuring the Lissajous patterns of the oscilloscope traces.

Gibson and coworkers (41) present an error analysis of the new and old techniques.

The new technique corrects for the displacement of the probe at its actual location instead of assuming that the displacement measured is at the tip, reducing errors associated with locating the probe at a specific distance from the specimen tip and then assuming that the probe is located near a nodal point of the displacement. Their results then showed that the new technique is less susceptible to measurement errors for the calculation of the loss factor than the original technique. They also found that the results using the aluminum blocks more closely matched the damping provided by the specimen itself. This was determined by testing the material first with the aluminum blocks, then replacing the aluminum block with a polyester shoulder and repeating the test. Using the polyester shoulder resulted in higher damping loss factors than when the aluminum blocks were used, indicating that the polyester blocks provide additional damping to the specimen.

Sheen (43) presented results on the damping of composite materials in a gravity-free environment. He reported that previous research has revealed that many material physical characteristics affect the damping of composites. He noted that Putter and coworkers (44) showed that temperature, humidity and ply orientation will affect damping. Adams and Bacon (45) showed that fiber volume fraction affected the damping. Mohr and Cawley (46) found that for angle-ply laminates, damping was slightly dependent on the stress and frequency of the vibration. Sheen (43) therefore indicates that the test method for determining the damping is critical for obtaining pertinent results.

Sheen's (43) experimental work included testing of $(0)_8$ and $(90)_8$ laminates at various frequencies. He mounted strain gages to the center of each specimen, a nodal point for this specific configuration, to obtain amplitude information. To vary the frequency yet

retain the center of the specimen as a node point, each specimen was cut to shorter lengths when a different frequency was to be tested. The damping results from this testing are presented in Table 6. The results given in Table 6 are averages of the values obtained by Sheen (43).

Table 6: Experimentally Determined Damping Loss Factor for Unidirectional Graphite/Epoxy Composite Materials (after Sheen(43)).

Material Orientation (degrees)	Frequency (Hz)	Stress x 10^3 psi (MPa)	Damping Loss Factor (x 10^{-4})
0	289.20	9.85 (67.9)	12.44
0	284.00	11.45(78.9)	10.38
0	288.20	9.51 (65.6)	12.84
0	301.10	10.62 (73.2)	10.11
0	485.84	3.85 (26.5)	12.01
0	931.50	3.12 (21.5)	9.88
0	1491.70	0.76 (5.2)	10.42
90	267.00	0.54 (3.7)	109.55
90	465.97	0.14 (1.0)	120.10
90	899.81	0.10 (0.7)	132.51
45/-45	17.95	5.07 (35.0)	108.33
45/-45	29.62	3.82 (26.3)	110.60
45/-45	54.16	1.85 (12.8)	119.52
45/-45	171.04	0.54 (3.7)	131.58

Sheen (43) used three methods to analytically determine the damping of the composite specimens. The first was the rule of mixtures approach, where the damping of the composite is given by

$$\eta = V_f \eta_f + V_m \eta_m \qquad (14)$$

where V_f and V_m are the volume fraction of the fibers and resin respectively, and η_f and η_m are the damping loss factors of the fibers and resin respectively. Since the damping loss factor for the matrix is at least an order of magnitude greater than that provided by the fibers, the loss factor of the composite can be merely approximated as

$$\eta = V_m \eta_m \tag{15}$$

In this case, the damping loss factor of the composite is assumed to be isotropic and not to vary as a function of fiber orientation.

The second method Sheen (43) used was developed by Hashin (35). Here, the loss tangent for the material was found to be proportional to the ratio of the imaginary part of the complex modulus divided by the real part. The approximation made in this analysis is that the fibers do not contribute to the damping of the composite, with the result that the imaginary part of the fiber modulus is zero. With this approximation, the damping loss factor of the composite in the fiber direction is given as

$$\eta_{11} = \frac{\eta_m}{1 + \left[\dfrac{E_f V_f}{E_m(1-\nu_f)}\right]} \tag{16}$$

where E_f and E_m are the modulus of the fiber and resin, respectively.

The third analytical technique Sheen (43) used was that developed by Adams and Bacon (45). They take into account the energy dissipation in each cycle due to shear. The results of this analysis establish the damping loss factor as

$$\eta_s = \frac{\eta_{12}\int_0^{L/2}\left(\frac{\partial^3 w}{\partial x^3}\right)^2 dx}{\int_0^{L/2}\left(\frac{\partial^3 w}{\partial x^3}\right)^2 dx + \frac{10\,G_{12}}{E_{11}\,h}\int_0^{L/2}\left(\frac{\partial^2 w}{\partial x^2}\right)dx} \qquad (17)$$

where L is the specimen length, w is the lateral deflection at a distance x along the beam, h is the specimen thickness, E_{11} is the composite Young's modulus along the primary axis, G_{12} is the shear modulus, and η_{12} is the longitudinal shear damping loss factor.

Sheen (43) tested the effect of frequency on the composite damping. His results convinced him that the variations in the damping loss factor observed were due solely to the frequency. He tested the same composite specimen at various frequencies so that any material characteristics which could affect the damping loss factor, such as the fiber volume fraction, width, thickness and internal nonuniformities remained constant. The specimen's natural frequencies were varied by cutting equal lengths from each end so that the specimen's center would correspond to a node of the vibration. The results of the testing showed that there was little change in the damping loss factor in the frequency range of 300 to 1492 Hz for the 0 degree specimens. These results are shown in Table 6. For the 90 degree specimens however, the damping loss factor was a function of the frequency, increasing as the frequency of oscillation increased. The same results apply to the (45/-45) specimens. These results are also shown in Table 6. Comparing the results of the experimental program with the theories, it was shown that the Hashin model (35) for unidirectional composites gives results consistent with the 0 and 90 degree unidirectional laminates tested. In the analysis that was performed, the damping capacity of the resin was approximated since this information was unavailable. The validity of the models,

therefore, still needs further verification.

Sun and coworkers (47) compared the two techniques currently used for experimentally determining the vibration damping characteristics of composites. The first was the forced vibration technique, where the specimen is continuously excited by an electromagnetic shaker at random frequencies. The advantages of this technique include easy control of the force level, the ability to control extraneous noise and nonlinearities, and the ability to remove distortion effects. The disadvantages of this technique are that it cannot measure the in-situ damping of actual structures and that the testing is limited to the natural frequencies of the test specimens.

The second technique available for measuring the damping characteristics of materials is the impulse hammer technique. In this technique, all higher modes of vibration are excited simultaneously, resulting in the ability to determine the damping at any desired frequency, a distinct advantage over the forced vibration technique.

In the impulse hammer technique, the input excitation and the response of the structure to a given forcing function are experimentally determined. This is done by defining H(f), called the transfer function, as the ratio of the Fourier transform of the system output to the Fourier transform of the system input. From the graph of the imaginary part of H(f) vs. f, a particular frequency is determined, at which the damping is to be determined. From the graph of the real part of H(f) vs. f, the ratio of the frequency at which H(f) attains its first maximum f(a) to the frequency at which H(f) attains its first minimum f(b) is obtained. The flexural damping loss factor is then determined as follows:

$$\eta = \frac{\left[\frac{f(a)}{f(b)}\right]^2 - 1}{\left[\frac{f(a)}{f(b)}\right]^2 + 1} \qquad (18)$$

This appears to be a variation on the half power band width technique. The use of a noncontact eddy current probe enables a more reliable method of determination of the damping of the composite. The previously used contact probe inevitably changed the modal form of vibration by virtue of the added mass as well as the natural frequencies of the specimen tested. Sun and coworkers (47) were able to achieve results consistent with other investigators, a comparison of which is given in their paper. Their results are presented in Table 7.

As can be seen in Table 7, all of the composite systems have a damping loss factor at least double that of aluminum. Of the composite systems investigated, the glass/polyester system has the highest damping. This high value can be attributed to the high damping imparted by the polyester resin compared to the Fiberite 934 epoxy resin and the epoxy system used for the Owens Corning hybrid laminate. In addition, there is a modal frequency effect on loss factor for all of the systems investigated. The values presented in Table 7 are similar to those obtained in previous investigations.

Haines (10) investigated the damping properties of graphite/epoxy composites tested in a free-free beam resonance mode subjected to forced sinusoidal excitation. His investigation was conducted to determine the effect of resin and fiber type on the damping loss factor. He tested 8 ply laminates in the 0, 90, and $(0/\pm45/90)_s$ configurations for all

Table 7: Comparison of the Damping Loss Factor for Aluminum, Glass/Polyester, Graphite/Epoxy, Kevlar/Epoxy, and Hybrid Composite (after Sun and coworkers(47))

Material	Laminate Configuration	Mode No.	Frequency Hz	Damping Loss Factor ($\times 10^{-4}$)
Aluminum	--	1	42	14.3
	--	2	275	3.3
	--	3	771	2.5
Glass/Polyester	[0]	1	75	103.5
		2	467	100.6
		3	1296	71.9
Graphite/Epoxy	$90_2/0_6/90_2]_s$	1	43	33.9
		2	287	40.8
		3	794	39.0
Kevlar/ Epoxy	[0]	1	56	42.0
		2	354	44.4
		3	976	32.1
Hybrid, Owens-Corning	[0]	1	45	41.9
		2	277	42.2
		3	773	40.5

the systems considered. The specimen dimensions were 5.9 x 0.5 x 0.079 in. (15 x 1.3 x 0.2 cm). Specimens were suspended on two fine taut threads at the calculated nodes of the beam.

The resin systems tested were Narmco 5213, Narmco 5208 and Fiberite 934. The latter two systems are extensively used in both composite research and production of composite parts. Three fiber systems were also used, Celion 3000, Celion 6000, and GY-70, all produced by the Celanese Corp. The first two fiber systems are conventional,

commercially utilized fibers having a modulus of approximately 34×10^6 psi (234 GPa). The latter fiber, GY-70, is an ultrahigh modulus fiber having a tensile modulus of approximately 74×10^6 psi (510 GPa), a factor of 2 higher than that of the former two fibers. The results from the investigation are given in Table 8. By using identical fiber systems in various matrices, Haines (4) was able to rank the resin systems in order of increasing damping that they provide with a particular fiber system as follows: Narmco 5213, Narmco 5208, and Fiberite 934. The fibers could likewise be ranked in order of increasing damping that they provide in a particular resin system as follows: Celion 3000, Celion 6000 and GY-70. Since the Celion 3000 and Celion 6000 fibers are identical, with the exception of the number of fibers in each individual tow used to manufacture the prepreg, Haines (6) was able to determine the effect of tow size on the damping by experimentally determining the damping of specimens using the two fibers in the same resin systems. His finding showed that the same fiber system with more fibers per tow, i.e., the Celion 6000, provides increased damping over a system with fewer fibers per tow, the Celion 3000. This seems to contradict the earlier findings by Adams and Short (15) who observed that as the surface to volume ratio of the fiber is increased (i.e., as the fiber diameter is reduced) the damping is also increased. Although the same fiber is used in both cases, the resin distribution within the tows and between tows is probably different. A possible explanation is that the packing of the fibers for the Celion 6000 system has more matrix between the actual tows but a more dense packing within the tows themselves, with the result that a larger effective surface to volume ratio results. If this is the case, then Haines's (10) results would support the findings of Adams and Short (18).

This work by Haines (10) also helps to identify a potentially high damping system. This can be seen if the earlier results of Adams and Bacon (19) are used. Adams and

Table 8: Experimentally Determined Damping Loss Factor for Celion 3000/5208, Celion 3000/5213, Celion 6000/5208, Celion 6000/5213, and GY 70/934 Unidirectional Graphite/Epoxy Composites using the Free-Free Vibration Test Method(after Haines (10)).

Material	Test Direction (degrees)	Frequency (Hz)	Young's Modulus x10^6 psi (GPa)	Damping Loss Factor (x 10^{-4})
C3000/5208	0	833	21.1 (145.5)	13.3
C3000/5213	0	881	19.7 (135.8)	9.7
C6000/5208	0	882	20.1 (138.6)	15.4
C6000/5213	0	909	19.2 (132.4)	10.5
GY70/934	0	1090	41.5 (286.1)	23.6
C3000/5208	90	673	1.8 (12.4)	251.6
C3000/5213	90	685	1.5 (10.3)	148.2
C6000/5208	90	699	1.7 (11.7)	279.7
C6000/5213	90	700	1.5 (10.3)	160.0
GY70/934	90	437	1.0 (6.9)	325.2
C3000/5208	(0/45/-45/90)	510	6.9 (47.6)	77.4
GY70/934	(0/45/-45/90)	592	10.6 (73.1)	61.5

Bacon (19) showed that, as the system is made stiffer, the damping loss factor of the system decreases. The GY-70/934 system tested by Haines (10) has a stiffness that is approximately double that of the other two fiber systems investigated. The GY-70/934 system, however, had a damping loss factor that was approximately double that of the other systems. Based on the above finding of Adams and Bacon (19), a composite system that incorporates the Celion 6000 with the 934 resin, having a stiffness much less than the GY-70/934, should yield a system that has superior damping to the systems shown in Table 8.

Suarez and coworkers (48) presented an analysis of the random and impulse

technique. The random technique is similar to the forced vibration technique mentioned above, except that the specimen is excited by a random frequency response generated by the noise source of a fast Fourier transform analyzer. The analysis still uses the transfer function [Sun and coworkers (47)] to determine the damping via the half power band width method. In the impulse technique the specimen is excited using an impulse from a hammer with a force transducer attached to its head. In this mode all the frequencies of vibration are excited simultaneously. The transfer function is again determined using the input from the force transducer as the input function and the response is measured using the noncontact eddy current probe. The loss factor for both techniques is also determined using the half power band width technique, previously given in equation 3. The results from the two techniques are similar. The impulse technique allows for low amplitude vibrations, which enables aerodynamic damping to be minimized. Obtaining low amplitude vibrations with the random vibration technique is more difficult. The consequence of using the random vibration technique, therefore, is that the aerodynamic damping can contribute to the measured damping of the specimen, as previously identified by Adams and Bacon (19). Because of this and other considerations, the impulse technique is considered by Suarez and coworkers (48) to be the easier of the two techniques to use experimentally.

The experimental results obtained using the impulse hammer technique were consistent over a larger frequency range and successive number of tests, and were consistent with proven theoretical models of metallic materials. With the impulse hammer technique, by keeping the vibration amplitude to a minimum, frictional losses at the clamp region of the specimen are also minimized, in addition to the above mentioned minimization of any aerodynamic damping effects.

The results of Suarez and coworkers (48) showed that the loss factor increases slightly with increasing frequency. The frequency of test varied from approximately 39 to 1000 Hz. It should also be noted that for the aluminum specimen tested, there was an initial increase in damping loss factor to a frequency of approximately 10 Hz followed by a decrease in loss factor with frequency, asymptotically approaching 0 at frequencies greater than 1000 Hz. For the chopped glass/polyester sample, the damping loss factor ranged from 100×10^{-4} at a frequency of approximately 40 Hz to a value of 120×10^{-4} at a frequency of approximately 1575 Hz. For the graphite/epoxy samples, the damping loss factor ranged from 25×10^{-4} at a frequency of 50 Hz to a value of approximately 30×10^{-4} at a frequency of approximately 950 Hz. Suarez and coworkers (48) also present results of the damping loss factor for the epoxy material. Values were approximately 180×10^{-4} up to a frequency of approximately 420 Hz.

Hoa and Ouellette (49) experimentally determined the damping loss factor of plain weave Kevlar 49 fabric impregnated with Narmco's 5208 epoxy resin, unidirectional T-300 Graphite/5208 epoxy, and various hybrid combinations of these two materials. The goal of their work was to obtain a laminate that had twice the stiffness of aluminum along with twice the damping loss factor of a graphite/epoxy panel. Initially, the loss factor of the Kevlar fabric and the unidirectional graphite/epoxy materials were determined. Next, various hybrid configurations were fabricated and tested to determine the resulting loss factor. Their results are given in Table 9. It can be seen that the maximum damping occurred when the Kevlar/epoxy was subjected to the largest axial stress level and the graphite/epoxy was subjected to the largest shear stress. The specific configuration used to meet their goal was a Kevlar/graphite/Kevlar laminate with the orientation of $[(0/90)_2/0_3/(0/90)_2]_T$.

Table 9: Effect of Material and Laminate Configuration on the Damping Loss Factor of Plain Weave Kevlar 49/5208 Epoxy, T-300 Graphite/5208 Epoxy and Kevlar/Graphite/Epoxy Hybrid Composite Materials(after Hoa and Ouellette (49)).

Material	Configuration	Initial Strain (μ in/in)	Frequency (Hz.)	Loss Factor ($\times 10^{-4}$)
Kev/epoxy	$[0/90]_{5T}$	300	34.0	134
Kev/epoxy	$[\pm 45]_{5T}$	300	17.1	197
Gr/epoxy	$[0]_{8T}$	300	63.0	42
Gr/Kev/Gr/epoxy	$0_2/\pm 45_3/0_2]_T$	300	67.8	41
Gr/Kev/Gr/epoxy	$[0_2/(0/90)_2/0_2]_T$	300	65.6	42
Kev/Gr/Kev/epoxy	$[(0/90)_2/0_3/(0/90)_2]_T$	300	50.6	138
Kev/Gr/Kev/Gr/Kev/epoxy	$[(0/90)/0/(0/90)/0/(0/90)]_T$	300	34.1	119
Kev/Gr/Kev/epoxy	$[(0/90)_2/0_2/(0/90)]_s$	300	83.3	88
Kev/Gr/Kev/epoxy	$(0/90)_3/0_2/(0/90)]_s$	300	97.1	96

Theoretical Determination of Damping

There have been numerous analytical models which have been developed for determination of the damping loss factor for composites. These approaches have attempted to determine the damping of a lamina from a micromechanical approach, the damping of a laminate using a macromechanical approach, and the damping that a composite structure would possess. Each of the individual approaches is important for the overall design of a damped composite. Each of the approaches ultimately builds upon damping or viscoelastic characteristics of the material constituents. This interrelationship is depicted in Figure 9. An understanding of this interrelationship is manifested in the design process of composite structures. From knowledge of the structural requirements of a component, a designer chooses the appropriate fiber and matrix system, or laminae. For the determination of the damping of the laminae, an understanding of the contributions of the material constituents and their combined response is necessary. These lamina characteristics are then required to determine the damping of a laminated composite. In addition, the stacking sequence and ply orientation effects must be considered in determining the damping response of a laminated composite. These stacking sequence and ply orientation effects are then necessary inputs to the damping analysis of composite structures. Again, additional characteristics, such as damping provided at joints, and aerodynamic and hydrodynamic damping, must be taken into account to obtain an accurate determination of the damping of the composite structure.

Analytical models that have been presented in the literature have typically attempted to determine the damping associated with one of the three general areas discussed above. The

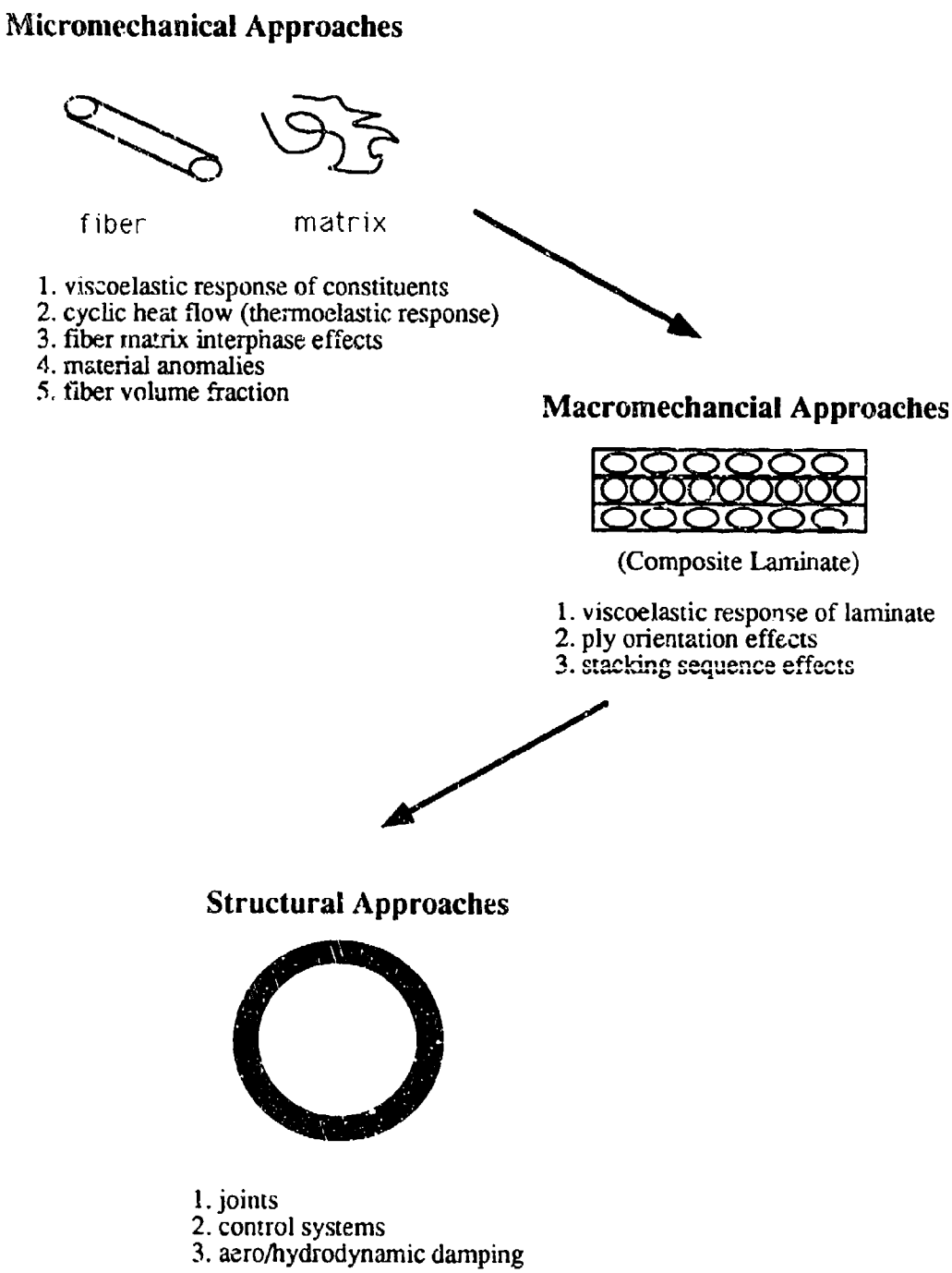

Figure 9: Damping mechanisms of composites.

review that follows will discuss the analytical models that have been formulated to determine the damping of composites on the micromechanical, macromechanical and structural levels.

Micromechanical Models

Three models that had moderate success at predicting the damping loss factor of various composite systems were presented earlier. These models were the rule of mixtures approach (43), the model of Hashin (35), and the model of Adams and Bacon (45). The modified rule of mixtures, as was introduced in the previous section gives the in-plane loss factor of the composite as

$$\eta_{11} = \eta_m V_m \tag{15}$$

where V_m is the volume fraction of the matrix and η_m is the loss factor of the resin system. This indicates that the loss factor of the composite is fixed once the resin system is chosen.

The model of Hashin(35) is an extension of the rule of mixtures approach. He incorporates the fiber elastic properties in the calculation of the material loss factor. In this case the in plane loss factor is given as

$$\eta_{11} = \frac{\eta_m}{1 + \left[\frac{E_f V_f}{E_m(1-\nu_f)} \right]} \tag{16}$$

where E_f and V_f are the elastic modulus and volume fraction of the fibers. This would indicate that as the stiffness of the fibers increase, the loss factor of the composite decreases, when a particular resin system is used with identical fiber volume fractions.

A third analytical model that has been used successfully to predict the loss factor of metals, and which may be operative for composites is the Zener Thermoelastic Theory (26). As was previously indicated, according to this theory, the loss factor for a beam vibrating in flexure is given by

$$\eta = \frac{\alpha^2 E T}{C} * \frac{\omega \tau}{(1 + \omega^2 \tau^2)} \qquad (6)$$

where α is the coefficient of thermal expansion, E the Young's modulus, T the absolute temperature, C the heat capacity, ω the angular frequency, and τ the relaxation time for heat flow across a beam of rectangular cross section. The value of τ is determined by

$$\tau = \frac{h^2 C}{\pi^2 K} \qquad (7)$$

where h is the beam thickness, and K is the thermal conductivity of the beam material. This analysis takes into account only the energy dissipation which results from thermal currents and ignores the viscoelastic contribution that the constituents may have. This in itself would not be recommended as an appropriate model to determine the loss factor of composites. However, this contribution in conjunction with the Hashin model would provide a more accurate estimate of the material damping loss factor of composites.

Using the Zener thermoelastic theory, the loss factor as a function of material thickness was investigated for a graphite/epoxy unidirectional composite. Literature values for the thermal conductivity, heat capacity, and coefficient of thermal expansion were used in equations 6 and 7. For a beam with a thickness of 0.04 in (1.02 mm), the peak value occurs at a frequency of approximately 10 Hz. At frequencies greater than 100 Hz., the calculated loss factor is less than 10×10^{-4}. As the thickness is increased to 0.125 in (3.18 mm), the peak is shifted to a frequency of approximately 1 Hz. At frequencies greater than 10z, the calculated loss factor is less than 10×10^{-4}. As the thicknesses increase, the frequency at which the peak value occurs is shifted to lower frequencies with a smaller bandwidth of significant contribution. As such, the energy dissipated from cyclic heat flow in composite materials is minimal at best for typical frequencies of interest.

Mallik and Ghosh (50) developed a theory concerning the damping of composites that have high damping particulate inclusions incorporated into their structure. In this analysis, they considered the inclusions to be uniformly distributed in the matrix material. They divide the material into unit cells which are cubes of side "b," each with a spherical inclusion at its center. They then subjected the cell to a tensile stress T and computed the stress field around the inclusion.

The damping capacity was computed as the equivalent logarithmic decrement given by

$$\delta = \frac{D}{2W} \tag{19}$$

where D is the energy dissipated per cycle, and W is the maximum elastic energy during the cycle. The values of D and W are computed as follows:

$$D = \iiint J(\sigma_1^2 + \sigma_2^2 + \sigma_3^2 - \sigma_1\sigma_2 - \sigma_2\sigma_3 - \sigma_3\sigma_1)^{n/2} dV \tag{20}$$

$$W = \frac{1}{2E}(\sigma_1 + \sigma_2 + \sigma_3)^2 - \frac{1-\nu}{E}(\sigma_1\sigma_2 + \sigma_2\sigma_3 + \sigma_1\sigma_3) \tag{21}$$

where E is the modulus of elasticity, ν is the Poisson's ratio, and J and n are material constants. This integration was carried out numerically.

A parametric study was carried out using various inclusions and the material properties $\nu = 0.3$ and $n = 2.5$, where n is the damping index of the matrix. Although the value of ν is actually variable with the material, its effect on the damping capacity was insignificant. Results indicated that rigidity is not affected by the inclusions, while damping capacity is enhanced greatly. No indications were given concerning the values used in the study and to what materials the appropriate damping capacity values would theoretically correspond.

This work appears to support the work of Lameris and coworkers (51). In their experimental investigation, these authors determined that adding a weight to the composite structure at various locations could enhance the damping of the structure. The work of Mallik and Ghosh (50) shows that, as one adds particulates to the composite, which can be considered as the degeneration of macroscopic weights added to the exterior of the composite, the damping is substantially enhanced. For the composite materials currently in use, the incorporation of a very dense, uniformly distributed particulate into the composite

during fabrication may substantially enhance the structural damping of the system.

Kishore and coworkers (52) presented a theoretical analysis on the effect of the bonding of the fiber to the resin on the damping of the composite system. In their analysis, they assumed that if the bonding is poor, there is a loading above which slip will occur. When this happens, there is a resultant dissipation of energy from friction at the interface. By varying the coefficient of friction at the interface, the loss factor is determined from the maximum strain energy stored during loading of the composite. The loss factor is then calculated as

$$\eta = \frac{W}{2\pi U} \tag{22}$$

where W is the energy dissipated during one loading cycle and U is the maximum strain energy stored in one cycle.

From their analysis, they showed that a loss factor for a composite which is as high as 1200×10^{-4} can be achieved. The loss factor is also a function of the applied load. No slip occurs until the critical load is reached, resulting in a loss factor that one would normally anticipate for a properly made composite. After this critical loading, further increases in loading increase the loss factor of the composite up to a certain large amplitude. A maximum is reached because eventually a separation occurs within the composite between the fiber and the resin, so that no frictional loss of energy is available. In general, using this analysis, the loss factor was shown to vary between 300×10^{-4} and 800×10^{-4}, typical of values expected for some composite materials.

These models do not take into account the numerous factors that have been shown to affect the damping loss factor of the composite, such as the fiber orientation and thickness, fiber diameter and fiber volume fraction to name but a few. In addition, the viscoelastic characteristic of the matrix material, or the frequency effect, is also ignored. A comprehensive micromechanical analytical model should account for these various microscopic aspects in determining the lamina damping characteristics of composite materials.

Macromechanical Models

Two macromechanical approaches predominate the literature, the elastic-viscoelastic correspondence principle and strain energy approach. These approaches are used to determine the laminate damping loss factors.

Numerous investigators have suggested the use of the elastic-viscoelastic correspondence principle for determination of the damping loss factor of composites (53-57). This procedure utilizes as input the lamina loss factor characterstics to determine the effective laminate loss factor.

Typically, the fibers are assumed to be elastic and the matrix is assumed to be linearly viscoelastic. As such, the composite behaves macroscopically as a linearly viscoelastic body. For a material subjected to oscillatory loading, the time varying local average stresses and strains can be expressed as

$$\varepsilon^* = \varepsilon_{ij} e^{i\omega t} \tag{23}$$

$$\sigma^* = \sigma_{ij} e^{i\omega t} \tag{24}$$

Hashin (35) has developed a general theory of complex moduli of viscoelastic composites which indicates that the macroscopic dynamic behavior may be approximated by classical continuum dynamics for relatively low frequencies. The composite viscoelastic response can then be determined by replacing the phase elastic moduli with the identical phase geometry by the effective complex moduli.

The elastic stress strain relationship for a material can be expressed as

$$\sigma_{ij} = Q_{ijkl}\, \varepsilon_{kl} \tag{25}$$

where Q_{ijkl} is the classical stiffness tensor. Applying the elastic viscoelastic correpondence principle to a material elastic behavior characterized by equation 25, the viscoelastic response is then given by

$$\sigma_{ij}^* = Q_{ijkl}^* \varepsilon_{kl}^* \tag{26}$$

A continuous fiber composite lamina possesses orthotropic symmetry. If the material is subjected to plane strain conditions, the number of elastic constants required to characterize the reduced stiffness components, Q_{ij}, given in equation 25 reduces to three: E_1, E_2, and G_{12}. Utilizing the elastic viscoelastic correpondence principle, the corresponding components in equation 26 become

$$E_1^* = E_1' + iE_1'' \tag{27}$$

$$E_2^* = E_2' + iE_2'' \tag{28}$$

$$G_{12}^* = G_{12}' + iG_{12}'' \tag{29}$$

where E_1', E_2', and $G_{12}'$are the real in-plane modulus, of storage modulus, of the composite and E_1'', E_2'', and G_{12}'' are the imaginary part of the complex modulus, or loss modulus. The components of the stiffness matrix, Q^*_{ijkl} can be written in terms of the complex moduli given in equations 27-29. For a general laminated plate, the components of the reduced stiffness matrix become

$$Q_{11}^* = \frac{E_1^*}{(1-\upsilon_{21}^* \upsilon_{12}^*)} \tag{30}$$

$$Q_{12}^* = \frac{\upsilon_{12}^* E_2^*}{(1-\upsilon_{21}^* \upsilon_{12}^*)} = \frac{\upsilon_{21}^* E_1^*}{(1-\upsilon_{21}^* \upsilon_{12}^*)} \tag{31}$$

$$Q_{22}^* = \frac{E_2^*}{(1-\upsilon_{21}^* \upsilon_{12}^*)} \tag{32}$$

$$Q_{66}^* = G_{12}^* \tag{33}$$

To determine the viscoelastic response of a general laminated composite, tensor transformations of the stiffness matrix is performed. These reduced stiffnesses are obtained by multiplying the Q^*_{ij} by the direction cosines. These values are given as

$$\bar{Q}_{11}^* = m^4 Q_{11}^* + 2m^2 n^2 [Q_{12}^* + 2Q_{66}^*] + n^4 Q_{22}^* \tag{34}$$

$$\bar{Q}_{12}^* = \bar{Q}_{21}^* = m^2 n^2 [Q_{11}^* + Q_{22}^* - 4Q_{66}^*] + (m^4 + n^4) Q_{12}^* \tag{35}$$

$$\bar{Q}_{22}^* = n^4 Q_{11}^* + 2m^2 n^2 [Q_{12}^* + 2Q_{66}^*] + m^4 Q_{22}^* \tag{36}$$

$$\bar{Q}^{*}_{16} = m^3 n [Q^{*}_{11} - Q^{*}_{12}] + m n^3 [Q^{*}_{12} - Q^{*}_{22}] - 2mn (m^2 - n^2) Q^{*}_{66} \quad (37)$$

$$\bar{Q}^{*}_{26} = m n^3 [Q^{*}_{11} - Q^{*}_{12}] + m^3 n [Q^{*}_{12} - Q^{*}_{22}] + 2mn (m^2 - n^2) Q^{*}_{66} \quad (38)$$

$$\bar{Q}^{*}_{66} = m^2 n^2 [Q^{*}_{11} + Q^{*}_{22} - 2Q^{*}_{66}] + (m^4 + n^4) Q^{*}_{66} \quad (39)$$

where m is the cosine of Θ and n is the sine of Θ where Θ is the angle the fibers make with the principle load direction.

The elastic response of a general laminated plate can then be defined in terms of these reduced stiffnesses as

$$A^{*}_{ij} = A'_{ij} + iA''_{ij} = \sum_{k=1}^{N} (\bar{Q}_{ij}' + i\bar{Q}_{ij}'')^{(k)} (h_k - h_{k-1}) \quad (40)$$

$$B^{*}_{ij} = B'_{ij} + iB''_{ij} = \frac{1}{2} \sum_{k=1}^{N} (\bar{Q}_{ij}' + i\bar{Q}_{ij}'')^{(k)} (h_k^2 - h_{k-1}^2) \quad (41)$$

$$D^{*}_{ij} = D'_{ij} + iD''_{ij} = \frac{1}{3} \sum_{k=1}^{N} (\bar{Q}_{ij}' + i\bar{Q}_{ij}'')^{(k)} (h_k^3 - h_{k-1}^3) \quad (42)$$

where h is the distance of the ply interface from the midplane of the composite laminate.

The manner in which the loss factor would be determined for a general laminated plate would be to determine the effective complex elastic constants. Taking the ratio of the imaginary to the real part of the effective modulus will result in the effective loss factor for the particular system. For example, the effective loss factor in tension could be estimated by using the relation for the effective longitudinal modulus,

$$E_x = \frac{A_{11}A_{22} - A_{12}^2}{hA_{22}} = \frac{1}{h\,A_{11}^{-1}} \tag{43}$$

and through the substitution of the complex quantities, the resulting loss factor can be determined using equation 5 as

$$\eta_x = \frac{E_x''}{E_x'} = \frac{A_{11}''^{-1}}{A_{11}'^{-1}} \tag{44}$$

In theory, the utilization of the elastic viscoelastic correspondence principle will allow for the determination of the damping loss factor of any general laminated plate of composite materials, including hybrid systems. An underlying assumption in the above development is that the matrix properties, and therefore the composite properties, are temperature and frequency dependent. As such, this frequency dependence should be carried through the analysis, yet is typically ignored in the literature. In addition, another major limitation to the theory is a lack of experimental information on the damping loss factor of the various composite systems which can be implemented into the above analysis.

The other macromechanics approach to determine the damping loss factor of a general laminated structure is through the computation of the strain energies. Many investigators have used this approach. A discussion of two variations of this technique are given below.

Plunkett (36) presents an analysis for predicting the damping loss factor of an isotropic homogeneous material. For general dynamic deformation, he states that the only

way to consistently define damping is to define it for the deformation state, which is exactly cyclic. For one cycle, the energy dissipation is given by

$$\Delta W(x) = \int_{t}^{t+T} \tau_{ij}(x,t) \frac{d\varepsilon_{ij}(t)}{dt} dt \tag{45}$$

where τ_{ij} is the shear stress as a function of position and time and ε_{ij} is the shear strain. This formulation determines the change in strain energy of the system over one cycle of vibration. Any losses due to the various damping mechanisms in the material will be included in the value of the strain energy. Since the deformation is exactly cyclic, the following stress relation holds:

$$\tau_{ij}(t + T, x) = \tau_{ij}(t, x) \tag{46}$$

The maximum strain energy of the system is determined to be

$$U(x) = \int_{0}^{\varepsilon_{max}} \tau_{ij}\, d\varepsilon_{ij} \tag{47}$$

Plunkett (36) then assumes that the strains are sinusoidal. Also, by expanding the stresses into a Fourier series, only the fundamental component of the stress contributes to the energy dissipation over one cycle, ΔW. Using this Fourier expansion and the elastic properties of the material, the stresses, even for an anisotropic material, can be written as

$$\tau_{ij} = C^{*}_{ijkl}\, \varepsilon_{kl} \tag{48}$$

where C^{*}_{ijkl} is the complex stiffness tensor. The local energy dissipation and the maximum strain energy can then be written as

$$\Delta W = \pi C''_{ijkl}\, \varepsilon_{ij}\, \varepsilon_{kl} \tag{49}$$

$$U = \frac{1}{2}\, C'_{ijkl}\, \varepsilon_{ij}\, \varepsilon_{kl} \tag{50}$$

where C'_{ijkl} and C''_{ijkl} are the real and complex parts of the complex modulus. Through further reductions, Plunkett (36) arrives at an analytical determination of the material's loss factor as

$$\eta_s = \frac{\Delta W}{2\pi U} \tag{51}$$

In this analysis, then, accurate determination of the complex modulus is required for the prediction of the damping loss factor. In composite materials, values of the loss modulus are not readily available for either the lamina or laminate.

Although the procedure is capable of analytically determining the loss factor, Plunkett (36) indicates that the values of the energy dissipation and the maximum strain energy at the particular location are not experimentally measurable quantities. It is necessary to integrate these values over the volume of the material, thus determining the system damping loss factor. This is the experimental quantity that is determined by the various test methods. Plunkett (36) points out that as a result, the loss factor measured in any experimental system determines the system damping loss factor and not the material damping loss factor.

Plunkett (36) indicates that if the damping is small enough, less than 0.1, then the out of phase stress is sufficiently small and therefore does not affect the in-phase vibratory

strain. Because this causes the mode shapes to remain the same, the nonlinear damping can be handled in the classical way, using equivalent damping coefficients, as long as the interaction is properly accounted for.

Plunkett (36) also compares the analytical predictions with experimental results of other investigators. He concludes that almost all of the energy dissipation in the composite materials tested is due to the strain field in the organic matrix materials, with some contribution by the fibers in the fiber direction.

Alam and Asnani (58) provide a more rigorous approach to the determination of the strain energy for a general laminated composite material. They point out that, currently, composites are dynamically analyzed by replacing the laminated plate structural characteristics with that of a homogeneous orthotropic material. Because of this, the true deformation of the individual layers may not be accurately represented. To account for this, Alam and Asnani (58) consider the elastic properties of each layer separately. In their analysis, they also consider the extension, bending, in-plane shear, and transverse shear deformations in each layer of the laminate.

They first determine the displacement at a point z from the mid plane of the i^{th} layer along the x and y directions respectively as

$$u_{z_i} = \frac{1}{2}(u_{i+1} + u_i) + \frac{z_i}{t_i}(u_{i+1} - u_i) \tag{52}$$

$$v_{z_i} = \frac{1}{2}(v_{i+1} + v_i) + \frac{z_i}{t_i}(v_{i+1} - v_i) \tag{53}$$

where u_i, v_i, u_{i+1}, and v_{i+1} are the displacements of the two surfaces of the i^{th} layer along the x and y directions respectively, and t_i is the thickness of the i^{th} layer. The strains are computed in the classical manner as the derivatives of the displacements. The resulting stresses are then determined from the strains by using the stiffness matrix, which has components of Q_{11}, Q_{12}, Q_{22}, Q_{66}, Q_{44}, and Q_{55}.

The strain energy of the system is then determined by summing the contributions of each layer to the strain energy, which is given by

$$U=\sum_{i=1,2}^{N}\int_0^b\int_0^a\int_{-\frac{t_i}{2}}^{\frac{t_i}{2}}\frac{1}{2}(\sigma_{xx,i}\varepsilon_{xx,i}+\sigma_{yy,i}\varepsilon_{yy,i}+\tau_{xy,i}\gamma_{xy,i}+\tau_{xz,i}\varepsilon_{xz,i}+\tau_{yz,i}\varepsilon_{yz,i})dz_i dx dy \tag{54}$$

where N is the total number of plies in the laminate and a and b are the lengths of the plate along the x and y directions respectively.

The kinetic energy of the plate is then determined from the displacements by the following equation

$$T=\sum_{i=1,2}^{N}\int_0^b\int_0^a\frac{1}{2}\rho_i t_i\left\{\dot{w}^2+\left(\frac{\dot{u}_i+\dot{u}_{i+1}}{2}\right)^2+\left(\frac{\dot{v}_i+\dot{v}_{i+1}}{2}\right)^2+\left(\frac{\dot{u}_i-\dot{u}_{i+1}}{2}\right)^2\frac{t_i^2}{12}+\left(\frac{\dot{v}_i-\dot{v}_{i+1}}{2}\right)^2\frac{t_i^2}{12}\right\}dxdy \tag{55}$$

where the $\dot{}$ is the time derivative.

The work done by the external excitation f(x,y)sin(wt) is the force times the displacement, given by

$$V = \int_0^b \int_0^a w\, f(x,y) \sin \omega t \quad dxdy \tag{56}$$

where the integration is carried out over the plane of the material.

The strain energy and the kinetic energy are next computed from the displacements and the normal stress transformations. They then utilize the Reissner Variational Theorem, which uses the kinetic and strain energies, and the work done by the system, and apply Hamilton's principle. The minimization process yields the governing equations of motion. From the governing equations and the boundary conditions, which must specify the initial displacement and velocity, the displacements are obtained as a functions of time and position.

In the series solution for the displacements that satisfy the boundary conditions, the real moduli are replaced by the complex moduli. The system is then solved as a complex eigenvalue problem. The real part of the complex eigenvalue is the resonant frequency parameter. The ratio of the imaginary to the real part of the complex eigenvalue is the system loss factor.

Again, the utility of this theory is limited due to the lack of experimental values for the complex modulus for composites. This theory also fails to take into consideration the frequency dependence of the material. Estimations were made on the loss factor of various fiber orientations using the above analysis. They assumed that the loss factor of the fiber was zero, while the loss factor of the matrix was assumed to be 0.5. Alam and Asnani(58) acknowledge that the material has a frequency, temperature and strain dependence which is

ignored in their analysis. The calculated loss factor results that were obtained for certain orientations were equal to the assumed loss factor of the resin. In practice, this level should never be approached, based on the volume fraction of the resin and configurations that are utilized. It is not known if the utilization of more appropriate values of the loss factor for the various orientations would result in more appropriate values for the various orientations. What is evident from this analytical effort is the need for appropriate experimental information which can be utilized in the model.

Two other results of the work of Alam and Asnani (58) are that the damping loss factor decreases with increasing thickness of a cross-ply material and that the damping loss factor increases with decreasing values of E_{11}/E_{22}. The first finding is consistent with the earlier work of Clary (16).

Structural Models

Approaches that have been used to determine the loss factor of composite structures have been to utilize finite element models to determine the energy dissipated and strain energy stored in the system. The following will present some of the variations that have been used for damping determination in composites.

Brockman(59) provides a summary of the finite element solution methodologies for determination of the damping loss factor of composites. Common to these techniques are the following assumptions: 1. displacements and strains are infinitesimal; 2. the material

behavior is linear and viscoelastic; 3. the steady-state viscoelastic behavior of the materials can be characterized by three parameters, namely the bulk modulus, shear modulus, and damping coefficient; 4. the applied loading varies sinusoidally with time.

With these assumptions, the strain displacement equations are given as

$$\varepsilon_{ij} = \frac{1}{2}\left(\frac{\partial u_i}{\partial x_j} + \frac{\partial u_j}{\partial x_i}\right) \tag{57}$$

the momentum and moment of momentum equations are

$$\frac{\partial \sigma_{ji}}{\partial x_j} + \rho \bar{b}_i = \rho \dot{v}_i \tag{58}$$

$$\sigma_{ij} = \sigma_{ji} \tag{59}$$

and the displacement and force boundary conditions are

$$u_i = \bar{u}_i \qquad \text{on } \partial V_u \tag{60}$$

$$\sigma_{ji}\, \eta_j = \bar{t}_i \qquad \text{on } \partial V_f \tag{61}$$

The assumption is made that each component of displacement varies sinusoidally with time at a given frequency, for both the free vibration and forced vibration at a single frequency. Thus, ui can be expressed in the product form

$$u_i (x_k, t) = U_i(x_k)\, e^{i\omega t} \tag{62}$$

The material model results in a linear relationship between stress and strain of the form

$$\sigma_{ij} = C_{ijkl}\,\varepsilon_{kl} \tag{63}$$

where C is the tensor for an isotropic material. The bulk and shear modulus are then assumed to be complex-valued. They are described as

$$G = G'(1 + \eta) \tag{64}$$

$$K = K'(1 + \eta) \tag{65}$$

In the above relationship, the damping loss factor that is used for both the shear and the bulk modulus is assumed to be the same. This use of a single loss factor by the finite element techniques is their major limitation for calculation of the composite damping loss factor. Although this limitation is acknowledged by most investigators, it is the result of the limitation of the source code. In addition, there are no provisions available to incorporate the frequency dependence of the material.

In addition, the strains and stresses are assumed to be complex-valued, with the real componen. denoting the in-phase contribution and the imaginary component denoting the out of phase component of the stress and strain.

A system of simultaneous equations, obtained from the finite element discretization, is then solved. These equations are of the form

$$([K] - \omega^2[M])\{U\} = \{F\} \tag{66}$$

where

[K] = system stiffness matrix (complex valued)

[M] = system mass matrix (real valued)

{U} = nodal displacements (complex valued)

{F} = nodal force amplitude (usually real valued)

ω = frequency of vibration

The solution techniques that are utilized to solve this system of equations are the complex eigenvalue solution, the frequency response solution, and the real eigenvalue solution. The complex eigenvalue solution solves for the frequency and mode shape by considering the unforced motion of the system, using the ratio of energy dissipated to energy stored for system loss factor determination. The frequency response solution solves the system of complex-valued linear equations, thereby obtaining the corresponding displacement shapes and plotting the resulting amplitude and phase quantities versus the forcing function at several frequencies, followed by the calculation of the energy dissipated and energy stored. The real eigenvalue solution solves the real eigenvalue problem for frequency and mode shape, assuming the system stiffness matrix to be real. By substitution of the damping loss factor of the material, the strain energy stored and dissipated by the system is determined.

Bert (60) presents a survey on the vibration damping of composite materials. He presents some of the analytical models that have been used to predict damping in

composites. Bert (60) notes that, to his knowledge, no analytical models available can predict the damping loss factor in composites in which the fibers are anisotropic. Graphite, boron and Kevlar fibers are anisotropic. Thus, according to Bert, the only composite system that presently can be modeled is one which utilizes glass fibers. Furthermore, the models that are available assume that the fibers are perfectly bonded to the matrix and that there is no interphase region around the fiber.

Bert (60) concludes that for designers concerned with the damping of composite materials, only trends are available for design considerations. Bert (60) says that to maximize the damping loss factor in a composite system, the designer must incorporate the effect of the fiber and matrix material, the volume fractions, orientations, and laminate arrangements into a model, although no currently available model incorporates these factors.

Summary

Two experimental techniques have predominated in the testing of the damping loss factor for composites: the forced vibration technique and the free vibration technique. Both techniques test the material in flexure. The impulse hammer method using the noncontacting eddy current probe appears to be the currently accepted premiere technique for experimentally determining the damping loss factor of composite materials.

The damping loss factor for composite materials has been shown experimentally to be dependent on the fiber angle, specimen thickness, the resin system used, the frequency of

test, the fiber volume fraction, fiber diameter, beam stiffness, state of damage in the material, and, in some cases, on the stress amplitude. A fiber angle of 45 degrees appears to maximize the damping loss factor with the other fiber orientations ranked as follows: 45 > 60 > 75 > 90 > 30 > 15 > 0. For the Kevlar/epoxy composite, however, the damping loss factor in the 0 and 90 degree directions were approximately equivalent. Polyester resin has a higher loss factor than epoxy. These resins can be ranked in order of decreasing damping loss factor as follows: Polyester > Fiberite 934 > Narmco 5208 > Narmco 5213. It should be noted here that the Fiberite 934 and Narmco 5208 are both high temperature curing epoxy, 350° F, with very similar mechanical properties. The type of fiber used also affects the damping loss factor. This can be due to the fiber's contribution to the damping or to the difference in the interface properties of the fiber and resin systems investigated. Increasing the fiber volume fraction, the fiber diameter, the specimen thickness, and the beam stiffness reduces the damping loss factor. In most cases, increasing the amount of damage in the material, the stress amplitude of test, or the frequency of test increases the damping loss factor. The maximum damping loss factor for glass/epoxy, graphite/epoxy, Kevlar/epoxy and glass polyester tested at 45 degrees are 110×10^{-4}, 325×10^{-4}, 190×10^{-4}, and 103×10^{-4} respectively. These results have to be viewed with caution since in no investigation was it indicated that the panels were inspected for quality. Since damage in the material will enhance the damping loss factor of the composite, it is unknown whether the indicated damping loss factor was the result of the particular characteristics of the material or the result of material quality.

The results that are summarized above indicate that there are numerous material constituent characteristics that affect the loss factor of the composite material. In addition, these investigations have not appropriately characterized the frequency dependence of this

viscoelastic material.

The theoretical models currently available to predict the damping loss factor for composites are inadequate for design purposes. Any micromechanical approach for determining the loss factor of composite laminae which could incorporate the material characteristics that have been shown to affect the loss factor and which could be experimentally validated would be virtually impossible. The macroscopic approaches do not account for the frequency dependence, i.e., the viscoelastic characteristic, of the material. In addition, there does not exist an adequate characterization of the material loss factor which could be utilized as input to these models. The structural approaches do not account for either the frequency dependence of the loss factor or the anisotropic variation in loss factor. This latter limitation may be the direct result of lack of appropriate input.

Chapter 3

ANALYTICAL MODEL DEVELOPMENT

There have been numerous approaches undertaken to determine the damping of composites. These approaches can be grouped into micromechanical, macromechanical and structural approaches. The most fundamental approach would derive the damping response of composites from the material constituents in an analogous manner to that in which the elastic behavior of composites is determined. This approach would provide the most utility. However, in addition to the characteristics of the material constituents, their interaction and physical characteristics have also been shown to affect their damping response. The incorporation of these effects as well as the necessary experimental validation of a micromechanical approach would be difficult if not virtually impossible.

In the structural analysis of composites, the fundamental building block is the composite lamina. The elastic response of the lamina incorporates the elastic response of the material constituents as well as their interaction and physical characteristics. Because of this, most composite design utilizes material characteristics of the lamina in lieu of the characteristics of the individual constituents. In addition, the lamina characteristics can be readily determined through numerous standardized test procedures.

In a similar vein, the determination of the damping of a composite from knowledge of the composite laminae damping characteristics will automatically incorporate the material constituent characteristics, e.g., the fiber diameter, fiber matrix interface, fiber and matrix loss factor, and fiber volume fraction. With knowledge of the anisotropic damping loss factors of the laminae, the damping response of a general laminated composite could then be determined. In addition, experimental techniques have been developed which can determine the laminae material loss factors. Therefore, one should be able to experimentally determine the material characteristics required for such a model. For these reasons, the approach that will be developed in this dissertation is a macromechanical approach.

There have been two approaches previously undertaken to model the macromechanical damping response of composites, the elastic viscoelastic correspondence principle and the strain energy approach. Of these two models, the elastic viscoelastic correspondence principle is the most utilitarian since fundamental parametric studies can be readily undertaken. This is the result of the model's ability to determine the fully populated complex reduced elastic stiffness matrices from the in-plane material complex elastic properties. As the model currently appears in the literature, there is one major material characteristic missing: the viscoelastic characteristic of the composite.

The polymer matrix material utilized in the composites materials discussed herein possesses temperature and frequency dependent damping loss factors, as illustrated in Figure 1. Because of this, the composite material should also exhibit a frequency and temperature dependent loss factor. In fact, in the discussion of the elastic viscoelastic

correspondence principle, many of the authors refer to this fact, yet omit its effect from the subsequent analysis. To provide a more accurate description of the damping of composites, their frequency dependence should be incorporated. The analytical model that will be developed in this dissertation will be a modification of the elastic viscoelastic correspondence principle to incorporate the frequency dependent anisotropic loss factor of the laminae for the analytical determination of the damping loss factor of a general laminated composite.

Macromechanical Model Development

The development of the elastic viscoelastic correspondence principle for composites has been given in Chapter 2. A detailed discussion of the development of this model for use with laminated plate theory will be presented. This is necessary to ensure that the principles associated with the elastic viscoelastic correspondence principle are not violated in the application to laminated plate theory.

The correspondence principle states that if the elastic solution for any dependent variable having a time varying component exists, then the viscoelastic problem can be solved by replacing the equations of the elastic material by the equations that describe the viscoelastic material. The principle can be applied if (1) the elastic solution is known, (2) no operation in obtaining the elastic solution has a corresponding operation in the viscoelastic solution that involves separating complex modulus into real and imaginary parts with the exception of the final determination of that response, and (3) the boundary

conditions for the elastic and viscoelastic cases are identical (61). These conditions are satisfied for the case of the vibrating beam.

Schapery (62,63) discusses the mathematical implications of the correspondence principle. If one performs the Laplace transform on the governing field and boundary equations with respect to time, they can be reduced so that they are mathematically equivalent to the elastic problem. Consider an isothermal problem, which is the same condition implemented in this dissertation. Schapery (62,63) begins his development using the fundamental constitutive relationship for linear viscoelastic materials which provides the relationship between stresses, σ_{ij}, and strains ε_{ij}, for a material with arbitrary degree of anisotropy. This relationship can be expressed as

$$\sigma_{ij} = \int_0^t C_{ij}^{kl}(t-\tau) \frac{\partial \varepsilon_{kl}}{\partial \tau} d\tau \tag{67}$$

Taking the Laplace Transform of equation 67 and through some simplifications, Schapery shows that the resulting equation becomes

$$\bar{\sigma}_{ij} = \tilde{C}_{ij}^{kl} \bar{\varepsilon}_{kl} \tag{68}$$

where the $\tilde{C}_{ij}^{kl}$ term is the product of the Laplace transform of C_{ij}^{kl} and the s term of the Laplace transform procedure. The time dependent equilibrium equations are given as

$$\frac{\partial \sigma_{ij}}{\partial x_j} + F_i = 0 \tag{69}$$

where F_i are the components of the prescribed body force vectors. The six strain displacement relations are given as

$$\varepsilon_{ij} = \frac{1}{2}\left(\frac{\partial u_i}{\partial x_j} + \frac{\partial u_j}{\partial x_i}\right) \tag{70}$$

Equations 67, 69 and 70 completely describe the viscoelastic body. It should be noted that in the above equations 69 and 70 that the dependent variables are actually functions of four independent variables, x_i and t. Equations 69 and 70 are then operated on by the Laplace transform, which yields

$$\frac{\partial \bar{\sigma}_{ij}}{\partial x_j} + \bar{F}_i = 0 \tag{71}$$

$$\bar{\varepsilon}_{ij} = \frac{1}{2}\left(\frac{\partial \bar{u}_i}{\partial x_j} + \frac{\partial \bar{u}_j}{\partial x_i}\right) \tag{72}$$

Christensen (64) shows that the time dependent solution for the dynamic and quasi-static problems can be readily obtained if an analytical solution to the associated elastic problem exists. In this case, the substitutions

$$\begin{aligned} \bar{C}_{ijkl} &\rightarrow C^{*}_{ijkl} & \bar{u}_i &\rightarrow u_i \equiv u_{iA}\, e^{i\omega t} \\ \bar{\sigma}_{ij} &\rightarrow \sigma_{ij} \equiv \sigma_{ijA}\, e^{i\omega t} & \bar{\varepsilon}_{ij} &\rightarrow \varepsilon_{ij} \equiv \varepsilon_{ijA}\, e^{i\omega t} \end{aligned} \tag{73}$$

can be made, where the subscript A denotes a time independent amplitude and ω is the frequency.

Hashin (35) extends this theory with further simplifications for composite materials. Letting F represent one of the elastic moduli of the composite, it can be described in terms of N phase properties as $F = F(p_j)$ where p_j are the phase properties for the composite.

These phase properties form the set of all elastic constants of all phases which are needed to predict the effective property F. The effective complex viscoelastic property is then given as

$$F^* = F(p_j^*) \tag{74}$$

where F is still the elasticity solution. Its arguments, however, are now complex phase properties. These complex phase properties can also be written as

$$p_j^* = p_j' [\, 1 + i\,\eta_j \,] \tag{75}$$

where p_j^* is the complex modulus. The effective modulus is then expanded in a multiple, complex Taylor series, using the real part of the complex phase property p_j' as the set of values about which the expansion is made. Assuming that all constituent loss factors are sufficiently small, the second and higher order terms in η_j can be neglected. This results in the Taylor expansion of F^* as

$$F^* = F' [\, 1 + i\,\eta] \equiv F' + iF'' \tag{76}$$

where F' is the elastic solution in terms of the real part of the phase properties. This development shows that with small damping, the effective complex properties can be derived directly from analytical elasticity solutions. If the constituent loss factors are not small, this same procedure can be used with a minor modification. In this case, second or possibly higher order terms in the Taylor series would need to be included, making the resulting equations much more complex. In the development that follows, then, the substitution of the viscoelastic comp. moduli, in the form given in equation 76 will be made.

An additional assumption that is made in this development is that the composite is linearly viscoelastic. A viscoelastic material possesses a time dependent elastic and viscous response to either an applied stress or strain loading. A linearly viscoelastic material is a subset of this having the property that the time dependent mechanical properties are independent of the level of stress or strain loading.

The local material behavior is governed by the elastic constitutive law as

$$\sigma_{ij} = C_{ijkl}\,\varepsilon_{kl} \tag{77}$$

In contracted notation, equation 77 can be expanded and written as

$$\begin{aligned}
\sigma_x &= C_{11}\varepsilon_x + C_{12}\varepsilon_y + C_{13}\varepsilon_z + C_{14}\gamma_{yz} + C_{15}\gamma_{zx} + C_{16}\gamma_{xy} \\
\sigma_y &= C_{21}\varepsilon_x + C_{22}\varepsilon_y + C_{23}\varepsilon_z + C_{24}\gamma_{yz} + C_{25}\gamma_{zx} + C_{26}\gamma_{xy} \\
&\vdots \quad \cdots \\
\tau_{xy} &= C_{61}\varepsilon_x + C_{62}\varepsilon_y + C_{63}\varepsilon_z + C_{64}\gamma_{yz} + C_{65}\gamma_{zx} + C_{66}\gamma_{xy}
\end{aligned} \tag{78}$$

The elastic viscoelastic correspondence principle can be applied to equations 77 and 78 since these equations meet the conditions stated in the principle. For the specific case of a vibrating beam, the stress and strain have time varying components. As such, σ_{ij} and ε_{ij} are given as

$$\varepsilon^* = \varepsilon_{ij}\, e^{i\omega t} \tag{79}$$

$$\sigma^* = \sigma_{ij}\, e^{i\omega t} \tag{80}$$

It is also assumed that the complex moduli are frequency dependent, consisting of a real and imaginary term, called the storage and loss modulus, respectively. It will be assumed that the storage modulus is independent of frequency. In the frequency range of interest, up to 1000 Hz., this is a very good approximation based on the work of other investigators (27,35,41,64). The frequency dependence of the complex modulus is therefore the result of the frequency dependence of the loss modulus. This frequency dependence of the loss modulus is the result of the frequency dependence of the loss modulus of the matrix material which has been been shown to occur by various investigators (1,2,3,64). As such, using the elastic viscoelastic correspondence principle, equation 77 is given as

$$\sigma_{ij}^{*} = C_{ijkl}^{*} \varepsilon_{kl}^{*} \tag{81}$$

where

$$C_{ijkl}^{*} = C_{ijkl}^{Real} + i\, C_{ijkl}^{Imag}(f) \tag{82}$$

Two assumptions are now made. First, that the fiber composite material can be approximated as a homogeneous material with orthotropic material properties. This reduces the number of elastic constants given by equations 77 and 81 from 36 to 9. A second assumption is that the material is in a state of plane stress assumption, where the stresses normal to the plane of the plate are assumed to be zero, i.e. $\sigma_3 = \tau_{23} = \tau_{13} = 0$. Without loss in generality, the time-varying components of the stress, $\sigma_3 e^{i\omega t} = \tau_{23} e^{i\omega t} = \tau_{13} e^{i\omega t}$ can likewise be assumed to be zero. This assumption further reduces the number of elastic constants to 4 independent values. The viscoelastic constitutive relationships can now be expressed as

$$\sigma_x^* = Q_{11}^* \varepsilon_x^* + Q_{12}^* \varepsilon_y^* + Q_{16}^* \gamma_{xy}^* \tag{83}$$

$$\sigma_y^* = Q_{21}^* \varepsilon_x^* + Q_{22}^* \varepsilon_y^* + Q_{26}^* \gamma_{xy}^* \tag{84}$$

$$\tau_{xy}^* = Q_{61}^* \varepsilon_x^* + Q_{62}^* \varepsilon_y^* + Q_{66}^* \gamma_{xy}^* \tag{85}$$

Equations 83-85 reduce to the elastic case if there is no frequency variation in stresses and strains. This is equivalent to setting the frequency equal to 0. As such, the time varying component for $\omega = 0$ gives the result that $e^{i\omega t} = 1$. In this case equations 83-85 become

$$\sigma_x = Q_{11}\varepsilon_x + Q_{12}\varepsilon_y + Q_{16}\gamma_{xy} \tag{86}$$

$$\sigma_y = Q_{21}\varepsilon_x + Q_{22}\varepsilon_y + Q_{26}\gamma_{xy} \tag{87}$$

$$\tau_{12} = Q_{61}\varepsilon_x + Q_{62}\varepsilon_y + Q_{66}\gamma_{xy} \tag{88}$$

The flat plate may be acted upon by applied moments, M, distributed applied loads, q, in-plane loads, N, and point loads P. It is assumed that the plate consists of multiple layers of composite laminae, with the fibers in each plate being parallel to the plane of the plate. Kirchhoff's hypothesis is then applied to the plate, i.e. lines that are straight and normal to the laminate's geometric mid-surface remain straight and normal to this geometric midplane and do not change length. This means that the lamina interfaces remain parallel to each other after application of the applied loads. It is therefore possible to express the displacement of the material points which lie along a line perpendicular to the laminates geometric midsurface in terms of the displacement and rotation of the point on the line located at the laminates geometric midplane. The implication of this hypothesis is that the displacement at any point (x,y,z) depends linearly on z. The time dependent displacement

in the x, y and z directions, given as u^*, v^* and w^* respectively, can be written in terms of the midplane displacements denoted by the ^{o} superscript, as

$$u^*(x,y,z) = u^o(x,y)\, e^{i\omega t} - z\,\frac{\partial w^o(x,y)}{\partial x}\, e^{i\omega t} \tag{89}$$

$$v^*(x,y,z) = v^o(x,y)\, e^{i\omega t} - z\,\frac{\partial w^o(x,y)}{\partial y}\, e^{i\omega t} \tag{90}$$

$$w^*(x,y,z) = w^o(x,y)\, e^{i\omega t} \tag{91}$$

In the case where these displacements do not vary with time, equations 89-91 reduce to the elastic case, again making use of the fact that $e^{i\omega t} = 1$ for $\omega = 0$. These displacements are then given as

$$u(x,y,z) = u^o(x,y) - z\,\frac{\partial w^o(x,y)}{\partial x} \tag{92}$$

$$v(x,y,z) = v^o(x,y) - z\,\frac{\partial w^o(x,y)}{\partial y} \tag{93}$$

$$w(x,y,z) = w^o(x,y) \tag{94}$$

The effect of Kirchhoff's hypothesis on the strain response, using the definition of the strain in the x direction on equation 89, results in

$$\varepsilon_x^* = \frac{\partial u^*(x,y,z)}{\partial x} = \frac{\partial u^o(x,y)\, e^{i\omega t}}{\partial x} - z\,\frac{\partial^2 w^o(x,y)}{\partial x^2}\, e^{i\omega t} = \left(\frac{\partial u^o(x,y)}{\partial x} - z\,\frac{\partial^2 w^o(x,y)}{\partial x^2}\right) e^{i\omega t} \tag{95}$$

The frequency independent strain is readily seen to result from the last equality, giving

$$\varepsilon_x(x,y,z) = \frac{\partial u(x,y,z)}{\partial x} = \frac{\partial\, u^o(x,y)}{\partial x} - z\,\frac{\partial^2 w^o(x,y)}{\partial x^2} \tag{96}$$

In equation 95, the first term in the last equality is due to the extensional strain of the reference surface. The second term is the curvature of the reference surface in the x direction since the material is limited to small rotations, which will henceforth be given by κ_i^o. Using this information, equation 96 can be rewritten as

$$\varepsilon_x^*(x,y,z) = \varepsilon_x^o(x,y)e^{i\omega t} + z\,\kappa_x^o(x,y)e^{i\omega t} \tag{97}$$

This again reduces that the classical case when the frequency is set equal to zero as

$$\varepsilon_x(x,y,z) = \varepsilon_x^o(x,y) + z\,\kappa_x^o(x,y) \tag{98}$$

In an analogous manner, the time dependent strain in the y direction can be determined using equations 90 in the same manner that the strain in the x direction was determined. This development results in the transverse strain given as

$$\varepsilon_y^* = \frac{\partial v^*(x,y,z)}{\partial y} = \frac{\partial v^o(x,y)\,e^{i\omega t}}{\partial y} - z\,\frac{\partial^2 w^o(x,y)}{\partial y^2}\,e^{i\omega t} = \left(\frac{\partial v^o(x,y)}{\partial y} - z\,\frac{\partial^2 w^o(x,y)}{\partial y^2}\right)e^{i\omega t} \tag{99}$$

The resultant frequency independent transverse strain is derived from equation 99 as

$$\varepsilon_y(x,y,z) = \frac{\partial v(x,y,z)}{\partial y} = \frac{\partial\, v^o(x,y)}{\partial y} - z\,\frac{\partial^2 w^o(x,y)}{\partial y^2} \tag{100}$$

In equations 99 and 100, the first term in the last equality is the result of the extensional strain of the reference surface. The second term is the curvature of the reference surface in the y direction since the material is limited to small rotations. Using this information, equations 99 and 100 can be rewritten as

$$\varepsilon_y^*(x,y,z) = \varepsilon_y^o(x,y)e^{i\omega t} + z\,\kappa_y^o(x,y)e^{i\omega t} \tag{101}$$

$$\varepsilon_y(x,y,z) = \varepsilon_y^o(x,y) + z\,\kappa_y^o(x,y) \tag{102}$$

Similarly, using the definition of the in-plane shear strains, the complex and conventional in-plane shear strains are given as

$$\gamma_{xy}^* = \frac{\partial v^*(x,y,z)}{\partial x} + \frac{\partial u^*(x,y,z)}{\partial y} = \gamma_{xy}^o e^{i\omega t} + z\,\kappa_{xy}^o e^{i\omega t} \tag{103}$$

$$\gamma_{xy}(x,y,z) = \frac{\partial v(x,y,z)}{\partial x} + \frac{\partial u(x,y,z)}{\partial y} = \gamma_{xy}^o + z\,\kappa_{xy}^o \tag{104}$$

Using the strains which were obtained using the Kirchhoff hypothesis, equations 83-85 can be written in the alternative form

$$\begin{Vmatrix} \sigma_x^* \\ \sigma_y^* \\ \tau_{xy}^* \end{Vmatrix} = \begin{Vmatrix} \bar{Q}_{11}^* & \bar{Q}_{12}^* & \bar{Q}_{16}^* \\ \bar{Q}_{12}^* & \bar{Q}_{22}^* & \bar{Q}_{26}^* \\ \bar{Q}_{16}^* & \bar{Q}_{26}^* & \bar{Q}_{66}^* \end{Vmatrix} \begin{Vmatrix} \varepsilon_x^o + z\,\kappa_x^o \\ \varepsilon_y^o + z\,\kappa_y^o \\ \gamma_{xy}^o + z\,\kappa_{xy}^o \end{Vmatrix} e^{i\omega t} \tag{105}$$

where σ_i^* are the frequency dependent stresses as given in equation 80. These relationships again clearly reduce to the general elastic case when the frequency dependence is taken to be zero. The resulting relations are given below.

$$\begin{Vmatrix} \sigma_x \\ \sigma_y \\ \tau_{xy} \end{Vmatrix} = \begin{vmatrix} \bar{Q}_{11} & \bar{Q}_{12} & \bar{Q}_{16} \\ \bar{Q}_{12} & \bar{Q}_{22} & \bar{Q}_{26} \\ \bar{Q}_{16} & \bar{Q}_{26} & \bar{Q}_{66} \end{vmatrix} \begin{Vmatrix} \varepsilon_x^o + z\,\kappa_x^o \\ \varepsilon_y^o + z\,\kappa_y^o \\ \gamma_{xy}^o + z\,\kappa_{xy}^o \end{Vmatrix} \tag{106}$$

The Q_{ij}, both real and complex, are the reduced stiffnesses for a composite with arbitrary fiber orientation.

The frequency dependent force and moment resultants are now defined as

$$(N_x, N_y, N_{xy})e^{i\omega t} = \int_{-\frac{h}{2}}^{\frac{h}{2}} (\sigma_x^*, \sigma_y^*, \tau_{xy}^*)\,dz = \int_{-\frac{h}{2}}^{\frac{h}{2}} (\sigma_x, \sigma_y, \tau_{xy})e^{i\omega t}\,dz \tag{107}$$

$$(M_x, M_y, M_{xy})e^{i\omega t} = \int_{-\frac{h}{2}}^{\frac{h}{2}} (\sigma_x^*, \sigma_y^*, \tau_{xy}^*)\,z\,dz = \int_{-\frac{h}{2}}^{\frac{h}{2}} (\sigma_x, \sigma_y, \tau_{xy})e^{i\omega t}\,z\,dz \tag{108}$$

where h is the laminate thickness. These reduce to the analogous elastic case by letting ω equal zero. This then gives the force and moment resultants as

$$(N_x, N_y, N_{xy}) = \int_{-\frac{h}{2}}^{\frac{h}{2}} (\sigma_x, \sigma_y, \tau_{xy})\,dz \tag{109}$$

$$(M_x, M_y, M_{xy}) = \int_{-\frac{h}{2}}^{\frac{h}{2}} (\sigma_x, \sigma_y, \tau_{xy})\, z\, dz \tag{110}$$

The substitution of equation 105 into equation 107 yields for the time varying or complex normal force in the x direction

$$N_x e^{i\omega t} = \int_{-\frac{h}{2}}^{\frac{h}{2}} [\bar{Q}_{11}^{*}(\varepsilon_x^o + z\,\kappa_x^o) + \bar{Q}_{12}^{*}(\varepsilon_y^o + z\,\kappa_y^o) + \bar{Q}_{16}^{*}(\gamma_{xy}^o + z\,\kappa_{xy}^o)]\, e^{i\omega t}\, dz \tag{111}$$

which is seen to reduce in the frequency independent case to the classical force resultant

$$N_x = \int_{-\frac{h}{2}}^{\frac{h}{2}} [\bar{Q}_{11}(\varepsilon_x^o + z\,\kappa_x^o) + \bar{Q}_{12}(\varepsilon_y^o + z\,\kappa_y^o) + \bar{Q}_{16}(\gamma_{xy}^o + z\,\kappa_{xy}^o)]\, dz \tag{112}$$

The integrand in equation 111 can be distributed over the six resultant terms. In addition, the strains and curvatures can be taken outside the integral since they are not functions of position z. Further simplifications can be made by considering each of the integrals separately. The first integral in equation 111 is given as

$$\varepsilon_x^o\, e^{i\omega t} \int_{-\frac{h}{2}}^{\frac{h}{2}} \bar{Q}_{11}^{*}\, dz \tag{113}$$

The reduced stiffnesses are material properties which vary from layer to layer but are constant within any given layer. Since the reduced stiffnesses are piecewise constant, the integral can be expanded through the thickness to give

$$\int_{-\frac{h}{2}}^{\frac{h}{2}} \bar{Q}_{11}^{*} dz = \int_{z_0}^{z_1} \bar{Q}_{11_1}^{*} dz + \int_{z_1}^{z_2} \bar{Q}_{11_2}^{*} dz + \ldots + \int_{z_{N-1}}^{z_N} \bar{Q}_{11_N}^{*} dz \tag{114}$$

Since each of the Qij are only functions of frequency within the integral, they can be taken out of the integration. The integration then becomes simply the thickness of the particular layer of the materiai. Equation 114 can be written as a finite summation, given as

$$\int_{-\frac{h}{2}}^{\frac{h}{2}} \bar{Q}_{11}^{*} dz = \sum_{k=1}^{N} \bar{Q}_{11_k}^{*} (z_k - z_{k-1}) \tag{115}$$

In the classical elastic case, this is typically denoted as A_{11}. As such, this term will be denoted as A_{11}^{*}.

The same procedure can be applied to the other terms of equation 107 with similar reductions being made. The mathematical manipulations performed do not violate any fundamental principles. The results are presented below

$$\int_{-\frac{h}{2}}^{\frac{h}{2}} \bar{Q}_{12}^{*} dz = A_{12}^{*} = \sum_{k=1}^{N} \bar{Q}_{12_k}^{*} (z_k - z_{k-1}) \tag{116}$$

$$\int_{-\frac{h}{2}}^{\frac{h}{2}} \bar{Q}_{16}^{*} dz = A_{16}^{*} = \sum_{k=1}^{N} \bar{Q}_{16_k}^{*} (z_k - z_{k-1}) \tag{117}$$

$$\int_{-\frac{h}{2}}^{\frac{h}{2}} \bar{Q}_{11}^{*} z \, dz = B_{11}^{*} = \sum_{k=1}^{N} \bar{Q}_{11_k}^{*} (z_k^2 - z_{k-1}^2) \tag{118}$$

$$\int_{-\frac{h}{2}}^{\frac{h}{2}} \bar{Q}_{12}^{*} z \, dz = B_{12}^{*} = \sum_{k=1}^{N} \bar{Q}_{12_k}^{*} (z_k^2 - z_{k-1}^2) \tag{119}$$

$$\int_{-\frac{h}{2}}^{\frac{h}{2}} \bar{Q}_{16}^{*} z \, dz = B_{16}^{*} = \sum_{k=1}^{N} \bar{Q}_{16_k}^{*} (z_k^2 - z_{k-1}^2) \tag{120}$$

With the utilization of equation 82, it is readily seen that equations 116-120 reduce to the classical elastic case when there is no frequency dependence.

Continuing this process for the moment resultants, the frequency dependent complex general laminated plate theory reduced stiffness matrix can be determined. Since the development is straightforward, involving only simple mathematical manipulations, all that will be given here is the summary of the results in contracted notation.

$$A_{ij}^{*} = \sum_{k=1}^{N} \bar{Q}_{ij_k}^{*} (z_k - z_{k-1}) \tag{121}$$

$$B_{ij}^{*} = \sum_{k=1}^{N} \bar{Q}_{ij_k}^{*} (z_k^2 - z_{k-1}^2) \tag{122}$$

$$D_{ij}^{*} = \sum_{k=1}^{N} \bar{Q}_{ij_k}^{*} (z_k^3 - z_{k-1}^3) \tag{123}$$

In matrix form, the above frequency dependent or complex reduced elastic constants are used to relate the in-plane stresses to strains. The specific relationship is given as

$$\left|\begin{array}{c} N_x(f) \\ N_y(f) \\ N_{xy}(f) \\ \hline M_x(f) \\ M_y(f) \\ M_{xy}(f) \end{array}\right| = \left|\begin{array}{ccc|ccc} A_{11}^*(f) & A_{12}^*(f) & A_{16}^*(f) & B_{11}^*(f) & B_{12}^*(f) & B_{16}^*(f) \\ A_{12}^*(f) & A_{22}^*(f) & A_{26}^*(f) & B_{12}^*(f) & B_{22}^*(f) & B_{26}^*(f) \\ A_{16}^*(f) & A_{26}^*(f) & A_{66}^*(f) & B_{16}^*(f) & B_{26}^*(f) & B_{66}^*(f) \\ \hline B_{11}^*(f) & B_{12}^*(f) & B_{16}^*(f) & D_{11}^*(f) & D_{12}^*(f) & D_{16}^*(f) \\ B_{12}^*(f) & B_{22}^*(f) & B_{26}^*(f) & D_{12}^*(f) & D_{22}^*(f) & D_{26}^*(f) \\ B_{16}^*(f) & B_{26}^*(f) & B_{66}^*(f) & D_{16}^*(f) & D_{26}^*(f) & D_{66}^*(f) \end{array}\right| \left|\begin{array}{c} \varepsilon_x^o(f) \\ \varepsilon_y^o(f) \\ \gamma_{xy}^o(f) \\ \hline \kappa_x^o(f) \\ \kappa_y^o(f) \\ \kappa_{xy}^o(f) \end{array}\right| \tag{124}$$

The A_{ij}^*, B_{ij}^*, and D_{ij}^* terms are funtions of the the Q_{ij} terms. The Q_{ij} terms are functions of the elastic constants. This can be seen by using equations 83-85 with a uniaxial composite laminate. Using the relationship given in equation 3 that the loss factor η is the ratio of the imaginary to real part of the elastic moduli, and the development of Hashin(35) which was given in equation 76, the relationship of the Q_{ij}'s in terms of elastic constants can be written as

$$Q_{11}^*(f) = \frac{E_{11}^*(f)}{(1-\upsilon_{21}^*\upsilon_{12}^*)} = \frac{E_{11}(1+i\,\eta_{11}(f))}{(1-\upsilon_{21}^*\upsilon_{12}^*)} \tag{125}$$

$$Q_{12}^*(f) = \frac{\upsilon_{12}^* E_2^*(f)}{(1-\upsilon_{21}^*\upsilon_{12}^*)} = \frac{\upsilon_{21}^* E_1^*(f)}{(1-\upsilon_{21}^*\upsilon_{12}^*)} = \frac{\upsilon_{21}^* E_1(1+\eta_{11}(f))}{(1-\upsilon_{21}^*\upsilon_{12}^*)} \tag{126}$$

$$Q_{22}^*(f) = \frac{E_2^*(f)}{(1-\upsilon_{21}^*\upsilon_{12}^*)} = \frac{E_{22}(1+i\,\eta_{22}(f))}{(1-\upsilon_{21}^*\upsilon_{12}^*)} \tag{127}$$

$$Q_{66}^*(f) = G_{12}^*(f) = G_{12}(1+i\,\eta_{12}(f)) \tag{128}$$

where the * denotes a complex value. Equations 125-128 will reduce to the classical elastic case when there is no frequency dependence.

In equations 125-128, all of the elastic constants can be readily determined through various experimental procedures that have been discussed in Chapter 2, with the exception of the complex Poisson's ratios. Since there have been no experimental techniques identified to determine the complex Poisson's ratios, two assumptions will be made concerning them. First, it is assumed that the Poisson's ratios are independent of frequency. Secondly, it is assumed that they are real. The consequences of these assumptions will be discussed in Chapter 6. There it will be shown that this assumption results in only minor differences in the resultant analytical response of the material.

These stiffness terms are the basic building blocks for the analysis of the frequency response of a general laminated plate. Using this information developed for the unidirectional material characteristics, the response of a general laminated composite material can be determined using conventional tensor transformations. The transformed reduced stiffnesses can be determined as

$$\bar{Q}^{*}_{11}(f) = m^4 Q^{*}_{11}(f) + 2 m^2 n^2 [Q^{*}_{12}(f) + 2 Q^{*}_{66}(f)] + n^4 Q^{*}_{22}(f) \tag{129}$$

$$\bar{Q}^{*}_{21}(f) = \bar{Q}^{*}_{12}(f) = m^2 n^2 [Q^{*}_{11}(f) + Q^{*}_{22}(f) - 4 Q^{*}_{66}(f)] + (m^4 + n^4) Q^{*}_{12}(f) \tag{130}$$

$$\bar{Q}^{*}_{22}(f) = n^4 Q^{*}_{11}(f) + 2 m^2 n^2 [Q^{*}_{12}(f) + 2 Q^{*}_{66}(f)] + m^4 Q^{*}_{22}(f) \tag{131}$$

$$\bar{Q}^{*}_{16} = m^3 n [Q^{*}_{11}(f) - Q^{*}_{12}(f) - 2Q^{*}_{66}(f)] + m n^3 [Q^{*}_{12}(f) - Q^{*}_{22}(f) + 2Q^{*}_{66}(f)] \tag{132}$$

$$\bar{Q}^{*}_{26} = m n^3 [Q^{*}_{11}(f) - Q^{*}_{12}(f) - 2Q^{*}_{66}(f)] + m^3 n [Q^{*}_{12}(f) - Q^{*}_{22}(f) + 2Q^{*}_{66}(f)] \tag{133}$$

$$\bar{Q}_{66}^{*} = m^2 n^2 [Q_{11}^{*}(f) + Q_{22}^{*}(f) - 2Q_{12}^{*}(f) - 2Q_{66}^{*}(f)] + (m^4 + n^4) Q_{66}^{*}(f) \quad (134)$$

where m is the cosine of Θ and n is the sine of Θ, and Θ is the angle the fibers make to the principle loading direction of the laminate. For the general laminate, the extensional, coupling and bending stiffness matrices can be determined from the $\bar{Q}_{ij}^{*}$ terms. In contracted notation, the explicit frequency dependence of A_{ij}^{*}, B_{ij}^{*}, and D_{ij}^{*} are defined as

$$A_{ij}^{*}(f) = A_{ij}^{'} + iA_{ij}^{''}(f) = \sum_{k=1}^{N} (\bar{Q}_{ij}^{*}(f))^{(n)} (h_n - h_{n-1}) \quad (135)$$

$$B_{ij}^{*}(f) = B_{ij}^{'} + iB_{ij}^{''}(f) = \frac{1}{2} \sum_{k=1}^{N} (\bar{Q}_{ij}^{*}(f))^{(n)} (h_n^2 - h_{n-1}^2) \quad (136)$$

$$D_{ij}^{*}(f) = D_{ij}^{'} + iD_{ij}^{''}(f) = \frac{1}{3} \sum_{n=1}^{N} (\bar{Q}_{ij}^{*}(f))^{(n)} (h_n^3 - h_{n-1}^3) \quad (137)$$

From the reduced stiffness matrix, the loss factor of a general laminated plate can be determined. This is readily done by utilizing the relationship given in equation 3. The relationship states that the loss factor is the ratio of the imaginary to the real part of the complex moduli. Other investigators have utilized a similar development. In their work, however, the frequency dependent loss modulus is not accounted for. Another assumption that is made in their efforts is in the determination of the laminated composite loss factors. Their development indicates that the effective loss factor in tension, for example, is given as

$$\eta_x = \frac{A''_{11}}{A'_{11}} \tag{138}$$

where A''_{11} is the imaginary part of A^*_{11} and A'_{11} is the real part of A^*_{11} (55). The assumption that is being made here is that the effective stiffness of the laminate is given as

$$E^*_x = \frac{A'_{11} + i\,A''_{11}}{h} \tag{139}$$

In actuality, the effective moduli is determined from the ABD inverse matrix. The inverse ABD matrix takes into account the stress couplings that may occur from the various orientations of the fibers used in the laminate. As such, the effective moduli is given as

$$E^*_x = \frac{1}{h\,(A'^{-1}_{11} + A''^{-1}_{11})} \tag{140}$$

Using this correct formulation of the effective extensional moduli of the composite the material effective loss factor is given as

$$\eta_x = \frac{A'^{-1}_{11}}{A'^{-1}_{11}} \tag{141}$$

Similarly, the transverse modulus is again given in terms of the inverse ABD matrix as

$$E^*_y = \frac{1}{h\,A^{*-1}_{22}} \tag{142}$$

Using the relationship for the loss factor from equation 3, the transverse loss factor is then given as

$$\eta_y = \frac{A_{22}^{*-1}}{A_{22}^{'-1}} \tag{143}$$

In a similar manner, the other components of the inverse ABD matrix can be used to determine the loss factor in shear, η_{xy} of the laminate.

In the typical cantilever beam testing of a general laminated composite sample, the effective bending stiffness will govern the beam motion. For the 0° and 90° composite orientations, the stiffness of the beam in bending is equal to the modulus of the material in that direction, or can be described as E_x. However, in the case of the general laminated beam, the beam motion will be governed by the effective bending stiffness of the specific construction. It has been shown analytically and experimentally that the effective bending stiffness of a general laminated beam is given as (65)

$$E_{effective_{bending}} = \frac{12}{h^3 D_{11}^{-1}} \tag{144}$$

where h is the beam thickness. Following the same lines of reasoning as given above, in complex notation, the complex effective bending stiffness is given as

$$E^*_{effective_{bending}} = \frac{12}{h^3 D_{11}^{*-1}} \tag{145}$$

With the effective bending stiffness determined, the loss factor as a function of frequency can be determined as the ratio of the complex to real parts of the value, or

$$\eta_{bending}(f) = \frac{E''_{effective_{bending}}(f)}{E'_{effective_{bending}}} \tag{146}$$

where

$$E^{*}_{effective_{bending}}(f) = E'_{effective_{bending}} + i\, E''_{effective_{bending}}(f) \tag{147}$$

For a general laminated beam, then, the loss factor can be analytically determined by first determining the material complex elastic moduli through cantilever beam testing over the frequency range of interest. The complex reduced stiffnesses can then be determined as given above. Depending on the type of test method utilized, the longitudinal, transverse or bending loss factor can then be determined using equations 141, 143, 146, respectively.

Although the use of the elastic viscoelastic correspondence principle has been proposed for use with composites to predict the loss factor, the incorporation of the frequency effect of the material constituents has not been attempted. The most probable reason for this is twofold. First, there does not appear to have been a complete loss factor characterization performed on any composite system, as was evident from the discussion in the Chapter 2. Typically, the investigators reported a loss factor at a specific frequency. The frequency of test was dependent on the specific geometry and material used. To carry out a complete characterization is both time consuming and expensive. Secondly, the mathematics of complex matrix manipulation is quite difficult and is not easily done by hand. Matrix manipulation using computers has been feasible, using real variables. However, the incorporation of complex terms into the matrix manipulations has until recently been difficult, if not impossible. With the advent of symbolic manipulators such as Mathematica$_{TM}$, this type of manipulation can now be readily performed.

Chapter 4

DEVELOPMENT OF EXPERIMENTAL TECHNIQUE

The proposed analytical model requires as input the in-plane damping loss factors of the composite, η_{11}, η_{12} and η_{22}. An experimental technique that can determine these loss factors was designed and developed using various aspects of techniques that were previously described in the Chapter 2. One decision made in considering the design of a technique was that only one testing methodology would be utilized. It was felt that this would keep constant any errors associated with the test procedure.

There have been numerous techniques utilized to experimentally determine the vibration damping loss factor of composites, as was previously detailed in the Chapter 2. Of these techniques, those used most recently are the forced resonant vibration technique(30,41) and the impulse technique(47,48,66), of which the impulse technique appears to be the most widely accepted. In the impulse technique, the specimen is normally held in a cantilever beam configuration, and is excited via an impact near the clamped end. The beam response is measured using either accelerometers or a noncontact eddy current probe. From the beam displacement versus time information, the frequency response function is determined. The data reduction scheme that is then typically employed to determine the damping loss factor is the half power band width method.

The impulse technique uses a cantilever beam specimen configuration for loss factor determination. To determine the loss factors η_{11} and η_{22} for the composite, unidirectional 0° and 90° specimens, respectively can be used. To determine η_{12} a specimen orientation of $\pm$45° will be used as an initial estimate. These experimental values will later be used to determine a more accurate estimate of η_{12} by using the analytical model along with these experimental values to back calculate the shear loss loss factor. This will be discussed in further detail in Chapter 6.

The manner in which the sample is supported is of vital importance to the accurate determination of the material damping loss factor. Care must be taken to ensure that the fixturing and materials used in the apparatus dissipate a minimal amount of energy. Losses that can occur at the clamping area include frictional losses and dissipation by any interface material used between the specimen and clamp block.

There are numerous technical reasons why the impulse technique has gained wide acceptance for testing composites. First, all vibrational frequencies are excited when the specimen is subjected to an impact. The fundamental frequencies and the various modes of vibration can therefore be investigated using a single specimen. This can be accomplished by determining the loss factor of the various modes of vibration for a single beam length or by varying the beam length to obtain different resonant frequencies. Secondly, to minimize external energy losses from such sources as friction at the clamped region or from aerodynamic damping, beam tip displacements must be minimized. For low frequencies, which are of major concern for various structural applications, placing the beam into resonant forced vibration usually results in large tip displacements. The damping loss

factor that is determined may be a combination of the material internal damping and external losses. This information would therefore be of little use for design purposes. With an impulse excitation, minimal force levels can still be used with resultant tip displacements being kept to a minimum.

The following will describe the experimental apparatus designed and developed for the experimental determination of the damping loss factors for composite materials, including both the fixturing and the hardware and software used for data acquisition. In addition, the results of the experimental calibration of this system are reported. This testing utilizes 2024 T-4 aluminum beams as the calibration specimen. The 2024 T-4 aluminum was chosen because it has been well characterized experimentally and has been shown to analytically follow Zener thermoelastic theory (26,62) for the damping loss factor as a function of frequency (8, 63).

Experimental Apparatus

For vibration damping testing, there are two primary considerations when designing fixturing for testing materials. First, it is necessary that the specimen be isolated from its surroundings. No vibrational energy from external sources should be allowed to influence the vibrational response of the specimen being tested. Accomplishment of this likewise infers that the vibrational energy imparted to the specimen will not be dissipated by the fixturing due to an energy transfer from the specimen. Secondly, care must be taken to minimize all other possible sources of energy dissipation so that the measured damping is the material inherent damping loss factor. Two prevalent sources for external energy

dissipation which should be minimized are frictional losses at the clamping egions(67) and aerodynamic damping (30,37,41,68,69).

In order to isolate the specimen from the surroundings, the specimen fixturing was attached to the load frame of a Sontag fatigue test machine, model SF-1U. This machine consists of a 36 x 36 x 3 in. solid steel top attachment plate to which the components for fatigue testing are attached. The entire system is isolated from the machine frame via four springs, effectively isolating it from the surroundings. In addition, the mass of this support system is several hundred pounds, which was experimentally shown to be not easily excited by the impulse excitation, the vibration of the test specimens, or other external energy sources.

The fixturing that was designed and fabricated for this program and used in subsequent testing of the composite materials is shown in Figure 10. This consists of a steel base plate, 12 x 16 x 1 in., which is bolted to the top plate of the Sontag machine with four 0.75 in. diameter bolts. A solid aluminum breadboard is then bolted to this plate with four screws. The breadboard consists of a 12 x 12 inch plate with 1/4-20 mounting holes on a 1 inch spaced square pattern starting 1.5 inches from the edge. This breadboard allows for easy accurate positioning of the eddy current probe. A 8 x 14 x 1.25 in. vertical support plate is bolted to the 12 x 16 in. base plate at one end of the base plate. This vertical support plate has two machined 12 inch long 0.75 in slots which are centered 6 in. apart. A movable attachment block, which consists of a 7 x 1.25 x 1.25 in steel bar, is then bolted to the support plate using two 0.75 in. bolts. Two 0.75 in. diameter holes are machined into this attachment block to accept two tool steel guide rods 5 in. in length. A

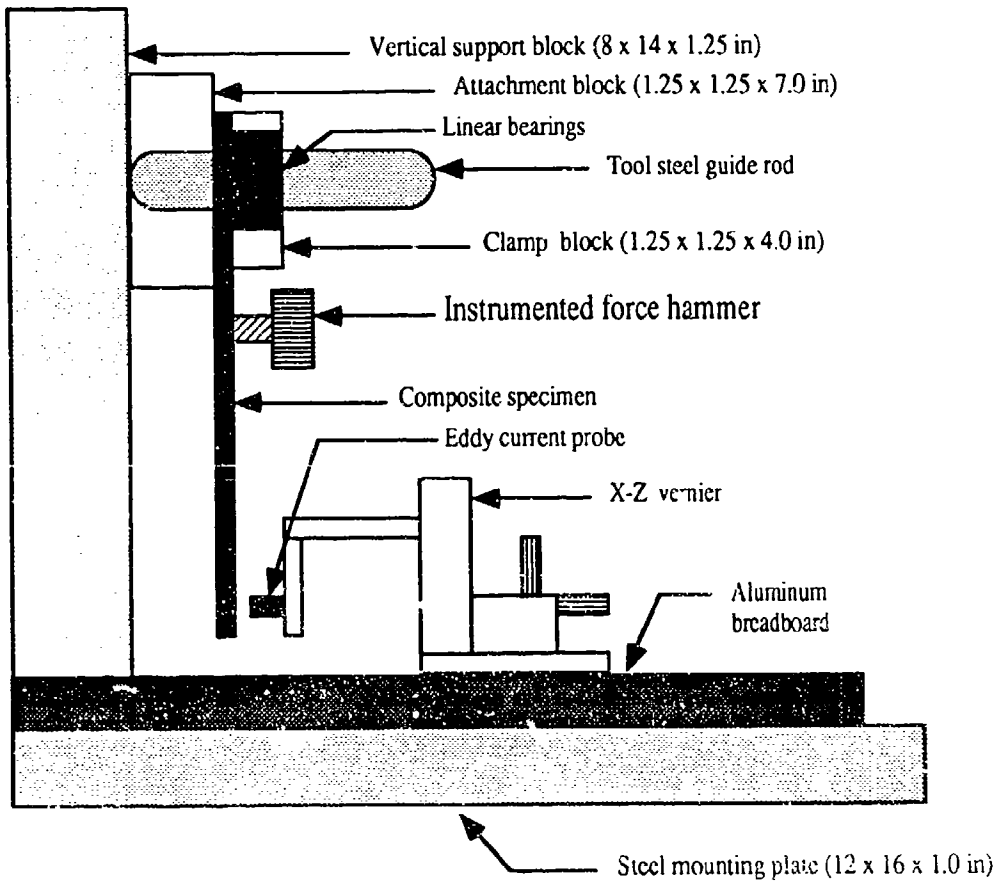

Figure 10 Schematic of the apparatus for testing the vioration damping loss factor of composites using a vertically oriented cantilever beam.

movable clamping block is then bolted to the attachment block. This consists of a 4 x 1.25 x 1.25 in. steel plate which is machined to accept linear bearings through which the guide posts will pass. The use of the guide rods and linear bearings is to ensure uniform clamping on the test specimens. By minimizing eccentric clamping of the specimen, perturbation from the beam true modal response should be minimized. Test specimens with widths up to 1.5 in. and of any thickness can be clamped by this fixture using two 1/4-20 screws.

The eddy current probe is positioned in proximity to the beam tip using an X-Z vernier. The vernier is attached to the breadboard with four cap screws. This specific vernier has a 0.5 inch travel in each direction. By repositioning the vernier at different bolt locations on the breadboard, beams of any thickness can be interrogated with the eddy current probe. It should be noted that a Plexiglas fixture, to which the eddy current probe is fastened, was fabricated to attach the eddy current probe to the vernier. The use of Plexiglas was required since the eddy current probe was unshielded and metallic structures near the sensor can result in spurious displacement determination. A schematic of the entire assembly is given in Figure 11.

Experimental Procedure

For damping loss factor determination, beam tip displacement versus time information is required. The eddy current probe is used to measure the tip displacement. This probe is electrically excited and outputs a voltage dependent on its distance from a conducting medium. This particular probe can be used for both magnetic and non-magnetic

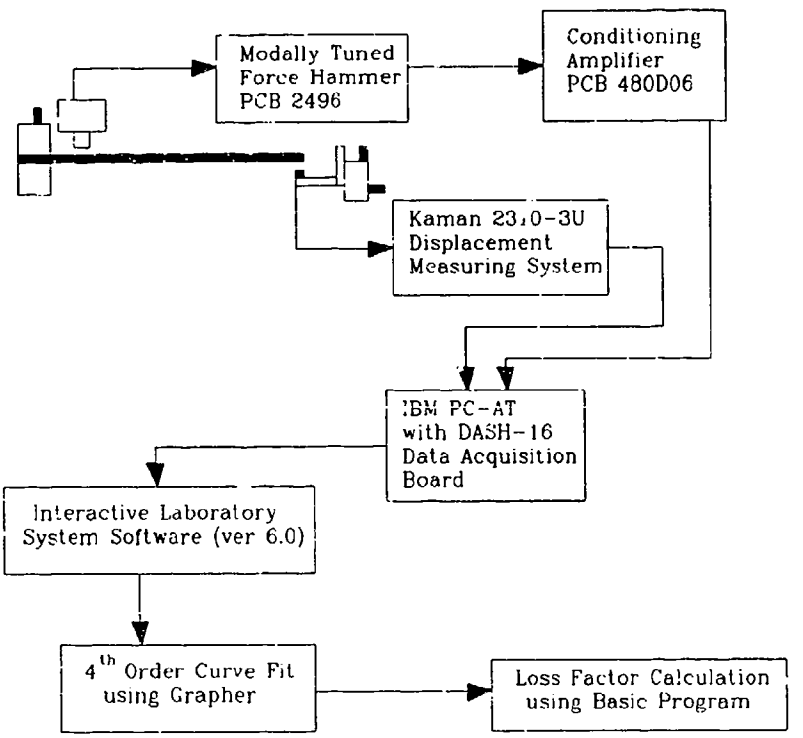

Figure 11 Schematic of instrumentation for vibration damping testing

materials. The probe has a measuring range of 0.120 inches with a resolution of 0.01% of the measuring range. The probe must be calibrated before use. To accomplish this, it is placed into a micrometer calibration fixture, Kaman part number 850854-001. Following the calibration procedure, the output of the eddy current probe is adjusted to the requirements of the test. The gain can be adjusted to optimize sensitivity for particular tests. For this testing program, the probe was calibrated so that 1 volt was equal to 0.040 in. of displacement. Displacement vs. voltage information was obtained with the fixture using increments of 0.005 in. A linear fit was then performed on the data shown in Figure 12. This linear fit had a correlation coefficient of 99.98%. The linear fit of the voltage vs. displacement data was used in the software written to determine the beam vibration response.

In the vibration testing, the beam specimen response is normally recorded using an FFT analyzer or a high speed A-D board. For this investigation, a high speed A-D board was utilized. This type of system required a minimal capital investment, approximately $2,000 as apposed to approximately $50,000 for the FFT analyzer. In addition, the use of the A-D board allows for maximum flexibility in system design and data manipulation. The data acquisition board purchased for this program was a MetraByte Das-16 A-D board. This system has a maximum acquisition rate of 76 kHz, which was verified using the output of a digital oscilloscope.

The specimens were excited using an impulse excitation from a modally tuned impact hammer. This hammer is a PCB Piezotronics, Inc., Model No. 086B01 impulse hammer with a 0-100 lb. force output. The hammer is supplied with impact tips of varying

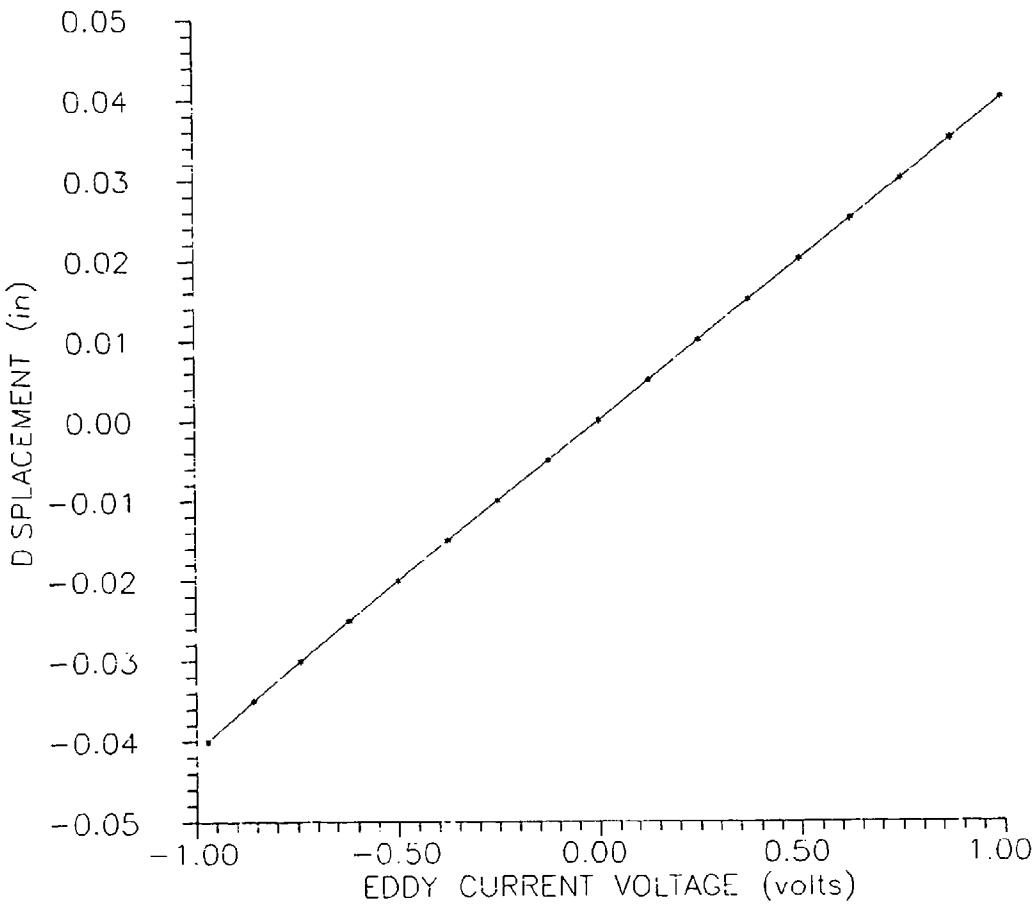

Figure 12 Calibration curve for the noncontact eddy current probe.

hardness. It was observed in the testing that for the higher frequencies, the harder tips were required to ensure a reproducible tip displacement vibration.

The output from the eddy current probe and the force hammer are attached to the MetraByte DAS-16 screw terminal accessory board using BNC connectors. The accessory board is connected to the DAS-16 data acquisition board installed in an IBM PC-AT. This is a 16 channel high speed A/D interface with direct memory access (DMA). This system has a 10 MHz on-board crystal-controlled oscillator to provide the time base. The system can be set up to read voltage ranges of 0 to 10 volts, -10 volts to 10 volts, or -5 volts to +5 volts. For this program the -5 to +5 volt range was used. The information is stored and read in bits with a range of -2048 to 2047 bits corresponding to -5 and +5 volts, respectively. The system resolution, then, with the eddy current probe calibration set to 0.04 in. per volt, is 9.78×10^{-5} in.

The DAS-16 A-D board is controlled by computer programs which are written in basic. There are numerous call routines available that activate various functions of the board. The program that was written to acquire the beam tip displacement and impulse force excitation utilized many of the capabilities of the hardware. The program was written to be interactive, prompting the user throughout its execution. Initially, the user is instructed to attach the instrument output leads to the appropriate input positions on the accessory board. To allow for the positioning of the eddy current probe to its calibrated zero, the program initially monitors only the eddy current probe output. A single positioning of the probe is not possible since there are slight variations in the thickness from specimen to specimen and specimens of different thickness were used throughout the

program. To allow for this positioning, the program is set up to monitor the output of the eddy current probe continuously at an acquisition rate of 76 kHz. The computer routine records this output as bits in sets of 1266 data points using direct memory access. These values are summed and averaged and output to the CRT screen. The user views this output, again in bits, which is updated 4 times a second. By adjusting the x positioning vernier of the eddy current probe, the output is reproducibly kept to a variation of ± 0.1 bits.

After this positioning, the program is automatically set to read two channels, which correspond to the output of the eddy current probe and the impulse hammer. The program then allows the user to choose the acquisition rate. It also allows the user to choose the number of data points to record, up to a maximum of 12000. Choosing an acquisition rate which is greater than 20 times the resonant frequency of the beam using the maximum data set size captures only a portion of the beam vibration response. This results in a loss of resolution in the FFT. The ability to vary the acquisition rate allows the user to zoom into a particular frequency range. In order to prevent aliasing, or distortion of the Fourier transform (70), however, the acquisition rate should be at least 8 times the frequency of interest. This is shown through the calibration testing that was performed.

The are several trigger routines available for the board. The trigger that was settled on was a manual trigger. The user is instructed to hit any key on the computer keyboard to activate the program to continue execution and record the output of the instrumentation. Typically what is done then is to hit the enter key on the keyboard and strike the beam with the hammer in quick succession. At this point the program records the specified number of data points to memory.

The data is then transferred from memory, converted to actual displacement and force, and stored as an array. The user then has two graphic options. First, the data can be plotted to the CRT screen as the log of the displacement versus time and force versus time. This first option allows the user to make a quick check on the amplitude decay to ensure qualitatively that there are no secondary sources of energy dissipation. This would be indicated by the appearance of two distinct slopes of the peak height values from the log displacement versus time plot. Figure 13 is an example of the log displacement versus time plot from the vibration response of 2024 T-4 aluminum subjected to an impact excitation. The second option allows a screen plot of the displacement versus time. This ensures proper positioning of the eddy current probe by viewing the symmetry of the beam response about the zero displacement. Figure 14 shows a representative displacement versus time plot of the same sample.

The user can likewise continue through the computer routine without plotting the data. At this point, the program prompts the user for the file name and address where the data will be transferred. The data can be transferred as the digital stored information, or it can be stored as actual displacements. An option in the program allows the user to input the specific scaling factors obtained from the calibration of the eddy current probe. This is useful if different probes are used. The program then creates and opens the storage file and transfers the appropriate data there. In addition, the program places a header in the data file that includes the acquisition rate and interval between data points. An annotated copy of this data acquisition program is given in Appendix A.

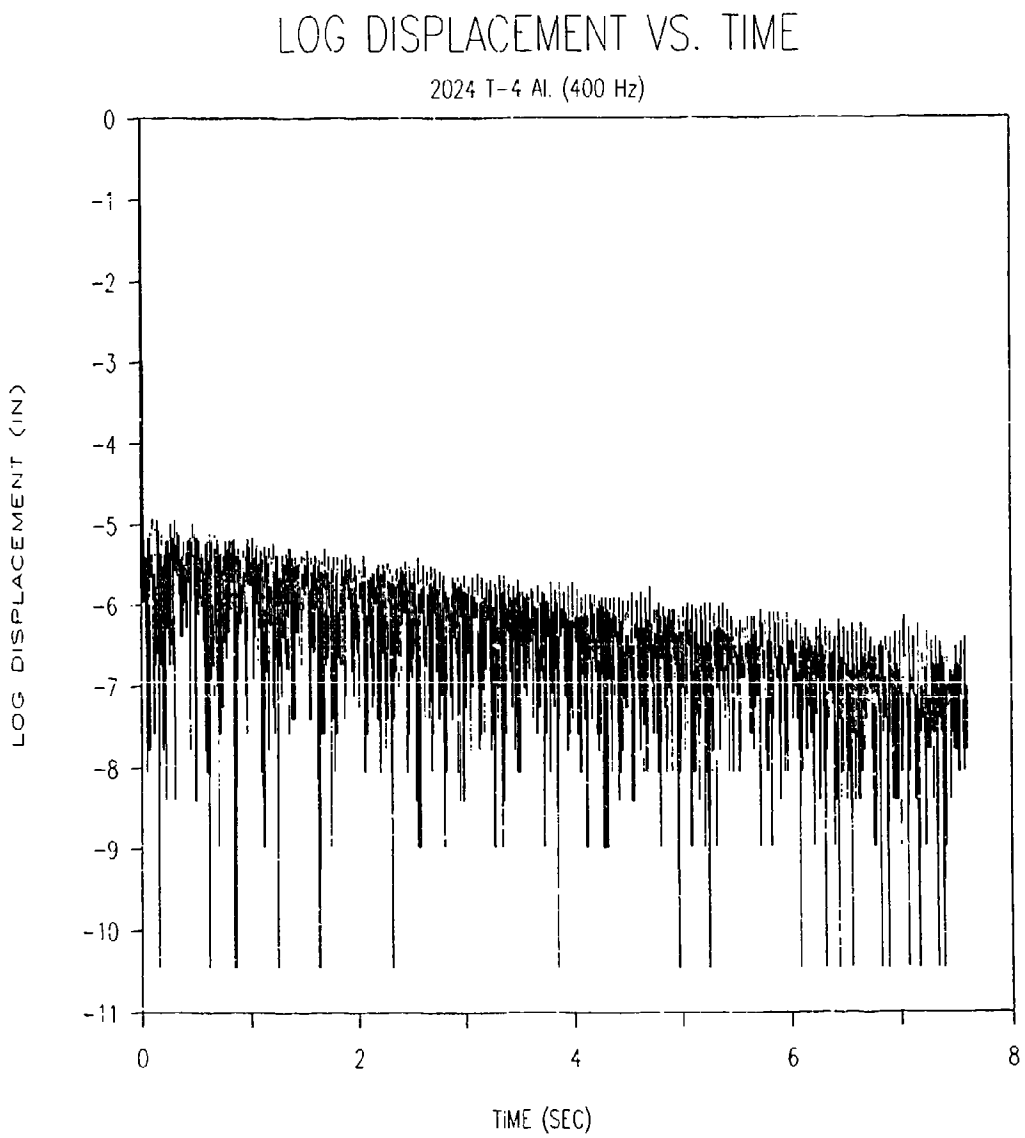

Figure 13 Log displacement vs. time curve for 2024 T-4 aluminum.

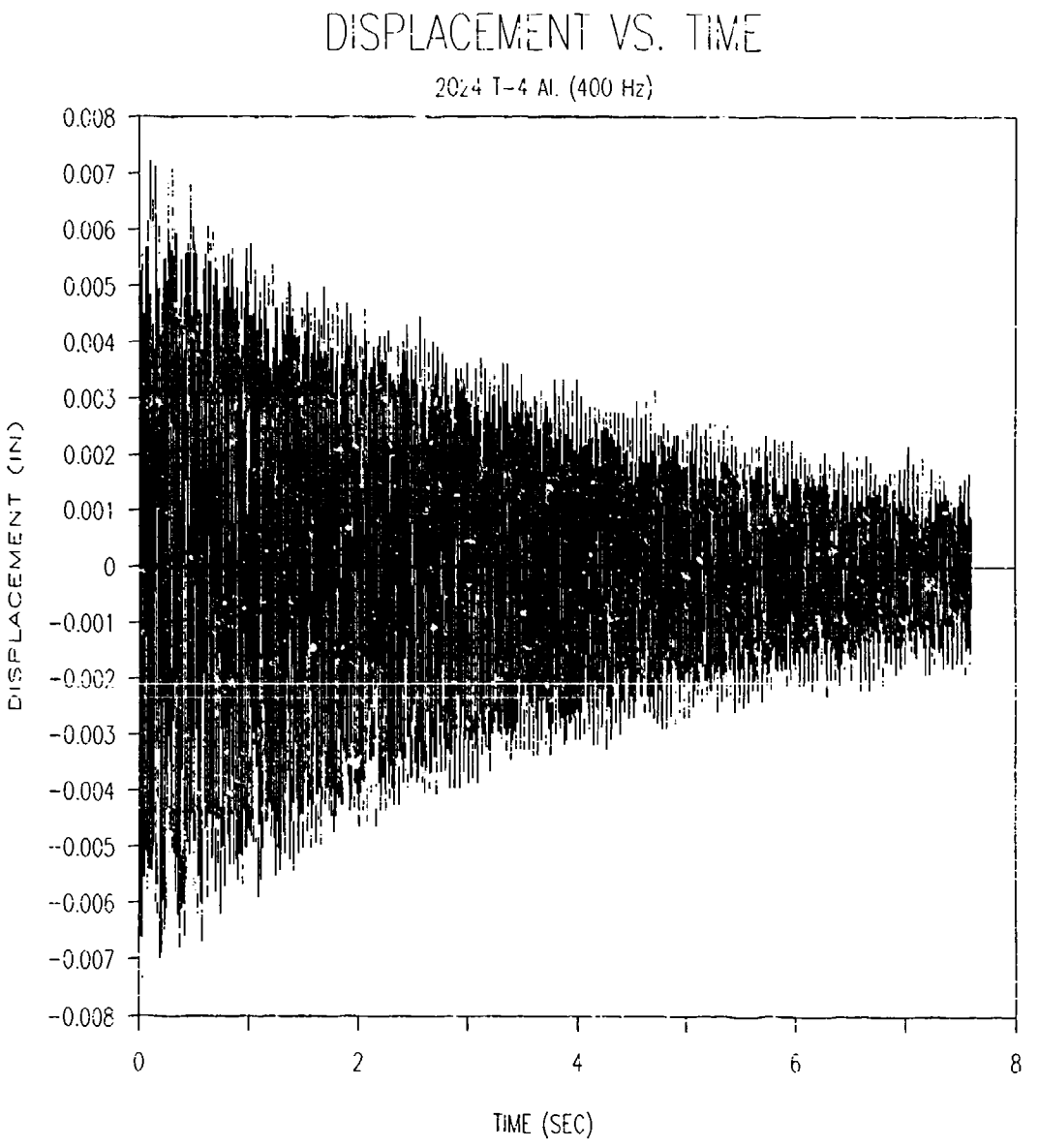

Figure 14 Displacement vs. time curve for 2024 T-4 aluminum.

To perform the Fast Fourier Transform (FFT) on the data, the Interactive Laboratory System software from Signal Technologies Incorporated is utilized. The displacement vs. time data is first read and stored as a sample file using the ILS software. The system partitions this data into records of up to 2048 data points. The size of these data sets used in the inves ations that follows were either 512 or 2048. The ILS software is then used to perform the FFT on any record and the information is stored to a file. The software is then used to transfer the FFT information as an ASCII file which can be manipulated and read by various other software routines. The information that is transferred includes the frequency, dB magnitude and phase for each data point.

The FFT that is obtained is the net vibration amplitude at various frequencies, or the frequency response of the time domain signal. When this net vibration amplitude is plotted vs. frequency, a series of resolved peaks occur. These peaks correspond to the resonant frequencies of the beam. As long as the resonant peaks have negligible overlap, the loss factor for the material can be determined using the half power band width method which was previously given as equation 3 (1). Figure 15 shows the FFT for the beam vibration shown in Figure 14. It is readily seen that no overlap occurs in any of the resonant peaks.

It is not intuitively obvious how damping loss factor determination can be determined using the half power band width. To convince the reader that this methodology is valid, an analytical development of the determination of the loss factor using the half power band width method for a cantilever beam is given in Appendix B. This is derived using the general equations of motion of a beam.

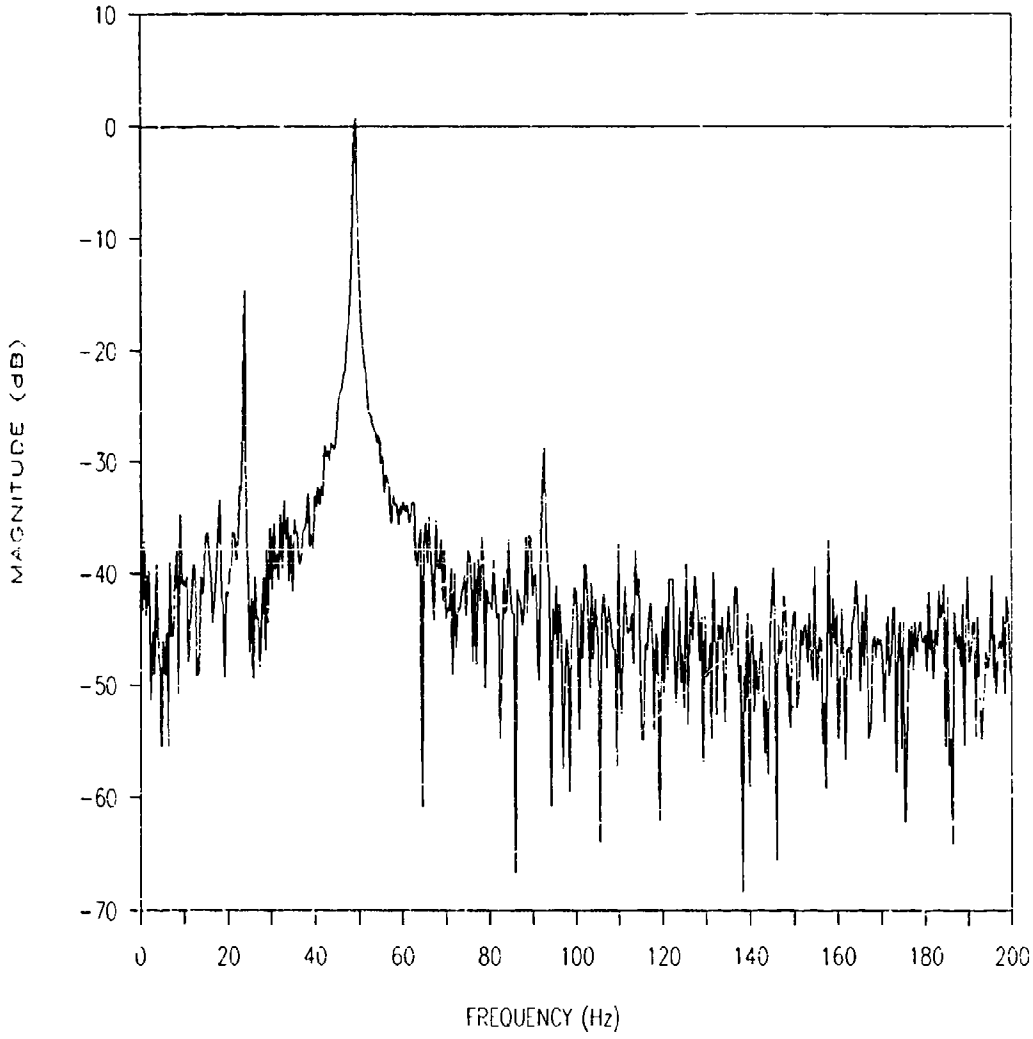

Figure 15 FFT of displacement vs. time data from given in Figure 14.

In order to determine the loss factor, then, the peak height and the half power points need to be determined. Initially, a graphical representation of the dB magnitude of the FFT versus frequency is obtained within a narrow band of the calculated resonant frequency. This is accomplished using a commercially available graphics software called Grapher, written by Golden Software. A curve fit is performed on the digital data on each side of the resonant frequency. The values which correspond to the left and right side of the peak are readily identifiable by a 2π phase shift as is shown in Figure 16. Through experimental investigations, it was determined that a fourth order polynomial using orthogonal coefficients provided the best fit to each side of the peak height values. The orthogonal coefficients and the recursion factors for the data which describe each side of the resonant frequency are recorded and written to a file. The curve fits for the sample data set shown in Figure 16 are given in Table 10.

The specific fourth order equation with orthogonal coefficients used for the curve fit routine is given as follows

$$y = B_1 + (x-\alpha_2)[B_2 + (x-\alpha_3)\{B_3 + (x-\alpha_4)(B_4 + (x-\alpha_5)B_5) - \beta_4 B_5\} - \beta_3(B_4 + [x-\alpha_5]B_5)] - \beta_2 [B_3 + (x-\alpha_4)\{B_4 + (x-\alpha_5)B_5\} - \beta_4 B_5] \qquad (148)$$

where the B_i are the orthogonal coefficients, and the a_i and b_i are the recursion factors. The value of x used in equation 148 is calculated from the experimental frequency data using the following equation

$$x = (x_{input} - x_{mid})\, x_{scal} \qquad (149)$$

where x_{input} is a specific frequency and the x_{mid} and x_{scal} are scaling factors for the original

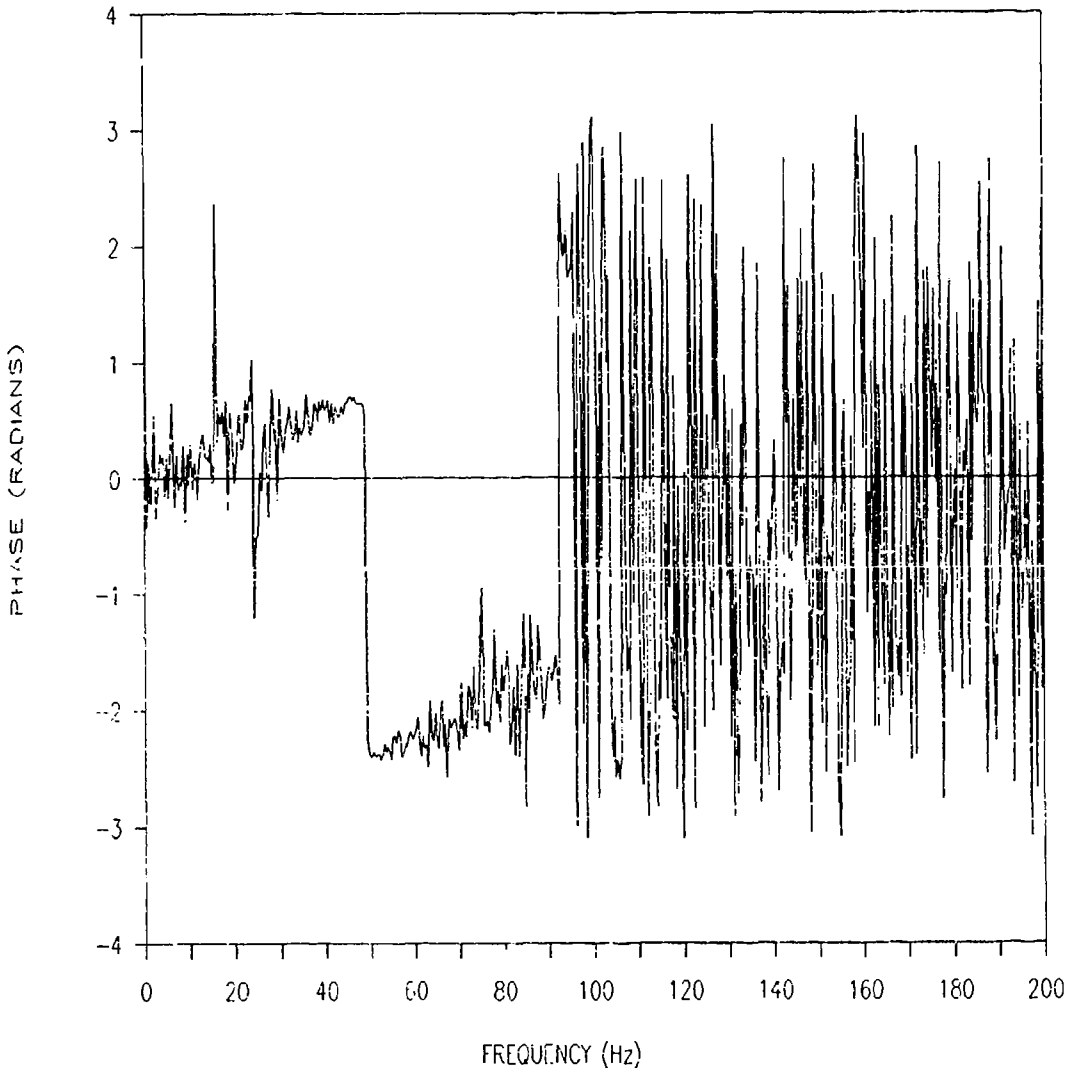

Figure 16 Phase vs. frequency of FFT given in Figure 15.

Table 10: Fourth order polynomial fit statistics for peak values from the FFT given in Figure 16.

LEFT SIDE OF PEAK

Degree	Orthogonal Factors	Recursion Factors	
		Alpha	Beta
0	-3.6147	0	0
1	1.24339	-0.000321833	1.55585
2	0.458577	0.000065269	1.22238
3	0.161536	0.000107365	1.1425
4	0.0916427	0.000147984	1.07872

RIGHT SIDE OF PEAK

Degree	Orthogonal Factors	Recursion Factors	
		Alpha	Beta
0	-3.86925	0	0
1	-1.39188	-0.000219959	1.52375
2	0.496194	-0.000141179	1.20287
3	-0.234782	0.000124755	1.13346
4	0.122776	0.000279605	1.08324

frequency data that is determined using the fourth order polynomial curve fit routine of Grapher.

The file that was created with the values of the orthogonal factors, and the alpha and beta recursion factors is then used as input to a basic computer routine which was written for this dissertation. This program determines the dB magnitude of the intersection of the

two curves, i.e. the left and right curves for the resonant frequency peak, and the frequencies corresponding to the half power points for the specific curves. The half power points are the values of the frequency that correspond to -3dB of the magnitude of the peak height value for the resonant peak. The loss factor is then determined using equation 3, or as follows

$$\eta = \frac{\Delta f_n}{f_r} \tag{3}$$

where Δf_n is the difference in the frequencies at the half power points and f_r is the resonant frequency calculated as the intersection of the two curves. An annotated version of this program is given in Appendix C.

A schematic of the instrumentation and computer routines used to determine the damping loss factor of the cantilever beams was previously given in Figure 11.

Calibration of Experimental Apparatus

In order to calibrate the system and to determine the accuracy and precision of the procedure, a material with a well characterized damping loss factor over the frequency range of interest was tested. The material used here, as well as by numerous other investigators, was 2024 T-4 aluminum. The materials loss factor can be analytically determined at any frequency using Zener Thermoelastic Theory. In addition, since the magnitude of loss factor of this material is very low, experimental replication of the analytical results will ensure that extraneous sources of energy dissipation are minimized.

Initially, beams were machined from 0.125 in. plate to specimens with widths of 1.0 inches and lengths of 12 inches. The 12 inch lengths were machined parallel to within 0.001 in. to minimize any errors in the test results. After the initial vibration tests, one end of these beams was machined to a specific length. By changing the beam length, the first resonant frequency was changed. By testing beams of various lengths, then, it was possible to characterize the loss factor of the 2024 T-4 aluminum over a frequency range of 10-300 Hz.

Beam lengths to be used to obtain a specific frequency in the calibration were analytically determined. The first resonant frequency of a cantilever beam can be determined using the following equation (30)

$$f_i = \sqrt{\frac{EIg}{W_l L^4}} \times C_i \qquad (150)$$

where E is the bending stiffness, I is the moment of inertia of the beam, g is the acceleration due to gravity, W_l is the weight per unit length, L is the beam length and C_i is the constant for the i^{th} mode of vibration.(1)

As was previously mentioned, there are two sources of energy dissipation that must be minimized to ensure that the damping loss factor experimentally determined is of the material internal damping and not from external dissipation sources. These sources are aerodynamic damping and frictional losses at the clamped region of the beam.

A study was conducted to determine explicitly the contribution of the aerodynamic

damping for this experimental program. The aluminum calibration beam was excited with increasing force levels to obtain increasing tip displacements. The results of the testing indicated that no variation in loss factor was obtained in the range of 0.006 to 0.012 in (67,71). Two other investigations have shown that aerodynamic damping could be minimized if tip displacements were kept less than 30% of the specimen thickness.(41,69)

Baker et al (72) conducted an extensive investigation on the effect of air damping on beam vibrations. Thin metallic beams were tested in both air and under vacuum. From their work, they conclude that as vibration amplitude is decreased, the damping due to air becomes less, but never zero. Using their analysis to estimate the air damping which results from the beam tip amplitudes obtained in the calibration study for this program, the additional damping from aerodynamic sources would be approximately 5×10^{-4}. Since this value is within the experimental accuracy of the testing procedure, it will be assumed that the measured loss factor is from material damping.

To minimize aerodynamic damping in this program, loss factors were only determined for samples where maximum tip displacements were less than ± 0.012 in. This represents a displacement less than 11% of the total beam thickness. This displacement level falls within those recommended to ensure a minimal contribution from aerodynamic damping.

The second source of energy dissipation that can be controlled and should be minimized are the frictional losses at the clamped region of the beam. An investigation was conducted where various materials were placed between the specimen and the clamping

block. These materials included tapered aluminum clamping blocks, tapered fiberglass blocks, fiberglass fabric reinforced polyurethane sheet, fiberglass fabric reinforced Teflon, and no clamping block. These systems were positioned between the sample to be tested and the clamping blocks. The specimens were tested using the procedure described above. The experimentally determined loss factors were compared to that analytically predicted from Zener Thermoelastic Theory. The clamping material which resulted in the lowest experimental value of the loss factor for the beam was the fiberglass fabric reinforced Teflon sheet. The loss factor determined using this material also exhibited superior correlation with theory. Since all other clamping materials gave results that were higher than anticipated, it was assumed that they were providing additional source for energy dissipation. The material that was used for the rest of the testing was therefore the fiberglass fabric reinforced Teflon sheet.

In addition, the effect of clamping pressure on the loss factor was determined by determining the loss factor as a function of the clamp block bolt torque. A clamping force that is too small will result in a sliding action, causing high frictional losses. A clamping pressure that if too high may cause damage to the specimen. This damage will result in higher loss factors either from stress concentrations or from friction at the damage sites. The clamping pressure that resulted in consistent results with no degradation to the specimen was 10 ft-lb.

To conduct a test, a specimen is first placed into the test fixture. The eddy current probe is positioned so that its center was approximately 0.5 in. from the specimen end and in the middle of the specimen width. The probe distance from the beam is then adjusted,

while monitoring the output, until the voltage output is near zero.

Beam lengths were varied so that the first resonant frequency was varied from approximately 38 Hz. to 300 Hz. The test procedure given above was followed and the loss factors determined. The results from the testing are given in Table 11.

The results of the test program were compared with the predictions determined using Zener thermoelastic theory. The 2024 T-4 aluminum beam specimens have been shown to follow predictions for the loss factor given by this theory by numerous investigators. (30,41,47,68). The loss factor determined using Zener thermoelastic theory was previously given as

$$\eta = \frac{\alpha^2 E T}{C} \times \frac{\omega \tau}{(1 + \omega^2 \tau^2)} \qquad (6)$$

where α is the coefficient of thermal expansion, E is the bending stiffness of the beam, T is the absolute temperature, C is the heat capacity, ω is the angular frequency and τ is the relaxation time for the heat flow across a beam of rectangular cross section. The value of τ is determined by

$$\tau = \frac{h^2 C}{\pi^2 K} \qquad (7)$$

where h is the beam thickness and K is the thermal conductivity of the beam material. The values used for input to equations 6 and 7 for the determination of the damping loss factor for the aluminum calibration specimen were obtained from the literature. The specific

Table 11: Experimentally determined vibration damping loss factor results for 2024 T-4 aluminum tested in cantilever beam configuration.

Calculated Resonant Frequency (Hz)	Experimental Resonant Frequency (Hz)	Experimentally Determined Loss Factor ($\times 10^{-4}$)	Average Loss Factor ($\times 10^{-4}$)	Loss Factor from Zener Thermoelastic Theory ($\times 10^{-4}$)
38.85±1.40	38.563082 38.57834 38.58244	19.66 21.91 25.45	22.34	22.21
48.91±1.76	49.0575 49.0637 49.0639 49.0684 49.0706 49.0909 49.5670	22.12 21.99 22.79 20.29 24.85 23.02 22.57	22.74	22.94
78.29±2.82	77.17365 77.18895 77.20165 77.2040 77.25243	20.30 21.24 18.52 20.85 20.25	20.23	20.70
80.38±2.89	80.1034 80.1891 80.2092 80.2496	20.00 21.28 19.99 20.88	20.54	20.04
96.82±3.49	95.328 96.47	18.44 18.60	18.52	18.62
195.20±7.03	197.2326 197.2516 197.1793	11.85 11.35 10.08	11.09	10.90
199.73±7.19	198.1793 198.2263 198.5398	9.84 8.62 10.31	9.59	10.64
223.92±8.06	219.628 219.645 219.856 220.041	8.28 8.59 9.35 10.09	9.08	9.61
312.08±11.24	305.1664 305.1771 305.1800 305.1902	8.00 7.69 5.83 8.80	7.58	7.05

values used are given in Table 12.

For each of the beam lengths used in the testing, the first resonant frequency was analytically determined using equation 149. These results are compared with those determined experimentally in Table 11. All of the experimental values of the first resonant frequency are within experimental error for the analytically determined values.

Also given in Table 11 are the experimentally determined loss factors. For comparison purposes, the anticipated loss factor of the specimens using Zener thermoelastic theory are given. The experimental loss factors are within 2.5% of those analytically anticipated for frequencies less than 196 Hz. At frequencies greater than 196 Hz., the experimental results were within 10% of those anticipated analytically.

Table 12: Input values used in equations 3 and 4 for the determination of the damping loss factor for the aluminum calibration specimen using Zener thermoelastic theory.

Input Parameter	Coefficient of Thermal Expansion	Bending Stiffness	Temperature (absolute)	Heat Capacity	Thermal Conductivity
Symbol	α	E	T		K
Value	23.2×10^{-6} $\left(\frac{\text{in/in}}{^{o}\text{K}}\right)$	73.097 GPa	298.72 (^{o}K)	2560511.2 $\left(\frac{\text{J}}{\text{m}^3\ ^{o}\text{K}}\right)$	126.47 $\left(\frac{\text{kg m}}{\text{sec}^3\ ^{o}\text{K}}\right)$

The results from the testing are plotted along with the analytical curve of the loss factor from Zener thermoelastic theory in Figure 17. In this figure, the solid curve is the analytically determined values of the loss factor using equations 6 and 7. A fourth order curve fit was performed on the experimental data to determine the degree of fit of the testing at frequencies between those at which tests were conducted. A plot of the curve fit, also given in Figure 17 shown by the dotted line, shows excellent agreement with the plot of the analytically determined values of the loss factor. As can be seen from the plot, the curve fit for the data matches the results predicted by Zener thermoelastic theory to within 2% in the range for which data was taken.

The experimental apparatus that was designed for determination of the damping loss factor for materials in the cantilever beam configuration accurately determines the damping loss factor with a high degree of precision. Resonant frequencies determined from curve fitting of the frequency response function are within the error of the analytically determined resonant frequencies. The variation in discrete values of the loss factor at a specific frequency have variations of less than 14% with the exception of the data at 312 Hz. where the spread was 22%. The anticipated trends in loss factor for the 2024 T-4 aluminum are determined to within 2% through appropriate curve fitting of the data compared to Zener thermoelastic theory for frequencies from 38 to 100 Hz, and less than 5% for frequencies between 100 and 312 Hz. Secondary sources of energy dissipation have therefore been minimized.

Comparison of these results to the calibration tests of other investigators should be noted. Typically, their calibration is performed at frequencies on the monotonically

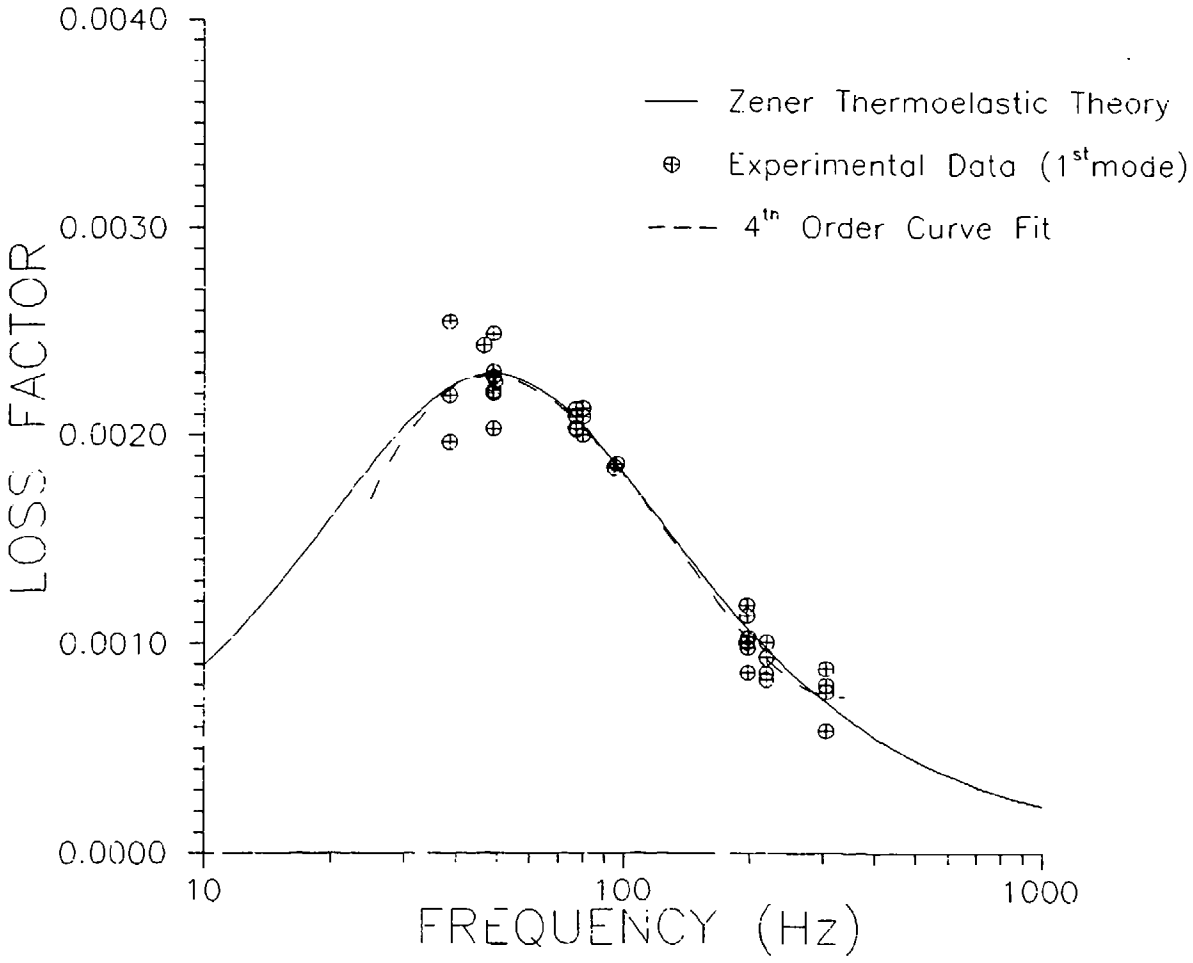

Figure 17 Loss factor vs. frequency for 2024 T-4 aluminum.

decreasing portion of the analytical curve. In addition, the range of frequencies tested are minimal, showing little variation in the magnitude of the loss factor with frequency. Finally, the scatter in their data would indicate that the loss factor at the frequencies tested are statistically equivalent.

Summary

An experimental technique has been designed and developed for determination of the vibration damping loss factor of composites. The technique utilizes a cantilever beam specimen oriented vertically to minimize eccentric type loads during vibration. An impulse excitation is utilized, provided by an instrumented impact hammer. The beam response is measured using a noncontact eddy current probe. Utilization of a Teflon impregnated glass interface material between the specimen and the clamp block has been shown to minimize frictional losses. Using a maximum torque of 10 ft-lb on the two bolts used to clamp the specimen has been shown to result in consistent loss factor results and causes no damage to the specimen. The apparatus was calibrated using a well characterized material, 2024 T-4 aluminum. The results from the calibration testing produced results which were within 5% of the analytically determined values using an appropriate curve fit to the data. The variation in the loss factor at any specific frequency tested was less than 14%, with the exception of the data at 312 Hz, where the spread was approximately 22%. The experimentally determined resonant frequency using the curve fitting routine for the half power bandwidth data reduction methodology was within 3% of the analytically determined value. This apparatus was then utilized for the testing of the composite materials for this research.

Chapter 5

DEVELOPMENT OF A ROBUST TESTING METHODOLOGY

Two material systems were investigated as part of this research. These included S-2 glass/3501-6 epoxy and AS4 graphite/3501-6 epoxy. These two composite systems were chosen because of their differences in material constituents. The fiber characteristics of the graphite and glass are significantly different. The glass is an isotropic fiber whereas the graphite is highly anisotropic. Carbon fibers are composed of long ribbons of turbostratic graphite oriented more or less in the fiber direction (73). These ribbons are grouped together in stacks about 20 angstrom thick (73). The normals to the basal plane of the stacks are randomly oriented perpendicular to the fiber axis, i.e., diffraction patterns of carbon fibers have fiber texture. Consequently, carbon fibers have high stiffness and strength only in the fiber direction, in which carbon-carbon covalent bonds can bear the load. The turbostratic graphite ribbons are held together by van der Waals bonds, resulting in low strength and stiffness transverse to the fiber axis.

All testing in this investigation is performed at room temperature, approximately 75° F. At room temperature, the polymer material is actually considered to be glassy. Here, the amorphous chain conformations are frozen into a rigid network, yielding a high modulus and low loss factor (1). Although the loss factor is considered low compared with that achievable in the glass transition region, these linear viscoelastic materials have been shown to have loss factors more than an order of magnitude greater than structural

metallic materials. When used in the composite form, even though the polymeric material typically constitutes only about 40% of the composite by volume, the matrix material should provide a significant contribution to the material damping loss factor. As such, the polymeric materials used as the matrix for organic matrix composites can be considered to have a high vibration damping loss factor.

Material damping can be defined as any material characteristic which allows for the conversion of mechanical energy into heat. In conventional metallic systems, this energy dissipation occurs through the relaxation of temperature across the specimen which is caused by internal friction. For composite materials, there are numerous sources of energy dissipation like the viscoelastic response of the material constituents, such as that found in polymer systems, thermoelastic conversion of mechanical energy into heat, frictional losses which can occur at the fiber matrix interface, and energy dissipation caused by stress variations that result from the nonhomogeneous material characteristics of the composite.

Although polymer matrix composites are normally considered to be linearly viscoelastic, most experimental investigations report loss factor for a specific material or laminate configuration without mention of the frequency at which the material was tested. Through the investigation of the loss factor as a function of frequency, the viscoelastic characteristic of the glass and graphite fiber reinforced epoxy matrix composites is determined.

In the previous chapter, the design and calibration of the test apparatus was presented. In the initial investigation of the vibration damping testing of composites, it

became evident that a modification to the data analysis procedure was required because of the higher damping loss factor of the composites being tested. This chapter will discuss the the details which made it necessary to modify the analysis procedure previously used to test the 2024 T-4 aluminum. The proposed procedure that follows describes a methodology for minimizing the effect of environmental sources of energy dissipation in order to provide a more accurate measure of the material loss factor. This procedure is being proposed as a robust testing methodology for the vibration damping loss factor determination of composite materials.

Composite Material Specimen Preparation

Two material systems were tested as part of this research. They were both obtained in prepreg form from the Hercules Corp. All specimens were fabricated in-house using the manufacturers recommended cure cycle using the autoclave vacuum bag procedure. This process resulted in samples which had fiber volume fractions of 63%. The specific procedures followed are included in Appendix D for the reader's information.

Machining of the specimens was performed using a diamond-impregnated cutoff wheel mounted on a milling machine. This procedure was followed to minimize damage to the composite specimens prior to testing. This is important since it has been previously shown that any damage that may be present in the composite is a potential source of energy dissipation through friction that will occur at the interface (20-22,36). In addition, samples were stored in a desiccant-filled enclosure in the interim between specimen fabrication and

testing. This was done to ensure that the samples were in the same moisture equilibrium state prior to testing.

Specimen Design and Testing: Elastic Modulus

In order to implement the analytical model to determine the loss factor of a general laminated composite material, the material elastic constants and loss factors need to be determined. To determine the elastic constants, there are conventional, well established procedures which are typically utilized. Specifically, the ASTM test methodologies were utilized. To determine E_1, E_2, ν_{12}, and ν_{21}, unidirectional composite panels were made having thicknesses as specified in the ASTM D3039-76 test procedure . After fabrication, these panels were nondestructively inspected using a J.B. Engineering C-scan immersion tank with software control being provided by Infometrics Test Pro system. In addition, specimens were cut from the scrap ends of the fabricated plate and destructively tested to determine fiber and void volume fractions. To determine the fiber and void volume, a different test procedure was necessary for the two composite materials used in this program. For the AS4/3501-6 graphite epoxy, the ASTM D3171-76 Fiber Content of Resin-Matrix Composites by Matrix Digestion procedure was used on the tag end specimens for each plate. For the S-2 glass/3501-6, the ASTM D2584-68 Ignition Loss of Cured Reinforced Resins test procedure was used. In all cases, the fiber volume fraction was approximately 63% with void content of less than 1%.

Specimens were cut to widths and lengths in accordance with ASTM D3039-76. The specimens were instrumented with Micromeasurements 0/90 strain gage :, gage type

EA-06-125TQ-350. These specimens were loaded in tension using a Baldwin Universal Test machine using a cross head loading rate of 0.05 in/min. The strain/load information was digitally recorded using a MetraByte Das-8 A-D data acquisition board installed in an IBM PC. E_1 is determined from the slope of the linear fit of the longitudinal stress vs. strain response. To determine ν_{12}, the longitudinal vs. transverse strain was graphed for each specimen. A least squares linear fit was then performed on each curve.

For determination of E_2 and ν_{21}, the same procedure was utilized. In this case, however, the unidirectional panel had its fibers oriented transverse to the loading direction. Again, 0/90 strain gage rosettes were utilized so that both E_2 and ν_{21} could be determined. These values were determined using the same test procedure and data analysis reduction as was given above.

For determination of G_{12}, the ASTM D3518-76 test procedure was followed. Here, a $\pm 45°$ specimen was fabricated and instrumented with the 0/90 strain gage rosettes. The specimen is loaded in tension and the stress strain response recorded as previously indicated. The shear strain is obtained from the difference in the longitudinal to transverse strains and the shear stress is given as one-half the load divided by the cross sectional area of the specimen. A linear fit is then performed on the initial portion of the shear stress versus shear strain curve to determine G_{12}.

The test results of the mechanical properties are given in Table 13. It should be noted that the information presented is the average of 5 tests for each property indicated in the table.

Table 13: Elastic properties of S-2 Glass/3501-6 and AS4/3501-6

MATERIAL	TEST METHOD	CONFIGURATION	PROPERTY	EXPERIMENTAL VALUE
AS4/3501-6	ASTM D3039-76	$[0]_8$	E_1	20.95 (Msi)
AS4/3501-6	ASTM D3039-76	$[0]_8$	ν_{12}	0.305
AS4/3501-6	ASTM D3039-76	$[90]_{20}$	E_2	1.70 (Msi)
AS4/3501-6	ASTM D3039-76	$[90]_{20}$	ν_{21}	0.0203
AS4/3501-6	ASTM D3518-76	$[\pm 45]_{8S}$	G_{12}	0.87 (Msi)
S2/3501-6	ASTM D3039-76	$[0]_8$	E_1	8.39 (Msi)
S2/3501-6	ASTM D3039-76	$[0]_8$	ν_{12}	0.264
S2/3501-6	ASTM D3039-76	$[90]_{24}$	E_2	2.88 (Msi)
S2/3501-6	ASTM D3039-76	$[90]_{24}$	ν_{21}	0.0913
S2/3501-6	ASTM D3518-76	$[\pm 45]_{8S}$	G_{12}	0.885 (Msi)

Specimen Design and Testing: Loss Factor

The methodology that is used to determine the loss modulus of the composite is by initially determining the material damping loss factor using the apparatus which was described in Chapter 4. Using the relationship previously given in equations 5 and 76, the loss modulus can then be determined as

$$E''_{ij}(f) = \eta_{ij}(f)\, E'_{ij} \tag{151}$$

where it should be noted that the storage modulus is assumed to be independent of frequency. Since it is also assumed that the Poissons' ratios are real and frequency

independent, a complete characterization of the loss modulus is possible by determination of η_{11}, η_{22} and η_{12}. This will be accomplished by utilizing 0° and 90° unidirectional beam specimens and ±45° angle-ply beam specimens.

The approximation for the unidirectional specimens should be valid. For the unidirectional specimens subjected to a bending moment, there is no in-plane shear strain resultant. Since the material is linearly viscoelastic, the material characteristics are independent of stress or strain amplitude. As such, the strains occurring in the material are the axial strain caused by the bending moment and the transverse strain which results from the Poisson effects. In addition, the axial modulus and the effective bending stiffness determined using equation 144 are equivalent. The difference in the two specimens is the through-thickness shear strains that occur as a result of a bending moment which are absent from an application of an axial load. Since the bending moment is small, due to the restriction placed on the maximum tip displacement allowed, the contribution to damping will be assumed to be minimal.

For the ±45° specimen subjected to a bending moment, axial and transverse strains are present in addition to the in-plane shear strains. As such, the loss factor determined using this specimen has contributions from the various strain components. A more accurate estimate of the in-plane shear loss modulus can be obtained, however, using the experimental values of the loss factor determined using this specimen and the analytical model which was developed in Chapter 3. As such, this specimen orientation is used to obtain frequency dependent loss factor measurements. Details on the calculation of the in-plane shear loss factor will be provided later in this chapter.

Modification of the Data Reduction Scheme

The testing methodology utilized for the loss factor determination of the 2024 T-4 aluminum specimen was initially utilized to determine the loss factor for the composite materials. To summarize, this procedure utilized a cantilever beam specimen which was excited with an impulse excitation using an instrumented force hammer. The beam response was measured using a noncontact eddy current probe. The data acquisition rate was varied to be at a minimum 8 times the first resonant frequency of the specific beam length tested. The beam tip displacement vs. time was digitally recorded using a PC based A-D converter to a sample size of 2048 data points. The loss factor was then determined at a particular frequency using the half power band width method.

The initial testing was conducted on the 90° S-2 glass/epoxy material. Five beams were utilized for each test length. The damping loss factor information was desired in the frequency range up to 1000 Hz. Only the first resonant frequency was utilized for loss factor determination since it was unknown what effect the different modes of vibration would have on the resultant loss factor. To obtain different frequencies to characterize the frequency dependence of the damping loss factor using beams with the same width and thickness, it was necessary to test beams of different length. To minimize sources of errors in the determination of the loss factor, one set of beams was used for the entire series of tests. After tests were conducted using a particular beam length, i.e., a specific frequency, they were cut to the next desired length and tested.

Initially, using the longer beam lengths, the beam response appeared similar to that of the aluminum calibration specimen. However, as the beam length became shorter, on the order of 5.0 in (12.7 mm), the beam displacement versus time response began to decay at a much higher rate, an indication of the higher damping loss factor of the specimen. In fact, at this beam length, using a data acquisition rate of 10 times the first resonant frequency of the beam, the tip displacement became unmeasurable, or was within the noise of the system, near the end of the data acquisition.

This type of decay in vibration amplitude to an unmeasurable value did not occur in the calibration of the apparatus using the 2024 T-4 aluminum specimens. The displacement vs. time curves that were analyzed typically had displacements which remained greater than $\pm$ 0.002 in. for the complete data set being analyzed. For the composite specimens, although the initial beam displacements were greater than that of the aluminum, in many cases the final beam displacements recorded were within the noise of the data acquisition instrumentation, less that $\pm$ 0.001 in. The reason for this is that the damping of the composite specimens are significantly higher than that of the aluminum. The question that arose was, " What effect does the incorporation of these nonmeasurable tip displacements have on the determination of the damping loss factor ?"

This was addressed by comparing the loss factor which was calculated with and without the incorporation of the very low amplitude vibrations. For the purpose of clarity, the discussion that follows will be limited to the 11.0 and 5.0 in (27.9 and 12.7 cm) 90° S-2 Glass/3501-6 beams.

Figures 18 and 19 show the displacement vs. time information that was taken for cantilever beams which had an unsupported test length of 11.0 and 5.0 in (27.9 and 12.7 cm). The data acquisition rate used for these two specimens was 250 and 1000 Hz., respectively. These rates were chosen since they are greater than 8 times the first resonant frequency of the beams. The theoretical resonant frequency of the beams was 14.5 and 70.1 Hz. The initial maximum tip displacement for both beams are approximately the same in both cases, about 0.023 in (0.6 mm). In each case, there are 2048 data points shown. Because of the higher resonant frequency of 12.7 cm. beam, the time interval is much less than the 27.9 cm. beam. As a point of reference for each specimen, vertical lines have been placed in Figures 18 and 19 which indicate the location of each 512 interval of data points.

In typical FFT analysis using conventional FFT analyzer equipment, the user can control the sensors' input to the analyzer, but little else. The acquisition rate is automatically controlled, as well as the number of data points that will be used for the FFT analysis. In Figures 18 and 19, there is an obvious variation in the rate of decay of the beam tip displacement from the first 512 interval to the last. It should also be noted that in the case of the 5.0 in (12.7 cm) beam, the maximum tip displacement for the last 512 data points is on the order of 0.0008 in (0.02 mm). In this range, the measured tip displacements occurring from the vibration decay may be lost in the noise of the electronic signal. If there is no decay in the tip displacement amplitude, the loss factor that would be calculated using this data only would be zero. This can be readily seen by considering the loss factor as calculated using the log decrement method, given in equation 2. If this portion of the data is included in the calculation of the loss factor for the specimen, the resultant average loss factor would be lower than the actual material loss factor. This characteristic will later be shown to occur. This problem can be reduced by utilizing an

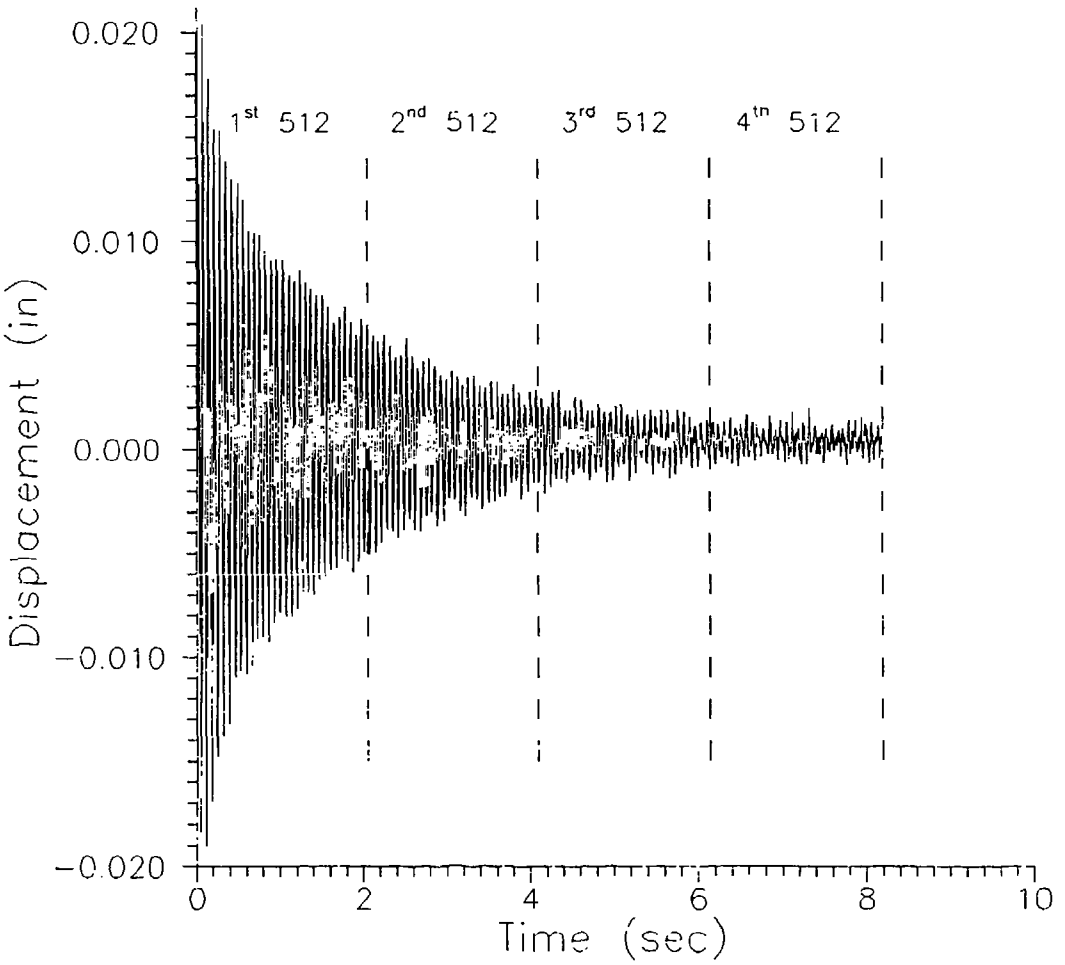

Figure 18 Beam tip displacement vs. time for 11.0 in 90° S-2 Glass/3501-6.

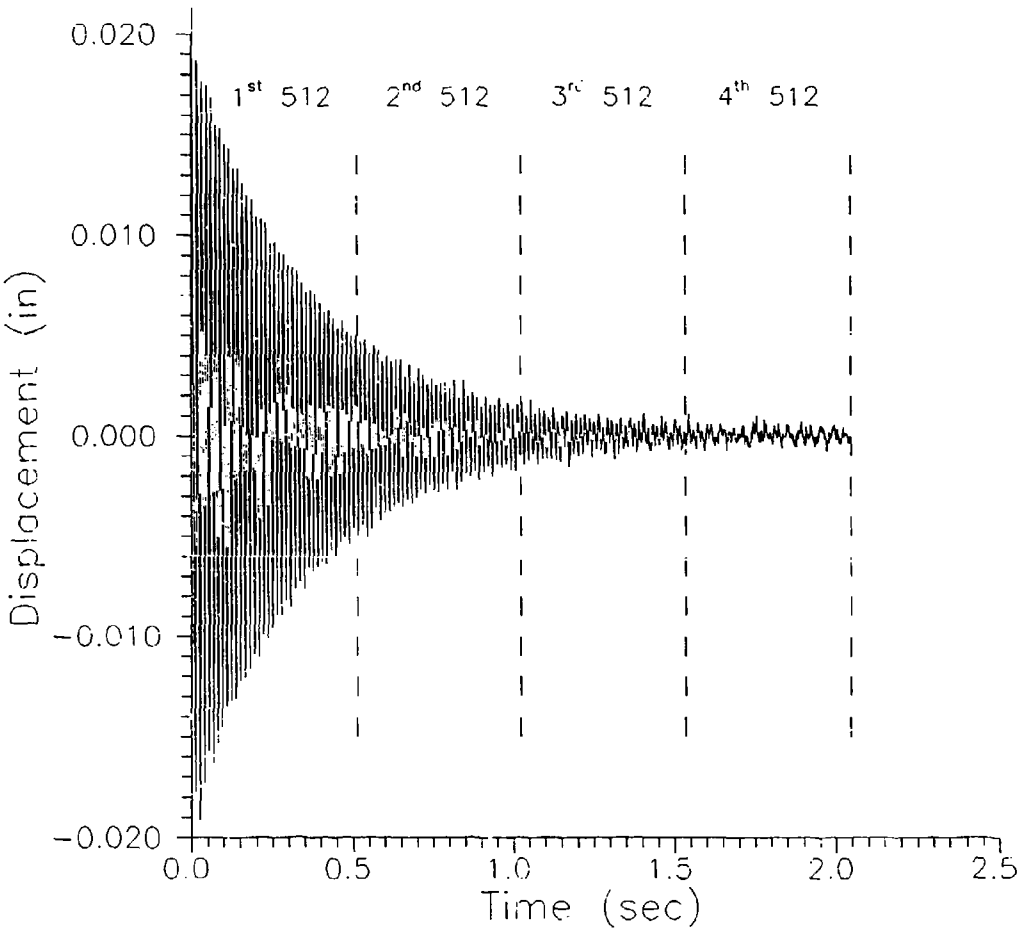

Figure 19 Beam tip displacement vs. time for 5.0 in 90° S-2 Glass/3501-6.

increased data acquisition rate, so that the maximum number of data points can be used in the FFT analysis. However, resolution is lost in doing this by reducing the capability to zoom into an appropriate frequency interval so that an accurate characterization of the half power band width can be obtained.

Characterization of the Effect of Vibration Amplitude on Damping Loss Factor

Initially, the damping loss factor for 5 specimens of each beam length was determined using 2048 data points using the procedure described in Chapter 4. Each data set was then divided into 4 subsets, containing the four successive 512 data points. The loss factor was then determined using each of these 512 data points which made up the initial 2048 data point set. The purpose of this exercise was to determine if the loss factor varied with tip displacement. In each interval, the magnitude of the stresses that the beam is subjected to, the frictional loss at the clamped end, and any variation in the aerodynamic damping will be a function of tip displacement which may affect the calculated material loss factor.

Within each 512 interval, there is a decay in the beam tip displacement as a function of time. For comparison purposes, it was decided to determine the maximum beam tip displacement in each of these intervals. In the graphical presentations that follow, it is this maximum value of tip displacement in each of these intervals which will be used.

Figure 20 shows the dB magnitude FFT vs. frequency for the 11 inch 90° S-2 glass/3501-6. The four curves are the dB magnitude FFT for the four consecutive 512 data sets. The loss factor is determined directly from these curves. Several features are

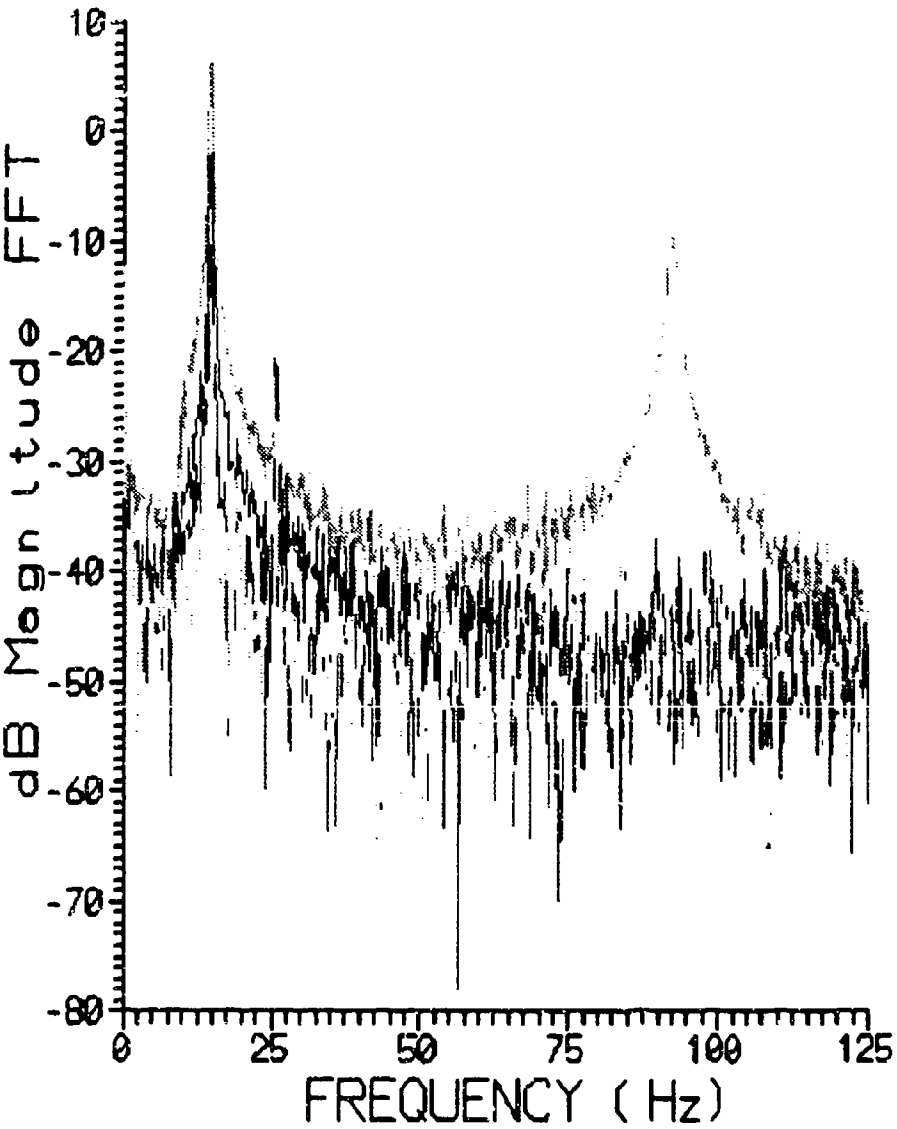

Figure 20 dB Magnitude FFT vs. frequency for four successive partitions of 512 tip displacement vs. time data points given in Figure 18.

evident. First, the first resonant frequency of the beam is evident by the large peak around 15 Hz. Secondly, the second mode is evident on the first 512 data point sets at a frequency of about 90 Hz but becomes unresolvable for the latter three sets. The reason for this is that the higher modes have a higher loss factor, and they have been damped out in that time interval. A third feature that shows up in all of the curves is a peak around 23 Hz. This peak is due to the excitation of the fixture. This resonant frequency of the fixture was determined following similar procedures as was given in Chapter 4. It is seen that the peak at this frequency is very sharp, indicating that it contributes little to the damping of the specimen. This signal can be reduced but not eliminated. The magnitude of this peak is dependent on the amplitude of vibration of the specimen and the resonant frequency of the specimen. As the resonant frequency of the specimen becomes further away from the resonant frequency of the apparatus, the apparatus does not become excited. For the testing of the other specimen lengths, the peak height at 23 Hz was negligible. Even at this low frequency, it should also be noted that the response of the fixture does not overlap the beam response. As such, it should not affect the determination of the loss factor of the composite sample (1).

Figure 21 shows the damping loss factors determined using the procedure given above for the five 11 in. (27.9 cm) specimens. Two distinct sets of data are shown. The five individual triangular points with loss factors of approximately 65 $x10^{-4}$ and tip displacements greater than 0.02 in. are the loss factors that were determined using the half power band width technique and all 2048 tip displacement vs. time data points. The other data points shown in Figure 21 are the loss factors determined for each successive 512 data point set. The lines shown in Figure 21 are linear fits to the four successive 512 data point

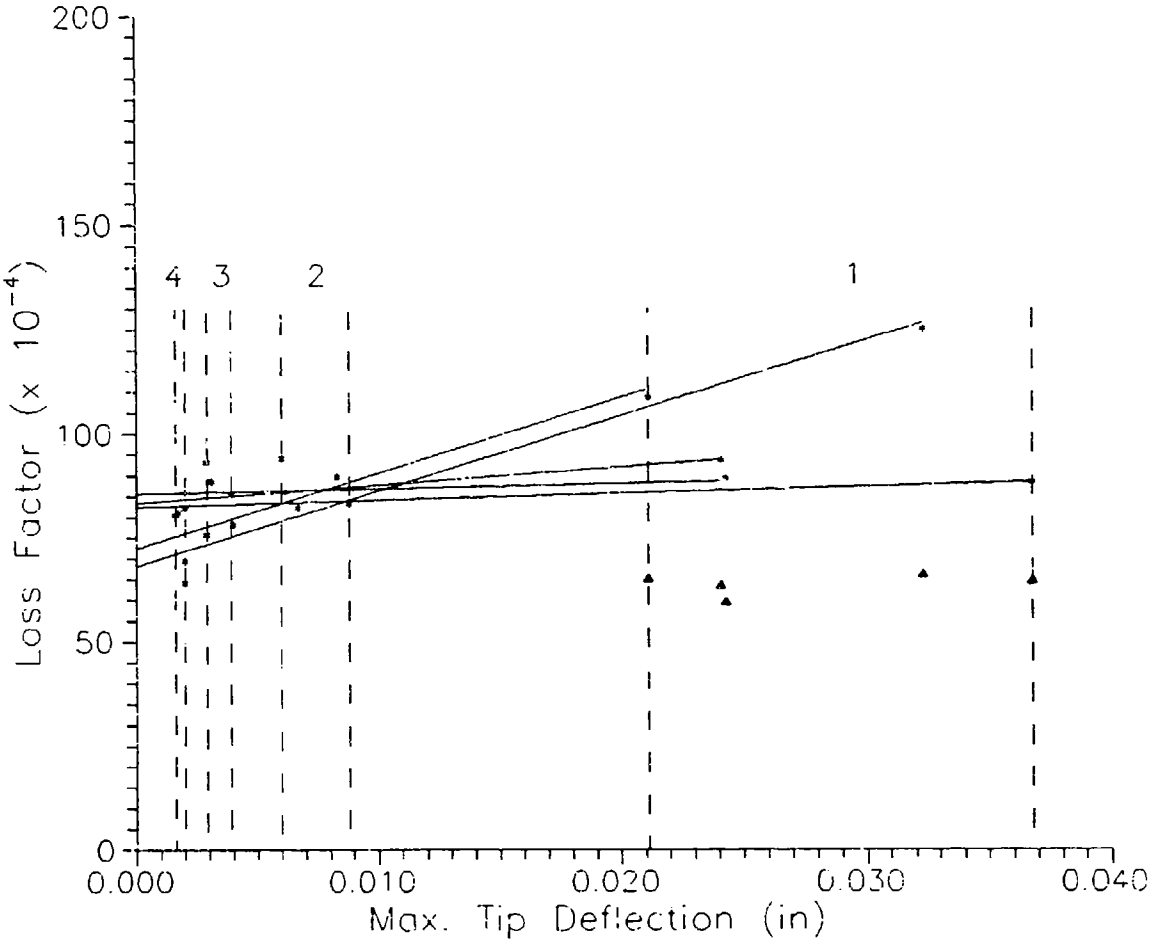

Figure 21 Loss factor vs. maximum tip displacement for successive partitions of 512 tip displacement vs. time data points for five 11.0 in specimens.

loss factors for each of the five specimens. It should be noted that these lines are extrapolated to zero displacement. In addition, the dashed vertical lines in Figure 21 partition the figure into four sections, indicated by the numbers 1-4. Each interval indicates the range of maximum tip displacements for each of the 512 data point sets for each of the specimens. For example, region 1 shows the range of the maximum tip displacements for the first 512 recorded tip displacements of the five test samples.

Some significant results can be extracted from Figure 21. First, there is little variation in the loss factor determined using all 2048 data points. It should be pointed out that for all five specimens, the beam tip amplitude had oscillations which remained greater than $\pm$ 0.002 in. for the entire data set. Second, for each specimen, the loss factor determined using the first 512 data points of each specimen data set was greater than the loss factor determined using all 2048 data points. Third, the loss factors determined for a given specimen using the four successive intervals decreased as the maximum amplitude of vibration decreased. And finally, the loss factor extrapolated to zero displacement using the four successive intervals is approximately equal to the loss factor determined using the entire data point set. The average of the zero extrapolated loss factors from the five specimens was 75.1×10^{-4}. For the case where all 2048 data displacement points are utilized, the average value of the loss factor was 63.9×10^{-4}. The reason that a difference exists may be due to the resolution and accuracy of the data in the last 512 data point set.

For the 5.0 in (12.7 cm) beams, the same test and analysis procedure was utilized. Figure 22 shows the calculated loss factors using 2048 and 512 data point sets. The various features shown in Figure 22 are the same as those utilized in Figure 21. Many of the same

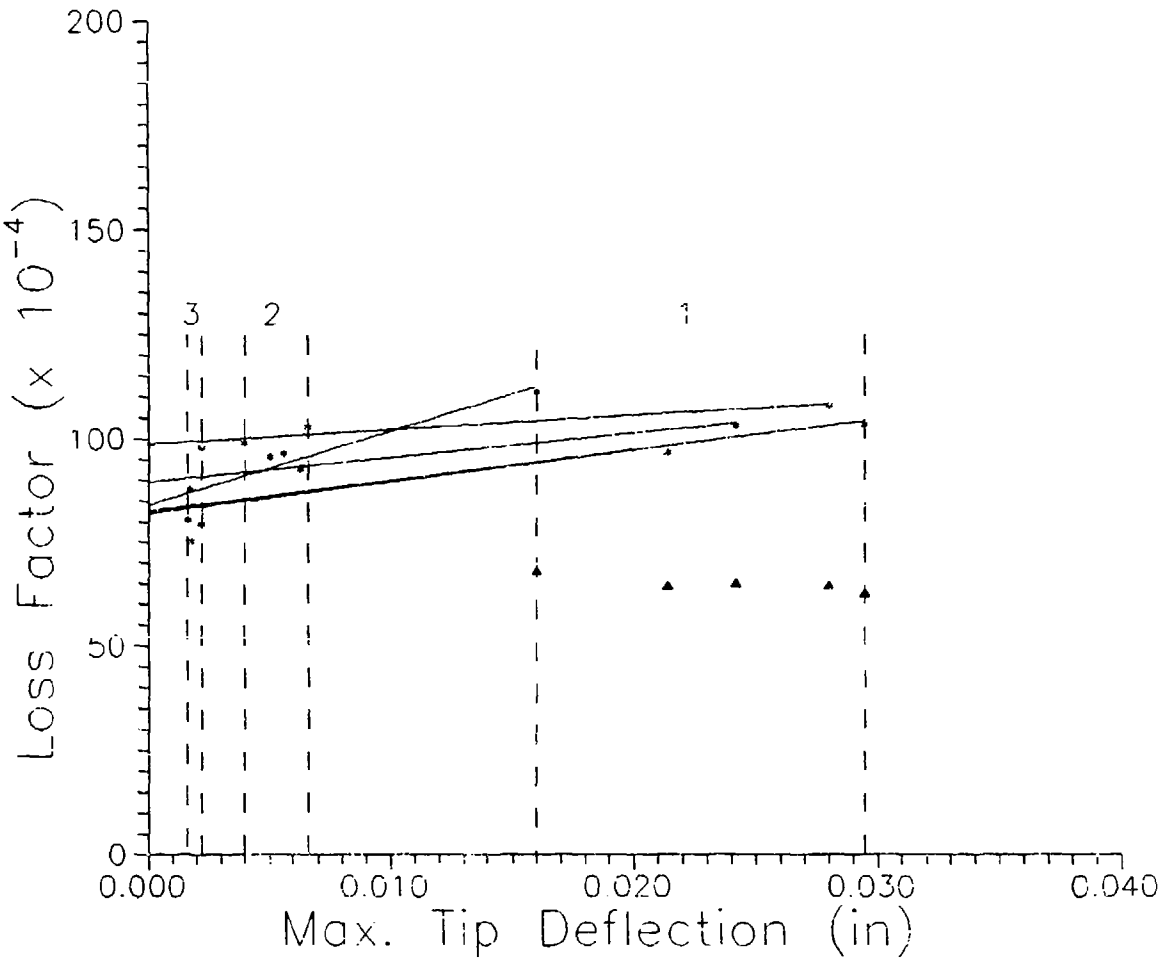

Figure 22 Loss factor vs. maximum tip displacement for successive partitions of 512 tip displacement vs. time data points for five 5.0 in specimens.

characteristics shown to occur for the 11.0 in (27.9 cm) specimen are also shown to occur for the 5.0 in (12.7 cm) specimen. First, there is a variation in loss factor with beam tip displacement as seen using the loss factors determined in the successive 512 data point sets. For this beam length, however, there is less of a decrease in loss factor as the amplitude of vibration decreases. It should be noted that it was not possible to resolve a peak in the dB magnitude FFT vs. frequency curves for the fourth 512 data point interval of any of the 5.0 in. specimen data sets. If a loss factor was determined using the log decrement method, the resultant loss factor would be very low. The loss factor determined using all 2048 data points is significantly lower than the zero extrapolated loss factor, 65.0 x 10^{-4} versus 84.6 x 10^{-4}. This shows that the incorporation of displacement information which becomes masked by the noise of the acquisition system, or has virtually come to rest, has the effect of lowering the value determined for the loss factor.

It should be noted that for the 5.0 in (12.7 cm) beams, the acquisition rate used was approximately 14 times the first resonant frequency. Even at this acquisition rate, the beam displacements for the last 512 data points of a 2048 set were on the order of the resolution of the sensor. This shows that as the resonant frequency of the beam is increased, the acquisition rate should be increased nonlinearly so that tip displacements are significantly greater than the sensor resolution over the entire 2048 data set. This will provide a more accurate description of the beam tip displacement history.

Similar findings were obtained for the series S-2 Glass/3501-6 90 degree beams tested for this investigation with lengths ranging down to 2.0 in.(5.0 cm). In all cases, the loss factor determined using the sets of 2048 data points resulted in loss factors that were

significantly lower than the zero extrapolated loss factor using the methodology described above. Again, this result occurred due to the incorporation of the displacement information which was within the noise of the data acquisition system.

A Proposed Robust Testing Methodology for the Loss Factor Determination of Composite

The finding of the variation in loss factor as a function of tip displacement amplitude has significant ramifications. In vibration testing that is normally performed to determine the damping loss factor of materials, care is taken to ensure that all external sources of energy dissipation are minimized. The magnitude of the damping provided by these sources is, however, difficult if not impossible to determine and eliminate. In general, then, the loss factor determined using any of the methodologies discussed in chapter 2 will be the summation of the material loss factor and the environmental losses associated with the test itself.

In addition, it has been shown that it is necessary to determine the applicability of the displacement information prior to performing data reductions for loss factor determination. Incorporation of near zero displacement information, or displacements that are on the same order of magnitude as the noise of the system, has the effect of lowering the calculated value of the loss factor. This occurs because of the effective averaging of this loss factor with the losses that occur at the larger more resolvable displacements. Another reason for errors occurring when the near zero displacements are included in the determination of the damping loss factor is due to the relationship of the magnitude of the tip displacements relative to the sensitivity of the sensors measuring the beam tip displacements. For large

beam displacements, on the order of ±0.010 in. (±0.25 mm), and a sensor resolution of ±0.0001 in (±0.0025 mm), tip displacements have an error of ± 1%. However, when tip displacements are on the order of ±0.001, the sensitivity of the sensor does not change. In this case there is an associated error of ±10%. This is in addition to the other sources of error that can arise in the instrumentation, such as noise.

This phenomenon has been observed by other researchers investigating the vibration damping of composites. Hoa and Oullette(49) conducted an investigation on the effect of microstrain on the damping loss factor of hybrid composite beams. The beams were given an initial step excitation followed by a free decay. The loss factor was measured using the log decrement test methodology. The results of their testing are shown in Figure 23. Although they attribute the decrease in the calculated loss factor to the decrease in the strain or amplitude of vibration, it may be the result of the sensitivity of their instrumentation as was described above.

Based on the results described above, a robust testing methodology for determination of the material loss factor of composites is proposed. First, a well designed apparatus is required which is calibrated using a well characterized test specimen. The apparatus described in Chapter 4 is an example of such a system. The magnitude of the beam tip displacement vs. time must remain greater than the noise and resolution of the sensor and data acquisition system. As such, the data needs to be visually or numerically interrogated to insure that this condition is met. If not, then a possibility exists that the resultant loss factor will be lower than the actual material loss factor. If displacements over the time interval which are utilized in the FFT are allowed to become smaller than 0.001 in.

(0.025 mm) for more than 25% of the displacement vs. time curve, the loss factor that is calculated appears to be lower than the actual material loss factor.

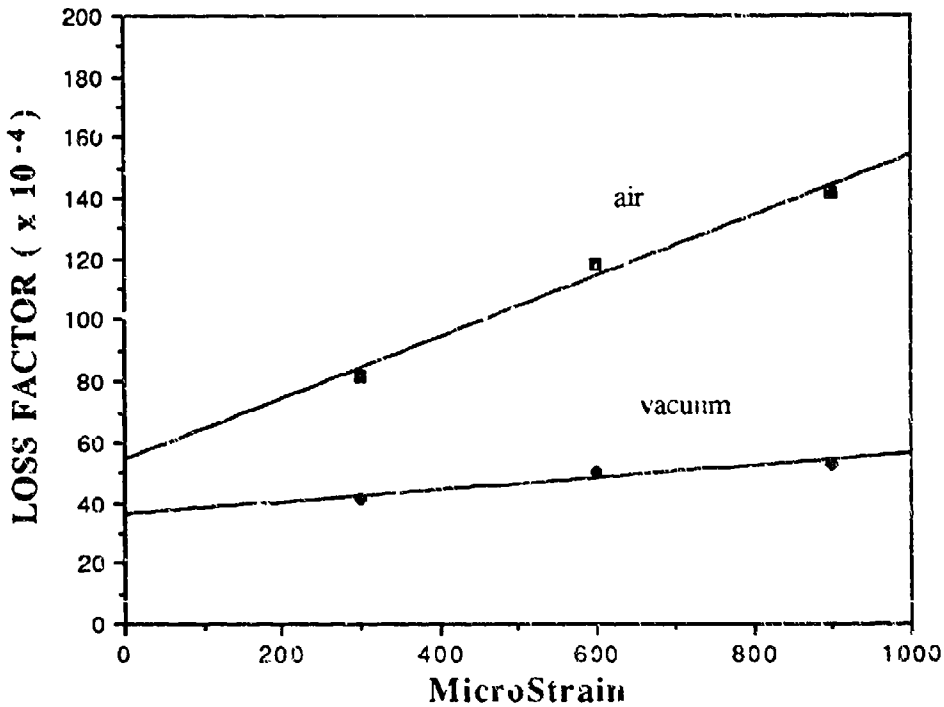

Figure 23: Loss Factor vs.MicroStain for $(0_{Gr})_2/(45_{Kev})_3/(0_{Gr})_2$ (after Hoa & Oullette(49))

The displacement versus time data should then be partitioned into 512 data point intervals. A Fourier transform should be performed on each data set and loss factor determined using the half power band width method. The maximum tip displacement in each set should then be determined The loss factor as a function of this tip displacement should then be plotted. A least squares fit should be performed on the data, with an extrapolation being made to zero displacement. This is done in an attempt to eliminate extraneous source of energy dissipation. As the beam's tip displacements increase, various sources of energy dissipation can occur. The extrapolation to zero displacement should

reduce the extraneous losses, providing a more robust testing protocol. In addition, it is hypothesized that the loss factors that result are more representative of that which would be experienced by an actual structure since, in the majority of cases, displacements are small and/or the structures are restrained from experiencing large displacements. This testing methodology should provide increased accuracy and precision for the determination of the damping loss factor of materials.

Chapter 6

S-2 GLASS/3501-6 AND AS4/3501-6 DAMPING LOSS FACTOR DETERMINATION

In Chapter 5, a robust testing methodology for the determination of the material damping loss factor determination of composites was presented. This testing procedure provides an accurate measure of the material loss factor of composites. This testing methodology was utilized to determine the damping loss factor of S-2 Glass/3501-6 and AS4/3501-6 glass and graphite composites. The damping loss factor testing is being conducted to provide the input required to the analytical model developed in Chapter 3 for the determination of the damping loss factor of general laminated composites made with these two composite systems.

The epoxy matrix used in this investigation is a viscoelastic material. Although the fibers are assumed to be elastic, the composite response is expected to be viscoelastic. Consequently, the loss factor for the composite is expected to be a function of frequency. To properly characterize the composite, then, it is necessary to determine the loss factor at various frequencies, i.e. beam lengths. The material loss factors that are required for the analytical model are η_{11}, η_{22}, and η_{12}. This chapter will present the results of the testing conducted on the composite materials using the robust test procedure given in Chapter 5.

In addition, methodology is presented for analytically determining an accurate

estimate of η_{12} using the experimental results and analytical model. In addition, a discussion is presented on the validity of the assumptions made on the Poisson's ratios being real and independent of frequency.

Vibration Damping Loss Factors of S-2 Glass/3501-6 and AS4/3501-6

All composite specimens were tested using the methodology given in Chapter 5. In summary, the composite materials manufactured in this research were machined to the desired beam length. A specimen was placed into the clamping fixture with the fiberglass-reinforced Teflon pieces placed between the specimen and the movable clamp block. The clamp block bolts were tightened to a torque of 10 ft-lb. The eddy current probe was then positioned, centered approximately 0.5 in. from the end of the beam. The resonant frequency was calculated and the desired acquisition rate chosen, which was at least 8 times the first resonant frequency of the beam. The data acquisition program was then run. The specimen was excited with an impulse near the clamped end of the specimen. The displacement and force versus time information was stored for later manipulation. The size of the data set was reduced to 2048 data points. This information was then read into ILS and stored with a record size of both 2048 and 512 data points. An FFT was performed on the data and stored as a file. The stored FFT files were then input into the graphics routine, Grapher, where a fourth order curve fit of each side of the first resonant peak was determined. The orthogonal coefficients and the alpha and beta recursion numbers were then input into a file. These files were then used as input to a basic computer program which computed the intersection of the two curves, the resonant frequency and the half power points. For each specimen, the maximum displacement in the

512 data point sets and the appropriate loss factors were stored as a data file. This data file was then used as input to the graphics routine, Grapher. A linear fit was then performed for each specimen, extrapolating the curve to zero displacement. These zero displacement extrapolated loss factor values with the appropriate frequency were then input into a file which is used to characterize the frequency dependence of the damping loss factor.

The specimen configurations tested included 0°, 90° and $\pm$ 45° for both the S-2 glass and AS4 graphite epoxy systems. The beam lengths were chosen so that the first resonant frequency would be between 10 and 1000 Hz. To properly characterize the frequency response of the material in the frequency range of 10 to 1000 Hz., a series of beam lengths had to be chosen so that their first resonant frequency was in this interval. The lengths were chosen so that the loss factor at approximately 100 Hz intervals could be determined. There were some restrictions on beam length that were imposed by the specific apparatus. The longest beam length that could be tested was 12 in. (30.5 cm). This results in a different lower bound for the lowest first resonant frequency for different material configurations tested. For given beam dimensions, the effective bending stiffness of the beam will govern the beam response, as was shown previously by equation 149. In addition, the shortest beam tested had to have a minimum of 20:1 length to thickness ratio in order to minimize the effects of shear and rotary inertia corrections to the damping loss factor determination (1). The results of the testing are shown in graphical form in Figures 24-29. The specific information for each beam length is also given in tabulated form in Appendix E.

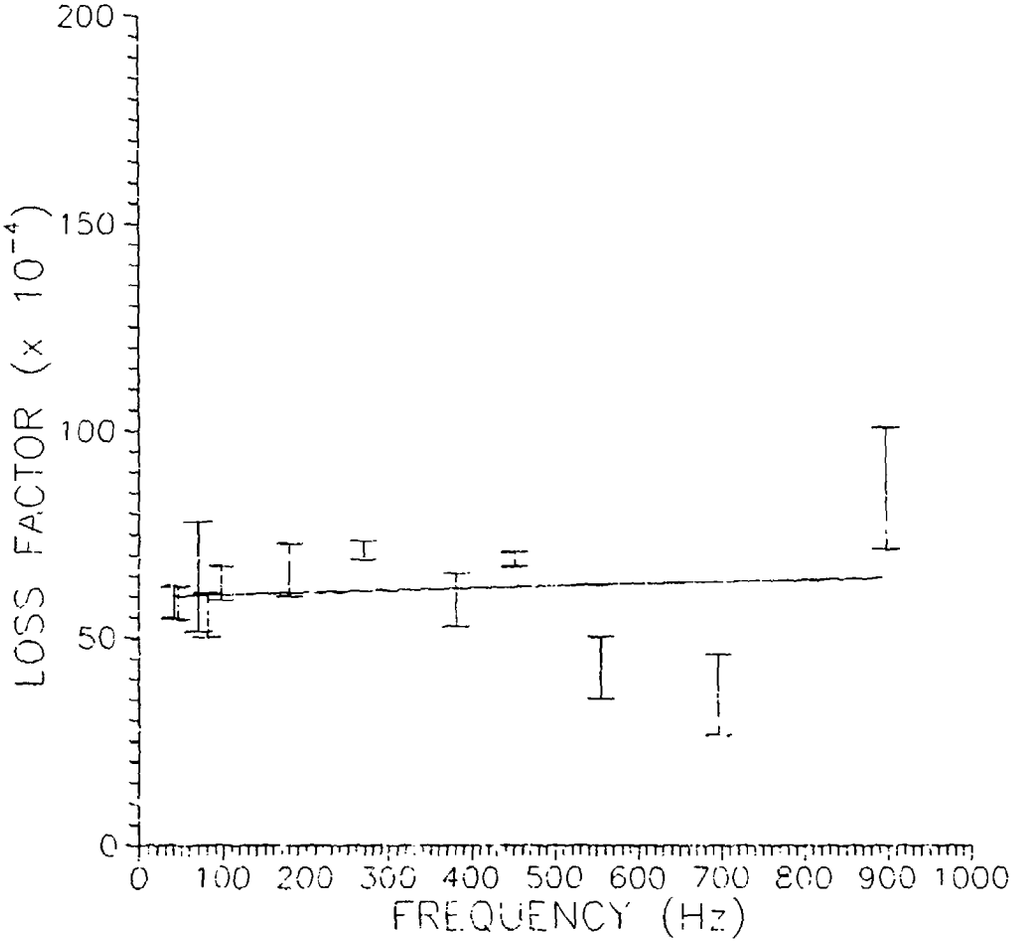

Figure 24 Loss factor vs. frequency for 0° S-2 Glass/3501-6.

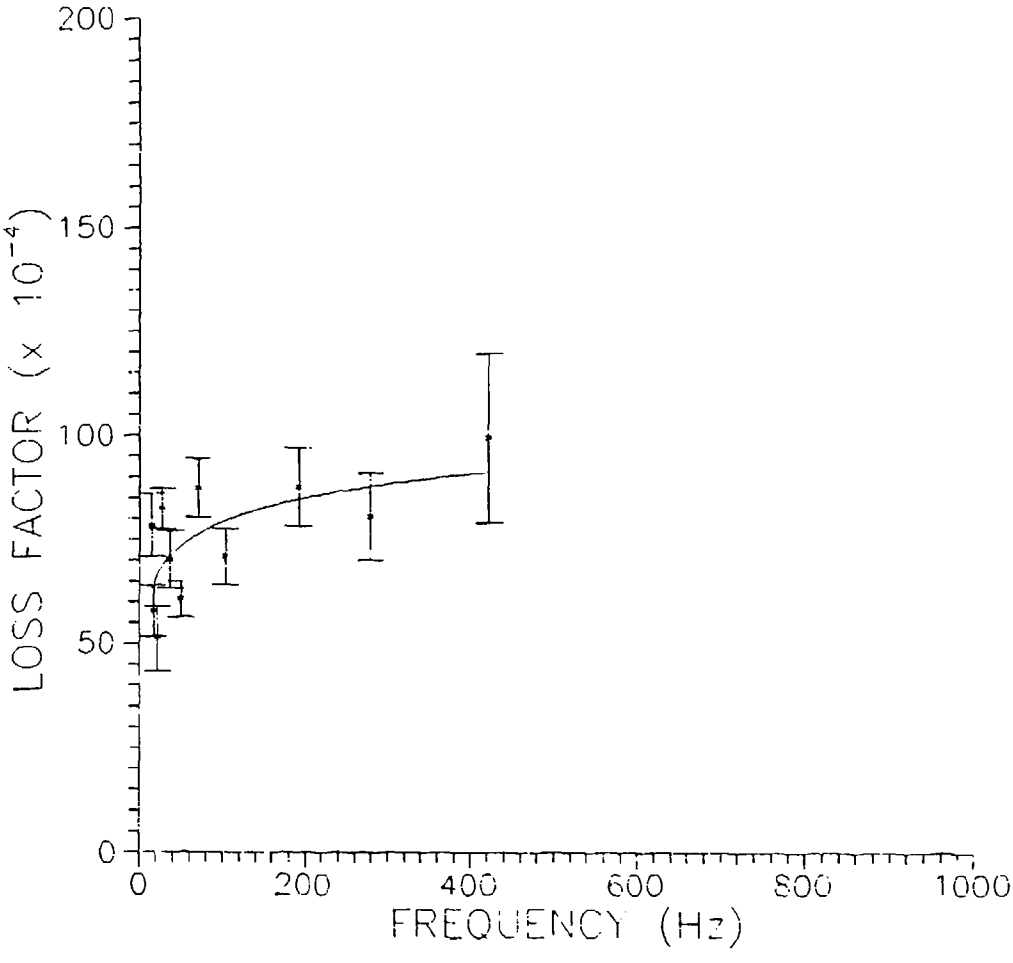

Figure 25 Loss factor vs. frequency for 90° S-2 Glass/3501-6.

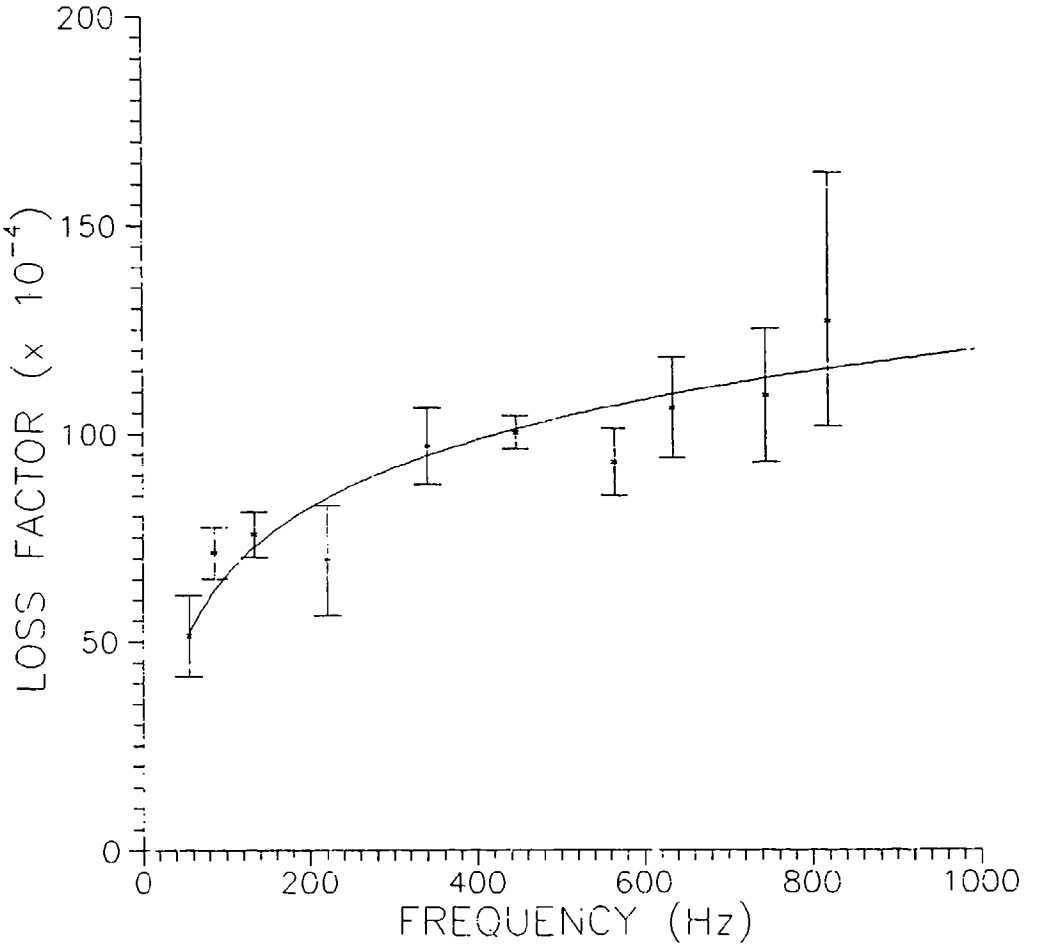

Figure 26 Loss factor vs. frequency for ±45° S-2 Glass/3501-6.

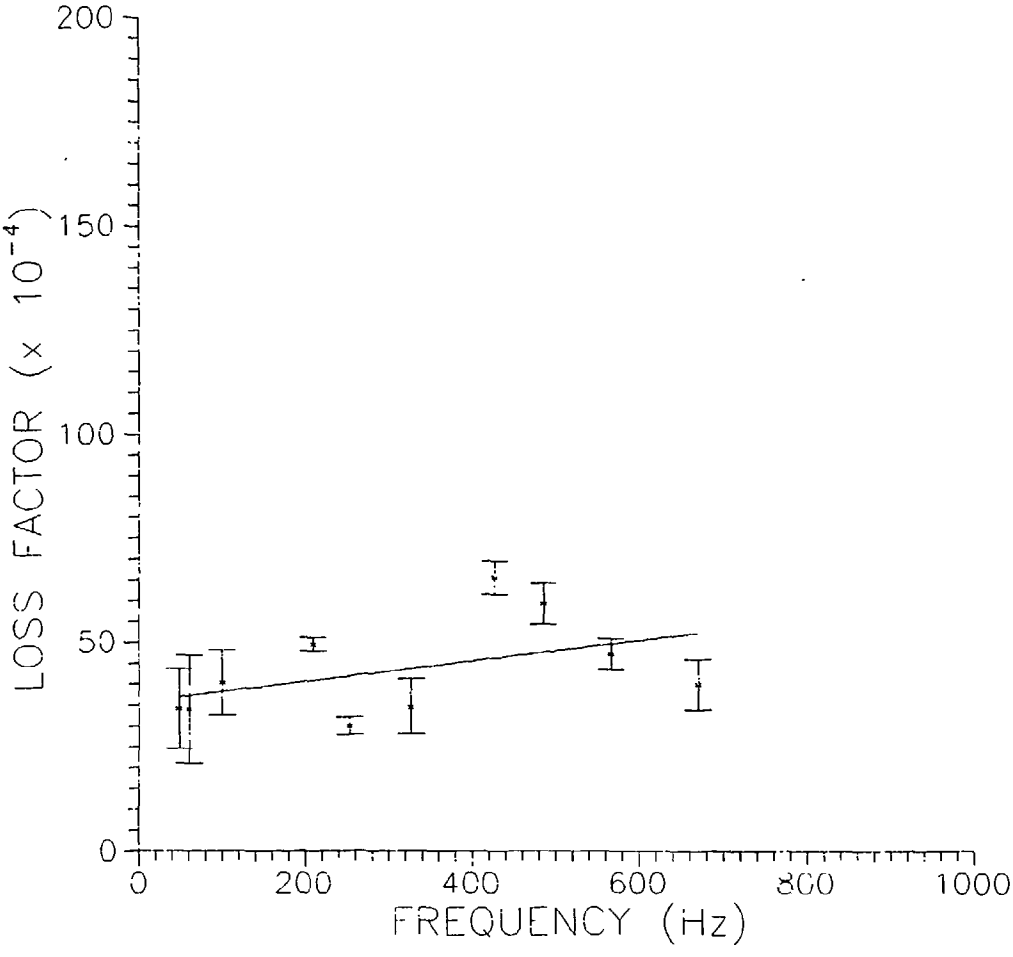

Figure 27 Loss factor vs. frequency for 0° AS4/3501-6.

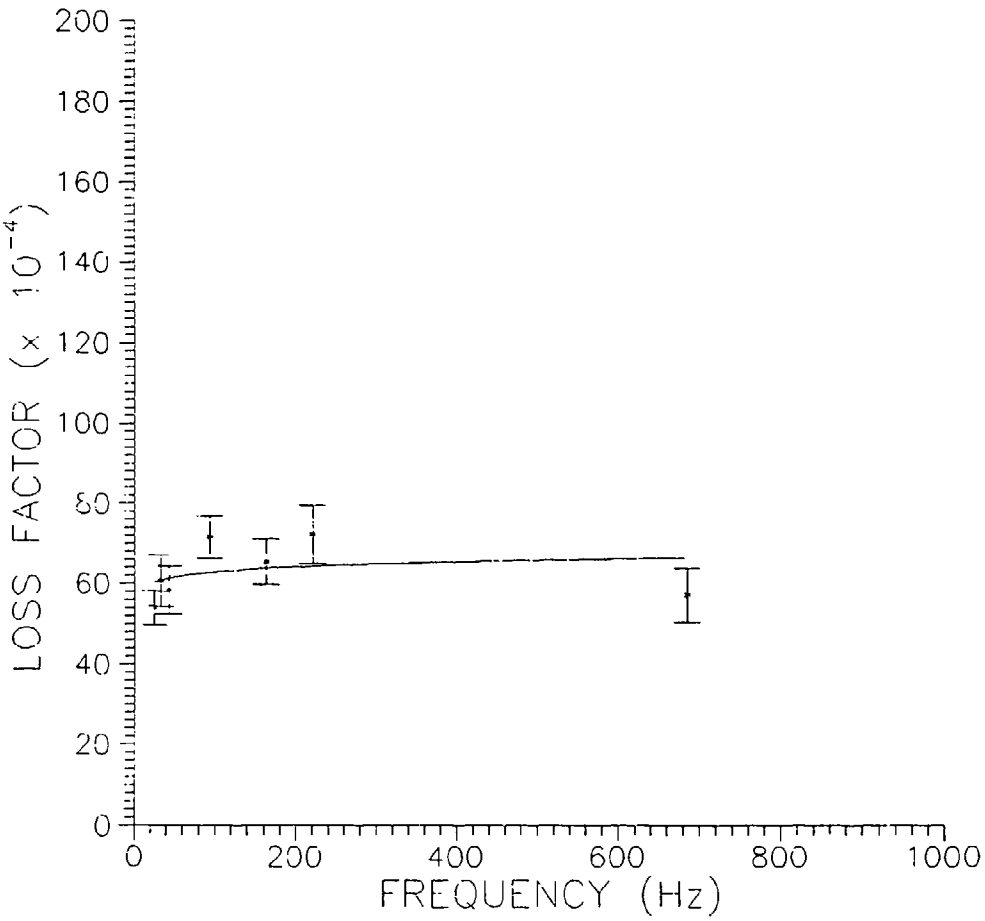

Figure 28 Loss factor vs. frequency for 90° AS4/3501-6.

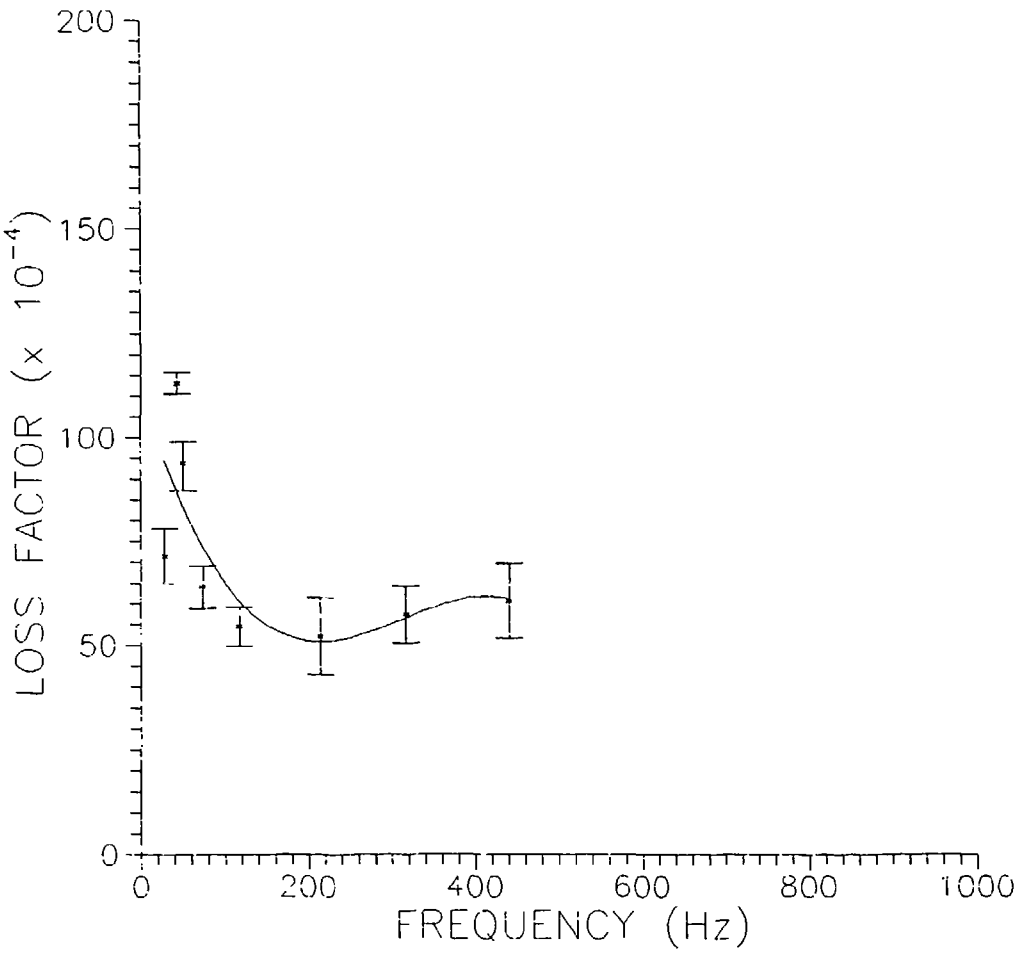

Figure 29 Loss factor vs. frequency for ±45° AS4/3501-6.

For a typical resonant frequency, the zero displacement extrapolated loss factor has some interesting characteristics. First, for a given beam length, there appears to be a variation in the rate of decay in loss factor as a function of the maximum displacement. This may occur as the result of material variations from specimen to specimen. Any material anomaly within the specimen, such as fiber waviness or fiber misorientation, that are possible sources of energy dissipation are minimized when displacements are small. As the displacements are increased, the energy dissipation caused by these material anomalies should also increase. In addition, a scatter in the experimentally determined resonant frequency occurs, the result of minor variations in beam length within one data set. This variation in beam length may also affect the loss factors. These characteristics are evident in the results presented in Figures 21 and 22.

Another interesting characteristic of the zero displacement extrapolated loss factor curves is the variation in their slope as a function of beam length, or frequency. This variation in slope may be the result of a change in stress distribution in the composite material or it may be the result of the viscoelastic character of the matrix. It may also be the result of a variation in aerodynamic damping as a function of frequency. Some investigators have indicated that the aerodynamic damping is a function of the velocity of the beam center of gravity (74,75). As the resonant frequency is increased for a given amplitude of vibration, there is an associated increase in velocity of the center of gravity of the specimen.

In order to extrapolate the values of the material loss factors of the two material systems in the range of frequencies up to 1000 Hz, the experimental values were curve fit.

For the 90° beam configuration, there were two curve fits used on the experimental data: a logarithmic fit and a linear fit. The best fit to the experimental data, determined using a least squares approach, was the logarithmic fit. It will be shown later in this chapter that the epoxy resin system also possesses a logarithmic frequency dependence of the loss factor. The similarity in the frequency dependence of the loss factor between the 90° composite beam and the unreinforced resin is expected, since a composite with a 90° orientation will possess matrix dominated characteristics.

A mechanical analogue that can be used to approximate the response of the 0° orientation would be the Voigt-Kelvin model of the spring dashpot in parallel. In this model, the loss factor should be directly proportional to the loss factor of the matrix. Since the loss factor of the matrix possesses a logarithmic dependence with frequency, it is assumed that a logarithmic fit would most accurately describe the frequency dependence of the 0° orientation. Because of the nonuniform trends in the loss factor as a function of frequency for this orientation, a logarithmic and linear fit were again used to fit the data. The best fit to the experimental data, determined using a least squares approach, was the linear fit. It should be pointed out that the variation in the two fits was minimal. Since the linear fit provided the most accurate description of the data, this is the fit that will be used to extrapolate the loss factors in the frequency range up to 1000 Hz. For an extrapolation outside this range, the logarithmic fit should provide the most accurate representation of the frequency dependence of the loss factor.

For the $\pm 45°$ beams, two different approximations were used. For the S-2 glass/epoxy, the experimental data was fit using logarithmic and linear approximations.

The curve fit that provided the most accurate representation of the data, again based on a least squares analysis, was the logarithmic fit. The logarithmic form should be from a physical standpoint. The $\pm 45°$ configuration in bending will experience in-plane shear stresses along with in-plane normal stresses. The shear characteristics of the composite are dominated by the shear characteristics of the resin. As such, it is anticipated that the loss factor characteristics of this configuration should parallel that of the resin.

The $\pm 45°$ AS4/3501-6 material showed trends that were not anticipated. As such, a polynomial fit was used to approximate the data. Although the loss factor values at low frequency were very reproducible, the low frequency values are still questionable. However, in order to determine trends in the frequency range up to 1000 Hz., the third order polynomial fit will be utilized.

The curve fits that were obtained for the specific material and orientation are given as follows:

0° glass	η_1	$= 5.1476 \times 10^{-7}\ f + 5.98698 \times 10^{-3}$	(152)
90° glass	η_2	$= 8.37194 \times 10^{-4} \ln(f) + 4.06544 \times 10^{-3}$	(153)
$\pm 45°$ glass	η_{12}	$= 2.08645 \times 10^{-3} \ln(f) - 2.95132 \times 10^{-3}$	(154)
0° graphite	η_1	$= 2.44682 \times 10^{-6}\ f + 3.56884 \times 10^{-3}$	(155)
90° graphite	η_2	$= 1.87469 \times 10^{-4} \ln(f) + 5.42504 \times 10^{-3}$	(156)
$\pm 45°$ graphite	η_{12}	= third order polynomial with orthogonal coefficients of the form given in equation 147 where the orthogonal and recursion factors are given as	(157)

$a_0 = 70.925 \times 10^{-4}$	$\alpha_1 = 0$	$\beta_1 = 0$
$a_1 = 7.94784 \times 10^{-4}$	$\alpha_2 = -0.715559$	$\beta_2 = 1.86312$
$a_2 = 6.68701 \times 10^{-4}$	$\alpha_3 = 0.503032$	$\beta_3 = 1.0759$
$a_3 = -2.87757 \times 10^{-4}$	$\alpha_4 = 0.202372$	$\beta_4 = 0.962746$

A statistical analysis of the curve fits was conducted using the Student t analysis method. For the comparison of the loss factors, the t distribution was used as the basis to determine if the difference between two means is significant or due to random variations in the data. For this analysis, the pooled variance, S^2_p, and the standard deviation of the difference in means, $S_{(x_2-x_1)}$, were determined. The pooled variance is given by

$$S_p^2 = \frac{(n_1 - 1)\, S_{x1}^2 + (n_2 - 1)\, S_{x2}^2}{n_1 + n_2 - 2} \tag{158}$$

where n_1 and n_2 are the number of samples in the data set and S^2_{x1} and S^2_{x2} are the standard deviations for sample sets 1 and 2 respectively. The standard deviation of the difference in means is given as

$$S^2_{(\bar{x}_2 - \bar{x}_1)} = S_p^2 \left(\frac{1}{n_1} + \frac{1}{n_2} \right) = S_p^2 \frac{n_1 + n_2}{n_1 n_2} \tag{159}$$

The statistic t is then computed as

$$t = \frac{|\bar{x}_2 - \bar{x}_1|}{S_{(\bar{x}_2 - \bar{x}_1)}} \tag{160}$$

The value of t determined in equation 160 was then compared to the value of $t(\alpha)$ given in a

Student's t distribution for d degrees of freedom table given in reference 76. From this table, a degree of confidence was determined for each successive mean frequency. The statistical information generated using equations 158-160 are presented in Appendix F. The results can be summarized as follows; there is at least a 95% confidence that the data at each frequency is significantly different from the previous frequency. The curves that were generated to indicate the trends in the loss factor as a function of frequency are significant.

In addition to the damping loss factor characterization for the composite material, characterization of the loss factor of a similar matrix system was also performed. The matrix material used in this portion of the dissertation was a 350° F epoxy from the Narmco Division of BASF, which they designate 5208. The Hercules Corp. 3501-6 resin was not tested because it was not sold in bulk form. The characterization of the damping loss factor of the matrix will provide an additional check of the test procedure. The testing procedure used was the robust testing methodology given in Chapter 5. A summary of the results of the testing are presented in Figure 30. The specific loss factors for the various beam lengths are presented in Appendix G. In general, Figure 30 shows that the resin possesses similar damping loss factor characteristics to the composite materials. The loss factor exhibits a logarithmic increase with increasing frequency. The logarithmic curve fit shown in Figure 30 is given as

$$\eta_m = 28.13 \times 10^{-4} \ln(f) + 72.53 \times 10^{-4} \qquad (161)$$

It should also be noted that the magnitude and frequency dependence of the loss factor determined herein showed trends that were similar in magnitude and shape to another 350° F cure epoxy, 934 epoxy made by the Fiberite Division of ICI (64).

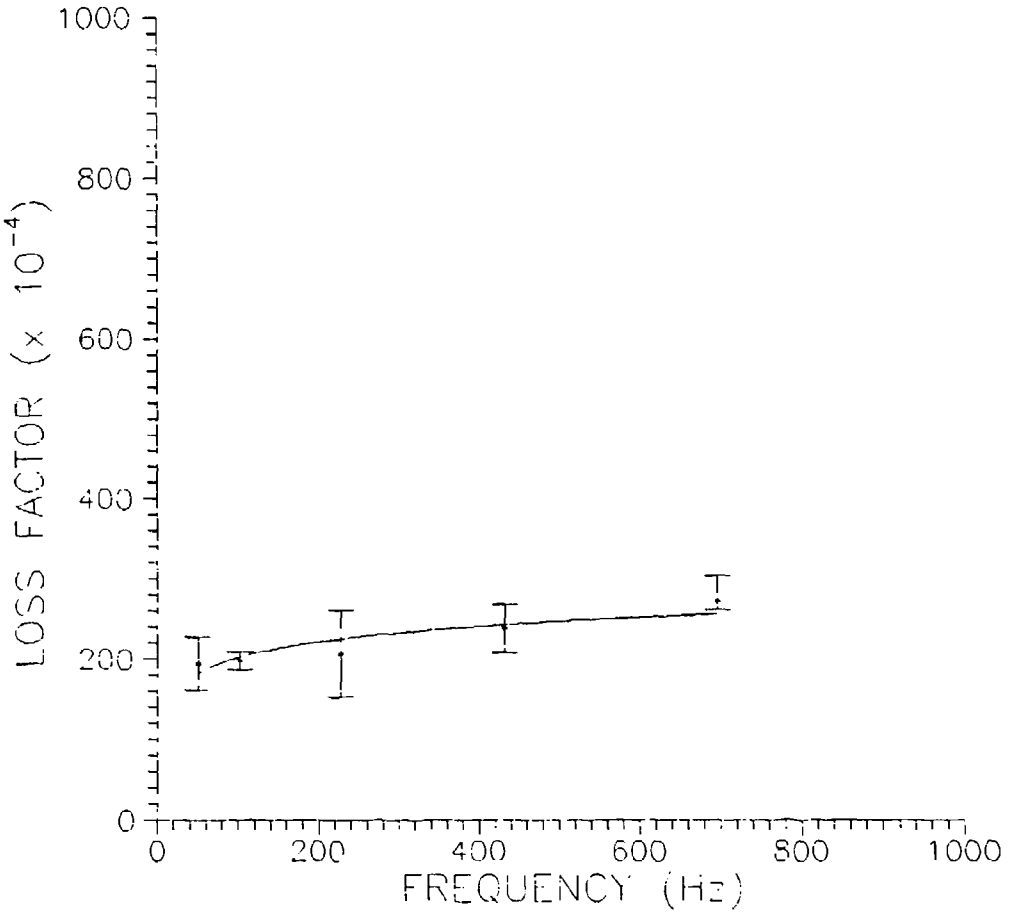

Figure 30 Loss factor vs. frequency for 5208 neat epoxy resin.

As a further comparison of the loss factor of the resin to that of the composite systems, the loss factor of the composite is divided by the loss factor of the resin, and this normalized loss factor is graphed as a function of frequency for the S-2 glass/epoxy material for the 90°, 0° and the ± 45° orientations. These are shown in Figures 31, 32 and 33, respectively. This normalization allows easy visualization of the effect of the fiber on the loss factor of the composites. For the 90° orientation, the normalized loss factor is linear at frequencies above approximately 50 Hz. Since the 90° orientation is matrix dominated, it would be assumed that the loss factor should be linearly proportional to the resin. It is interesting to note that the volume fraction of the resin is approximately 40%. The normalized loss factor of the S-2 Glass/3501-6 in the 90° orientation is also approximately 40%. This would indicate that an estimate of the loss factor of a polymer in its glassy region can be obtained by using a simple rule of mixtures approach.

For the 0° orientation, the normalized loss factor decreases with increasing frequency. This characteristic is reasonable since the composite in this configuration is fiber dominated and will respond more elastically than as a viscoelastic. As the frequency is increased, the viscoelastic characteristic of the matrix becomes more elastic also, thereby resulting in a slight decrease in loss factor with increasing frequency.

The normalized loss factor for the ± 45° orientation exhibits an increase with increasing frequency. The normalized loss factor for the ± 45° orientation is also seen to be greater than that of the 90° orientation. This result is probably due to the in-plane shear strains that are present in the ± 45° specimens and which are not present with the 90° specimens. Since the dominant mode of energy dissipation by a viscoelastic is through

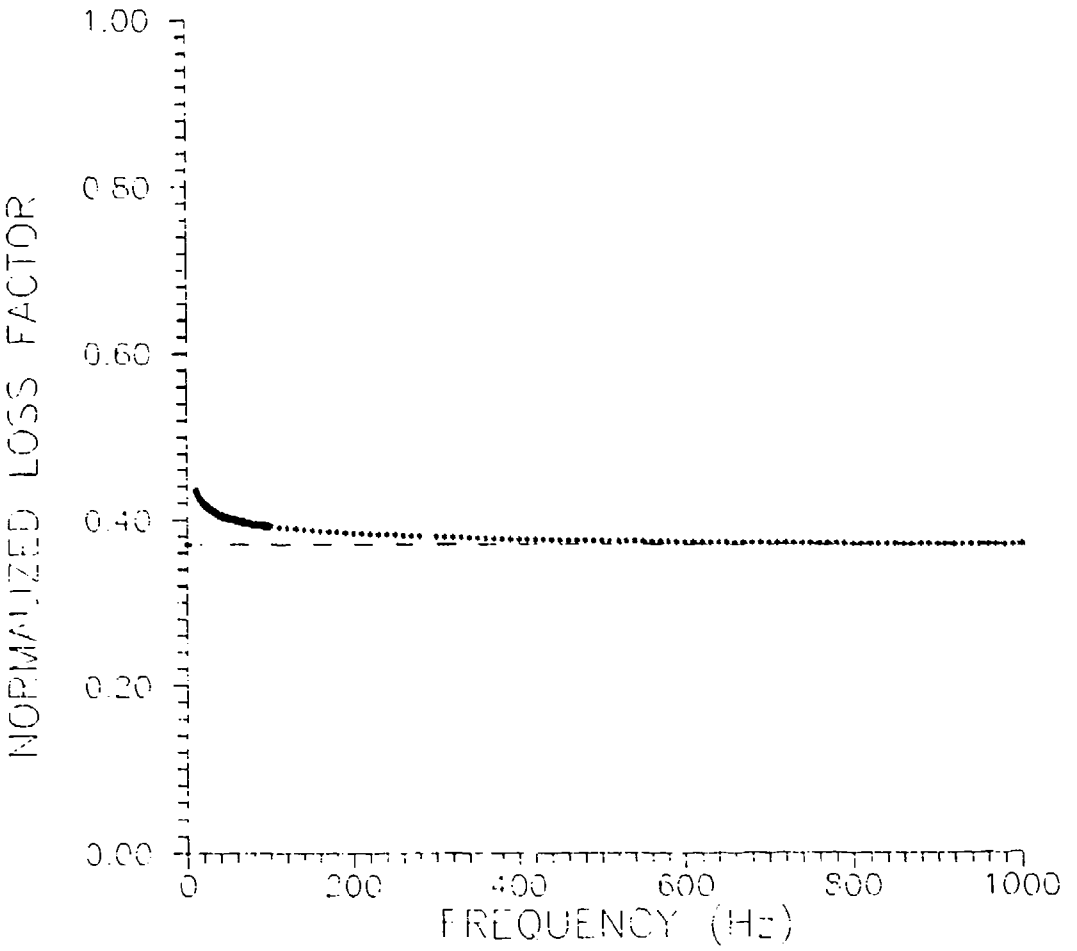

Figure 31 Normalized loss factor of 90° S-2 Glass/3501-6 vs. frequency.

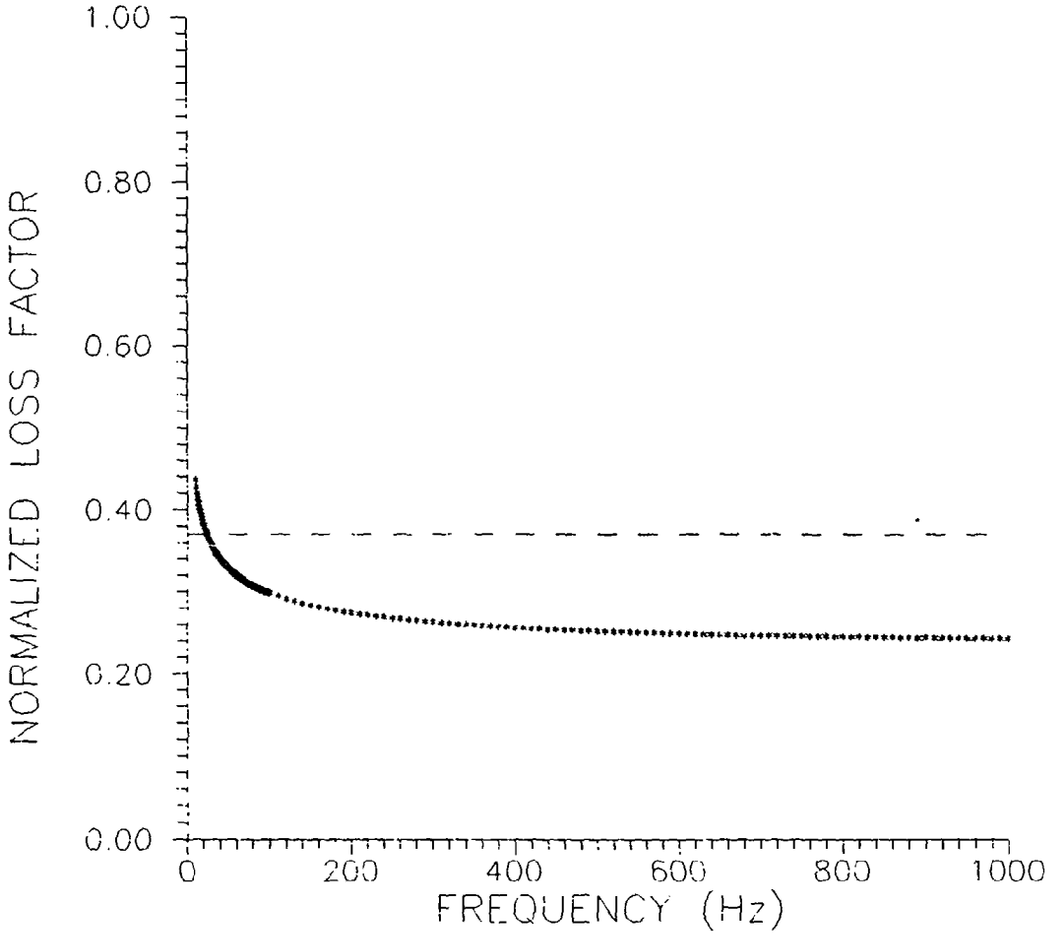

Figure 32 Normalized loss factor of 0° S-2 Glass/3501-6 vs. frequency.

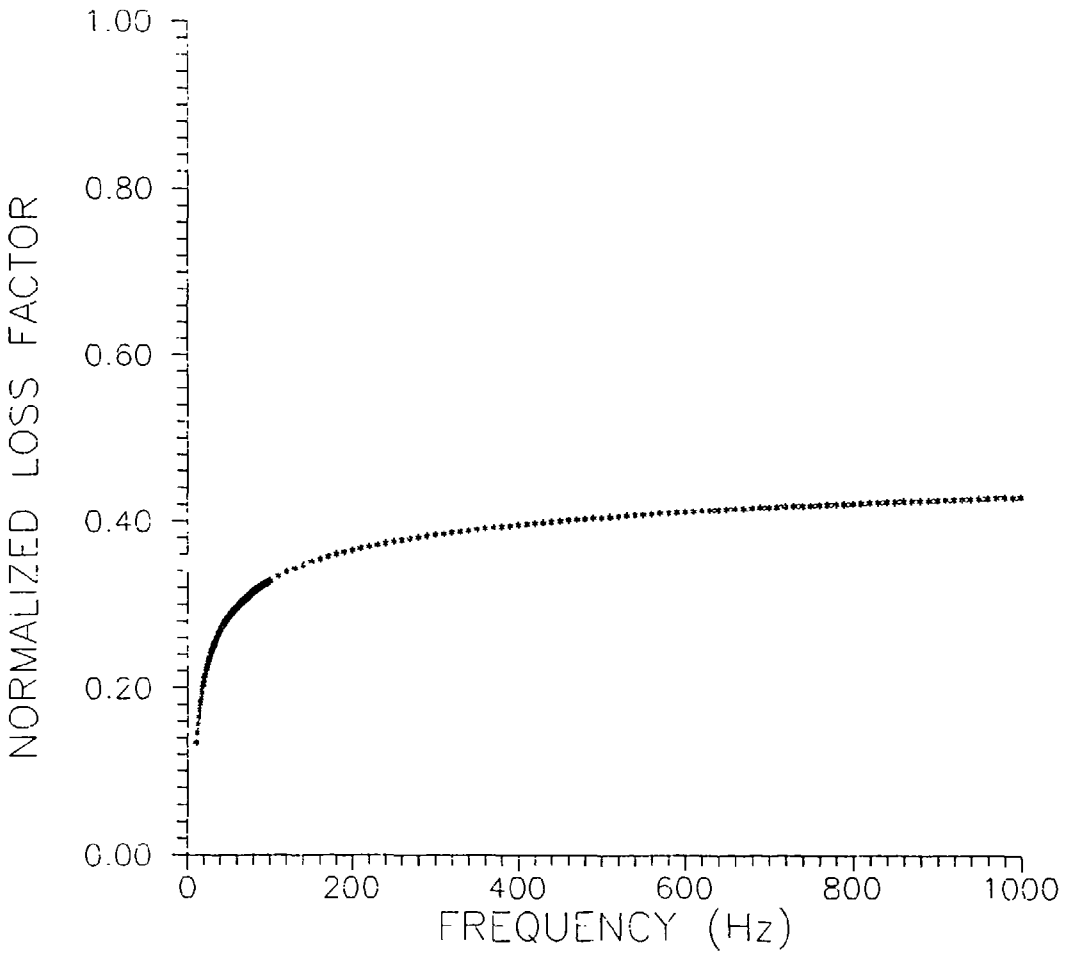

Figure 33 Normalized loss factor of ±45° S-2 Glass/3501-6 vs. frequency.

shear, it is reasonable that the $\pm 45°$ normalized loss factor increases with increasing frequency.

Analytical Determination of η_{12}

It should be recalled that the shear loss factors of the composites were estimated using a $\pm 45°$ beam specimen. For this specimen orientation, the application of a bending moment results in a combination of longitudinal, transverse and shear in plane stresses. The assumption that the loss factor of the $\pm 45°$ beam specimen is equal to the shear loss factor, η_{12}, is therefore in error. The loss factor that is determined using this specimen is actually the summation of the losses attributable to the these stresses.

It is possible, however, to determine the shear loss factor of the composite using experimental values of the loss factor of the $\pm 45°$ specimen. This is done by using the proposed analytical model along with the longitudinal and transverse loss factors that were experimentally determined. One of the test frequencies of the $\pm 45°$ specimen is first chosen. The values of η_{11} and η_{22} are then determined for this frequency using equations 152 and 153. An estimated value of η_{12} is chosen. The values of η_{11}, η_{22}, and η_{12} are then used as inputs for the model described in Chapter 3 to analytically determine the loss factor for the $\pm 45°$ specimen. The value of η_{12} is adjusted until the predicted and experimental values of the loss factor for the $\pm 45°$ specimen are within 0.1%. This value of η_{12} is then taken to be the loss factor in shear for the material.

To determine η_{12}, the analytical model was programmed using the symbolic manipulator program, Mathmatica$_{TM}$. The complex moduli E_1^* and E_2^* that were used as input for the model are those given in equations 152 and 153 for the S-2 Glass/3501-6 and by equations 155 and 156 for the AS4/3501-6. The program uses these complex moduli to determine the values of the ABD matrix. The various terms for the reduced stiffnesses are complex. As such, conventional laminated plate theory routines would not be able to perform the manipulations required by the model. The inverse ABD matrix is then determined. This operation, although straightforward for the symbolic manipulator program, Mathmatica$_{TM}$, is quite difficult to perform either by hand or using conventional computer algorithms. Since the $\pm 45°$ specimen is subjected to a bending moment, the loss factor is determined using the equation for the effective bending stiffness, equation 146. This calculated value of η_{+45} is then compared with the experimental value. The estimated value of η_{12} was then increased or decreased based on the analytically determined value of $\eta_{\pm 45}$. This iterative process was continued until the estimated value of η_{12} in the analytical model gave results that were within 0.1% of the experimental value.

This process was used to determine the value of η_{12} from 50 to 1000 Hz. The results of this analysis are given in Table 14. The results are also presented in graphical format in Figure 34. It should be noted that the loss factor that was experimentally obtained for the $\pm 45°$ specimen is slightly lower than the estimated shear loss factor. These results are consistent with current thinking of energy dissipation of viscoelastic materials. The predominant source of energy dissipation in a viscoelastic material is in shear. Since the $\pm 45°$ specimen is not in a state of pure shear, the loss factor calculated should be less than the shear loss factor.

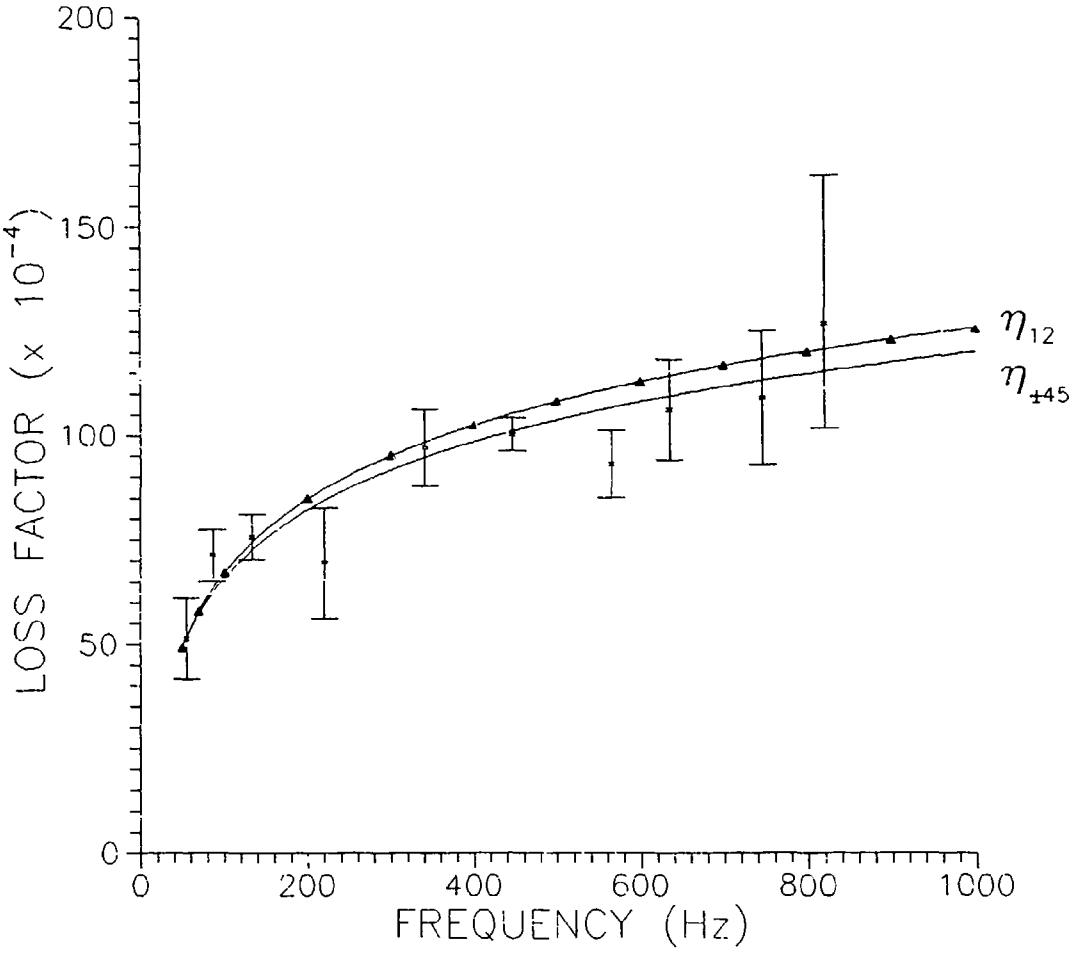

Figure 34 Analytical η_{12} vs $\eta_{\pm 45}$ as a function of frequency for S-2 Glass/3501-6.

Table 14 : Determination of η_{12} using Experimental Values of η_{11}, η_{22}, and η_{+45} for S-2 Glass/3501-6.

Frequency (Hz)	η_{11} (x 10^{-4})	η_{22} (x 10^{-4})	η_{12} (x 10^{-4})	η_{+45} model (x 10^{-4})	η_{+45} experimental (x 10^{-4})
50	60.13	73.41	49.24	52.11	52.11
70	60.23	76.22	57.90	59.13	59.13
100	60.38	79.21	67.07	66.57	66.57
200	60.90	85.01	84.86	81.03	81.03
300	61.41	88.41	95.22	89.49	86.49
400	61.93	90.81	102.55	95.50	95.50
500	62.44	92.68	108.20	100.15	100.15
600	62.96	94.21	112.81	103.96	103.96
700	63.47	95.50	116.69	107.18	107.17
800	63.99	96.62	120.03	109.96	109.96
900	64.50	97.60	122.96	112.41	112.41
1000	65.02	98.49	125.58	114.61	114.61

This same procedure was used to analytically determine the shear loss factor for the AS4/3501-6 material. Similar results occurred. The calculated value of η_{12} was greater than the experimental value obtained using the $\pm 45°$ specimen. The results from this procedure are given in Table 15. Figure 35 shows the comparison graphically between $\eta_{\pm 45}$ and η_{12}. It should be noted in this comparison, the curve fit for the calculated value of η_{12} is determined for frequencies greater than 50 Hz only. The reason for this is that the experimental results for frequencies less than 50 Hz cannot be phenomenologically explained. In addition, it should be noted that the estimated value of η_{12} would not be expected to continue to increase at higher and higher frequencies. Instead, this value should reach some upper limit asymptotically, similar to the curve generated for the loss

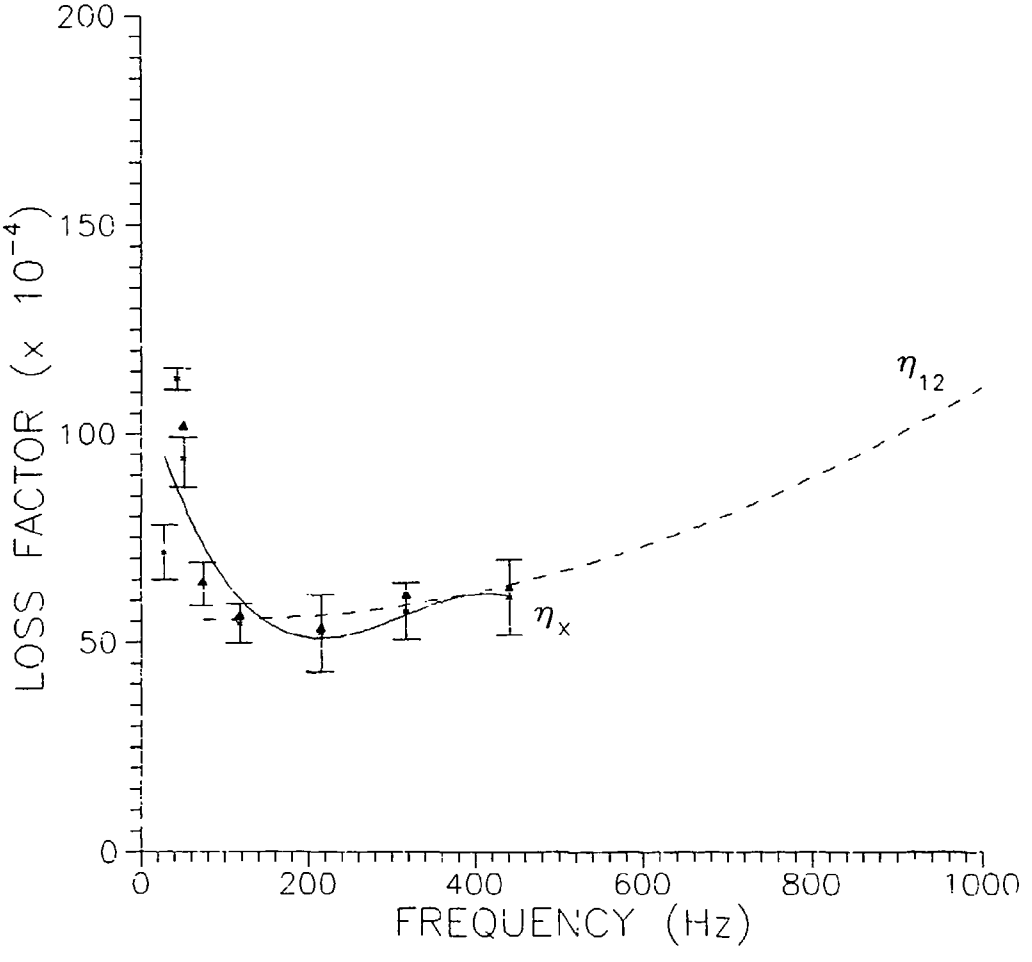

Figure 35 Analytical η_{12} vs $\eta_{\pm 45}$ as a function of frequency for AS4/3501-6.

Table 15 : Determination of η_{12} using Experimental Values of η_{11}, η_{22}, and η_{+45} for AS4/3501-6.

Frequency (Hz)	η_{11} (x 10^{-4})	η_{22} (x 10^{-4})	η_{12} (x 10^{-4})	η_{+45} model (x 10^{-4})	η_{+45} experimental (x 10^{-4})
50.81	36.93	61.61	102.07	93.94	93.94
73.74	37.49	62.31	67.67	64.03	64.02
117.44	38.56	63.19	56.58	54.50	54.49
214.42	40.93	64.31	53.59	52.18	52.18
317.10	43.45	65.02	61.49	59.37	59.37
441.12	46.48	65.67	62.99	61.05	61.05

factor of the resin. As such, there is a limitation on the validity of the estimated value of η_{12} to be limited to the frequency range of 50 to 1000 Hz.

The frequency dependence of η_{12} is then determined for both material systems by performing a curve fit to the analytically determined values given in Tables 14 and 15. The equations that describe the loss factor as a function of frequency are given as follows

$$\eta_{12_{Glass}} = 25.4998 \times 10^{-4} \ln(f) - 50.371 \times 10^{-4} \tag{161}$$

$\eta_{12_{Graphite}}$ = second order polynomial with orthogonal coefficients of the form given in equation 147 where the orthogonal and recursion factors are given as

$a_0 = 58.6615 \times 10^{-4}$ $\quad \alpha_1 = 0 \quad \beta_1 = 0$

$a_1 = 2.06069 \times 10^{-4}$ $\quad \alpha_2 = -0.0835393 \quad \beta_2 = 2.20824$

$a_2 = 0.441874 \times 10^{-4}$ $\quad \alpha_3 = 0.120602 \quad \beta_3 = 1.45132$ (162)

Throughout the remainder of this report, the shear loss factors for the materials given by equations 161 and 162 will be utilized.

Determination of η_{11} and η_{12} for S-2 Glass/3501-6 using Micromechanical Model

An investigation was performed to determine the accuracy of the micromechanical models for predicting the lamina loss factors of composites. The analytical model developed by Hashin that was described in Chapter 2 will be used The material information required by the model are the matrix frequency dependent loss factor, the axial and shear modulus of the fiber and resin, and the matrix volume fraction. The shear properties of the fiber and matrix were approximated using the relationship of the axial to shear modulus for isotropic materials. All other values used for this exercise were experimentally determined. Table 16 lists the specific input values used in the analytical model.

Table 16 Material Property Input for Micromechanical Model

Material	Volume Fraction (%)	Shear Modulus (x 10^6 psi)	Axial Modulus (x 10^6 psi)
S-2 Glass	63	4.77	12.4
Epoxy	37	0.2	0.5

The micromechanical model developed by Hashin provides a methodology for determining the in-plane axial, η_{11}, and shear, η_{12}, loss factors as a function of the materials properties given in Table 16. The equations used are given below as

$$\eta_{11} = \frac{\eta_m}{1 + \frac{E_f v_f}{E_m v_m}} \tag{163}$$

$$\eta_{12} = \frac{\eta_m v_m \left[\left(\frac{G_f}{G_m} + 1 \right)^2 + v_f \left(\frac{G_f}{G_m} - 1 \right)^2 \right]}{\left[\frac{G_f}{G_m} (1 + v_f) + v_m \right] \left[\frac{G_f}{G_m} v_m + (1 + v_f) \right]} \qquad (164)$$

where η_m is the loss factor of the resin, E_f and E_m are the axial moduli of the fiber and matrix, respectively, G_f and G_m are the shear moduli of the fiber and matrix, respectively and v_f and v_m are the volume fraction of the fiber and matrix in the composite, respectively.

The axial and shear loss factors as a function of frequency determined using equations 163 and 164 are shown graphically in figures 36 and 37, respectively. Also included in these figures are the experimental results obtained for the corresponding composite beams.

The micromechanical analytical determination of η_{11} is significantly lower than the experimental values obtained over the entire frequency range. One possible explanation for this is that the analytical model fails to take into consideration the shear at the fiber matrix interface. Any shear deformation in the matrix would result in a significant increase in loss factor of the system. Another possible explanation is that the matrix material near the fiber has different material characteristics than the bulk matrix. It has been proposed by numerous investigators that this interphase region of the matrix occurs in an area which is a fraction of the fiber diameter around the fiber. This material can possess a glass transition temperature which is lower than the bulk matrix, which results in a frequency dependent loss factor that is different than the bulk matrix. These two conditions would have the effect of increasing the loss factor of the composite. As such, it is not surprising that the

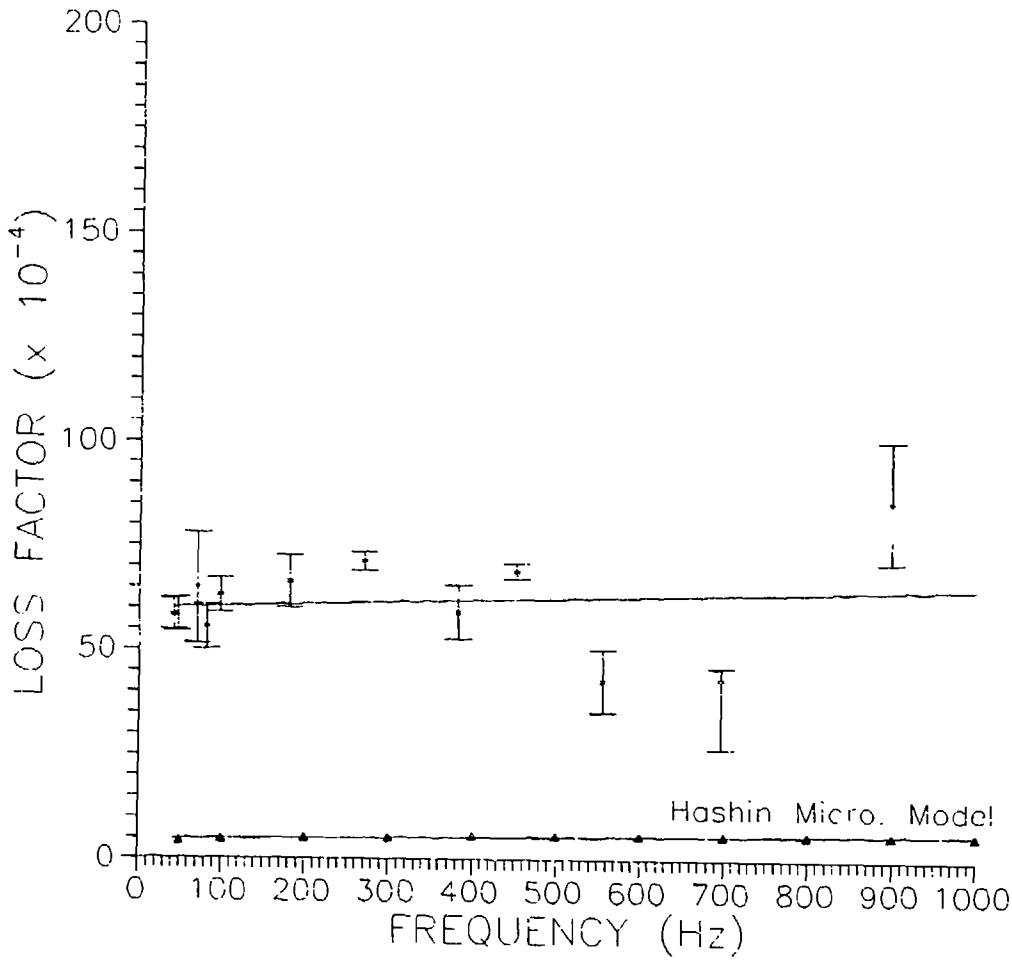

Figure 36 Analytical determination of η_{11} for S-2 Glass/3501-6 using Hashin Micromechanical Model

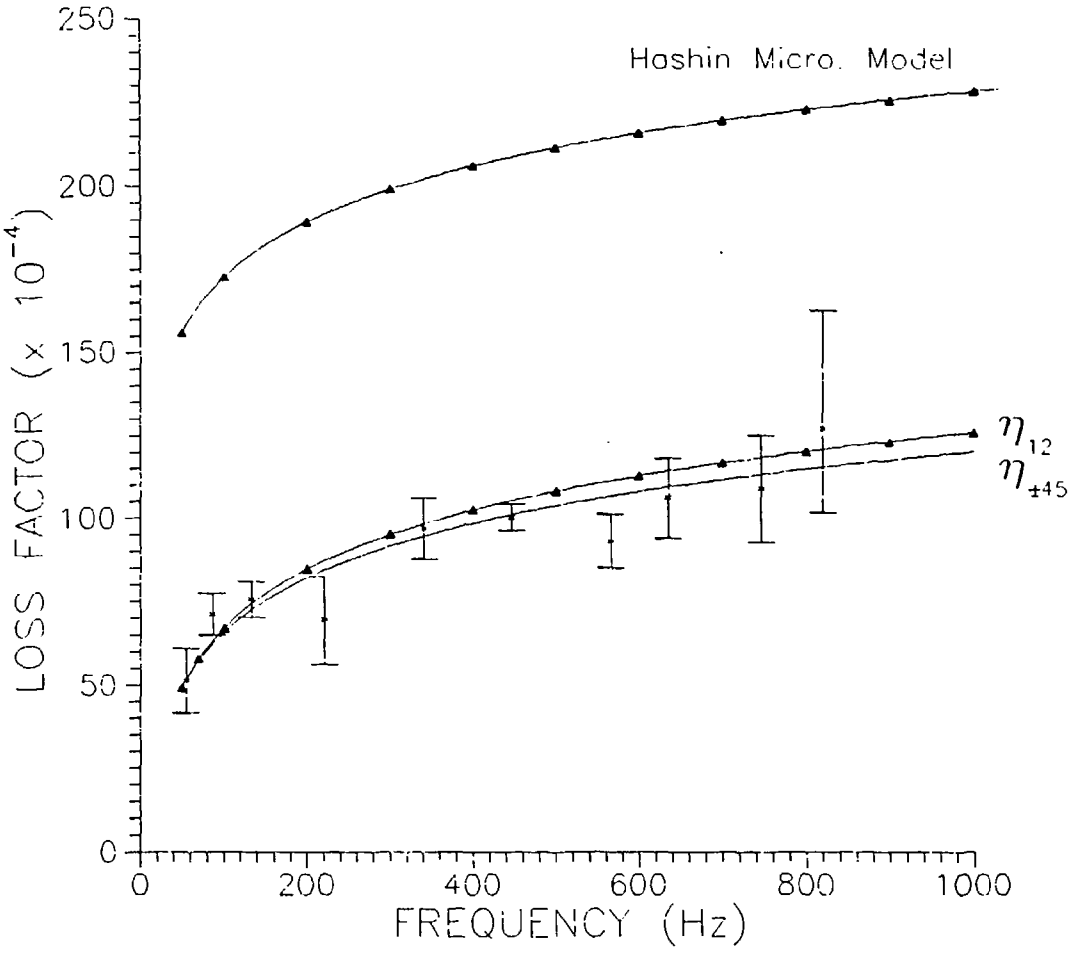

Figure 37 Analytical determination of η_{12} for S-2 Glass/3501-6 using Hashin Micromechanical Model

experimentally determined loss factor is greater than the analytical value.

The analytical determination of η_{12} using the Hashin micromechanical model is shown to give results that are approximately a factor of two greater than the experimentally determined values in the frequency range up to 1000 Hz, as seen in Figure 37. The micromechanical model assumes that the composite shear loss factor is directly proportional to the loss factor of the matrix. This appears to be an accurate general description of the composite shear loss factor since the general form of the experimentally determined shear loss factor for both the matrix and composite have a logarithmic frequency dependence. In the micromechanical model determination of η_{12} for the S-2 Glass/3501-6, however, the effective constant of proportionality, determined using Equation 164, is approximately 0.85. If this constant of proportionality was approximately 0.43, the micromechanical model would provide an accurate approximation of the shear loss factor for the S-2 Glass/epoxy system. It should be noted that this constant of proportionality is greater than the volume fraction of the matrix, which was determined to be 37%, making a simple rule of mixtures approach inappropriate. The fact that the value of η_{12} is greater than a rule of mixture prediction seems appropriate since no consideration is given for any shear at the fiber matrix interface. To account for this, the incorporation of some form of relationship between the fiber and matrix shear modulus would seem appropriate. It appears that the specific form used by Hashin should be modified in order to provide a more accurate determination of the shear loss factor of composites.

Comments of the Poisson's Ratios Assumptions

In the development of the analytical model given in Chapter 3, two assumptions were made concerning the Poisson's ratios: (1) they are real; and (2) they are independent of frequency. A contradiction arises when these assumptions are enforced with the reciprocity relation. For a material subjected to a set of forces, considering the work done by these forces and by utilizing the Maxwell-Betti Reciprocal Theorem along with some simple mathematical manipulations results in the generation of the reciprocity relation

$$\frac{\upsilon_{12}}{E_1} = \frac{\upsilon_{21}}{E_2} \tag{163}$$

This same relation will hold in complex notation, by utilizing the elastic viscoelastic correspondence principle. As such, the corresponding relationship between the elastic moduli and Poisson's ratios will be given as

$$\frac{\upsilon_{12}^*}{E_1^*} = \frac{\upsilon_{21}^*}{E_2^*} \tag{164}$$

In the model presented in Chapter 3, substituting the assumptions on Poisson's ratio into equation 164 yields

$$\frac{\upsilon_{12}}{E_1^*} = \frac{\upsilon_{21}}{E_2^*} \tag{165}$$

Since the real part of the complex modulus is assumed to be real, equation 165 yields the result that the frequency dependence is the same for both the axial and transverse moduli.

Experimentally, this does not occur. This indicates the possible need to incorporate a frequency dependence and also possibly assume that the Poisson's ratios are complex.

The reason the Poisson's ratios were assumed to real and independent of frequency was the lack of experimental procedure to determine these values. Some assumptions can be made, however, in an attempt to analytically determine them using the complex moduli which have been experimentally determined. By definition, υ_{21} is the negative of the ratio of the strain in the 1 direction to the strain in the 2 direction that occurs from the loading of the specimen in the 2 direction. Upon application of a load in the 2 direction, i.e. an axial extension of a 90° specimen, there will be an extension of the material in that direction. Since the material is viscoelastic, this strain will lag the load. As the material is elongated in the 2 direction, there will be a contraction of the material in the 1 direction. Since this direction is fiber dominated, an assumption will be made that this strain is in phase with the strain in the 2 direction. From this assumption, it is seen that υ_{21} is real. Since the assumption is made that there is no lag in strain, there should also be no frequency dependence.

Using the approximation that υ_{21} is real and independent of frequency, υ^*_{12} can be determined using the complex reciprocity relation given in equation 164. It should be noted that υ^*_{12} is assumed to be complex and a function of frequency. Rearranging terms, υ^*_{12} can be given as

$$\upsilon^*_{12} = \left(\frac{E^*_1}{E^*_2} \right) \upsilon_{21} \tag{166}$$

Using the relationship for the Poisson's ratios given in equation 166, then, the reciprocity relation is maintained.

A sensitivity study was conducted to determine the significance of assuming that all Poisson's ratios are real and frequency independent compared with the results that are obtained using equation 166. The Q^*_{ij} were determined using the complex frequency dependent υ^*_{12} given in equation 166 and the value of υ_{12} determined from the experimental investigation. These values were determined at 50 and 1000 Hz to obtain the range of variation in these values. In all cases, the maximum difference in the real and imaginary terms of the Q^*_{ij}, which occurs at 1000 Hz, were less than 1.5%. These values are therefore well within the experimental accuracy of the testing procedure. As such, there will only be an insignificant variation in the resulting solutions employing the assumption that the Poisson's ratios are real and frequency independent. This assumption has therefore been shown to be applicable to this material system.

Parametric Studies of the Flexural Damping Loss Factor of S-2 Glass/3501-6

Some general comments can be made about the information that can now be generated using the analytical model given in Chapter 3. A complete characterization of the damping loss factor as a function of frequency has never been reported in the literature. As such, the analytical determination of the loss factor of a general laminated composite over a given frequency range was never determined. This model has the utility of being able to determine the effect of stress couplings on the loss factor. It has been proposed by some investigators that the difference in loss factor as a function of fiber orientation between the

off-axis and angle-ply laminates is due to the stress coupling terms. These stress couplings should then lend themselves to loss factors which are higher than that achievable in pure shear. For an angle-ply composite, the material is balanced and symmetric, which results in minimal values of D_{16} and D_{26}, i.e. minimal stress coupling effects. For the off-axis configuration, however, since the material is unbalanced, significant stress couplings are present. The loss factor determined for the off-axis configuration has a peak at an orientation of approximately 30°, whereas the angle-ply configuration shows a loss factor maximum at a fiber orientation of approximately $\pm$ 45°, as seen in Figures 5 and 6. Calculating the magnitude of the coupling terms D_{16} and D_{26}, a peak occurs at a fiber orientation of approximately 30°. This gives the intuitive indication that the loss factor of a general laminated composite can be greater than the material's shear loss factor, by taking advantage of the flexibility in material design. It should be pointed out the loss factor information presented in Figures 5 and 6 were not determined at the same frequency for all orientations.

The loss factors in bending of 16 ply angle-ply and off-axis S-2 glass/3501-6 beams were analytically determined over a frequency range of 50 to 1000 Hz. The fiber orientations used were from 0° to 90° in increments of 15°. The model was used to analytically determine the complex inverse ABD matrix for each orientation and at frequencies of 50 Hz and from 100 to 1000 Hz in increments of 100 Hz. The loss factor was then determined using the D^{-1}_{11} term in equation 146. The results from this modeling are presented in Figures 38 and 39 for the angle-ply and off-axis material, respectively.

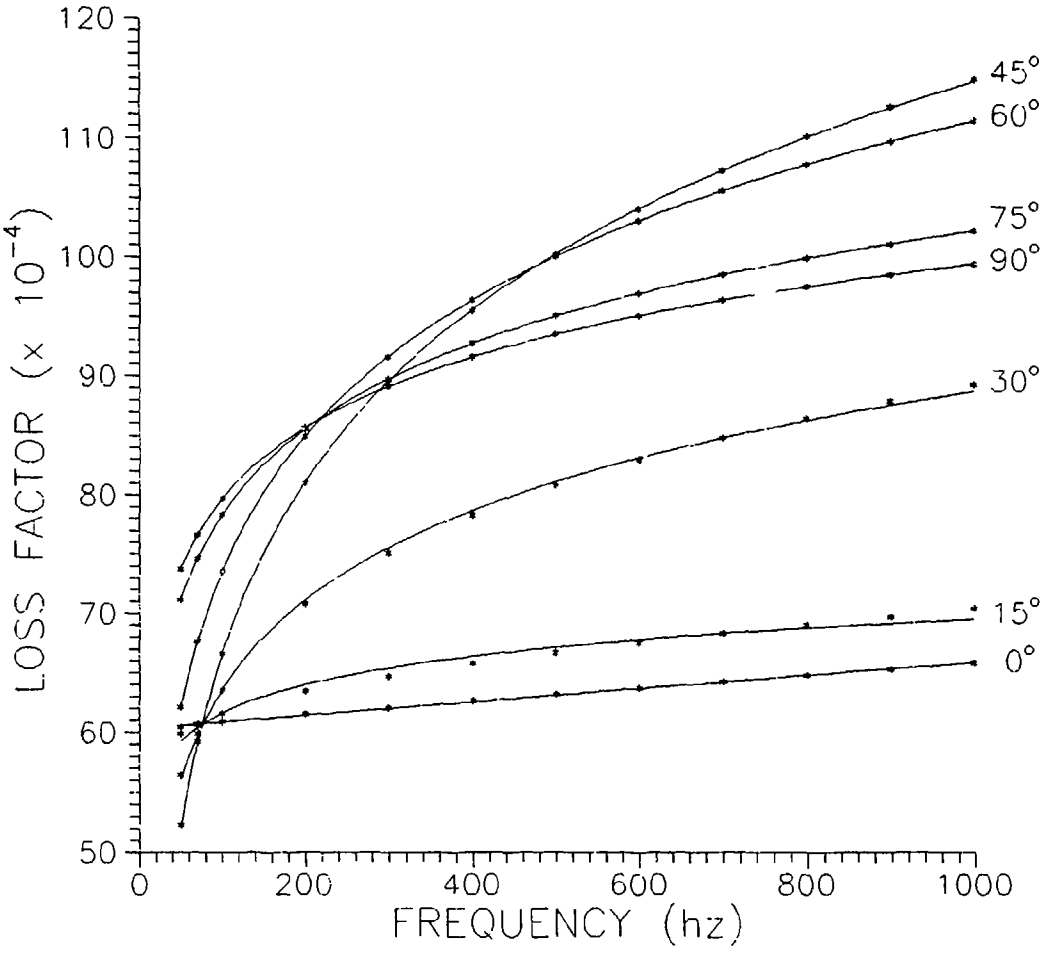

Figure 38 Loss factor vs. frequency for angle ply S-2 Glass/3501-6.

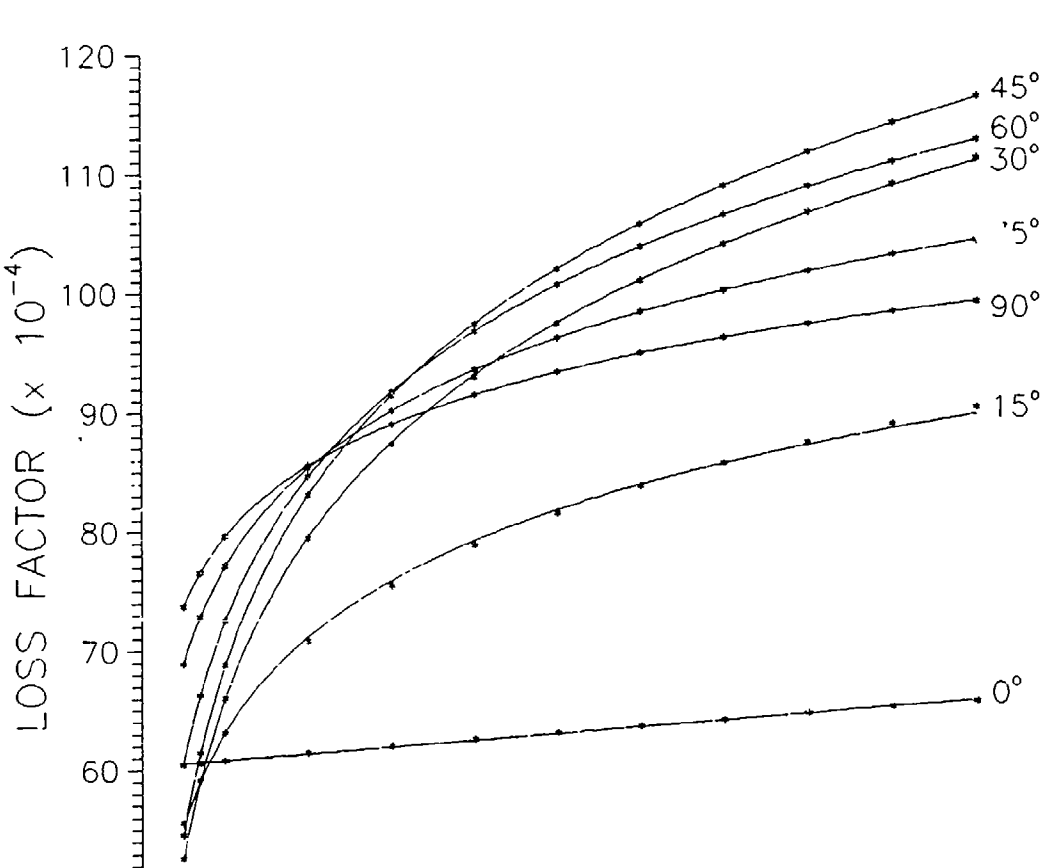

Figure 39 Loss factor vs. frequency for off axis S-2 Glass/3501-6.

Several results are evident by comparing the loss factors as a function of fiber orientation for these two configurations. The major difference in the two configurations is that the off-axis configuration has significant stress couplings because it is unbalanced. The first obvious difference in the two configurations is that the loss factor for a specific orientation over the entire frequency range is greater for the off-axis orientation with the exception of the 0° and 90° orientations where the loss factors are identical. Secondly, the effect of the stress coupling on loss factor is more pronounced for the 15° and 30° orientations then any of the other configurations. At a frequency of 1000 Hz, the 15° off-axis loss factor was 28.5% greater than the angle-ply loss factor, while the 30° off-axis loss factor was 24.8% greater than the angle-ply loss factor. This increase is attributed solely to the stress coupling terms. Third, the ranking of the loss factors as a function of material fiber orientation is different in the two configurations, as is evident in the magnitude of the loss factors at 1000 Hz.

In addition, there are also some similarities that can be pointed out. First, the general shapes of the curves are similar. Secondly, the maximum value of the loss factor - in both cases this occurs for the 45° orientation - is on the same order of magnitude. Third, in all cases, in the frequency range of 50 to 1000 Hz, the flexural damping loss factor increases as the frequency increases.

Some interesting results can be obtained using the analytical model and the information given above. For example, in the experimental determination of the loss factor for an angle-ply and off-axis S-2 Glass/3501-6 specimen, beams with the same dimensions are typically used. For a given orientation, the beam stiffness and therefore the resonant

frequency will vary. Since most investigators have not acknowledged the frequency dependence of the loss factor of composite materials, the frequency at which the test is conducted is of little concern. The information that they present, then, gives the loss factor as a function of orientation at different frequencies.

As an exercise, the effect of fiber orientation on loss factor will be analytically determined in the same manner that previous investigators have experimentally determined the loss factor. Specifically, an arbitrary beam length of 6.0 in (15.2 cm.) will be assumed. In addition, all beams will be assumed to have a thickness of 0.2 in (5.0 mm). To use the analytical model, the effective beam stiffness is first determined. This was done using a lamination plate theory routine to determine the ABD inverse matrix. The beam effective bending stiffness is then determined by substituting the $D^{-1}{}_{11}$ term into equation 144 for each of the orientations used. It should be noted that the effective beam stiffness of an off-axis beam is different than its angle-ply counterpart by virtue of the stress couplings that occur. Using this beam stiffness, the first resonant frequency of each beam is then determined using equation 149. The loss factor for each orientation at each of the frequencies is then determined using the analytical model given in Chapter 3. Tables 17 and 18 present the results for the angle-ply and off-axis beams, respectively. These tables show the variation in resonant frequency that occurs when the beam dimensions are kept constant.

The results of both the off-axis and angle-ply loss factor given in Tables 17 and 18 are presented graphically in Figure 40. This graph shows trends that are similar to those obtained by other investigators, as in Figures 5 and 6. First, there is a difference in the rate

Table 17: Analytical Determination of Loss Factor vs. Fiber Orientation for Angle-Ply S-2 Glass/3501-6

Orientation	Frequency (Hz)	Loss Factor ($\times 10^{-4}$)
0	186.36	61.42
$\pm$15	174.17	62.90
$\pm$30	139.71	66.91
$\pm$45	107.39	68.04
$\pm$60	101.55	73.79
$\pm$75	106.64	79.02
90	109.19	80.43

Table 18: Analytical Determination of Loss Factor vs. Fiber Orientation for Off-Axis S-2 Glass/3501-6

Orientation	Frequency (Hz)	Loss Factor ($\times 10^{-4}$)
0	186.36	61.42
15	155.14	68.05
30	119.73	69.55
45	103.93	69.66
60	101.39	72.83
[illegible]	105.86	77.85
[illegible]	109.19	80.43

of increase in loss factor for the two configurations. The off-axis material shows a more rapid increase in loss factor than the angle-ply configuration. The explanation for this is that additional losses are present by virtue of the stress couplings in the off-axis material, whereas the angle-ply configuration has no stress couplings, since it is both balanced and symmetric. At fiber orientations greater than 45°, the loss factor of the two configurations are within 2%.

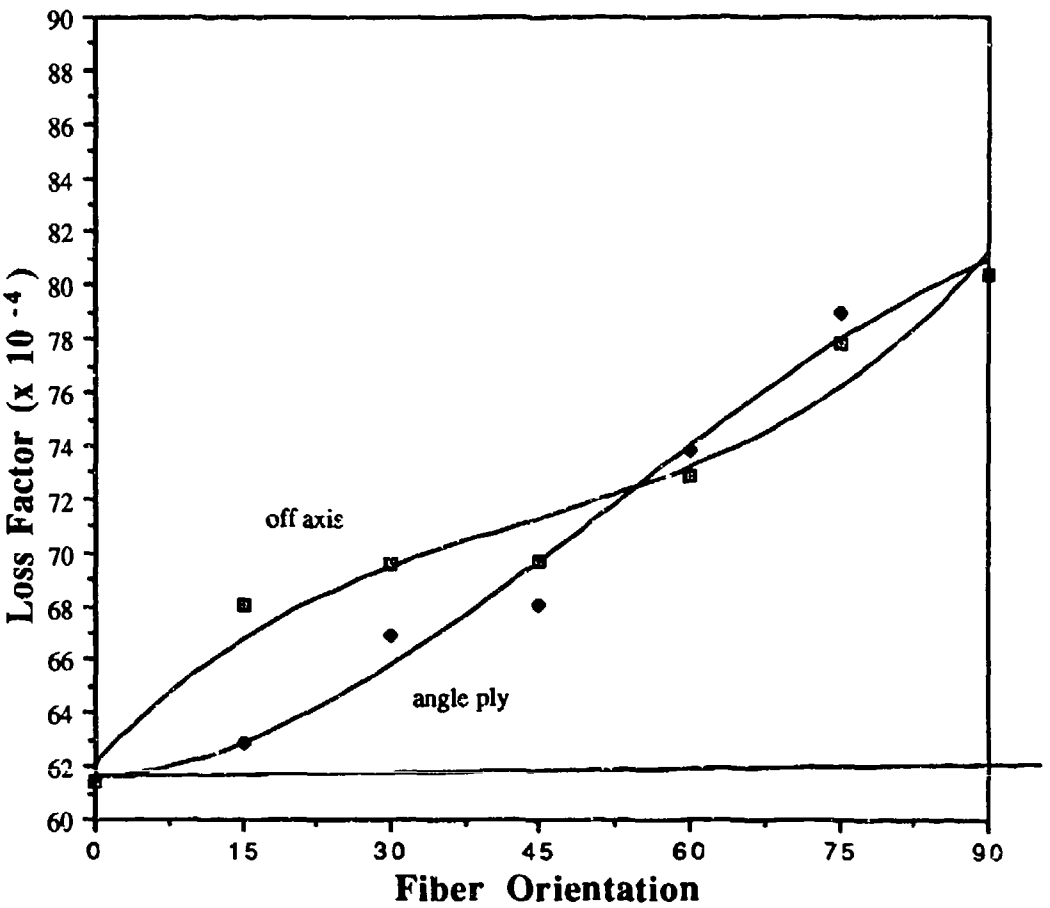

Figure 40 Loss factor vs fiber orientation for off-axis and angle-ply configurations for a 6.0 in long, 0.2 in thick beam.

Figures 38 and 39 can be used to visually determine the effect of orientation at a constant frequency. What is evident in these figures is that it is important to specify the frequency of interest. The shape of the curves of loss factor vs. fiber orientation at constant frequency will vary, showing maxima for different orientations at different frequencies. This helps to explain the inconsistency in the results of several investigators who report varying orientation at which the maximum in loss factor occurs.

It should also be pointed out that the model has the capability of determining the effect of hybridization on resultant loss factor. The affect of the incorporation of two or more different fibers within one test specimen on the resulting damping loss factor has not been considered in the literature. The hybrid configuration may provide an alternative means of attaining specific damping loss factor values which would currently be achievable only by varying the fiber orientations.

Summary of the Material Damping Loss Factors for S-2 Glass/3501-6 and AS4/3501-6

The loss factor for the 90 degree S-2 glass/3501-6 and AS4/3501-6 unidirectional composites is a nonlinear function of frequency, showing an increase in loss factor with increasing frequency. The loss factor for the 0 degree S-2 glass/3501-6 and AS4/3501-6 unidirectional composite appears to be linear, showing an increase with increasing frequency. From experimentally determined 0° and 90° loss factor information, a methodology is given to determine the shear loss factor based on the loss factor results obtained in a $\pm 45°$ beam specimen. The shear loss factor is greater in magnitude than the other orientations. The assumption that the Poisson's ratios are real and independent of frequency has been shown to be a plausible assumption, which will result in only minor variations from results obtained which include these dependencies. The results of experimental investigations in the literature which attempt to determine the effect of fiber orientation on loss factor can be analytically determined using the model described in Chapter 3. The differences that occur when considering angle-ply versus off-axis results has been shown to be the result of the stress coupling effects on loss factor.

Chapter 7

MODEL VERIFICATION

The analytical model that has been proposed in Chapter 3 has the capability to determine the damping loss factor of general laminated composites with any stacking sequence and with any combination of materials, provided the material loss factors are known. In this investigation, the material loss factors of two material systems were determined. The parametric studies that were performed can account for the trends that were obtained by other investigators. To gain added confidence in the model, however, it is necessary to show the correspondence between the analytical predictions of the damping loss factor with experimental determination of the loss factor of a general laminated composite configuration.

For this validation, it was decided to utilize two different laminated configurations using the S-2 Glass/3501-6 composite material. This material was chosen over the AS4/3501-6 material, due to its availability.

Test Specimens

There is an infinite variety of possible laminated configurations that could be used to

validate the analytical model. One material configuration that is often used in structural applications is the quasi-isotropic configuration, $[0/90/45/-45]_{ns}$. Although this configuration results in material properties which are isotropic in the plane of the material, the bending stiffness is a function of the orientation tested. In addition, there is a variation in the magnitude of the stresses or strains through the thickness of the material when it is subjected to a bending moment. As such, there should be a variation in the loss factor of this material as a function of the outer ply orientation.

A 16 ply laminate was fabricated having the configuration $[0/90/45/-45]_{ns}$. After fabrication, the panel was nondestructively inspected using the previously described ultrasonic C-scan inspection system. In addition, the fiber volume fraction was determined using the procedures previously indicated. This testing indicated that the panel was free of manufacturing defects and had the same fiber volume fraction as the glass material which had been previously tested, 63%.

Two sets of specimens were machined from this panel using a diamond-impregnated blade attached to a milling machine. One set had an outer fiber orientation of 90°, while the second set had an outer fiber orientation of 45°. The two beam configurations tested then were $[90/0/-45/45]_{2s}$ and $[45/-45/0/0]_{2s}$. In all cases the specimens had a width of 1.0 in. (25.4 mm).

Test Procedure

The material was tested using the apparatus described in Chapter 4 and the robust testing methodology described in Chapter 5. The material was to be characterized in the frequency range of 50 to 1000 Hz since this is the range in which the material loss factor was previously determined. This is accomplished by testing beams of various length. Five specimens of a specific length were used for each of the frequencies tested. Initial beam lengths for each configuration were chosen so that its first resonant frequency was approximately 50 Hz. The beam lengths were then reduced to obtain loss factors at frequencies which were multiples of 100 Hz. The minimum beam length tested was 2.0 in. (50.0 mm) to minimize shear and rotary inertia effects on the loss factor. The results of this testing are given in Table 19.

Table 19: Flexural loss factor determination of S-2 Glass/3501-6

Configuration	Frequency (Hz)	Loss Factor [Std. Dev] ($\times 10^4$)
$[45/-45/90/0]_{2s}$	53.4	61.52 [6.25]
	78.0	76.96 [1.8]
	115.1	65.90 [5.0]
	208.8	65.39 [2.3]
	326.8	77.68 [6.0]
	441.4	78.78 [8.0]
$[90/0/45/-45]_{2s}$	54.7	55.47 [6 5]
	98.6	64.31 [8.6]
	213.8	60.19 [3.6]
	487.4	67.33 [1.8]

Several features concerning the loss factor of these two configurations are evident in Table 19. First, for both configurations, there is an increase in loss factor with increasing frequency. This follows the general trend that was evident in the testing of the unidirectional composite samples. Second, the quasi isotropic configuration results fall within the range of values previously obtained for the angle-ply configuration. Intuitively this should occur, since the loss factor of the quasi-isotropic configuration should be some combination of the loss factors from the orientations used. Finally, the $[45/-45/90/0]_{2s}$ configuration had a higher loss factor than the $[90/0/45/-45]_{2s}$ configuration. Intuitively again, this should occur since the former configuration has the higher damping material subjected to a higher stress level.

Analytical Determination of Flexural Loss Factor

The analytical model developed in Chapter 3 is used to analytically determine the loss factor of the two quasi-isotropic configurations tested. The input required for the analytical model, i.e., the complex moduli, was previously given in Chapter 6. The complex moduli are necessary to determine the complex ABD inverse matrix. Once this matrix is determined, the flexural loss factor is determined using the D^{-1}_{11} term in equation 146. The specific inputs used in this development are given below as

$$E_1^* = 8.39 \times 10^6 (1 + i (5.1476 \times 10^{-7} f + 59.8698 \times 10^{-4})$$

$$E_2^* = 2.88 \times 10^6 (1 + i (8.37194 \times 10^{-4} \ln f + 40.6544 \times 10^{-4})$$

$$G_{12}^* = 0.885 \times 10^6 (1 + i (25.4998 \times 10^{-4} \ln f - 50.371 \times 10^{-4})$$

$$\nu_{12} = 0.264 \quad \nu_{21} = 0.0913$$

The analytical model was written into a computer program to determine the complex ABD matrix. The program that was utilized was Mathmatica$_{TM}$, a symbolic manipulator program. The program calculated the components of the complex ABD matrix as a function of frequency. The program then determines the inverse complex ABD matrix. The flexural loss factor is then determined using the $D^{-1}{}_{11}$ term in equation 146. The loss factor as a function of frequency was determined for three different outer ply orientations of the quasi-isotropic configuration. These orientations were $[45/-45/90/0]_{2s}$, $[90/0/45/-45]_{2s}$ and $[0/90/45/-45]_{2s}$. These analytically determined loss factors are presented graphically in Figure 41.

The loss factors shown in Figure 41 show trends similar to those seen with other configurations. First, the loss factor increases with increasing frequency. Second, the specific stacking sequence affects the loss factor of the laminate. For the quasi-isotropic laminate configuration, the orientations can be given in order of increasing loss factor as $[0/90/45/-45]_{2s}$, $[90/0/-45/45]_{2s}$, and $[45/-45/90/0]_{2s}$. This shows that to achieve the maximum damping loss factor, the stacking sequence used should have the orientation with the highest loss factor located near the surface of the laminate. The analytically determined loss factors for the quasi-isotropic configuration fall in the range of loss factors previously determined for the angle-ply configuration.

Comparison of the Analytically Determined Loss Factor with the Experimental Results

For comparison purposes, the experimental and analytically determined loss factors

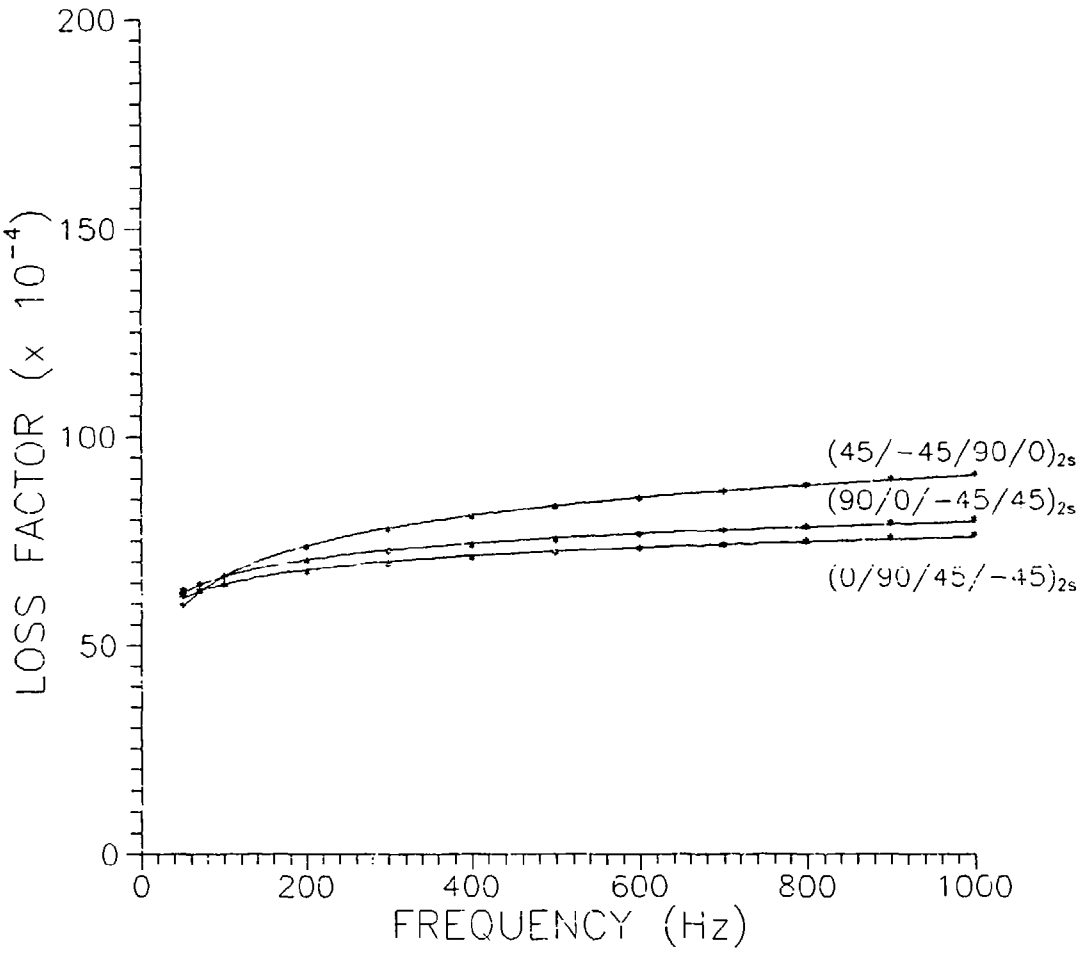

Figure 41 Loss factor vs. frequency for quasiisotropic S-2 Glass/3501-6 beams with varying outer ply orientations.

will be presented graphically. Figure 42 shows the comparison for the $[90/(\ '\text{-}45/45]_{2s}$ configuration. The two curves shown in Figure 42 are curve fits to the analytical and experimental loss factor values. The analytically determined loss factors are shown to follow the same trends as the experimental values. In general, the analytical values are on the upper side of the scatter, or as a maximum are on the order of 10% greater than the experimental values. This may be due to the manner in which the values of the experimental loss factor are determined. The linear extrapolation to zero displacement may not be appropriate. Instead, a nonlinear fit, such as a logarithmic fit, may be more appropriate.

Figure 43 shows the comparison of the experimental and analytically determined loss factors for the $[45/\text{-}45/90/0]_{2s}$ configuration. For this configuration, the analytical model provides an accurate description of the experimentally determined values of loss factor. The analytically determined loss factor falls within the scatter of the experimental values in the frequency range in which the experimental values were determined.

In general, the analytical model based on the elastic viscoelastic correspondence principle appears to provide an adequate prediction of the damping loss factor of a general laminated composite configuration. Trends occurring experimentally in the material are shown to occur using the analytical model. The analytical model has been shown to provide a loss factor which is within 15% of the experimentally determined values in the frequency range of 50 to 500 Hz.

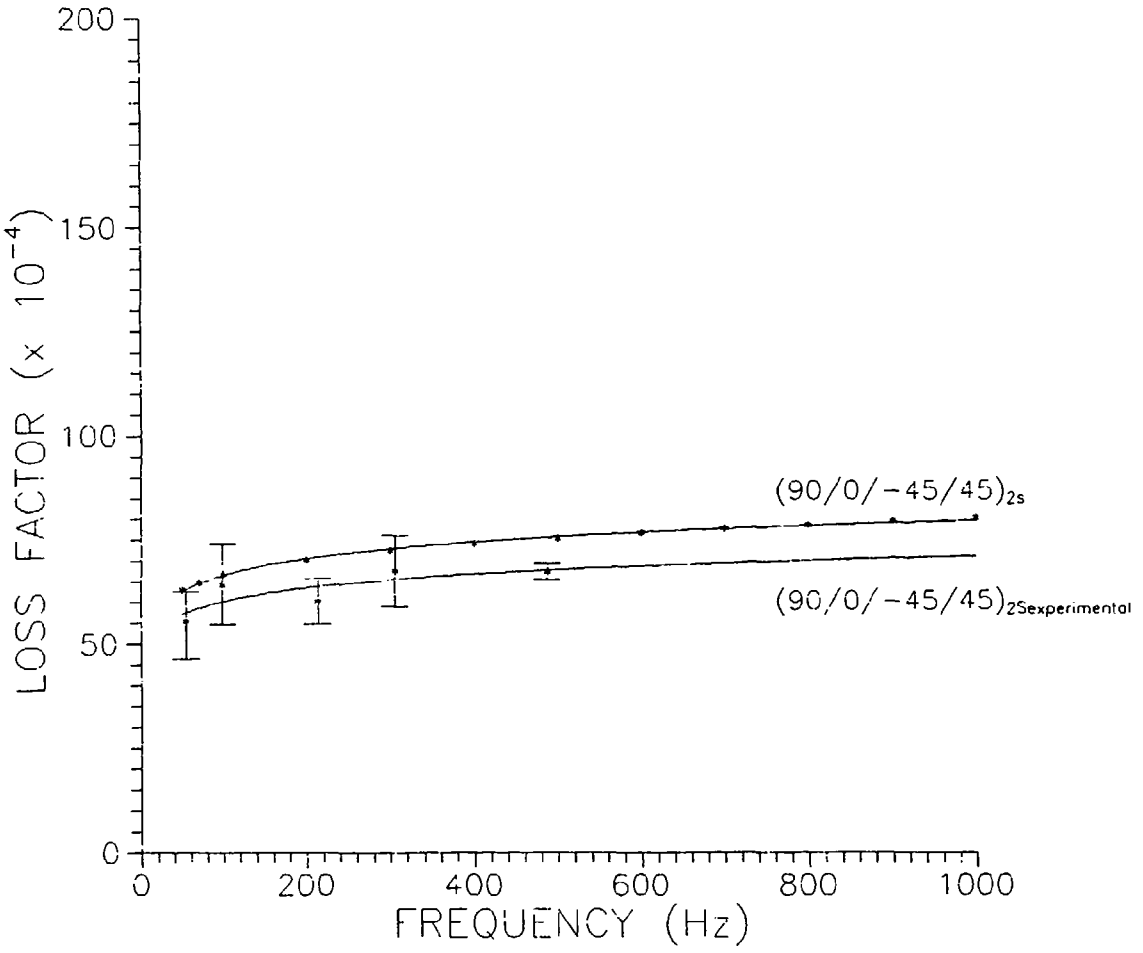

Figure 42 Analytical versus experimentally determined loss factor for $(90/0/-45/45)_{2s}$ laminate as a function of frequency.

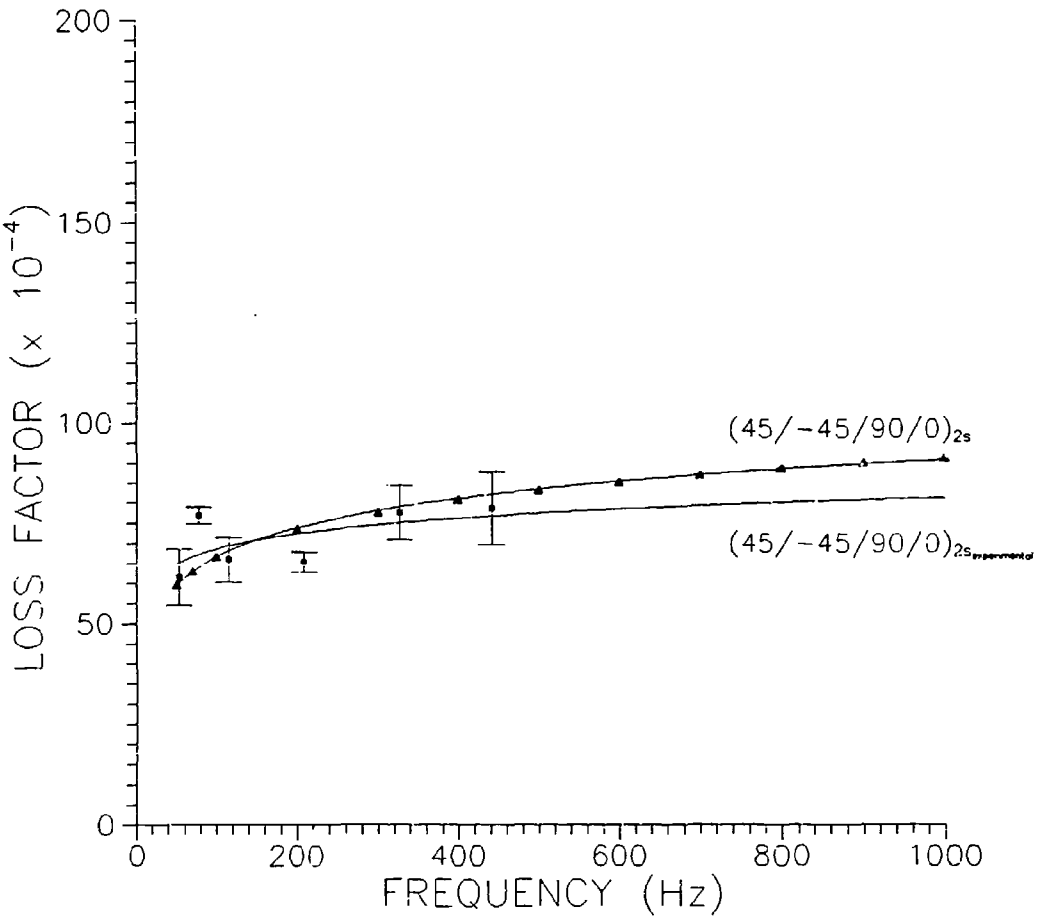

Figure 43 Analytical versus experimentally determined loss factor for $(45/-45/90/0)_{2s}$ laminate as a function of frequency.

Chapter 8

CONCLUSIONS

This research addresses the issue of the mechanical vibration damping of glass and graphite composite materials. In general, the loss factors of these composite materials have been shown to be a function of frequency. As the resonant frequency of the material is increased, the loss factor increases. The rate at which these increases occur is a function of the laminate configuration.

An analytical model was developed based on the elastic-viscoelastic correspondence principle. In this research, the frequency dependence of the damping loss factor is included, thereby extending the model as it is currently used in the literature. The incorporation of this frequency dependence has been shown to analytically explain the discrepancies in the literature on the loss factor as a function of fiber orientation. Different investigators have obtained conflicting experimental results for the composite laminate fiber orientation which results in the maximum loss factor. Using the analytical model developed in this research, all of their results can be shown to be valid. This occurs because for a given investigation, the test specimen dimensions are typically kept constant. When the fiber orientation of the test specimen is changed, the beam stiffness also changes. This results in a change in the first resonant frequency of the beam. The results of the model show that for a given frequency, the fiber orientation which has the highest loss factor is different.

The model has shown that the stress couplings that occur in unbalanced laminated constructions have a pronounced effect on the loss factor. The loss factor was shown to increase proportionally to the magnitude of the bending twisting coupling terms. The loss factor therefore showed the most pronounced increase for orientations of 15° and 30°.

The loss factors determined using the analytical model have shown excellent agreement to the experimental results. This model can therefore be used as an analytical tool to determine the material loss factor of composite materials at any frequency of interest. In addition, the loss factor in any direction can also be determined. This will enable the bounding of the structural loss factor to be obtained. This would be accomplished by using the following procedure. First, the maximum and minimum values of the material loss factor in the frequency range of interest is determined for the specific material configuration. This minimum and maximum value would then be used as input to one of the various finite element routines, since most finite element routines allow only a single value of damping loss factor as input. The finite element model would then determine the strain energy dissipated and stored in the structure. The loss factor is then determined using the ratio of the energy dissipated to the stored energy, as was previously discussed in Chapter 3. In addition, the structural loss factor at specific frequencies can also be determined by determineing the specific material loss factor at a given frequencyi and using this as input to the finite element routine. This capability, to the author's knowledge, has not been previously available to the structural designer.

The analytical model, as well as the experimental investigation, indicates that to achieve the highest flexural loss factor for a given set of laminae orientations, the

orientations that have the highest loss factor should be positioned near the surfaces of the specimen. This is demonstrated in the analytical determination of the loss factor for the quasi-isotropic configurations shown in figure 41.

An experimental apparatus has been designed, fabricated and calibrated for determining the in-plane vibration damping loss factors of composites. The use of a Teflon-impregnated glass fabric, commonly used as peel-ply material in the composites industry, and a bolt torque of 10 ft-lb. has been shown to result in consistent loss damping factor values, while at the same time causing no damage to the specimen. The calibration of the apparatus using a low damping material, 2024 T-4 aluminum, and employing this interface material and bolt torque resulted in loss factor values that were within 2% of the loss factors determined analytically using the Zener thermoelastic theory.

When utilizing the half power band width technique with materials that have high damping, i.e. greater than 60×10^{-4}, the tip amplitudes used in the calculation must be determined. If the loss factors have a magnitude lower than 0.001 in. for more than 25% of the sample time, the calculated loss factor will be reduced from the true loss factor for the material.

A robust testing methodology is proposed for determination of the damping loss factors of composite materials. This methodology is an attempt to minimize external sources of energy dissipation which occurs in vibration damping tested, such as aerodynamic and frictional losses and energy dissipated by the resultant excitation of testing apparatus. Specifically, this method calls for the partitioning of the tip displacement vs.

time information into 512 data point sets. The loss factor is determined as a function of the maximum beam vibration amplitude in each interval. A linear fit is then performed on this data, with the fit being extrapolated to zero displacement. This extrapolation is a quantitative way to extract the external sources of energy dissipation from the beam vibration response. This zero displacement loss factor value is then assumed to be the material loss factor.

In general, the three in-plane loss factors of the glass/epoxy composite are greater than that of the graphite/epoxy in the frequency range up to 1000 Hz. This trend should also carry over to other composite laminated orientations. The material loss factors for both systems are at least a factor of two greater than the loss factor of a conventional structural metal, such as steel or aluminum. In both systems, the 0° orientation loss factor, η_{11}, showed a linear increase as the frequency increased. The transverse and shear loss factors, η_{22} and η_{12}, showed a nonlinear increase as the frequency increased.

ACKNOWLEDGEMENTS

The author would like to acknowledge the financial and administrative support of James Kelly of ONT, Joseph Crisci and Dr. Bruce Douglas of DTRC, and Dr. A.K. Vasudaven of ONR. The author would also like to thank, John W. Gillespie, Jr., R.Byron Pipes, Jerold M Schultz, Roy L. McCullough, and Michael D. Greenberg of the University of Delaware for their review and comments on this research. The author would like to especially acknowledge the moral and technical support provided by Dr. Gillespie throughout this effort. Finally, the author would like to thank Thomas Juska, Harry Telegadas, Sandro D'Agaro, Darin Castro, Vincent Castelli, Eugene Camponeschi, Terry Morton and Eugene Fischer for their technical support in this effort.

Chapter 9

FUTURE WORK

Throughout the course of this research, numerous concerns were raised, investigated to a reasonable extent, and put aside as additional efforts that should be considered concerning the vibration damping testing of composites. A brief description of some of these issues follow.

Embedded Fiber Optic Displacement Sensor

In the determination of the damping loss factor of composites using the half power band width method, it is necessary to determine the amplitude of vibration of the end of the beam. Conventional techniques can only approximate this amplitude since the end of the beam alone can not be physically measured. All sensors require a finite volume of material on which to perform their measurement, such as for an accelerometer, strain gage or noncontact eddy current probe. In addition, these sensors in actuality measure average displacements in an indirect manner.

An alternative technique was briefly investigated as part of this research. This technique utilized an embedded optical fiber at the center of the beam. The optical fiber is cut incident with one end of the beam and is allowed to extend from the other end. A

helium neon laser is then coupled to the optical fiber. The light is guided through the optical fiber and exits the composite end. This light, visible to the unaided eye, can be detected by an array of optical sensors. Depending on the size of the sensors, the motion of the light exiting the embedded optical fiber can be accurately monitored. With the use of high-speed A-D data acquisition systems, a very accurate characterization of the beam tip displacement can be made. In addition, the displacement is measured using first principles, unlike the other techniques that are normally utilized. Accuracy can also be enhanced by increasing the distance from the beam end to the sensor.

This technique was investigated using equipment at the Fiber Optic Research Center at Virginia Polytechnic and State University. Composite specimens were made with embedded sensors. Two configurations were utilized. One was a 30° off-axis beam and the other was a unidirectional configuration. The off axis configuration was utilized since a bending twisting coupling should occur when it is subjected to a bending moment. It was hypothesized that this technique would be able to measure the degree of twist by utilizing two embedded optical fibers, one in the center of the beam width and one spaced 1/4 of the width away from an edge. If a twist occurred, the light should trace out an arc on a plane perpendicular to the end of the beam.

The sensor used to monitor the light exiting the optical fiber was a 512 by 512 array of optical detectors, which had planar dimensions of 0.5 x 0.5 in. This was coupled to a minicomputer with the sensor output being displayed on a CRT screen. At the time this investigation was carried out, the position of the incident light could not be digitally stored to a file. The response, however, could be visually monitored.

The results of this qualitative investigation were that the tip displacements and the degree of twist were measurable. In addition to its use as a sensor for damping measurements, this technique could also be utilized to nondestructively monitor the structural integrity of composite components. This would be done using the following procedure. Consider the composite wing of an aircraft such as the AV-8B. Initially, the vibrational response of this component would be measured by ultrasonic excitation. The resonant frequency could be determined as well as the damping loss factor. After a given period of service, the wing could be excited at the same location as was previously used and the resonant frequency and damping loss factor could be determined. If these were different than the original values, it would be hypothesized that some structural degradation had occurred. This could be quantitatively determined by backing out the component stiffness from the resonant frequency.

A more complete description of this technique has previously been published (77). In addition, a patent is currently pending (78).

Effects of Defects

In Chapter 2, mention was made of experimental work showing the effect of defects on the damping loss factors of composites. Plunkett (36) shows that the loss factor of composites increases as the transverse crack density increases. Other defects can also dissipate energy through the friction that occurs at the resulting interface. An investigation could be undertaken to determine the energy dissipated per area of defect

In this investigation, simulated delaminations could be fabricated in a section of a composite panel. Specimens with and without the defect would be cut from the panel and tested. The energy dissipated per area of defect could then be determined from the difference in the losses obtained from the two configurations.

This investigation could then be generalized to other defects, such as cracks. Transverse cracks can be easily created in composite panels by using a cross-ply configuration. Various densities of transverse cracks can be achieved by loading the material in tension to a predefined strain. The loss factor could then be determined as a function of transverse cracks. The dissipation per unit area from the transverse cracks could then be compared with that obtained from the delamination sample. This may lead to a universal dissipation of energy per unit volume of defect.

Effect of Beam Orientation on Damping Loss Factor

The initial experimental investigation to determine the damping loss factor of composites used the beam configuration that is commonly used in the literature, i.e. a horizontally oriented beam. The three in-plane composite material loss factors were determined in the frequency range of interest. The results of these efforts have been published elsewhere (67,79).

The results that were obtained at low frequencies, i.e., long beam lengths, for beams which had a low bending stiffness gave results that were not consistent with results reported elsewhere in the literature. What was occurring was a significant increase in loss

factor as the frequency decreased. In some cases, this increase was as high as a factor of two. One possible explanation would be that aerodynamic damping was influencing the results. However, for the aluminum beam, this did not occur. The aluminum beam had a much higher section stiffness than the composites that were affected. The 0° unidirectional graphite/epoxy also did not show this increase. This would discount the statement that the effect was caused by aerodynamic damping.

What may be occurring instead is an increased damping caused by gravitational effects. This can be shown to be a plausible explanation by considering one cycle of vibration. Without loss of generality, assume that the beam is initially excited downward. The beam's acceleration, and therefore displacement, is the result of the combined excitation force and the force due to gravity. After the beam reaches its maximum displacement, the energy stored in the beam causes a restoring force to act upward. This results in the acceleration of the beam which now has the gravitational acceleration acting against it. The resultant displacement is therefore less than it would have been in the absence of gravity. Since the displacement is less, the stored energy in the material is less. The restoring force to which the beam will respond will cause an acceleration which is less than it would have been in the absence of gravity. As such, the resultant displacement downward is less.

Since the amplitude of vibration is reduced with each subsequent motion, the apparent loss factor becomes greater. It is hypothesized that this effect is more pronounced on beams which have low stiffness. When the beam is oriented vertically, the gravitational force acts equally for each direction of motion. This is why the vertical beam orientation was used in this research. A comparison of the loss factor measurement in these two

orientations are given in references 80 and 81.

This effect could be experimentally modelled in the following manner. First, a composite specimen that has demonstrated a variation in loss factor when using a horizontal orientation compared to that obtained using a vertical would be fabricated. The loss factor would be determined using the horizontal orientation. These same specimens would be placed in the vertically oriented apparatus. The loss factor would then be determined. Before removing the specimen from the apparatus, a very compliant spring would be attached to the specimen. The loss factor would then be determined with this additional directional force applied. If the loss factor results were shifted toward the results obtained using the horizontal orientation, this would qualitatively demonstrate this phenomenon.

This would have a dramatic impact on damping testing, since currently the majority of the testing that is performed utilizes the horizontal beam orientation.

Damping Optimization using Hybrid Composite Design

The experimental investigation conducted in this program utilized specimens fabricated using one material system. What was not considered was the effect of hybridization on the damping loss factor.

The utilization of two distinct fibers in a composite has led to some interesting material properties. An example is the hybrid effect, the apparent improvement in tensile

strength from what would be anticipated using maximum stress theories. Although this can be explained by considering the effect of the difference in coefficients of thermal expansion of the two fiber systems, there is a synergistic enhancement of the composite strength.

The damping loss factor that may occur as a result of these residual stresses is unknown. The variation in coefficients of thermal expansion between adjacent layers of glass and graphite laminae should result in a shear stress through the matrix. This may result in added energy dissipation, since a maximum energy dissipation occurs through shear.

The most effective way to investigate the effect of hybridization on loss factor would be analytically. In this case, the modification to the analytical model would need to be twofold. First, the incorporation of residual stresses would need to be addressed, which may result in a damping equivalent hybrid effect. Secondly, the model modification would have to include three-dimensional stresses, such as the interlaminar and through-thickness shear stresses. A discussion on the three-dimensional extension to the model developed in Chapter 3 is given in the next section.

In addition to the modification to the analytical model, an experimental investigation would need to be undertaken. This would allow for the model modifications to be verified.

Generalized 3-D Elastic Viscoelastic Model

In the development of the analytical model given in Chapter 3, the plane stress

assumption was utilized. This reduced the complexity of the analytical model from a three dimensional problem to a two dimensional problem. If this simplification was not made, the development would have continued using the identical formulations. For the effort undertaken for this research, since thicknesses were small, the through thickness stresses can be assumed to be negligible.

For various structural applications, as the thickness of the material is increased, the need for incorporation of the through thickness stresses increases. When these thick structures are excited, their response will be governed by the three-dimensional elastic properties of the material. Likewise, the damping response will be governed by the three-dimensional loss factor characteristics.

An analytical three-dimensional model has been proposed by Trethewey and coworkers (82). In this development, the Q_{ij} terms have been determined as a function of the elastic properties of the composite. A generalized 3-D damping model could be readily proposed using the elastic viscoelastic correspondence principle, and making the substitution of the complex moduli for the real moduli given by Trethewey and coworkers (82).

With knowledge of the material loss factors in three dimensions, which for this case would mean the determination of the through thickness loss factor as a function of frequency, the reduced stiffnesses for a specific laminated stacking sequence can be determined. The energy dissipation that the structure would experience then could be determined by incorporating the appropriate loss factor in the structural analysis routine.

REFERENCES

1. Read, B.E. and Dean, G.D, The Determination of Dynamic Properties of Polymers and Composites, John Wiley and Sons, New York, 1978

2. Morozumi, M., Tsuge, K., and Hideshima, T., " Stress Relaxation Study of the Alpha Relaxation Process in a Mat of Single Crystals of Polyethylene," Proceedings of the Fifth International Congress on Rheology, Vol. 3, 1970, pp 325-334.

3. Hoffman, John D., Williams, G. and Passaglia, E., "Analysis of the α, β and γ Relaxations in Polychlorotrifluorethylene and Polyethylene: Dielectric and Mechanical Properties," Journal of Polymer Science: Part C, No. 14, 1966, pp 173-235.

4. Boyer, R.F., "The Relation of Transition Tempertures to Chemical Structure in High Polymers," Rubber Chemistry and Technology, Vol 36, 1963, pp. 1303-1421.

5. Macander, A.B. and Crane, R.M., "Literature Review and Experimental Data on Vibration Damping and Galvanic Properties of Advanced Composite Materials," David W. Taylor Naval Ship Research and Development Center, Ship Materials Engineering Department Report DTNSRDC-SME-83/24, Feb. 1983, 51 pp.

6. Crane, Roger M., "Literature Survey on the Vibration Damping Characteristics of Organic Matrix Continuous Fiber Composites," DTNSRDC, SME-87-81, November 1987.

7. Crane, R.M., Gillespie, J.W.,Jr. and Pipes, R. Byron, "Literature Review of the Vibration Damping Characteristics of Continuous Fiber Organic Matrix Composites," The University of Delaware, Center for Composite Materials Report, CCM-87-35, December 1987.

8. Crandall, S.H., "On Scaling Laws for Material Damping," National Aeronautical and Space Administration, Report TN D-1467, December 1960

9. Friend, C.A., Poesch, J.G. and Leslie, J.C., "Graphite Fiber Composites Fill Engineering Needs," SPI Reinforced Plastic Composite Institute, Proceedings of the 27th Annual Technical Conference, 8-11 Feb. 1972, Section 13-E, 8 pp.

10. Haines, Daniel W., "Material Damping of Carbon/Epoxy Composites by means of Free-Free Beam Resonance Tests," Vibration Damping 1984 Workshop Proceedings, Long Beach, CA, 27-29 Feb. 1984, AFWAL-TR-84-3064, Section R, 17 pp.

11. Suarez, S.A and Gibson, R.F., "Computer-Aided Dynamic Testing of Composite Materials," Proceedings of the Fall SEM Conference on Experimental Mechanics, Milwaukee, WI, Nov. 1984, pp. 118-123

12. Kurtze, G. and Mechel, F., "Structural Configurations for Increasing Fatigue Life at Temperatures up to 200° C," Summary report, Wright-Patterson AFB, Ohio, Report AFML-TR-67-39, Feb. 1967, 33 pp.

13. Schultz, Albert B. and Tsai, Stephen W., "Dynamic Moduli and Damping Ratios in Fiber Reinforced Composites," Journal of Composite Materials, Vol 2. No. 3, Jul. 1968, pp. 368-379

14. Newland, D.E., An Introduction to Random Vibrations and Spectral Analysis, Second Edition, New York, Longman, 1984

15. Adams, R.D., Fox, M.A.O., Flood, R.J.L., and Hewitt, R.J., "The Dynamic Properties of Unidirectional Carbon and Glass Fiber Reinforced Plastics in Torsion and Flexure," Journal of Composite Materials, Vol 3., Oct. 1969, pp. 594-603

16. Clary, R.R., "Vibration Characteristics of Unidirectional Filamentary Composite Material Panels," Composite Materials: Testing and Design (Second Conference), American Society for Testing and Materials STP 497, 1972, pp. 415-438

17. Schultz, Albert B. and Tsai, Stephen W., "Measurement of Complex Dynamic Moduli for Laminated Fiber Reinforced Composites," Journal of Composite Materials, Vol. 3, July 1969, pp. 434- 444

18. Adams, R.D. and Short, D., "The Effect of Fibre Diameter on the Dynamical Properties of Glass Fibre Reinforced Polyester Resins," Journal of Physics D: Applied Physics, Vol. 6, 1973, pp.1032-1039

19. Adams, R.D. and Bacon, D.G.C., "Effect of Fibre Orientation and Laminate Geometry on the Dynamic Properties of CFRP," Journal of Composite Materials, Vol. 7, Oct. 1973, pp. 402-428

20. Henneke, E.G. and Jones, K.L., "Detection of Damage in Composite Materials by Vibrothermography," American Society for Testing and Materials STP 696, Nondestructive Evaluation and Flaw Criticality for Composite Materials, Dec. 1979, pp. 83-95

21. Pye, C.J. and Adams, R.D., "Detection of Damage in Fiber Reinforced Plastics Using Thermal Field Generated During Resonant Vibration," NDT International, Vol. 14, No. 3, June 1981, pp.111-118

22. Wilson, D.W. and Charles, J.A., "Thermographic Detection of Adhesive Bond and Interlaminar Flaws in Composites," Center for Composite Materials, Report CCM-80-03, University of Delaware, 1980

23. Parker, B.A.,"High Damping Structural Materials," Noise, Shock, and Vibration Conference Proceedings, Melbourne, Australia, 22-25 May 1974, pp. 266-271

24. Adams, R.D., Bacon, D.G.C., Short, D. and Walton, D., "Dynamic Flexural Properties of Composite Materials," Composite Standards: Testing and Design Conference Proceedings, 1974, pp. 155-157

25. Paxson, Ernest B., Jr., "Real and Imaginary Parts of the Complex Viscoelastic Modulus for Boron Fiber Reinforced Plastic," Journal of the Acoustical Society of America, Vol 57, No. 4, April 1975, pp. 891-898

26. Zener, Clarence, Elasticity and Anelasticity of Metals, University of Chicago Press, Chicago, IL, 1965, 5th Impression

27. Gibson, Ronald F. and Plunkett, Robert, "Dynamic Mechanical Behavior of Fiber Reinforced Composites: Measurement and Analysis," Journal of Composite Materials, Vol. 10, Oct 1976, pp. 325-341

28. Bishop, R.E.D. and Johnson, D.C., The Mechanics of Vibration, Cambridge University Press, England, 1960

29. Maymon, G., Briley, R.P., and Renfield, L.W., "Influence of Moisture Absorption and Elevated Temperature on the Dynamic Behavior of Resin Matrix Composites: Preliminary Results," Proceedings of the Symposium on Advanced Composites, 1977

30. Gibson , R.F., and Plunkett, R., "A Forced-Vibration Technique for Measurement of Material Damping," Experimental Mechanics, Vol.11, No. 8, August 1977, pp. 297- 302

31. Pulgrano, L.J. and Miner, L.H., "Vibration Damping of Composites," Proceedings of the 25th National SAMPE Symposium and Exhibition, 6-8 May 1980, San Diego, CA, pp. 557-575

32. Shimizu, K., "The Damping Properties of Composites of Carbon Fiber and Enhanced Damping Matrix," Proceedings of the Japan-US Conference on Composite Materials; Mechanics, Mechanical Properties and Fabrication, Gakushi Kaikan, Tokyo, 12-14 Jan. 1981, pp.111-118

33. Adams, R.D. and Bacon, D.G.C., Journal of Physics D: Applied Physics, Vol. 6, No. 27, 1973

34. Yoshida, H., Bulletin of the Osaka Municipal Technical Research Institute, Vol. 57, 1979

35. Hashin, Z., "Complex Moduli of Viscoelastic Composites - I. General Theory and Application to Particulate Composites," International Journal of Solids and Structures, Vol. 6, 1970, pp. 539-552

36. Plunkett, R., "Damping Mechanisms in Fiber Reinforced Laminates," Mechanics of Composite Materials, Recent Advances, Proceedings of the IU TAM Symposium on Mechanics of Composite Materials, April 1982, pp. 93-104

37. Garrett, K.W. and Bailey, J.E., "Multiple Transverse Fracture in 90 Cross-Ply Laminates of a Glass Fibre-Reinforced Polyester," Journal of Material Science, Vol.12, 1977, p. 157

38. Parvizi, A., Garrett, K.W. and Bailey, J.E., "Constrained Cracking in Glass Fiber-Reinforced Epoxy Cross-Ply Laminates," Journal of Material Science, Vol. 13, 1978, p. 195

39. Bailey, J.E., Curtis, P.T., and Parvizi, A., "On the Transverse Cracking and Longitudinal Splitting Behavior of Glass and Carbon Fibre Reinforced Epoxy Cross Ply Laminates and the Effect of Poisson and Thermally Generated Strains," Proceedings of the Royal Society of London, A366, 1979, p. 599

40. Fukunaga, Hisao, Chou, Tsu-Wei, Peters, P.W.M., and Schulte, K., "Probabilistic Failure Strength Analysis of Graphite/Epoxy Cross-Ply Laminates," Journal of Composite Materials, Vol. 18, July 1984, p. 339

41. Gibson, R.F.. Yau, A., and Riegner, D.A., "An Improved Forced Vibration Technique for Measurement of Material Damping," Experimental Techniques, Vol.6 No.2, April 1982, pp. 10-14

42. Yau, A., "Experimental Technique for Measuring Dynamic Mechanical Behavior of Composite Materials," M.S. Thesis, Mechanical Engineering Department, University of Idaho, July 1980

43. Sheen, R.L., "Experimental Measurement of Material Damping for Space Structures in Simulated Zero-G," M.S. Thesis, Air Force Institute of Technology, Wright-Patterson AFB, Ohio, Report AFIT/CI/NR-83-84T, Dec. 1983, 120 pp.

44. Putter, S., Buchanan, D.L., Rehfield, L.W., "Influence of Frequency and Environmental Conditions on Dynamic Behavior of Graphite/Epoxy Composites," Composite Materials: Testing and Design (6th Conference) American Society for Testing and Materials, STP 787, 1982, pp. 414-424

45. Adams, R.D. and Bacon, D.G.C., "The Dynamic Properties of Unidirectional Fiber Reinforced Composites in Flexure and Torsion," Journal of Composite Materials, Vol. 7, Jan. 1973, pp.53-67

46. Mohr, D.G. and Cawley, E.F., "Experimental Measurements of Material Damping of Aluminum and Graphite/Epoxy in Free Fall with Tunable Excitation," MIT Space Systems Laboratory, No. 11-82, June 1982

47. Sun, C.T., Lee, B.T., Chaturvedi, S.K., "Composite Material Damping Using Impulse Technique," Vibration Damping 1984 Workshop Proceedings, Long Beach, CA, 27-29 Feb. 1984, Wright-Patterson AFB, Report No. AFWAL-TR-84-3064, Section P, 24 pp.

48. Suarez, S.A., Gibson, R.F., and Deobold, L.R., "Random and Impulse Techniques for Measurements of Damping in Composite Materials," Experimental Techniques, Vol. 8, No. 10, Oct. 1984 pp. 19-24

49. Hoa, S.V. and Ouellette, P., "Damping of Composite Materials," Polymer Composites, Vol.5, No.4, October 1984, pp. 334-338

50. Mallik, A.K. and Ghosh, A., "Damping Characteristics of Composite and Porous Materials," Journal of Composite Materials, Vol. 8, April 1974, pp. 207-211

51. Lameris, J., Stevenson, S., and Streeter, B., "Study of Noise Reduction Characteristics of Composite Fiber Reinforced Panels, Interior Panel Configuration, and the Application of the Tuned Damped Concept," National Aeronautical and Space Administration Report-CR-168745, March 1982, 163 pp.

52. Kishore, N.N., Ghosh, A., and Agarwal, B.D., "Damping Characteristics of Fiber Composites with Imperfect Bonding Part II - Low Volume Fraction Composites," Journal of Reinforced Plastics and Composites, Vol.1, Jan. 1982, pp. 64-81

53. Hashin, Z., "Complex moduli of viscoelastic composites - II. Fiber reinforced materials," International Journal of Solids Structures, vol. 6, (1970) p. 797-807.

54. Hashin, Z., Damping characteristics of Fiber Composites," Israel Institute of Technology Department of Materials Engineering MED Report No. 36, July 1972, 30 pp.

55. Sun, C.T., Wu, J.K. and Gibson, R.F., "Prediction of material damping of laminated polymer matrix composites," Journal of Materials Science, Vol 22., 1987 p 1006-1012

56. Savaranos, D.A., and Chamis, C.C., "Tailoring of Composites for Optimal Damping Elasto-Dynamic Performance," NASA Publication No. NASA-TM-102094, Lewis Research Center, Cleveland, Ohio, 1989, 30 p.

57. Savaranos, D.A., and Chamis, C.C., "Unified Micromechanics of Damping for Unidirectional and Off-Axis Composites," Journal of Composites Technology and Research, Vol.12, No. 1, Spring 1990, pp. 31-40

58. Alam, N. and Asnani, N.T., "Vibration and Damping Analysis of Fibre Reinforced Composite Material Plates," Journal of Composite Materials, Vol. 20, January 1986, pp. 2-18

59. Brockman, R.A., On Vibration Damping Analysis Using The Finite Element Method, Vibration Damping 1984 Workshop Proceedings, Long Beacg, CA, 27-29 Feb. 1984, AFWAL-TR-84-3064, Section II, 9 pp.

60. Bert, C.W., "Composite Materials: A Survey of the Damping Capacity of Fiber Reinforced Composites," Damping Applications for Vibration Control, Proceedings of The American Society of Mechanical Engineers, AMD - Vol. 38, 16-21 Nov. 1980, Chicago, IL., pp. 53-64.

61. Bland, D.R., The Theory of Linear Viscoelasticity, Pergamon Press, New York, 1960.

62. Schapery, R.A., "Viscoelastic Behavior and Analysis of Composite Materials," Composite Materials, Volume 2, Mechanics of Composite Materials, Ed. by G.P Sendeckyj, 1974, Academic Press, New York, pp. 85-168.

63. Schapery, R.A., "Stress Analysis of Viscoelastic Composite Materials," Composite Materials Workshop, Ed. by S.W. Tsai, J.C. Halpin, and Nicholas J. Pagano, 1968, Technomic Pub. Co., Inc., Stamford, Conn., pp. 153-192.

64. Gibson, R.F. and Suarez, S.A., "Improvement and Optimization of Internal Damping in Fiber Reinforced Composite Materials," Report No.AFOSR-TR-86-0330, March 1986, 225 p.

65 . Whitney, J.M, Browning, C.E., and Mair, A., "Analysis of the Flexure Test for Laminated Composite Materials," Composite Materials: Testing and Design (Third Conference), ASTM STP-546, Williamsburg, Va., 21-22 March 1973, pp. 30-45.

66. Suarez, S.A., Gibson, R.F., Sun, C.T., and Chaturvedi, S.K., "The Influence of Fiber Length and Fiber Orientation on Damping and Stiffness of Polymer Composite Materials," Experimental Mechanics, vol.26, no.2, June 1986, pp. 175-184

67. Crane, Roger M. and Gillespie, John W., Jr., "Characterization of the Damping Loss Factor of Glass and Graphite Fiber Composites," Composite Science and Technology, Vol. 40, No. 4 1991, pp. 355-375

68. Granick, N. and Stern, J.E., "Material Damping of Aluminum by a Resonant Dwell Technique," NASA TN-D-2895, 1965, 24 p.

69. Gibson, R.F, Yau, A., and Reigner, D.A., "Vibration Characteristics of Automotive Composite Materials," Short Fiber Reinforced Composites, American Society for Testing and Materials STP 772, Minneapolis, Minn., 14-15 April 1982, pp. 133-150

70.Yang, C.Y., Random Vibration of Structures, John Wiley & Sons, Inc., New York, 1986

71. Yim, Y-H, Burmeister, J.S., Kaminski, R.L., and Gillespie, J.W., Jr., "Experimental Characterization of Material Damping in Laminated Polymer Matrix Composites," Center for Composite Materials Report No. CCM-88-39, University of Delaware, Jan. 1989, 70 p.

72. Baker, Wilfred E., Woolam, William E. and Young, Dana, "Air and Internal Damping of Thin Cantilever Beams," International Journal of Mechanical Science, Vol 9., 1967, pp.743-766.

73. D.M. Riggs, R.J. Shuford, and R.W. Lewis, "Graphite Fibers and Composites," Handbook of Composites, edited by G. Lubin, Van Nostrand Reinhold Co., New York, 1982.

74. Edberg, D.L., "Measurement of Material Damping in a Simulated Space Environment," SUDAAR Report No. 546, Department of Aeronautics and Astronautics, Stanford University, December 1984.

75. Spimak, G.T., "The Effect of Temperature on the Material Damping of Graphite/Epoxy Composites in a Simulated Space Environment," Master of Mechanical Engineering Thesis, University of Delaware, 1987, 80 p.

76. Dally, James W., Riley, William F., and McConnell, Kenneth G., Instrumentation for Engineering Measurements, John Wiley & Sons, Inc., New York, 1984.

77. Crane, Roger M. and Telegadas, Harry, "Experimental and Analytical Investigation on a Proposed Embedded Fiber Optic Displacement Sensor," David Taylor Research Center Report No. DTRC/SME-87-95, Nov. 1987, 29 p.

78. Crane, Roger M. and Fischer, Eugene, "Beam Displacement Measurement System for Vibrating Beams," Patent Application, DTRC Navy Case No. 70386, 9 February 1987.

79. Crane, Roger M. and Gillespie, John W., Jr., "Damping Loss Factor Determination of Glass and Graphite Composites," David Taylor Research Report No. DTRC SME-89-59, Sept. 1989, 35 p.

80. Crane, Roger M., "Damping Loss Factor Determination of Glass and Graphite Epoxy Laminated Composite using Vertically Oriented Cantilever Beams," David Taylor Research Center Report No. DTRC-SME-89/62, Nov. 1989, 51 p.

81. Crane, Roger M., "Composite Damping," Proceedings of the U.S. Navy Advanced Damping Materials Workshop. 12 Oct 1989, David Taylor Research Center, Annapolis, Md. pp. 109-135.

82. Trethewey, Bruce R., Jr., Wilkens, Dick J., and Gillespie, John W., Jr., "Three-Dimensional Elastic Properties of Laminated Composites," Center for Composite Materials CCM Report 89-04, 28 p.

Appendix A

Annotated Copy of Data Collection Program

```
''''''''''''''''''''''''''''''''''''''''''''''''''''''''''''''''''''''''''''
'                                                          '
' QBEX6.BAS       DAS16 Example of MODES 0, 1, 6, 7, 8, 9, 17    '
'                                                          '
' MetraByte Corporation      for QuickBasic 4.0   9-7-88      '
'                                                          '
''''''''''''''''''''''''''''''''''''''''''''''''''''''''''''''''''''''''''''

DIM DIO%(4)
DIM DT%(12000), CH%(12000)  'set up integer arrays for data/channel #

COMMON SHARED DIO%(), CH%(), DT%()
DECLARE SUB DAS16 (MODE%, BYVAL dummy%, FLAG%)

'$DYNAMIC
DIM dat%(12000)
'$STATIC

5 print "THE DATE OF THIS PROGRAM UPDATE IS 11/19/90, NEW CALIBRATION"
10 ' THIS PROGRAM IS THE DATA AQUISITION PROGRAM FOR THE VIBRATION DAMPING
20 ' PROJECT. THIS IS SET UP TO READ CHANNEL 0 AS THE DISPLACEMENT SENSOR
30 ' AND CHANNEL 1 AS THE FORCE HAMMER. THE PROGRAM TAKES DATA AT YOUR
40 ' PRESCRIBED RATE AND WRITES IT TO A DATA ARRAY, CH% AND DT. THE PROGRAM
50 ' PLOTS THE ABSOLUTE VALUE OF THE LOG OF THE DISPLACEMENT VS. TIME. THE
60 ' DATA CAN BE SAVED IN EITHER THE DIGITAL VALUE FORM (-2048 TO 2047) OR
70 ' CAN BE SCALED BEFORE BEING SAVED TO A FILE. THE DIGITAL DATA FILE NAME
80 ' WILL BE VIBDATA.DAT WHILE THE SCALED DATA WILL BE VIBDATA.PRN. THE
PROGRAM
90 ' WILL ALLOW YOU TO MAKE THE APPROPRIATE SCALING FACTOR CHANGES.
91 ' THIS PROGRAM SETS THE ZERO POINT OF THE SYSTEM TO 30 MILS FROM THE
92 ' SPECIMEN, WITH A 20 MIL OFFSET.
100 '*********************************************************************
110 ' THIS PROGRAM IS CALLED VIBDAMP.BAS
120 '*********************************************************************
125 'DIM DT%(12000)
126 'DIM CH%(12000)
```

```
127 KEYPRESSED = 0
128 CLS
130 '
140 ' LOAD DASH16.BIN DRIVER
150 '
160 'DEF SEG = &H5000
170 'BLOAD "C:\ILS\DAS\DASH16.BIN", 0
180 '
190 ' *** INITIALIZE WITH MODE 0
200 '
210 MD% = 0
220 DIO%(0) = &H330       ' SET I/O ADDRESS
230 DIO%(1) = 2           ' SET INTERRUPT LEVEL
240 DIO%(2) = 3           ' SET DMA LEVEL
250 FLAG% = 0
260 'DASH16 = 0
270 'CALL DASH16 (MD%, DIO%(0), FLAG%)
275 CALL DAS16(MD%, VARPTR(DIO%(0)), FLAG%)
280 IF FLAG%<>0 THEN PRINT "INSTALLATION ERROR":STOP
290 '
300 ' ***  SET MULTIPLEXER SCAN LIMITS
310 MD% = 1
360 PRINT
370 PRINT " ATTACH THE OUTPUT FROM THE EDDY CURRENT PROBE TO CHANNEL 0"
380 PRINT " AND THE OUTPUT FROM THE FORCE HAMMER TO CHANNEL 1"
390 INPUT " AFTER DOING THIS, HIT ANY KEY ",Z$
395 CLS
400 DIO%(0) = 2
410 DIO%(1) = 2
420 'CALL DASH16 (MD%, DIO%(0), FLAG%)
425 CALL DAS16(MD%, VARPTR(DIO%(0)), FLAG%)
430 IF FLAG%<>0 THEN PRINT "ERROR # ";FLAG%;"IN SETTING SCAN LIMITS":STOP
440 '
450 '  *** DO ONE A/D CONVERSION AND INCREMENT MUX
460 '
470 PRINT
530 '  *** DO 1266 A/D CONVERSIONS AND PRINT AVERAGE
540 PRINT
550 PRINT " THE FOLLOWING SECTIONS WILL ALLOW YOU TO ADJUST ZERO FOR THE"
560 PRINT " EDDY CURRENT PROBE. ADJUST THE VERNIER FOR THE PROBE HOLDER"
570 PRINT " UNTIL THE OUTPUT IS CLOSE TO 0. THEN HIT ANY KEY TO CONTINUE"
580 WHILE NOT KEYPRESSED
590  MD% = 17
600 DIO%(0) = 10 ' DIVIDE 10 MHz BY 10 TO GIVE 1MHz FREQUENCY
610 DIO%(1) = 13 ' DIVIDE 1 MHz BY 12 TO GIVE 83.3 KHz FREQUENCY
620 FLAG% = 0
630 'CALL DASH16 (MD%, DIO%(0), FLAG%)
635 CALL DAS16(MD%, VARPTR(DIO%(0)), FLAG%)
640 DIO%(0) = 1266
650 'DIO%(1) = &H6800   ' SEGMENT OF MEMORY TO RECIEVE DATA
655 DIO%(1) = VARSEG(DAT%(0))   'SEGMENT OF MEMORY TO RECIEVE DATA
```

```
660 DIO%(2) = 1   'INDICATES TYPE OF TRIGGER; 1 = TIMER, 0 = EXTERNAL TRIGGER
670 DIO%(3) = 0   ' 0 = ONE CYCLE,  1 = RECYCLE
675 'CALL DASH16 (MD%, DIO%(0), FLAG%)
680 MD% = 6
695 CALL DAS16(MD%, VARPTR(DIO%(0)), FLAG%)
700 MD% = 8
705 CALL DAS16(MD%, VARPTR(DIO%(0)), FLAG%)
710 'CALL DASH16 (MD%, DIO%(0), FLAG%)
720 IF DIO%(1) = 1 THEN GOTO 700
730 'MD% = 9
740 DIO%(0) = 1266          ' NUMBER OF WORDS TO TRANSFER
750 'DIO%(1) = &H6800       ' SEGMENT OF MEMORY TO TRANSFER FROM
755 DIO%(1) = VARSEG(dat%(0))
760 DIO%(2) = 0             ' SET TRANSFER TO BEGIN AT BEGINNING OF SEGMENT
770 DIO%(3) = VARPTR(DT%(0))  ' TO START TRANSFER AT BEGINNING OF ARRAY
780 DIO%(4) = VARPTR(CH%(0))  ' CHANNEL THAT DATA IS FROM
785 'CALL DASH16 (MD%, DIO%(0), FLAG%)
787 MD% = 9
789 CALL DAS16(MD%, VARPTR(DIO%(0)), FLAG%)
790 IF KEYPRESSED$<>"" THEN KEYPRESSED=-1
800 SUM = 0
810 FOR I = 1 TO 1266
820 SUM = SUM +DT%(I)
830 NEXT I
840 ZERO= SUM/1266
845 ZERO = ZERO - 122.82
850 LOCATE 15,20
860 PRINT USING "###.###";ZERO
870 KEYPRESSED$=""
880 KEYPRESSED$=INKEY$
890 WEND
895 '
896 '*** SET MULTIPLEXER SCAN LIMITS
897 MD% = 1
898 DIO%(0) = 2
899 DIO%(1) = 3
900 'CALL DASH16 (MD%, DIO%(0), FLAG%)
903 CALL DAS16(MD%, VARPTR(DIO%(0)), FLAG%)
905 IF FLAG%<>0 THEN PRINT "ERROR # ";FLAG%;"IN SETTING SCAN LIMITS":STOP
909 '
910 '*** SET PROGRAMMABLE TIMER RATE USING MODE 17
920 '    SO THAT TIMER CAN BE SET TO MAX. VALUE
930 ' NOTE THAT CURRENT TIME FOR 2 CHANNEL SCAN IS 1.30 E-5 SEC."
940 '
950 PRINT "DO YOU WANT TO CHANGE THE VALUES FOR THE PROGRAMMABLE TIMER"
960 PRINT " THE CURRENT SETTING IS FOR A FREQUENCY OF 76.9 KHz. THIS IS"
970 PRINT " THE MAXIMUM FREQUENCY. ANY NEW FREQUENCY WILL BE LOWER THAN"
980 INPUT " THIS. DO YOU WANT TO CHANGE FREQUENCIES ";A$
990 PRINT
1000 IF A$ = "N" OR A$ = "n" THEN GOTO 1140
1010 PRINT " TO SET A NEW FREQUENCY, INPUT TWO NUMBERS WHICH WILL"
```

```
1020 PRINT " BE DIVIDED INTO 10 MHz THAT WILL RESULT IN THE FREQUENCY"
1030 INPUT " THAT YOU DESIRE; A,B (CURRENT DIVISOR IS 130) ";D,V
1040 K = D*V
1050 PRINT
1060 TI#= 1E+07/K
1070 IF K>=130 GOTO 1170
1080 PRINT
1090 PRINT " YOU MUST CHOOSE A DIVIDE BY GREATER THAN 130 IN ORDER TO"
1100 PRINT " COLLECT DATA CORRECTLY. PLEASE INPUT VALUES WHICH HAVE A"
1110 PRINT " PRODUCT GREATER THAN 130 !!! "
1120 PRINT
1130 GOTO 1010
1140 D=5
1150 V = 26
1160 TI#= 1E+07/130
1170  MD% = 17
1180 DIO%(0) = D  ' DIVIDE 10 MHz BY 10 TO GIVE 1MHz FREQUENCY
1190 DIO%(1) = V  ' DIVIDE 1 MHz BY 12 TO GIVE 83.3 KHz FREQUENCY
1200 FLAG% = 0
1210 'CALL DASH16 (MD%, DIO%(0), FLAG%)
1215 CALL DAS16(MD%, VARPTR(DIO%(0)), FLAG%)
1220 '
1230 ' *** DO N A/D CONVERSIONS AND TRANSFER TO MEMORY VIA DMA - MODE 6
1240 '
1250 INPUT "ENTER NUMBER OF CONVERSIONS DESIRED (UP TO 12000): ",M
1270 PRINT
1280 PRINT "THE SYSTEM WILL BEGIN TAKING DATA FROM ASSIGNED CHANNELS"
1290 INPUT "WHEN READY, STRIKE ANY KEY AND DATA COLLECTION WILL BEGIN ",A$
1300 DIO%(0) = M
1310 'DIO%(1) = &H6800   ' SEGMENT OF MEMORY TO RECIEVE DATA
1315 DIO%(1) = VARSEG(dat%(0))
1320 DIO%(2) = 1   'INDICATES TYPE OF TRIGGER; 1 = TIMER, 0 = EXTERNAL TRIGGER
1330 DIO%(3) = 0   ' 0 = ONE CYCLE,  1 = RECYCLE
1340 MD% = 6
1350 'CALL DASH16 (MD%, DIO%(0), FLAG%)
1355 CALL DAS16(MD%, VARPTR(DIO%(0)), FLAG%)
1360 MD% = 8
1370 'CALL DASH16 (MD%, DIO%(0), FLAG%)
1375 CALL DAS16(MD%, VARPTR(DIO%(0)), FLAG%)
1380 IF DIO%(1) = 1 THEN GOTO 1360
1390 '
1400 PRINT CHR$(7)
1410 '
1420 '*** TRANSFER DATA FROM MEMORY TO ARRAY USING MODE 9
1430 MD% = 9
1440 DIO%(0) = M              ' NUMBER OF WORDS TO TRANSFER
1450 'DIO%(1) = &H6800        ' SEGMENT OF MEMORY TO TRANSFER FROM
1455 DIO%(1) = VARSEG(dat%(0))
1460 DIO%(2) = 0              ' SET TRANSFER TO BEGIN AT BEGINNING OF SEGMENT
1470 DIO%(3) = VARPTR(DT%(0)) ' TO START TRANSFER AT BEGINNING OF ARRAY
1480 DIO%(4) = VARPTR(CH%(0)) ' CHANNEL THAT DATA IS FROM
```

```
1490 'CALL DASH16 (MD%, DIO%(0), FLAG%)
1495 CALL DAS16(MD%, VARPTR(DIO%(0)), FLAG%)
1500 PRINT CHR$(2)
1510 '
1520 ' READ DATA FROM MEMORY SEGMENT AND PRINT GRAPHICS, LOG(DISPLACEMENT)
1530 ' VS. TIME AND FORCE VS. TIME
1540 '
1545 Q=0
1550 FOR I = 1 TO M-1 STEP 2          ' SEARCH HAMMER ARRAY FOR WHEN VALUE
1560 IF DT%(I) < 250 THEN GOTO 1600   ' REACHES A PRESET VOLTAGE INDICATING
1565 IF I<22 GOTO 1610
1570 B = I - 21                       ' HAMMER IMPACT. STORE ARRAY NUMBER AS B
1580 K = (M-B)/640                    ' K SCALES TIME TO FIT ON X-AXIS
1590 GOTO 1620
1600 NEXT I
1610 B = 20
1615 K = (M-B)/640                    ' K SCALES TIME TO FIT ON X-AXIS
1620 Q=0
1625 j = 0
1630 FOR I = B TO M-1 STEP 2          ' SEARCH FOR MAXIMUM VALUE OF DISPLACEMENT
1640 IF ABS(122.82-DT%(i)) < Q THEN GOTO 1660   ' SO THAT GRAPHICS CAN BE SCALED
1650 Q = ABS(122.82-DT%(I))
1655 j = i
1660 NEXT I
1670 R#=Q/50
1680 INPUT "DO YOU WANT TO PLOT LOG(DISPLACEMENT) VS. TIME ";A$
1690 IF A$ = "N" OR A$ = "n" THEN GOTO 1820
1700 CLS:SCREEN 2:KEY OFF
1710 W = (LOG(Q))/100                 ' W SCALES DISPLACEMENT TO FIT ON Y-AXIS
1720 FOR I = B TO M-1 STEP 2          ' LINES 1230 - 1410 PLOTS DISPLACEMENT
1730 Z = ABS(DT%(I)- 122.82)          ' AND FORCE VS. TIME USING LOG PLOT
1740 IF Z = 0 THEN GOTO 1780
1750 L = LOG(Z)
1760 PSET ((I-B)/K, (100 - (L/W)))
1770 GOTO 1790
1780 PSET ((I-B)/K, 100)
1790 PSET ((I-B)/K, (190-(DT%(I+1)/23)))
1800 NEXT I
1810 INPUT "",A$
1820 INPUT "DO YOU WANT TO PLOT THE SAME DATA USING DISPLACEMENT VS.
TIME";A$
1830 IF A$ = "N" OR A$ = "n" THEN GOTO 1900
1840 CLS:SCREEN 2:KEY OFF
1850 FOR I = B TO M-1 STEP 2
1860 PSET ((I-B)/K, (((DT%(I)-122.82)/R#))+51)
1870 PSET ((I-B)/K, 51)
1880 PSET ((I-B)/K, (195-(DT%(I+1)/23)))
1885 PSET ((I-B)/K, 195)
1890 NEXT I
1900 N = M-B
1902 M1 = 0.0984241*(Q/409.6)+ 3.000045E-4  'CALIBRATION AS OF 11/16 90
```

```
1903 'M1 = 4.69312E-02*(Q/409.6)+7.59419E-04 'calibration as of 10/23/90
1904 'M1 = 4.02424E-02*(Q/409.6)-1.883607E-04 'calibration as of 6/26/89
1905 PRINT "                MAX DISPLACEMENT IS ";M1
1910 INPUT "",A$
1920 PRINT "NUMBER OF DATA POINTS IS ";N
1925 PRINT
1930 INPUT "WOULD YOU LIKE TO CHANGE THE START OF THE DATA ";A$
1940 IF A$ = "N" OR A$ = "n" THEN GOTO 1970
1950 PRINT "THE CURRENT VALUE OF THE START FOR DATA IS ";B
1960 INPUT " ENTER NEW VALUE FOR START OF DATA TRANSFER ";B
1970 CLS:SCREEN 0
1980 '
1990 '*** TRANSFER DATA
2000 '
2010 PRINT " THE DATA WILL NOW BE PRINTED TO A FILE. INSERT A DATA DISK IN"
2020 PRINT " DRIVE A. INPUT THE NAME YOU WISH TO CALL THIS FILE"
2030 PRINT " PLEASE USE THE EXTENSION OF 'PRN' FOR YOUR FILE ";
2040 INPUT "",FILE$
2042 B$ = ":"
2044 IF INSTR(FILE$,B$) = 0 THEN GOTO 2047
2045 C$=FILE$
2046 GOTO 2050
2047 A$="A:"
2048 C$=A$+FILE$
2050 PRINT
2060 PRINT " CURRENT ARRAY WILL BE TRANSFERRED TO A FILE, ";C$
2065 PRINT
2070 PRINT " YOU CAN SCALE THE DATA OR PRINT THE DIGITAL DATA TO THIS FILE"
2075 PRINT
2080 PRINT " THE SCALING FACTORS ARE CURRENTLY SET WITH A "
2085 PRINT " SLOPE AND INTERCEPT FOR DISPLACEMENT OF 4.69312E-2 AND "
2087 PRINT " 7.59419E-4, RESPECTIVELY. DO YOU WANT TO PRINT THE DIGITAL"
2090 'PRINT " SLOPE AND INTERCEPT FOR DISPLACEMENT OF 4.02424E-2 AND "
2100 'PRINT "-1.883607E-4, RESPECTIVELY. DO YOU WANT TO PRINT THE DIGITAL"
2130 INPUT "DATA TO FILE";A$
2140 IF A$="Y" OR A$="y" THEN GOTO 2340
2145 PRINT
2150 PRINT "DO YOU WANT TO CHANGE THE SLOPE AND INTERCEPT OF THE EDDY"
2155 INPUT "CURRENT PROBE FROM 4.69312E-2 AND  7.59419E-4, RESPECTIVELY";A$
2160 'INPUT "CURRENT PROBE FROM 4.02424E-2 AND -1.883607E-4, RESPECTIVELY";A$
2170 IF A$ = "N" OR A$ = "n" THEN GOTO 2210
2180 PRINT
2190 INPUT " INPUT NEW SLOPE AND INTERCEPT IN FORMAT, S,I ";S#,E#
2200 GOTO 2230
2210 'S#= 4.02424E-02
2212 'E#= -1.883607E-04
2214 S# = 0.0984241
2216 E# = 3.000045E-4
2218 'S#= 4.69312E-02
2220 'E#= 7.59419E-04
2222 PRINT "THE CURRENT NUMBER OF DATA POINTS THAT WILL BE PRINTED IS ";M-B
```

```
2223 PRINT "DO YOU WANT TO CHANGE THE NUMBER OF DATA POINTS STORED ";
2224 INPUT "",A$
2225 IF A$="N" OR A$ = "n" THEN GOTO 2230
2226 PRINT
2227 PRINT "INPUT THE TOTAL NUMBER OF POINTS THAT YOU WANT TO STORE ";
2228 INPUT "",V
2229 M=B+2*V
2230 OPEN C$ FOR OUTPUT AS #1
2240 PRINT #1,"THE FREQUENCY OF TEST IS ";TI#/2
2250 PRINT #1,"THE TIME INTERVAL BETWEEN DATA POINTS IS ";2/TI#
2260 FOR I = B TO M STEP 2
2270 DT# = DT%(I)/409.4
2280 DT# = S# * DT# + E# - .03
2290 PRINT #1,DT#
2300 NEXT I
2310 CLOSE #1
2315 N = (M-B)/2
2316 PRINT
2320 PRINT "THE NUMBER OF CONVERSIONS THAT HAVE BEEN MADE IS ";N
2330 GOTO 2435
2340 PRINT "THE DIGITAL DATA WILL BE STORED IN FILE ";C$
2350 PRINT "THE NUMBER OF DATA POINTS ARE ";M-B
2360 OPEN C$ FOR OUTPUT AS #1
2370 PRINT "THE FREQUENCY OF DATA ACQUSITION IS ";TI#/2
2380 FOR I = B TO M-1 STEP 2
2400 PRINT #1, DT%(I)
2410 'PRINT #1,T#;DT%(I);DT%(I+1)
2420 NEXT I
2430 CLOSE #1
2435 PRINT
2440 PRINT "WOULD YOU LIKE TO RUN THIS PROGRAM AGAIN ? ";
2450 INPUT "",M$
2460 IF M$ = "Y" OR M$ = "y" THEN GOTO 127
2470 END
```

Appendix B

Half Power Band Width Development

The analytical technique that is used for the determination of the damping loss factor is called the half power band width method. In this technique, the loss factor is determined as the ratio of the difference in frequencies at which are -3dB of the value of the frequency response at resonance and the resonant frequency. The loss factor is then given as

$$\eta = \frac{\Delta f_n}{f_r} \qquad 1$$

The derivation of this relationship as a way in which the loss factor can be deteremined is not intuitively obvious. As such, a derivation will be given in the following.

Consider a beam which is subjected to a transverse displacement caused by a force $F_0(x)\delta(x)$ appled at the free end of the beam. The equation of motion which describes this beam is

$$EI_a \frac{\partial^4 w}{\partial x^4} + \rho A \frac{\partial^2 w}{\partial t^2} = F_o \delta(x) \qquad 2$$

where $\delta(x)$ is the Kronecker delta function. This function has the following values,

$\delta(x) = 1$ when x equals 0 and $\delta(x) = 0$ when x is not equal to 0. In this application, after the removal of the force, the beam response is given as

$$EI_a \frac{\partial^4 w}{\partial x^4} + \rho A \frac{\partial^2 w}{\partial t^2} = 0 \qquad 3$$

To solve equation 3 to obtain a description of the beam transverse motion, a solution is assumed which is of the form

$$w(x,t) = W(x)\, e^{i\omega t} \qquad 4$$

Substituting equation 4 into equation 3, using the relations as follows

$$\frac{\partial w}{\partial t} = i\,\omega W(x)\, e^{i\omega t} \qquad 5$$

$$\frac{\partial^2 w}{\partial t^2} = -\omega^2 W(x)\, e^{i\omega t} \qquad 6$$

$$\frac{\partial^4 w}{\partial x^4} = e^{i\omega t} \frac{d^4 w}{d x^4} \qquad 7$$

we obtain

$$E I_a e^{i\omega t} \frac{d^4 w}{dx^4} - e^{i\omega t}\, \omega^2 \rho A W = 0 \qquad 8$$

or

$$\frac{d^4 w}{dx^4} - \frac{\omega^2 \rho A}{E I_a} W = 0 \qquad 9$$

For low loss viscoelastic materials, it is assumed that the free vibrations are approximately harmonic. In equation 9, the real modulus, E, is then replaced with the

complex modulus, E^*. Using the relationship

$$\alpha^4 = \frac{\rho A l^4 \omega^2}{E^* I_a} \qquad 10$$

and substituting into equation 9, the differential equation of motion becomes

$$\frac{d^4 w}{dx^4} - \frac{\alpha^4}{l^4} W = 0 \qquad 11$$

A solution to this ordinary differential equation is assumed to be of the form

$$W = C_1 \sin\frac{\alpha x}{l} + C_2 \cos\frac{\alpha x}{l} + C_3 \sinh\frac{\alpha x}{l} + C_4 \cosh\frac{\alpha x}{l} \qquad 12$$

The boundary conditions required for the determination of the constants in equation 12 are at the clamped end of the beam

$$W = 0 \quad \text{and} \quad \frac{dw}{dx} = 0 \quad \text{at} \quad x = l \qquad 13$$

while at the free end of the beam

$$\frac{d^2 w}{d x^2} = 0 \quad \text{and} \quad \frac{d^3 w}{d x^3} = 0 \quad \text{at } x = 0 \qquad 14$$

Solving $\frac{d^2 w}{d x^2} = 0$ at $x = 0$, results in

$$0 = C_1 \frac{\alpha^2}{l^2} \sin\frac{\alpha x}{l} - C_2 \frac{\alpha^2}{l^2} \cos\frac{\alpha x}{l} + C_3 \frac{\alpha^2}{l^2} \sinh\frac{\alpha x}{l} + C_4 \frac{\alpha^2}{l^2} \cosh\frac{\alpha x}{l} \qquad 15$$

or

$$0 = -C_2 \frac{\alpha^2}{l^2} + C_4 \frac{\alpha^2}{l^2} \qquad 16$$

or $C_2 = C_4$. Substituting this into equation 12 results in

$$W = C_1 \sin\frac{\alpha x}{l} + C_2 \cos\frac{\alpha x}{l} + C_3 \sinh\frac{\alpha x}{l} + C_2 \cosh\frac{\alpha x}{l} \qquad 17$$

Solving $\frac{d^3w}{dx^3} = 0$ at $x = 0$, in equation 17 results in

$$0 = -C_1 \frac{\alpha^3}{l^3} \cos\frac{\alpha x}{l} + C_2 \frac{\alpha^3}{l^3} \cos\frac{\alpha x}{l} + C_3 \frac{\alpha^3}{l^3} \sinh\frac{\alpha x}{l} + C_2 \frac{\alpha^3}{l^3} \cosh\frac{\alpha x}{l} \qquad 18$$

or

$$0 = -C_1 \frac{\alpha^3}{l^3} + C_3 \frac{\alpha^3}{l^3} \qquad 19$$

or $C_1 = C_3$. Substituting this into equation 17 results in

$$W = C_1 \sin\frac{\alpha x}{l} + C_2 \cos\frac{\alpha x}{l} + C_1 \sinh\frac{\alpha x}{l} + C_2 \cosh\frac{\alpha x}{l} \qquad 20$$

Using the boundary condition that $W = 0$ at $x = l$, equation 20 becomes

$$0 = C_1 \sin\alpha + C_2 \cos\alpha + C_1 \sinh\alpha + C_2 \cosh\alpha \qquad 21$$

Using the boundary condition that $\frac{dw}{dx} = 0$ at $x = l$ in equation 20 results in

$$0 = C_1 \cos\alpha - C_2 \sin\alpha + C_1 \cosh\alpha + C_2 \sinh\alpha \qquad 22$$

Using equations 21 to solve for C_1 and substituting this into equation 22 yields

$$0 = -\frac{C_2(\cos\alpha + \cosh\alpha)^2}{(\sin\alpha + \sinh\alpha)} + C_2(\sinh\alpha - \sin\alpha) \qquad 23$$

or

$$0 = -\frac{C_2(\cos\alpha + \cosh\alpha)^2}{(\sin\alpha + \sinh\alpha)} + C_2\frac{(\sinh\alpha - \sin\alpha)(\sinh\alpha + \sin\alpha)}{(\sinh\alpha + \sin\alpha)} \qquad 24$$

The only nontrivial solution to the equation occurs for nonzero C_2, when the numerator of equation 24 is zero or when

$$0 = -\cos^2\alpha - 2\cos\alpha\cosh\alpha - \cosh^2\alpha + \sinh^2\alpha - \sin^2\alpha \qquad 25$$

Using the trigonometric identities where

$$(\sin^2\alpha + \cos^2\alpha) = 1 \quad \text{and} \quad (\cosh^2\alpha - \sinh^2\alpha) = 1 \qquad 26$$

in equation 25, the solution becomes

$$\cos\alpha\cosh\alpha = -1 \qquad 27$$

There are therefore an infinite number of solutions to equation 27. For each α_n, there are associated constants C_n which form the solution to equation 3.

The displacement of the beam at any position x can be normalized relative to the free end of the beam by dividing by $W_n(0)$. The value of $W_n(0)$ is $2C_2$ as can be readily seen by substituting $x = 0$ into equation 20. The normalized beam displacement is then given as

$$\frac{W_n(x)}{W_n(0)} = \frac{1}{2}\left(\cos\frac{\alpha_n x}{l} + \cosh\frac{\alpha_n x}{l}\right) + \frac{1}{2}\frac{C_{1n}}{C_{2n}}\left(\sin\frac{\alpha_n x}{l} + \sinh\frac{\alpha_n x}{l}\right) \qquad 28$$

where

$$\frac{C_{1n}}{C_{2n}} = \frac{\sin\alpha_n + \sinh\alpha_n}{\sin\alpha_n\cosh\alpha_n - \cos\alpha_n\sinh\alpha_n} \qquad 29$$

Substitution the values of α_n for α in equation 10, making the additional substitution that the complex modulus $E^* = E'(1 + i\eta)$ results in

$$\alpha_n = \frac{\rho A l^4 \omega^2}{E'(1 + i\eta) I_a} \qquad 30$$

Since the modulus is complex, the frequencies are also complex. The substitution is therefore made where $\omega^* = \omega_n' + i\,\omega_n''$ into equation 30 which results in

$$\alpha_n = \frac{\rho A l^4}{I_a}\,\frac{\omega_n'^2 - \omega_n''^2 + 2i\,\omega_n'\,\omega_n''}{E'(1 + i\eta)} \qquad 31$$

Separating the real and imiaginary parts of equation 31 results in

$$E' = \frac{\rho A l^4}{I_a \alpha_n^4}(\omega_n'^2 - \omega_n''^2) \qquad 32$$

$$\eta = \frac{2\,\omega_n'\omega_n''}{\omega_n'^2 - \omega_n''^2} \qquad 33$$

Solving now for the particular solution to the transverse displacement resulting from an applied force, we have as the equation of motion

$$EI_a \frac{\partial^4 w}{\partial x^4} + \rho A \frac{\partial^2 w}{\partial t^2} = F_o \delta(x) e^{i\omega t} \qquad 34$$

Following the same development as was performed for the complimentary solution to the beam equation, the solution to equation 34 can be written in terms of a series as

$$W(x,t) = \sum_{n=1}^{\infty} \frac{4F_o}{\rho A l} \frac{W_n(x)}{W_n(0)} \frac{e^{i\omega t}}{(\omega_n^{*2} - \omega^2)} \qquad 35$$

Using the realtionship $\omega^* = \omega_n' + i\,\omega_n''$, the value of $(\omega^{*2} - \omega^2)$ is given as

$$\omega_n^{*2} - \omega^2 = \omega_n'^2 - \omega_n''^2 + 2i\,\omega_n'\,\omega_n'' - \omega^2 \qquad 36$$

$$\omega_n^{*2} - \omega^2 = \omega_n'^2 - \omega_n''^2 \left(1 - \frac{\omega^2}{\omega_n'^2 - \omega_n''^2} + 2i \frac{\omega_n' \omega_n''}{\omega_n'^2 - \omega_n''^2} \right) \qquad 37$$

But $\dfrac{2\,\omega_n'\,\omega_n''}{\omega_n'^2 - \omega_n''^2} = \eta$. Substituting this into equation 37 yields

$$\omega_n^{*2} - \omega^2 = \omega_n'^2 - \omega_n''^2 \left(1 - \frac{\omega^2}{\omega_n'^2 - \omega_n''^2} + i\eta \right) \qquad 38$$

Substituting equation 38 into equation equation 35 yields

$$W(x,t) = \sum_{n=1}^{\infty} \frac{4F_o}{\rho A\, i\, (\omega_n'^2 - \omega_n''^2)} \frac{W_n(x)}{W_n(0)} \frac{e^{i\omega t}}{\left(1 - \dfrac{\omega^2}{\omega_n'^2 - \omega_n''^2} + i\eta \right)} \qquad 39$$

Using the relationship for E' that previously derived in equation 32, we have that

$$\frac{4F_o}{\rho A l (\omega_n'^2 - \omega_n^{-2})} = \frac{4 F_o l^3}{E' \alpha_n^4 I_a} \qquad 40$$

Substituting this into equation 39 yields

$$W(x,t) = \sum_{n=1}^{\infty} \frac{4 F_o l^3}{E' \alpha_n^4 I_a} \frac{W_n(x)}{W_n(0)} \frac{e^{i\omega t}}{\left(1 - \frac{\omega^2}{\omega_n'^2 - \omega_n'^2} + i\eta\right)} \qquad 41$$

Expanding part of equation 41 we have that

$$\alpha_n^4 \left(1 - \frac{\omega^2}{(\omega_n'^2 - \omega_n''^2)} + i\eta\right) = \alpha_n^4 - \frac{\omega^2 \alpha_n^4}{(\omega_n'^2 - \omega_n''^2)} + i\eta\alpha_n^4 \qquad 42$$

Using equation 32 and rearranging terms we have that

$$\frac{\alpha_n^4}{\omega_n'^2 - \omega_n''^2} = \frac{\rho A l^4}{I_a E'} \qquad 43$$

Letting $\omega_D^2 = \frac{\omega^2 \rho A l^4}{E' I_a}$ and substituting into equation 42 yields

$$\alpha_n^4 \left(1 - \frac{\omega^2}{(\omega_n'^2 - \omega_n''^2)} + i\eta\right) = \alpha_n^4 - \omega_D^2 + i\eta\alpha_n^4 \qquad 44$$

Substituting equation 44 into equation 41 yields

$$W(x,t) = \sum_{n=1}^{\infty} \frac{4 F_o l^3}{E' I_a} \frac{W_n(x)}{W_n(0)} \frac{e^{i\omega t}}{(\alpha_n^4 - \omega_D^2 - i\alpha_n^4 \eta)} \qquad 45$$

For a complex number, the denominator can be rewritten in polar form as

$$\alpha_n^4 - \omega_D^2 + i\alpha_n \eta = [\,(\alpha_n^4 - \omega_D^2)^2 + (\alpha_n \eta)^2\,]^{\frac{1}{2}}\, e^{i\phi_n} \qquad 46$$

where

$$\tan \phi_n = \frac{\eta}{1 - \dfrac{\omega_D^2}{\alpha_n^4}} \qquad 47$$

Substituting this relationship into equation 45 yields

$$W(x,t) = \sum_{n=1}^{\infty} \frac{4 F_o l^3}{E I_a} \frac{W_n(x)}{W_n(0)} \frac{e^{i(\omega t - \phi_n)}}{[\,(\alpha_n^4 - \omega_D^2)^2 - (\alpha_n^4 \eta)^2\,]^{\frac{1}{2}}} \qquad 48$$

or

$$\frac{w E I_a}{4 F_o l^3} = \sum_{n=1}^{\infty} \frac{W_n(x)}{W_n(0)} \frac{e^{i(\omega t - \phi_n)}}{[\,(\alpha_n^4 - \omega_D^2)^2 - (\alpha_n^4 \eta)^2\,]^{\frac{1}{2}}} \qquad 49$$

From equation 49 it is seen that the amplitude of vibration is proportional to

$$w \propto [\,(\alpha_n^4 - \omega_D^2)^2 + (\alpha_n \eta)^2\,]^{-\frac{1}{2}} \qquad 50$$

A maximum of equation 49 occurs when $\omega_D^2 = \alpha_n^4$ or when

$$\omega_D^2 = \frac{\omega_m^2 \rho A l^4}{E I_a} = \alpha_n^4 \qquad 51$$

or

$$\omega_{rn}^2 = \frac{E I_a \alpha_n^4}{\rho A l^4} \qquad 52$$

where ω_{rn} is the angular frequency at which the maximum amplitude occurs. The maximum for the resonant amplitude, W_{max}, occurs at this frequency, ω_{rn}. At this frequency, $W_{max} \alpha (\alpha_n^4 \eta)^{-1}$. Letting f_1 and f_2 be the two frequencies on either side of f_{rn} at which

$$W^2 = \frac{1}{C} W_{max}^2 = \frac{1}{C} \frac{1}{(\alpha_n^4 \eta)^2} \qquad 53$$

Solving equation 53 for η yields

$$\eta = \frac{1}{(C-1)^{\frac{1}{2}}} \left(\frac{f_{2n}^2 - f_{1n}^2}{2 f_{rn}^2} \right) \qquad 54$$

But $(f_{2n}^2 - f_{1n}^2) = (f_{2n} + f_{in})\ (f_{2n} - f_{in})$. In addition, using the approximation $f_{2n} + f_{in} \approx 2f_{rn}$ in equation 54 yields

$$\eta = \frac{1}{(C-1)^{\frac{1}{2}}} \frac{2 f_{rn} (f_{2n} - f_{1n})}{2 f_{rn}^2} = \frac{1}{(C-1)^{\frac{1}{2}}} \frac{(f_{2n} - f_{1n})}{f_{rn}} \qquad 55$$

Substituting $C = 2$ in equation 55, which corresponds to a 3 dB amplitude drop yields

$$\eta = \frac{(f_{2n} - f_{1n})}{f_{rn}} = \frac{\Delta f_n}{f_{rn}} \qquad 56$$

which is the well known half power band width formula.

Appendix C

Annotated Copy of Computer Program to Determine Damping Loss Factor.

```
10 ' ****** THE FOLLOWING PROGRAM IS CALLED 1ORTHOFIT *****
20 '
30 ' THIS PROGRAM PERFORMS A FIT TO DATA IN A DATA FILE FOR A
40 ' FOURTH ORDER POLYNOMIAL FIT WITH ORTHOGONAL COEFFICIENTS
50 ' THE INFORMATION IS READ FROM A FILE AND YOU ARE PROMPTED FOR
60 ' THE APPROPRIATE INFORMATION, DATA REDUCTION DONE IN dB
70 '
80 Y = 1
90 PRINT " IN ORDER TO RUN THIS PROGRAM, YOU NEED TO HAVE A DATA FILE "
100 PRINT " THAT HAS THE FOURTH ORDER POLYNOMIAL COEFFICIENTS ALONG WITH"
110 PRINT " THE ALPHA AND BETA VALUES.  THEY SHOULD BE INPUT FOR EACH"
120 PRINT " EQUATION IN THE FORM: "
130 PRINT " A, B, C, D, E"
140 PRINT " A1, A2, A3, A4, A5 "
150 PRINT " B1, B2, B3, B4, B5"
160 PRINT
170 PRINT " WHERE THE FORM OF THE EQUATION IS EX^4+DX^3+CX^2+BX+A "
180 PRINT " AND A1 - A5 AND B1 - B5 ARE THE ALPHA AND BETA COEFFICIENTS"
190 PRINT " AS DETERMINED USING GRAPHER POLYNOMIAL FIT "
200 PRINT
210 PRINT " INPUT THE NAME OF THE FILE THAT HAS THE COEFFICIENTS FOR THE "
220 PRINT " FOURTH ORDER POLYNOMIAL FIT WITH ORTHOGONAL COEFFICIENTS "
230 PRINT " IN THE FORMAT AS INDICATED ABOVE ";
240 INPUT "",A$
250 OPEN A$ FOR INPUT AS #1
260 INPUT #1,A#,B#,C#,D#,E#
270 INPUT #1,A1#,A2#,A3#,A4#,A5#
280 INPUT #1,B1#,B2#,B3#,B4#,B5#
290 INPUT #1,F#,G#,H#,I#,J#
300 INPUT #1,A11#,A12#,A13#,A14#,A15#
310 INPUT #1,B11#,B12#,B13#,B14#,B15#
320 PRINT
330 CLS
340 PRINT " THE COEFFICIENTS FOR THE FIRST EQUATION FOR THE POLYNOMIAL FIT"
350 PRINT " IN THE FORM EX^4+DX^3+CX^2+BX+A ARE "
360 PRINT E#;"X^4 + ";D#;"X^3 + ";C#;"X^2 + ";B#;"X + ";A#
370 PRINT
380 PRINT " THE VALUES FOR THE ALPHAS IN THE ORTHOGONAL FIT FOR THE FIRST"
390 PRINT " EQUATION ARE ";A1#;A2#;A3#;A4#;A5#
400 PRINT
```

```
410 PRINT  " THE VALUES FOR THE BETAS IN THE ORTHOGONAL FIT FOR THE FIRST "
420 PRINT " EQUATION ARE ";B1#;B2#;B3#;B4#;B5#
430 PRINT
440 PRINT " THE COEFFICIENTS FOR THE SECOND EQUATION FOR THE POLYNOMIAL FIT"
450 PRINT " IN THE FORM EX^4+DX^3+CX^2+BX+A ARE "
460 PRINT J#;"X^4 + ";I#;"X^3 + ";H#;"X^2 + ";G#;"X + ";F#
470 PRINT
480 PRINT " THE VALUES FOR THE ALPHAS IN THE ORTHOGONAL FIT FOR THE SECOND"
490 PRINT " EQUATION ARE ";A11#;A12#;A13#;A14#;A15#
500 PRINT
510 PRINT  " THE VALUES FOR THE BETAS IN THE ORTHOGONAL FIT FOR THE SECOND"
520 PRINT " EQUATION ARE ";B11#;B12#;B13#;B14#;B15#
530 PRINT
540 PRINT " INPUT THE LOWER AND UPPER BOUND FOR THE FREQUENCY FOR WHICH"
550 PRINT " PROGRAM WILL SEARCH FOR A SOLUTION ";
560 INPUT "",XL#,XR#
570 XM#=(XL#+XR#)/2
580 FL#=XL#
590 FR#=XR#
600 CLOSE #1
610 XL4#=E#
620 XL3#=D#-E#*A5#-A4#*E#-A3#*E#-A2#*E#
630 XL2#=E#*A5#*A4#-D#*A4#+C#-B4#*E#-A3#*D#+A3#*A5#*E#+A3#*A4#*E#
640 XL2#=XL2#-E#*B3#-A2#*D#+A2#*A5#*E#+A2#*A4#*E#+A2#*A3#*E#
650 XL2#=XL2#-B2#*E#
660 XL1#=A3#*A4#*D#-A3#*A4#*A5#*E#-A3#*C#+A3#*B4#*E#-B3#*D#+A5#*B3#*E#
670 XL1#=XL1#+B#+A2#*A4#*D#-A2#*A4#*A5#*E#-A2#*C#+A2#*B4#*E#+A2#*A3#*D#
680 XL1#=XL1#-A2#*A3#*A5#*E#-A2#*A3#*A4#*E#+A2#*B3#*E#-B2#*D#
690 XL1#=XL1#+A5#*B2#*E#+A4#*B2#*E#
700 XL0#=A2#*A3#*A4#*A5#*E#-A2#*A3#*A4#*D#+A2#*A3#*C#
710 XL0#=XL0#-A2#*A3#*B4#*E#+A2#*B3#*D#-A2#*A5#*B3#*E#-A2#*B#
720 XL0#=XL0#+A#+A4#*B2#*D#-A4#*A5#*B2#*E#+B2#*B4#*E#-B2#*C#
730 XR4#=J#
740 XR3#=I#-J#*A15#-A14#*J#-A13#*J#-A12#*J#
750 XR2#=J#*A15#*A14#-I#*A14#+H#-B14#*J#-A13#*I#+A13#*A15#*J#+A13#*A14#*J#
760 XR2#=XR2#-J#*B13#-A12#*I#+A12#*A15#*J#+A12#*A14#*J#+A12#*A13#*J#
770 XR2#=XR2#-B12#*J#
780 XR1#=A13#*A14#*I#-A13#*A14#*A15#*J#-A13#*H#+A13#*B14#*J#-B13#*I#
790 XR1#=XR1#+A12#*A14#*I#-A12#*A14#*A15#*J#-A12#*H#+A12#*B1   A12#  A13#*I#
800 XR1#=XR1#-A12#*A13#*A15#*J#-A12#*A13#*A14#*J#+A12#*B13#*      '#
810 XR1#=XR1#+A15#*B12#*J#+A14#*B12#*J#+A15#*B13#*J#+G#
820 XR0#=A12#*A13#*A14#*A15#*J#-A12#*A13#*A14#*I#+A12#*A13#*H#
830 XR0#=XR0#-A12#*A13#*B14#*J#+A12#*B13#*I#-A12#*A15#*B13#*J#-A12#*G#
840 XR0#=XR0#+F#+A14#*B12#*I#-A14#*A15#*B12#*J#+B12#*B14#*J#-B12#*H#
850 PRINT
860 CLS
862 IF Y = 1 GOTO 870
864 PRINT "IS THE MATERIAL TYPE ";M$;
866 INPUT "",Q$
867 IF Q$ = "Y" OR Q$ = "y" GOTO 890
870 PRINT "ENTER THE TYPE OF MATERIAL FROM WHICH THIS DATA WAS TAKEN ";
```

```
880 INPUT "",M$
890 PRINT
892 IF Y = 1 GOTO 900
894 PRINT "IS THE BEAM LENGTH STILL ";L$;
896 INPUT "",Q$
898 IF Q$ = "Y" OR Q$ = "y" GOTO 920
900 PRINT " ENTER THE BEAM LENGTH FOR THIS SAMPLE ";
910 INPUT "",L$
920 PRINT "INPUT THE VALUE OF X-MID AND XSCAL FOR THE FIRST "
930 PRINT " EQUATION ";
940 INPUT "",XMD1#,XSC1#
950 PRINT
960 PRINT "INPUT THE VALUE OF X-MID AND XSCAL FOR THE SECOND "
970 PRINT " EQUATION ";
980 INPUT "",XMD2#,XSC2#
990 CLS
1000 'XXLL#=(XL#-XMD1#)*XSC1#
1010 'XXRL#=(XL#-XMD2#)*XSC2#
1020 XXLM#=(XM#-XMD1#)*XSC1#
1030 XXRM#=(XM#-XMD2#)*XSC2#
1040 'XXLR#=(XR#-XMD1#)*XSC1#
1050 'XXRR#=(XR#-XMD2#)*XSC2#
1060 VAML#= XL4#*XXLM#^4 + XL3#*XXLM#^3 + XL2#*XXLM#^2 + XL1#*XXLM# +XL0#
1070 VAMR#= XR4#*XXRM#^4 + XR3#*XXRM#^3 + XR2#*XXRM#^2 + XR1#*XXRM# +XR0#
1080 IF VAMR#-VAML#<0 GOTO 1170
1090 ' S#=XR4#-XL4#
1100 ' T#=XR3#-XL3#
1110 ' U#=XR2#-XL2#
1120 ' V#=XR1#-XL1#
1130 ' W#=XR0#-XL0#
1140 XL#= XM#
1150 XM#=(XL#+XR#)/2
1160 GOTO 1190
1170 XR#= XM#
1180 XM#=(XL#+XR#)/2
1190 IF (XR#-XL#)<1E-13 GOTO 1220
1200 IF ABS(VAML#-VAMR#)<1E-14 GOTO 1220
1210 GOTO 1000
1220 PRINT "THE SOLUTION TO THE FREQUENCY THAT CORRESPONDS TO THE
INTERSECTION"
1230 PRINT "OF THE TWO QUARTIC EQUATIONS IS ";XM#
1240 PRINT
1250 V1#=XR4#*XXRM#^4+XR3#*XXRM#^3+XR2#*XXRM#^2+XR1#*XXRM#+XR0#
1260 V2#=XL4#*XXLM#^4+XL3#*XXLM#^3+XL2#*XXLM#^2+XL1#*XXLM#+XL0#
1270 PRINT "THE VALUE OF THE AMPLITUDE FROM EQUATION 1 & 2"
1280 PRINT "RESPECTIVELY ARE ";V2#,V1#
1290 PRINT
1300 FE1#= V2# - 3
1310 FE2#= V1# - 3
1320 LN2#= FE2#
1330 LN#= FE1#
```

```
1340 XL01#=XL0#-LN#
1350 XR01#=XR0#-LN2#
1360 XR#=XM#
1370 XL#=FL#
1380 XM1#=(XR#+XL#)/2
1390 XXLL#=(XL#-XMD1#)*XSC1#
1400 XXLM#=(XM1#-XMD1#)*XSC1#
1410 XXRM#=(XR#-XMD1#)*XSC1#
1420 VALM#=XL4#*XXLM#^4 + XL3#*XXLM#^3 + XL2#*XXLM#^2 + XL1#*XXLM# + XL01#
1430 IF ABS(VALM#)<1E-14 GOTO 1530
1440 IF (XR#-XL#)<1E-13 GOTO 1530
1450 IF ABS(VALM#)=VALM# GOTO 1490
1460 XL#=XM1#
1470 XM1#=(XL#+XR#)/2
1480 GOTO 1390
1490 XR#=XM1#
1500 XM1#=(XR#+XL#)/2
1510 GOTO 1390
1530 PRINT "THE FREQUENCY CORRESPONDING TO -3dB OF THE PEAK AMPLITUDE "
1535 VALM#=XL4#*XXLM#^4 + XL3#*XXLM#^3 + XL2#*XXLM#^2 + XL1#*XXLM# + XL0#
1540 PRINT "OF THE LEFT SIDE OF THE PEAK IS ";XM1#;VALM#
1550 PRINT
1560 XL#=XM#
1570 XR#=FR#
1580 XM2#=(XM#+XR#)/2
1590 XXRM#=(XM2#-XMD2#)*XSC2#
1600 VARM#=XR4#*XXRM#^4 + XR3#*XXRM#^3 + XR2#*XXRM#^2 + XR1#*XXRM# + XR01#
1610 IF ABS(VARM#)<1E-14 GOTO 1710
1620 IF (XR#-XL#)<1E-13 GOTO 1710
1630 IF ABS(VARM#)=VARM# GOTO 1670
1640 XR#=XM2#
1650 XM2#=(XL#+XR#)/2
1660 GOTO 1590
1670 XL#=XM2#
1680 XM2#=(XL#+XR#)/2
1690 GOTO 1590
1710 PRINT "THE FREQUENCY CORRESPONDING TO -3dB OF THE PEAK AMPLITUDE "
1715 VARM#=XR4#*XXRM#^4 + XR3#*XXRM#^3 + XR2#*XXRM#^2 + XR1#*XXRM# + XR0#
1720 PRINT "OF THE RIGHT SIDE OF THE PEAK IS ";XM2#;VARM#
1730 PRINT
1740 LF# = (XM2#-XM1#)/XM#
1750 PRINT " THE LOSS FACTOR FOR THIS DATA IS ";LF#
1760 OPEN AS FOR OUTPUT AS #2
1770 PRINT #2,A#,B#,C#,D#,E#
1780 LPRINT A#,B#,C#,D#,E#
1790 PRINT #2,A1#,A2#,A3#,A4#,A5#
1800 LPRINT A1#,A2#,A3#,A4#,A5#
1810 PRINT #2,B1#,B2#,B3#,B4#,B5#
1820 LPRINT B1#,B2#,B3#,B4#,B5#
1830 PRINT #2,F#,G#,H#,I#,J#
1840 LPRINT F#,G#,H#,I#,J#
```

```
1850 PRINT #2,A11#,A12#,A13#,A14#,A15#
1860 LPRINT A11#,A12#,A13#,A14#,A15#
1870 PRINT #2,B11#,B12#,B13#,B14#,B15#
1880 LPRINT B11#,B12#,B13#,B14#,B15#
1890 PRINT #2,""
1900 LPRINT ""
1910 PRINT #2,"THE LOSS FACTOR FOR THIS DATA IS ";LF#
1920 LPRINT "THE LOSS FACTOR FOR THIS DATA IS ";LF#
1930 PRINT #2,"THE VALUE OF THE PEAK HEIGHT IS ";V1#
1940 LPRINT "THE VALUE OF THE PEAK HEIGHT IS ";V1#
1950 PRINT #2,"AT A FREQUENCY OF ";XM#
1960 LPRINT "AT A FREQUENCY OF ";XM#
1970 PRINT #2,"FREQUENCIES AT -3dB OF PEAK HEIGHT ARE ";XM1#;XM2#
1980 LPRINT "FREQUENCIES AT -3dB OF PEAK HEIGHT ARE ";XM1#;XM2#
1990 PRINT #2,"THE FILE NAME FOR THIS DATA IS ";A$
2000 LPRINT "THE FILE NAME FOR THIS DATA IS ";A$
2010 LPRINT
2020 PRINT #2,"THE MATERIAL TESTED WAS ";M$
2030 LPRINT "THE MATERIAL TESTED WAS ";M$
2040 PRINT #2, " THE BEAM LENGTH WAS ";L$
2050 LPRINT " THE BEAM LENGTH WAS ";L$
2060 PRINT #2, "THE DATE IS ";DATE$
2070 LPRINT "THE DATE IS ";DATE$
2080 LPRINT CHR$(12);
2090 CLOSE #2
2095 Y = Y+1
2100 INPUT "WOULD YOU LIKE TO DO ANOTHER CURVE FIT ";A$
2110 IF A$="Y" OR A$="y" THEN GOTO 2130
2120 GOTO 2150
2130 CLS
2140 GOTO 90
2150 END
```

Appendix D

Processing Procedures used for Fabrication of Composite Materials

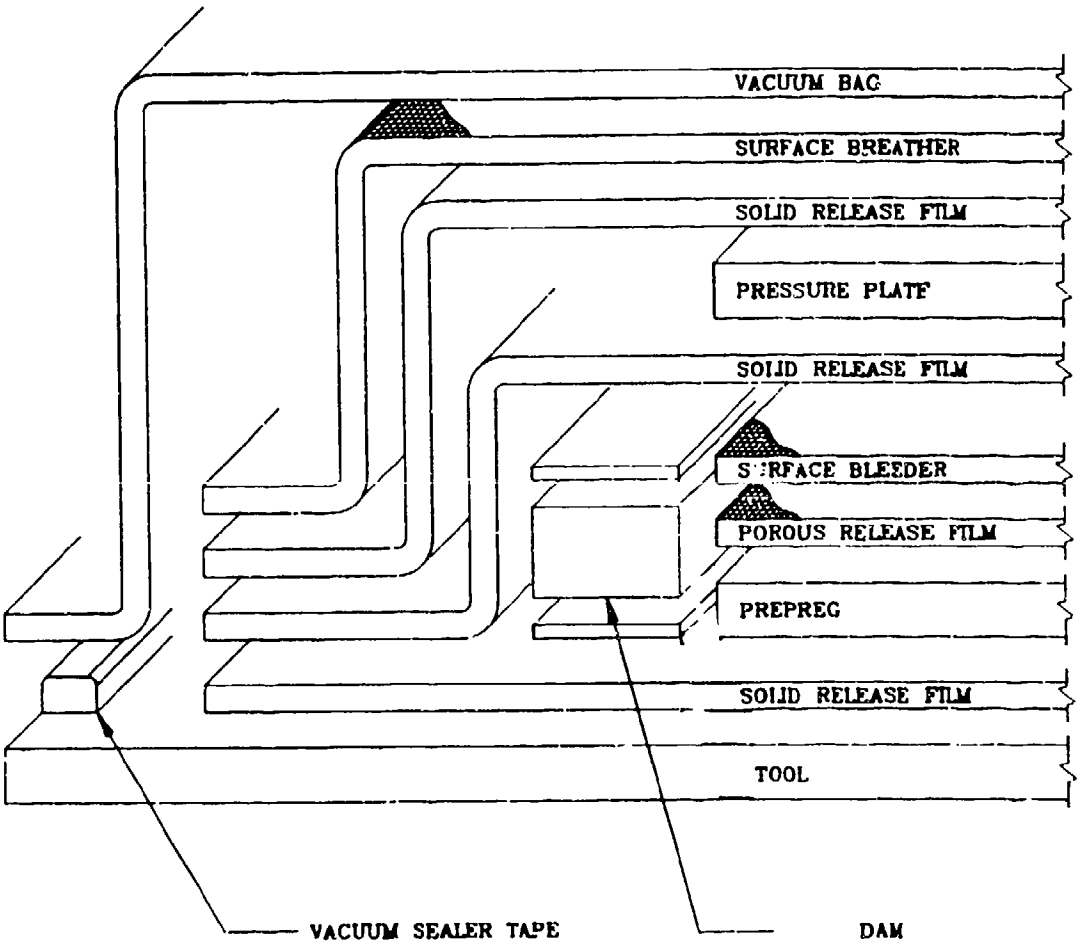

FIGURE 44 Vacuum bag layup used for processing composite materials

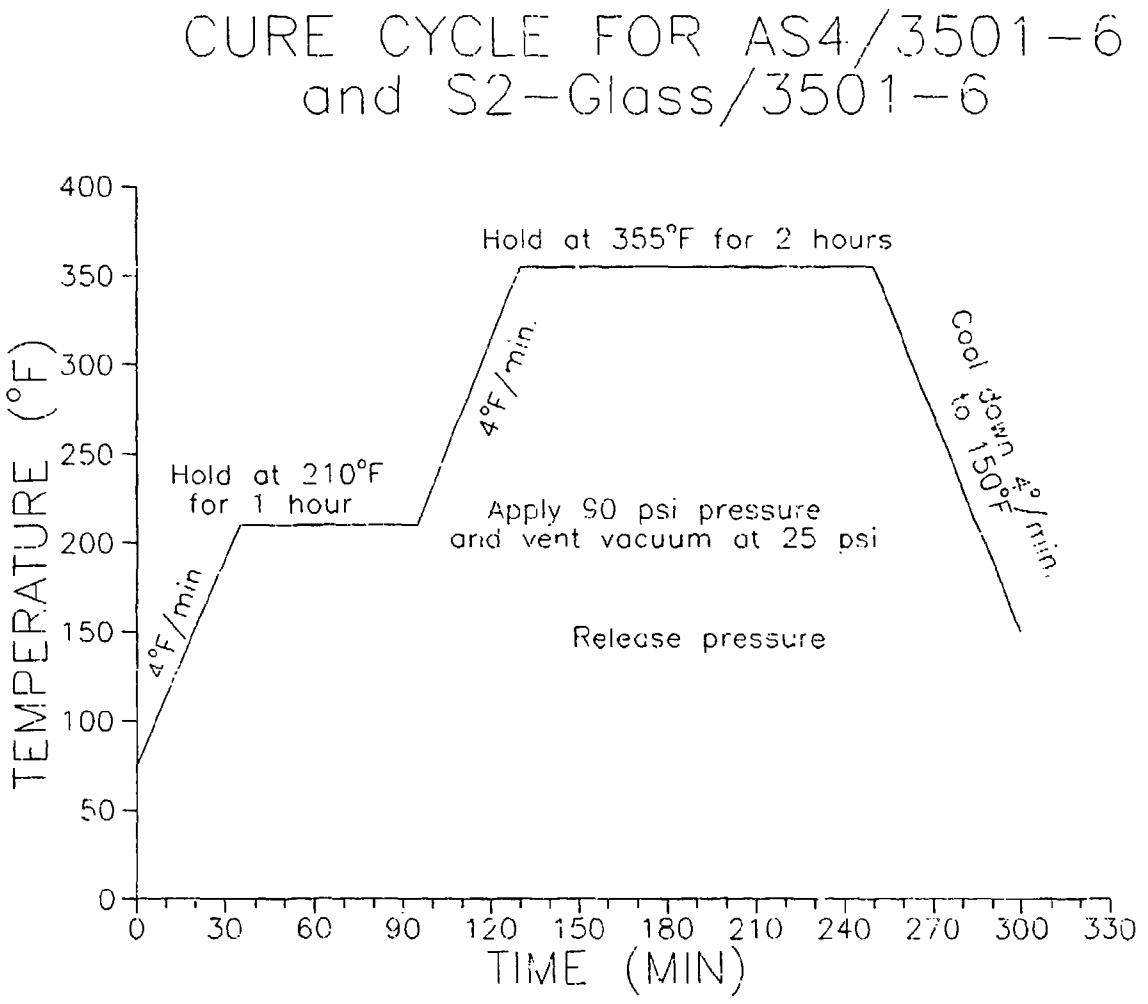

1) Apply 28 inches vacuum.
2) Heat part to 210°F at 1–5°/min.
3) Hold at 210°F for 1 hour.
4) Apply 90 psi pressure. Vent vacuum when pressure reaches 25 psi.
5) Raise temperature to 355°F at 1–5°/min.
6) Hold temperature at 355°F for 2 hours.
7) Cool to 150°F at rate of 1–5°/min.
8) Vent pressure at 150°F.
9) Hold at 355°F for 4 hours.
10) Cool to 75°F at rate of 2°/min. and vent pressure.

FIGURE 45 Autoclave cure cycle used for composite materials

APPENDIX E

Loss Factor vs. Frequency for Glass/epoxy and Graphite/epoxy

Table 19: Flexural Damping Loss Factor Results for 90° Unidirectional AS4/3501-6

Beam Length (in)	First Resonant (hz)	Loss Factors ($\times 10^{-4}$)	Ave. Loss Factor ($\times 10^{-4}$)	Standard Dev. ($\times 10^{-4}$)
8.00	25.05	54.61 47.92 57.01 56.39	53.98	3.06
7.00	33.27	58.94 57.29 58.58 71.95 57.12	60.778	5.63
6.00	43.89	54.26 63.51 61.03 50.20 63.15	58.43	5.29
4.00	93.45	70.6279 68.0501 76.4936 77.4548 65.3781	71.60	4.70
3.00	163.12	63.0139 63.558 59.9878 74.7062 65.8927	65.43	5.00
2.50	221.12	81.4684 61.926 69.3177 73.3073 75.7239	72.35	6.53
1.50	685.49	59.3865 51.9849 65.7985 52.0188	57.30	5.76

Table 20: Flexural Damping Loss Factor Results for 0° Unidirectional AS4/3501-6

Beam Length (in)	First Resonant (hz)	Loss Factors ($\times 10^{-4}$)	Ave. Loss Factor ($\times 10^{-4}$)	Standard Dev. ($\times 10^{-4}$)
10.34	48.51	40.8 27.31	34.06	6.75
9.38	60.66	47.05 33.76 21.22	34.01	10.55
7.25	100.23	40.43 32.4 48.04	40.29	3.87
5.00	209.93	50.97 47.66 49.89	49.51	1.38
4.50	253.37	31.04 27.25 31.89 29.66	29.96	1.76
4.00	326.61	34.91 27.91 41.18	34.67	5.42
3.50	427.59	62.18 62.3 66.57 70.1 60.66 65.54 70.79	65.45	3.68
3.25	486.56	59.58 64.73 51.42 59.16 61.09	59.20	4.36
3.00	567.15	46.46 50.32 41.35 47.61 50.24	47.2	3.28
2.75	671.08	38.32 33.89 41.35 48.59 43.96 32.83	39.82	5.52

Table 21: Flexural Damping Loss Factor Results for ±45° Cross Ply AS4/3501-6

Beam Length (in)	First Resonant (hz)	Loss Factors (x 10^{-4})	Ave. Loss Factor (x 10^{-4})	Standard Dev. (x 10^{-4})
8.00	28.10	74.01 79.25 61.31 71.29 71.28	71.43	5.84
6.50	43.07	108.8 115.53 113.9 113.85 113.87	113.189	2.29
6.00	50.81	85.65 100.33 95.76 88.61 95.15	93.10	5.28
5.00	73.74	61.36 66.84 68.51 67.06 56.31	64.02	4.56
4.00	117.44	51.51 61.20 57.63 50.90 51.21	54.49	4.18
3.00	214.42	51.76 40.67 47.37 64.95 56.15	52.18	8.18
2.50	317.1	57.06 47.51 60.57 51.42 64.93 62.89	57.40	6.20
2.125	441.12	54.52 70.08 54.66 48.09 60.03 65.95 71.95	60.75	8.25

Table 22: Flexural Damping Loss Factor Results for 90° Unidirectional S-2 Glass/3501-6

Beam Length (in)	First Resonant (hz)	Loss Factors ($\times 10^{-4}$)	Ave. Loss Factor ($\times 10^{-4}$)	Standard Dev. ($\times 10^{-4}$)
11.00	14.77	72.48 83.41 68.24 82.47 85.60	78.44	6.81
10.00	17.95	54.26 60.42 49.28 59.47 65.76	57.84	5.62
9.00	22.34	52.90 54.46 49.81 57.69	53.71	2.84
8.00	28.38	73.24 75.29 69.25 85.23 85.81	77.76	6.62
7.00	37.10	62.73 74.44 78.63 63.70 71.52	70.20	6.15
6.00	50.26	54.22 62.74 66.22 61.05 59.57	60.76	3.95
5.00	71.36	82.58 82.06 89.66 84.10 98.73	87.42	6.26
4.00	104.32	76.76 69.17 76.58 72.09 60.37	71.00	6.03

Table 22: Flexural Damping Loss Factor Results for 90° Unidirectional S-2 Glass/3501-6 (cont)

Beam Length (in)	First Resonant (hz)	Loss Factors ($\times 10^{-4}$)	Ave. Loss Factor ($\times 10^{-4}$)	Standard Dev. ($\times 10^{-4}$)
3.00	192.23	96.16 78.11 80.55 84.75 99.15	87.74	8.42
2.50	280.22	64.48 78.71 80.28 91.16 88.42	80.81	9.34
2.00	423.35	119.47 108.93 72.29 97.37	99.52	17.56

Table 23: Flexural Damping Loss Factor Results for 0° Unidirectional S-2 Glass/3501-6

Beam Length (in)	First Resonant (hz)	Loss Factors ($\times 10^{-4}$)	Ave. Loss Factor ($\times 10^{-4}$)	Standard Dev. ($\times 10^{-4}$)
8.50	41.07	53.98 61.01 55.52 62.86 58.67	58.41	3.30
8.00	46.30	52.66 58.20 62.96 56.84 61.25	58.38	3.59
6.50	70.40	45.70 75.80 56.50 75.98 69.79	65.75	11.87
6.00	81.70	58.58 53.14 59.74 58.78 47.11	55.47	4.78
5.50	97.30	61.74 62.96 61.23 59.37 69.98	63.05	3.65
4.00	180.80	66.85 60.94 73.47 71.33 59.18	66.35	5.59
3.25	269.90	70.65 74.19 72.42 70.34 68.30	71.18	1.99
2.75	381.50	60.95 65.57 50.81 54.05 64.35	59.15	5.78
2.50	451.50	66.89 71.28 69.40 69.49 67.54	68.92	1.56

Table 23: Flexural Damping Loss Factor Results for 0° Unidirectional S-2 Glass/3501-6 (cont)

Beam Length (in)	First Resonant (hz)	Loss Factors ($\times 10^{-4}$)	Ave. Loss Factor ($\times 10^{-4}$)	Standard Dev. ($\times 10^{-4}$)
2.25	555.60	44.55 51.11 33.64 48.11 36.67	42.82	6.66
2.00	696.60	44.60 26.85 42.78 42.65 24.51	43.34	0.89
1.75	898.70	82.72 56.12 94.74 91.27 89.77 85.11	83.29	12.77

Table 24: Flexural Damping Loss Factor Results for ±45° Cross Ply S-2 Glass/3501-6

Beam Length (in)	First Resonant (hz)	Loss Factors (x 10^{-4})	Ave. Loss Factor (x 10^{-4})	Standard Dev. (x 10^{-4})
10.10	55.37	42.94 41.44 62.35 60.34 49.78	51.37	8.64
8.00	86.33	77.07 68.99 62.65 70.29 77.50	71.30	5.53
6.50	133.66	75.13 76.41 80.39 66.84 79.66	75.69	4.84
5.00	221.02	68.68 61.74 59.73 55.29 86.33 84.66	69.41	12.05
4.00	341.03	94.61 91.68 94.86 113.71 87.16 99.93	96.99	8.40
3.50	446.27	102.69 105.79 96.89 99.19 96.34	100.18	3.59
3.125	565.78	88.76 102.08 98.48 81.69 94.32	93.07	7.21

Table 24: Flexural Damping Loss Factor Results for ±45° Cross Ply S-2 Glass/3501-6 (cont)

Beam Length (in)	First Resonant (hz)	Loss Factors ($\times 10^{-4}$)	Ave. Loss Factor ($\times 10^{-4}$)	Standard Dev. ($\times 10^{-4}$)
2.875	635.28	106.46 123.64 104.93 99.70 113.58 88.15	106.08	11.02
2.625	746.27	123.86 94.43 103.06 133.45 95.35 103.44	108.93	14.63
2.5	820.36	157.41 159.06 113.57 100.77 106.04 124.15	126.83	23.34

Appendix F

Statistical Analysis of the Damping Loss Factor for Glass/epoxy and Graphite/epoxy

TABLE 26 Statistical values for use in Equation 160 for 90° S-2 Glass/3501-6

S-2 GLASS/3501-6 90°				
FREQUENCY (hz)	T-VALUES (Confidence Level)	AVERAGE Loss Factor	STD DEV	NO. OF SAMPLES
14.77	5.217 (99%)	78.44	6.81	5
17.95	1.325 (90%)	57.84	5.62	5
22.34	4.074 (99%)	53.71	2.84	4
28.38	0.923 (95%)	77.76	6.62	5
37.10	2.890 (99%)	70.20	6.15	5
50.26	8.050 (99%)	60.76	3.95	5
71.36	4.227 (99%)	87.42	6.26	5
104.32	3.615 (99%)	71.00	6.03	5
192.23	1.223 (85%)	87.74	8.42	5
280.22	2.068 (96%)	80.81	9.34	5
423.35		99.52	17.56	4

TABLE 27 Statistical values for use in Equation 160 for 0° S-2 Glass/3501-6

S-2 GLASS/3501-6 0°				
FREQUENCY (hz)	T-VALUES (Confidence Level)	AVERAGE Loss Factor	STD DEV	NO. OF SAMPLES
41.1	0.0126 (<50%)	58.41	3.30	5
46.3	1.149 (85%)	58.38	3.59	5
70.4	1.622 (92%)	64.75	11.87	5
81.7	2.820 (98%)	55.47	4.78	5
97.3	1.105 (85%)	63.05	3.65	5
180.8	1.819 (94%)	66.35	5.59	5
269.9	4.400 (99.5%)	71.18	1.99	5
381.5	3.648 (99.5%)	59.15	5.78	5
451.5	3.532 (99.5%)	68.92	1.56	5
555.6	0.132 (55%)	42.82	6.66	5
696.6	5.250 (99.5%)	43.34	0.89	3
898.7		83.29	12.77	6

TABLE 28 Statistical values for use in Equation 160 for ±45° S-2 Glass/3501-6

S-2 GLASS/3501-6 ±45°				
FREQUENCY (hz)	T-VALUES (Confidence Level)	AVERAGE Loss Factor	STD DEV	NO. OF SAMPLES
55.37	4.340 (99.5%)	51.37	8.64	5
86.33	1.336 (89%)	71.30	5.53	5
133.66	1.087 (85%)	75.69	4.84	5
221.02	4.599 (99.5%)	69.41	12.05	6
341.03	0.786 (77%)	96.99	8.40	6
446.27	1.974 (95%)	100.18	3.59	5
565.78	2.257 (97%)	93.07	7.21	5
635.28	0.381 (63%)	106.08	11.02	6
746.27	1.413 (90%)	108.93	14.63	6
820.36		126.83	23.34	6

TABLE 29 Statistical values for use in Equation 160 for 90° AS4/3501-6

AS4/3501-6 90°				
FREQUENCY (hz)	T-VALUES (Confidence Level)	AVERAGE Loss Factor ($\times 10^{-4}$)	STD DEV ($\times 10^{-4}$)	NO. OF SAMPLES
25.05	2.080 (96%)	53.98	3.608	4
33.27	.678 (72.5%)	60.776	5.632	5
43.89	4.161 (99.5%)	58.432	5.290	5
93.45	2.009 (96%)	71.601	4.701	5
163.12	1.880 (95%)	65.432	5.004	5
221.12	3.612 (99.5%)	72.349	6.532	5
685.49		57.297	5.760	4

TABLE 30 Statistical values for use in Equation 160 for 0° AS4/3501-6

AS4/3501-6 0°				
FREQUENCY (hz)	T-VALUES (Confidence Level)	AVERAGE Loss Factor ($\times 10^{-4}$)	STD DEV ($\times 10^{-4}$)	NO. OF SAMPLES
48.51	0.005795	34.06	6.745	2
60.66	.882 (77%)	34.01	10.547	3
100.23	2.444 (95%)	40.29	3.686	3
209.93	15.85 (99.5%)	49.51	1.378	3
253.37	1.669 (91%)	29.96	1.755	4
326.61	10.661 (99.5%)	34.66	5.420	3
427.59	2.692 (97%)	65.45	3.683	7
486.56	4.919 (99.2%)	59.20	4.355	5
567.15	2.615 (96.2%)	47.20	3.284	5
671.08		39.82	5.518	6

TABLE 31 Statistical values for use in Equation 160 for ±45° AS4/3501-6

AS4/3501-6 ±45°				
FREQUENCY (hz)	T-VALUES (Confidence Level)	AVERAGE Loss Factor	STD DEV	NO. OF SAMPLES
28.10	14.906 (99.5%)	71.43	5.835	5
43.07	7.811 (99.5%)	113.19	2.287	5
50.81	9.325 (99.5%)	93.10	5.277	5
73.74	3.445 (99.5%)	64.02	4.558	5
117.44	.562 (70%)	54.49	4.181	5
214.42	1.206 (86%)	52.18	8.181	5
317.1	.815 (78%)	57.4	6.199	6
441.12		60.75	8.248	7

Appendix G

Loss Factor for 5208 Epoxy

TABLE 32 Loss Factor as a Function of Frequency for 5208 Neat Epoxy Resin

Frequency (hz)	Loss Factor ($\times 10^{-4}$)	Average Loss Factor ($\times 10^{-4}$)	Standard Dev. ($\times 10^{-4}$)
50	180.57 199.78 144.72 225.28 222.24	194.52	29.72
102.3	181.36 210.43 190.75 197.51 207.68 200.11	197.97	9.85
227.85	229.23 177.08 193.41 230.82 205.68	207.24	20.70
432.15	213.09 230.65 221.06 278.11 275.34 214.28	238.76	27.46
696.75	228.72 285.81 309.39 278.23 258.14	272.06	27.18

INITIAL DISTRIBUTION

Copies

12 DTIC

8 NAVSEA
- 1 05M3 (Pinto)
- 1 92RL (Swann)
- 1 92RP (Spero)
- 1 92RP (Troffer)
- 1 55Y2 (McCarthy)
- 1 55Y (Malakhoff)
- 1 55Y2 (Will)
- 1 56D2 (Fritsch)

3 PL
- 1 6383 (Badaliance)
- 1 6383 (Wolock)
- 1 6385 (Chaskelis)

1 NSWC
- 1 R31 (Augl)

5 ONR
- 1 1132SM (Rajapakse)
- 1 1131S (Fishman)
- 1 1132SM (Barsoum)
- 1 1216 (Vasudevan)
- 1 1132SM (Jones)

3 ONT
- 1 211 (Gagorik)
- 1 225 (Kelly)
- 1 233 (Remmers)

1
Dr. John P.Coulter
Lehigh University
Dept. of Mech. Eng. and Mechanics
Packard Lab. No. 19
Bethlehem, Pa. 18015

1
Dr. Michael L. Drake
University of Dayton
Research Institute - JPC 33
300 College Park
Dayton, Oh 45469

CENTER DISTRIBUTION

Copies	Code	Name
1	0113	Winegrad
1	0113	Douglas
1	0114	Becker
1	0115	Caplan
1	15	Morgan
1	17	Krenzke
1	1702	Corrado
1	172	Rockwell
1	1720.1	Tinley
1	1720.2	Dozier
1	1720.2	Phyillaier
1	1730.2	Critchfield
1	19	Sevik
1	1905.1	Blake
1	1940	Montroll
1	1940.2	Maga
1	1941	Cole
1	2723	Wilhelmi
1	2742	Lu
1	28	Wacker
1	2801	Crisci
10	2802	Morton
25	2802	Crane
1	2803	Cavallaro

Copies	CENTER DISTRIBUTION		
1 Longin Greszczuk McDonnell Douglas Space Systems Co. Mail Stop 13/3 5301 Bolsa Avenue Huntington Beach, CA 92647	1	2812	Wong
	1	284	Fischer
	1	2842	Jones
1 James Gauld Electric Boat Division General Dynamics 75 Eastern Point Rd. Groton, Ct. 06340-4909	1	2844	Castelli
	1	522.2	TIC (A)
	1	522.1	TIC (C)
	1	5231	Office Services

1
K. E. Hofer
L. J. Broutman & Assoc. Ltd.
3424 South State St.
Chicago, IL 60616

1
Dr. Ron Gibson
Mechanical Engineering Dept.
Wayne State University
2140 Engineering Building
Detroit, Michigan 48202

1
Bruce Sandman
NUSC
Code 8215, Building 679
Newport, RI. 02841

1
Dr. Stan Sattinger
Mechanics Department
Westinghouse
401-2X9C
1310 Beulah Rd
Pittsburgh, Pa. 15235

1
Ted Duclos
Thomas Lord Research Center
Lord Corp.
405 Gregson Drive, Box 8225
Cary, NC. 27512-8225

1
Dr. D. Wilkins
Center for Composite Materials
University of Delaware
Newark, DE 19716

1
Dr. Martin J. Pechersky
APL/Penn State University
Box 30
State College, Pa. 16804

1
Mr. Jack Woods
Foster Miller
350 Second Avenue
Waltham, MA 02154

1
Mr. Jim Dorr
McDonnell Douglas Corp.
D. 390 MC 1021310
P.O. Box 516
St. Louis, Mo. 63166-0516

1
Mr. Mark Sherman
Amoco Research Center
P.O. Box 400
Naperville, Il 60566

1
Kevin L. Smith
Dept. E78, Building 600
Newport News Shipbuilding Co.
4101 Washington Ave.
Newport News, VA. 23607

1
Dr. J. R. Vinson
Dept. of Mech. Engineering
Spencer Laboratory
Univ. of Delaware
Newark, DE 19716

1
Mr. F Xavier Speigel
Loyola College
Baltimore, Md. 21218

1
John M. Winter, Jr.
Center for Nondestructive Evaluation
102 Maryland Hall
The Johns Hopkins University
Baltimore, MD 21218

1
Charles Zanis
CASDE Corporation
2800 Shirlington Road
Suite 600
Arlington, VA 22206

1
Don E Pettit
Composites Development Center
Lockheed
Aeronautical Systems Company
D74-72, B369, B6
Burbank, CA 91520-7004

1
K. Benjamin Su
E. I. Du Pont De Nemours & Company
Engineering Technology Laboratory
Experimental Station - 80304
Wilmington, DE 19880-0304

1
Dr. Richard Norton
Science and Technology Dept.
Hercules, Inc.
Research Center, 8136-T6
Wilmington, De. 19894

1
Dr. R.B. Pipes
Dean of Engineering
University of Delaware
Newark, DE 19716

1
T.H. Tsiang, Sc.D.
Lockheed
Aeronautical Systems Company
Burbank, CA 91520-4717

1
R. H. Boschan
Composites Development Center
Lockheed
Aeronautical Systems Company
Burbank, CA 91520-7637

1
Douglas S. Cairns, Ph.D.
Hercules Incorporated
Science & Technology Department
Bacchus Works
Magna, UT 84044-0098

1
Bob Kolec
Westinghouse
Mail Stop EC-1
401 East Hendry Ave, Box 3499
Sunnyvale, Ca. 94088-3499

1
Dr. Charles Bersch
Institute for Defense Analysis
801 N. Beauregard Street
Alexandria, VA 22311

1
Dr.John W. Gillespie, Jr.
Assistant Director, CCM
Composites Manufacturing Science Laboratory
University of Delaware
Newark, DE 19716

1
Dr. Robert E. Green
Materials Science and Engineering
102 Maryland Hall
The Johns Hopkins University
Baltimore, MD 21218

1
Lowell Smith
Newport News Shipbuilding
& Drydock Company
4101 Washington Avenue
Newport News, VA 23607

1
Ms. Beverly Roberts
Fibers Department
EI du Pont de Nemours & Co.
P.O. Box 80702
Wilmington, De. 19880-0702

1
Mr. Jim Suarez
Grumman Aircraft Systems
M/S B 44-35
Bethpage, NY. 11714

1
Dr. Roy McCullough
Director, CCM
University of Delaware
Newark, DE 19716

1
George Leon
Electric Boat Division
General Dynamics
Mail Stop J11-431
Eastern Point Road
Groton, CT 06340

1
Dr. J. Economy
University of Illinois
104 S. Wright St.
Urbana, Il. 61801

1
Mr. Ron Trabocco
Code 6063
Naval Air Development Center
Warminster, Pa. 18974

1
Mr. B. Coffenberry
ICI Composite Structures
2055 East Technology Circle
Tempe, Az. 85284

REPORT DOCUMENTATION PAGE

Form Approved
OMB No. 0704-0188

1. AGENCY USE ONLY *(Leave blank)*	2. REPORT DATE	3. REPORT TYPE AND DATES COVERED
	April 1991	Research & Development

4. TITLE AND SUBTITLE
Vibration Damping Response of Composite Materials

5. FUNDING NUMBERS

6. AUTHOR(S)
Roger M. Crane

7. PERFORMING ORGANIZATION NAME(S) AND ADDRESS(ES)
David Taylor Research Center
Bethesda MD 20084–5000

8. PERFORMING ORGANIZATION REPORT NUMBER
DTRC–SME–91/12

9. SPONSORING /MONITORING AGENCY NAME(S) AND ADDRESS(ES)

10. SPONSORING /MONITORING AGENCY REPORT NUMBER

11. SUPPLEMENTARY NOTES

12a. DISTRIBUTION / AVAILABILITY STATEMENT
Approved for public release; distribution is unlimited.

12b. DISTRIBUTION CODE

13. ABSTRACT *(Maximum 200 words)*

This report involves the investigation of the mechanical vibration damping characteristics of glass/epoxy and graphite/epoxy composite materials. The objective was to develop an analytical model which incorporates the frequency dependence of the vibration damping loss factor and to experimentally characterize the loss factor for frequencies up to 100 Hz.

Numerous analytical models have been proposed to determine the loss factor of composites, including micromechanical, macromechanical and structural models. Of these generic types, the macromechanical models incorporate important material characteristics which can affect the loss factor. The most widely accepted model utilizes the elastic viscoelastic correspondence principle. Although investigators acknowledge the viscoelastic characteristic of composites, they fail to incorporate the frequency dependence in their analysis. In this effort, the elastic viscoelastic correspondence principle is extended to incorporate the frequency dependence of the composite material.

The analytical model requires as input the inplane material loss factors as a function of frequency. An experimental apparatus was designed and fabricated to accomplish this. Cantilever beam specimens were utilized which were excited using an impulse from an instrumented force hammer. The loss factor was calculated using the half power band width technique. The apparatus was calibrated using a well characterized low damping material. The effect of clamping pressure and of the clamp block to specimen interface material was also investigated.

While testing the composites, it became evident that the amplitude of vibration had a pronounced effect on the calculated loss factor. Calculated loss factors were significantly reduced if the tip displacement amplitudes vs. time were lower than 0.001 in. for more than 25% of the data set. To alleviate this problem, a robust testing methodology was proposed and tested. This test method is then utilized to determine the composite inplane loss factors.

The analytical model was validated using two generic laminated configurations. The model predictions were within the scatter of the experimental data. Parametric studies were also performed using the model. Trends shown by other investigators as well as inconsistencies between them were accounted for by this model.

14. SUBJECT TERMS	15. NUMBER OF PAGES
Damping loss factor, S–2 Glass/epoxy, Graphite/epoxy, Elastic-viscoelastic correspondence principle, Experimental test setup, Damping survey, Zener thermoelastic theory, Material complex modulus	278
	16. PRICE CODE

17. SECURITY CLASSIFICATION OF REPORT	18. SECURITY CLASSIFICATION OF THIS PAGE	19. SECURITY CLASSIFICATION OF ABSTRACT	20. LIMITATION OF ABSTRACT
Unclassified	Unclassified	Unclassified	Same as report